Doctoral Dissertation
Doctoral Program in Chemical Engineering (35th Cycle)

Innovative antibacterial biocomposite films based on biomacromolecules and nanostructured zinc oxide

By

Paolo Pino
******

Supervisor(s):
Prof.ssa F. Bosco
Prof.ssa B. Onida

Doctoral Examination Committee:
Prof.ssa B. Vigani, Referee, University of Pavia
Prof.ssa E. Ghedini, Referee, University of Venezia
Prof.ssa E. Verne', Referee, Polytechnic of Turin
Prof. M. Banchero, Referee, Polytechnic of Turin
Prof.ssa P. Santi, Referee, University of Parma

Politecnico di Torino
2023

Declaration

I hereby declare that the contents and organization of this dissertation constitute my own original work and does not compromise in any way the rights of third parties, including those relating to the security of personal data.

Paolo Pino

2023

* This dissertation is presented in partial fulfillment of the requirements for **Ph.D. degree** in the Graduate School of Politecnico di Torino (ScuDo).

I would like to dedicate this thesis to my parents,
and to their priceless, selfless, endless love.

Acknowledgment

It takes more than a village to raise a researcher. The work that you are about to read is the result of the relentless commitment and dedication of many people, whose contributions – either scientific, administrative, or emotional – have made this possible. To them I want to express my deepest gratitude.

First and foremost, I want to acknowledge my research team at Politecnico di Torino. I thank my two supervisors, Professors Francesca Bosco and Barbara Onida, for their attentive and insightful mentorship, their brilliant scientific leadership, and for being the best examples a young researcher could be inspired from. I thank Dr. Chiara Mollea, for her constant support and friendship, her firm resourcefulness, and for teaching me how to work and thrive in a scientific laboratory. I also want to thank the other faculty members and colleagues that took part to this journey as well. My gratitude goes to Professor Silvia Ronchetti and to Dr. Marta Gallo and Dr. Sara Mohammed, for being such a helpful presence in so many occasions. Thanks to all the other faculties that allowed me to keep on learning and growing. Thanks to all my thesis student for sharing so much work and hours with me, and for their young motivation and intelligence. Finally, thanks to all the administrative and technical personnel that supported us throughout.

Many thanks to Professor Silvia Rossi for giving me the opportunity to spend a research period at the University of Pavia. A huge thanks to Dr. Barbara Vigani for her invaluable support and collaboration during and after that period, for her monumental work at the BForDev Lab, and for being such a talented and driven

scientist. My gratitude also extends to the whole BForDev research group, for being so helpful in carrying out our research and for welcoming me in such a lovely and heartwarming way.

I also want to thank Professor Theo Van de Ven for allowing me to spend another research period with his group at McGill University. Thanks to Professors Hadi Moradian and Hassan Sawalha for their scientific acumen and for involving me in their research. Thank you to Amin Ojan, Yiwei Yang and Sarah Cranmer-Smith for being phenomenal co-workers and young researchers. Thank you to Ross Commodari for his warm welcome and administrative support. Thanks to my dearest Giulia, Cecilia, Sabrina and Serena for sharing with me this amazing experience and being *home away from home*.

These three years have been enriched by so many other beautiful things happening *outside* of the universities, and yet playing a central role in making this path worth being grateful for.

I express my deepest gratitude and affection to Justin Zipkin and to all the incredible Eternal Light Photonics Team. To what has been achieved so far and to all the great things that lie ahead. Thanks to Professor Andrew Aldrin for supporting us from the beginning. *Ad Luna*.

I warmly acknowledge the Collège des Ingénieurs for connecting me to an amazing network of bright *Fellows*. I thank and admire each and every one of you for being such outstanding individuals.

Thanks to all the true friends and loved ones who shared these years with me and had my back in every challenge. Thank you, Giuseppe, for your love, patience, adamant support, and brotherhood. Thank you, Nanna, for your presence and kindness.

Thank you Cecio, Valeria, my Londoners, my Frejus housemates, my beloved family, and all the friends and relatives building their lives in other cities and yet remaining close to me.

Thank you, Francesca. *Life will always be la vie en rose*.

Thank you, Mum and Dad. None of this would have been possible without your love and help. To you goes my biggest and sincerest gratitude.

In conclusion, I would like to dedicate a final thought to all the young doctoral students and researchers who spent countless hours and efforts inside the laboratories of the world. To all those who have failed experiments, wore out lab coats, broke glasses, lost data, faced doubts, received rejections, struggled with uncertainty, repeatedly questioned the purpose and quality of their activity, and yet tried again, moved by their passion for science: yours are the hands and minds that will shape a better future for this planet. Keep it up.

Abstract

Chronic wounds are a large global health issue affecting 2% of the population in western countries, with mortality rates becoming as high as 52% in some cases. Chronic wounds can be caused by – or cause – infections, as pathogens do not encounter the natural barrier represented by the skin and can interfere with the normal healing process. It has been estimated that these infections are responsible for 75% of post-operative deaths. In parallel, treating infections is becoming more difficult, due to antimicrobial resistance (AMR), i.e., the tendency of microorganism to adapt and develop resistance against the drugs that are used to eradicate them. Without further action, AMR is predicted to cause around 10 million deaths per year by 2050. This demands for urgent solutions, including new types of wound dressings. Many dressings have been used and developed over time, from traditional cotton gauzes to modern films, foams, hydrogels, and hydrocolloids. In recent years, a new class of dressing materials has emerged: bionanocomposites. These are composites made by biomacromolecule-based matrixes filled with nanostructured materials. The former primarily bring high biocompatibility and biodegradability, while the latter have been found to have antimicrobial properties. Bionanocomposites can also possess many other beneficial features, such as anti-inflammatory, hemostatic, cellular proliferation and tissue regeneration properties. Common biomacromolecules include polysaccharides like chitosan, cellulose, alginate and starch, to proteins like collagen, gelatin and chitin. Many nanostructured materials have been combined with these polymers. The most common are metal and metal oxide nanoparticles. Among all these, nanostructured zinc oxide (nZnO) is one of the most effective in terms of antibacterial properties, and showed lower toxicity compared to metal nanoparticles. Plus, zinc is an

essential element for the human body, and is involved in wound healing and the immune system. For all these reasons, this work concerns the development, characterization and testing of nZnO-containing bionanocomposites using biomacromolecules that have yet been poorly explored but that possibly hold good potential, in an effort to develop new solutions.

The research therefore started from the synthesis of a nanostructured zinc oxide following a simple wet chemical precipitation technique. The nZnO particles are spherical with an average size of 30 nm, a specific surface area of 49.5 m2/g, a wurtzite-type crystal structure, and a 3.49 eV bandgap. The oxide has positive electric charge in neutral pH water and shows the presence of some carbonate species on the surface. Its antibacterial efficacy has been tested against Gram-positive *Staphylococcus epidermidis* and Gram-negative *Escherichia coli*. The nZnO revealed far more effective than a commercial, micron-sized ZnO. The minimum inhibitory concentration of nZnO resulted equal to 120 and 480 μg/mL against *S. epidermidis* and *E. coli*, respectively, in line with other values reported in the literature.

At this point, several bionanocomposites with this nZnO were formulated. In a first instance, whey proteins were investigated. These are a byproduct of the dairy industry with uses as food additives and for encapsulation and delivery of nutraceuticals. Composite films were made with Whey Protein Isolate (WPI). These showed high transparency in the visible range (around 70%), which is important to ensure good wound inspection. Their swelling properties are comparable with those of some commercial alginate-based wound dressings. nZnO improved UV-barrier properties, swelling in phosphate buffered saline, elastic modulus and tensile strength, and decreased optical transmittance, mass degradation in artificial sweat, and elongation at break. The mechanical properties were comparable with those of the human skin, which is good to ensure dressing compliance with the underlying tissue. A nZnO concentration-dependent antibacterial activity was observed against *S. epidermidis* and *E. coli*. The values were higher for the first strain and in line with scientific literature.

After WPI, β-glucans were explored. They are known for their immune-stimulatory properties. Yeasts β-glucans/nZnO films were prepared via solvent casting. The films were amorphous and had lower transparency and swelling abilities compared to WPI, but had very good antimicrobial properties. Composites were also made with poly(3-hydroxybutyrate-co-3-hydroxyvalerate), which is often used in scaffolds for tissue engineering due to its high biocompatibility. However, the films were inhomogeneous and had the lowest water affinity and antibacterial activity.

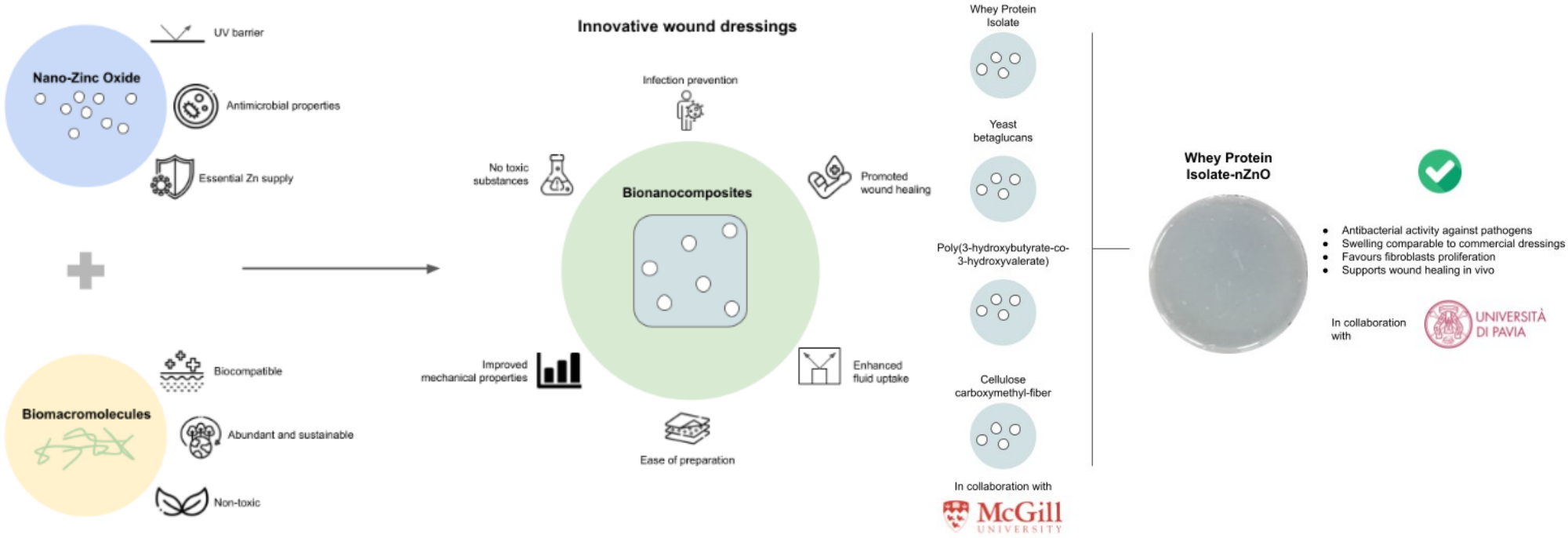
Finally, cellulose-based bionanocomposites were investigated at the Pulp & Paper Research Center of McGill University, Montreal, Canada. To this end, a recently developed mildly-carboxylated cellulose was used, denominated carboxymethyl fiber (CMF), and incorporated with nZnO for the first time. Films had good transparency and mechanical properties. The oxide increased water contact angle and surface roughness, as well as the swelling ability, which was the highest ever reported in this work. The antibacterial activity was slightly lower than that of WPI-based composites and decreases if a CMF matrix with a higher degree of substitution of carboxyl groups was used, due to the antibacterial Zn^{2+} being sequestered by the negative carboxyl groups.

Of all the bionanocomposites considered, WPI-nZnO offered the best compromise among high transparency, swelling, antibacterial action, ease of production, low cost and environmental impact, homogeneous nZnO dispersion, and mechanical properties comparable with the human skin. For this reason, WPI-nZnO composites underwent water contact angle measurements, hydration tests, viscoelastic properties measurements after hydration, and degradation tests in liquid oxidative environment. The presence of nZnO increased water contact angle while maintaining its values within the range of common wound dressings. Zinc oxide also improved hydration and allowed to better retain good viscoelastic properties. This indicates that the composite dressing is well suited to remain compliant with skin strains even after absorbing wound exudates upon use. The films were also stable in oxidative environments and degraded less when nZnO was present. WPI-nZnO composites were also tested against

pathogen *S. aureus* and *E. coli*. This time, the samples were more effective against the *E. coli*, showing that the films might also work well against some Gram-negatives. Subsequently, *in vitro* cytotoxicity and proliferation tests on human dermal fibroblasts were carried using culture media previously conditioned with WPI and WPI-nZnO samples (also called extracts). In the first test, cytotoxicity was observed when cells were exposed to non-diluted extracts, but disappeared at 1:2 dilution. This same dilution enhanced proliferation in the second test, compared with control samples. Finally, *in vivo* wound healing tests were carried on rats. Wounds treated with WPI or WPI-nZnO samples healed correctly and without any delay or sign of toxicity compared to non-treated wounds, as revealed by histological analyses, where clear evidence of re-epithelialization and tissue restoration could be found.

In conclusion, this work contributed to the progress in the field of advanced wound dressing materials through the design, preparation and study of new potential candidates. To this end, the systematic assessment of the materials explored allowed to outline a standard framework and set of tools to compare and mature different bionanocomposites, so that these new technologies can be developed more successfully. In doing so, a novel material – WPI-nZnO composites – was identified and its promising properties demonstrated, towards a potentially better future healthcare.

Graphical Abstract



Contents

Humans against microbes....1
1.1 Antimicrobial resistance and the quest for the next antibiotic....1
1.1.1 Approaches to contrast antimicrobial resistance....3
1.2 The skin....4
1.2.1 Wound types and healing....6
1.3 Wound treatments and infections....9
1.4 Wound dressings....12
1.4.1 Types of wound dressings....12
1.4.2 Advanced wound dressings properties....15
References....17
Biopolymers and nanomaterials: next generation healthcare....24
2.1 Hacking tissue repair....24
2.2 Biomacromolecules for wound dressings....25
2.2.1 Polysaccharides-based polymers....25
2.2.2. Protein-based polymers....27
2.3 Nano-antimicrobials....31
2.3.1 Nanostructured Zinc Oxide....33
2.4 Biomacromolecules-nZnO composites....37
2.4.1 Preparation methods....38
2.4.2 Mechanical and functional properties....40
2.5 Biomedical applications....46

2.5.1 Antimicrobial properties 46
2.5.2 Wound healing properties 50
References 53
Big problems, small solutions: nanostructured zinc oxide 78
3.1 Introduction 78
3.2 Experimental 78
3.2.1 Materials 78
3.2.2 Synthesis of nanostructured zinc oxide 79
3.2.3 Characterization of nanostructured zinc oxide 79
3.2.4 Antibacterial activity 80
3.3 Results and discussion 81
3.3.1 Characterization of nZnO 81
3.3.2 Antibacterial activity 87
3.4 Conclusions 91
References 92
Upcycling food by-products: whey proteins as bionanocomposite matrix 94
4.1 Introduction 94
4.2 Experimental 96
4.2.1 Materials 96
4.2.2 Preparation of Whey Protein films 96
4.2.3 Preparation of WP-ZnO films 96
4.2.4 Characterization of the films 97
4.2.5 Swelling tests 97
4.2.6 Degradation tests 98
4.2.7 Antibacterial tests 98
4.3 Results 99
4.3.1 Characterization of the films 99
4.3.2 Swelling tests 102

4.3.3 Degradation tests....106
4.3.4 Antibacterial tests....107
4.4 Conclusions....109
References....110
Macromolecules from microorganisms: polysaccharides and polyesters....116
5.1 Introduction....116
5.2 Experimental....118
5.2.1 Materials....118
5.2.2 Preparation of BG and BGZ films....119
5.2.3 Preparation of PHBV and PHBV-Z films....119
5.2.4 Characterization of BG and BGZ films....120
5.2.5 Characterization of PHBV and PHBV-Z films....120
5.2.6 Swelling tests....121
5.2.7 Antibacterial tests....121
5.3 Results....122
5.3.1 Characterization of BG and BGZ films....122
5.3.2 Preparation and characterization of PHBV and PHBV-Z films....127
5.3.3 Swelling tests....130
5.3.4 Antibacterial tests....133
5.4 Conclusions....136
References....137
Wound healing made green: cellulose-based dressings....144
6.1 Introduction....144
6.2 Experimental....145
6.2.1 Materials....145
6.2.2 Preparation of CMF dope....145
6.2.3 Preparation of CMF films....147
6.2.3 Preparation of CMC films....147

6.2.4 Films characterization 148
6.2.5 Swelling tests 149
6.2.6 Antibacterial tests 149
6.3 Results 150
6.3.1 Films characterization 150
6.3.2 Swelling test 157
6.3.3 Antibacterial tests 158
6.4 Conclusions 162
References 163
Taken to the next level: a biopharmaceutical characterization of Whey Protein Isolate-nZnO bionanocomposites 166
7.1 Introduction 166
7.2 Experimental 168
7.2.1 Water Contact Angle Measurements 168
7.2.2 Hydration test 168
7.2.3 Viscoelastic Properties after Hydration 170
7.2.4 Degradation test 170
7.2.5 Antimicrobial test 171
7.2.6 *In vitro* cytocompatibility test 171
7.2.7 *In vitro* proliferation test 172
7.2.8 *In vivo* studies 172
7.2.9 Statistical analysis 173
7.3 Results 174
7.3.1 Water Contact Angle 174
7.3.2 Hydration test 175
7.3.3 Viscoelastic Properties after Hydration 176
7.3.4 Degradation Test 177
7.3.5 Antimicrobial test 179

7.3.6 *In vitro* cytocompatibility test 180
7.3.7 In-vitro proliferation test 182
7.3.8 In-vivo wound healing test 183
7.4 Conclusions 185
References 185
Conclusions and Perspectives 185

List of Figures

Figure 1.1: Representation of human skin. Source: (Kordestani, 2019a). 5

Figure 1.2: Wound prevalence by type in the Medicare population. Source (Nussbaum et al., 2018). 9

Figure 2.1: Antibacterial mechanisms of nano-ZnO. Source (A. Singh et al., 2018). 35

Figure 2.2: Differences in Gram-negative and Gram-positive cell walls. Source: (Berezin et al., 2017).....36

Figure 2.3: Nano-ZnO design through selection of reagents and synthesis parameters.....37

Figure 2.4: Schematic representation of BNCs preparation techniques.....39

Figure 2.5: Antibacterial action mechanisms of BNCs.....48

Figure 3.1: FESEM image of nZnO (A) and cZnO (B) 82

Figure 3.2: nZnO particle size distribution. 83

Figure 3.3: TEM image of nZnO 83

Figure 3.4: UV-visible absorbance spectrum of nZnO 84

Figure 3.5: X-rays diffraction pattern of nZnO corresponding to a wurtzite-type crystalline structure.....84

Figure 3.6: Nitrogen adsorption-desorption isotherms of nZnO.....85

Figure 3.7: FTIR spectrum of nZnO. 85

Figure 3.8: Particle size distribution for different pH values. 86

Figure 3.9: Modified Kirby-Bauer agar diffusion test against *S. epidermidis* (a) and E. coli (b). Red frames indicate the nZnO concentrations tested against both microorganisms. Black arrows indicate the MIC values, 3.75 and 6 mg/mL, for S. epidermidis and *E. coli* respectively. 88

Figure 3.10: Inhibition zones for different nZnO concentrations against *S.epidermidis* and *E.coli*. 89

Figure 3.11: Modified Kirby-Bauer agar diffusion test against *S. epidermidis* (left) and *E. coli* (right) using cZnO. Red frames indicate the concentrations tested against both microorganisms. 90

Figure 4.1: A WPC film sample (top left) and a WPI film sample (bottom left) and their UV-visible spectra. 99

Figure 4.2: WPI and WPI-ZnO film samples (left) and their UV-visible spectra. 100

Figure 4.3: XRD spectra of WPI and WPI-ZnO films. 101

Figure 4.4: ATR-FTIR spectra of WPI and WPI-ZnO films. 101

Figure 4.5: Mechanical properties of WPI and WPI-ZnO films. 102

Figure 4.6: Swelling ratio of WPI and WPI-ZnO composites in water (left) and in PBS (right). 103

Figure 4.7: Swelling ratio in water of WPI films versus commercial wound dressings at neutral pH 105

Figure 4.8: Percentage of degraded mass in different fluids versus nZnO content 106

Figure 4.9: Inhibition zones of WPI and WPI-ZnO films with different nZnO contents against *S. epidermidis* and *E. coli* 109

Figure 4.10: Inhibition zones of WPI and WPI-ZnO films top and bottom faces against *S. epidermidis* 109

Figure 5.1: A1) FESEM image of BG film surface; A2) EDS carbon and oxygen distribution map of BG film surface; A3) FESEM image of BG film cross section; B1) FESEM image of BGZ-6 film surface; B2) Elemental maps of C, O and Zn of BGZ-6 film surface in a generic point of the sample (1) and in correspondence of a nZnO aggregate (2); B3) Close-up FESEM image of a nZnO aggregate in the BGZ-6 film cross section; B4) Elemental maps of C, O and Zn in the BGZ-6 film cross section. 123

Figure 5.2: A) XPS survey of the samples and B) high-resolution XPS peaks of Zn2p3. 123

Figure 5.3: XRD pattern of BG and BGZ films. 124

Figure 5.4: UV-Visible spectra of BG and BGZ films. Sample photographs are shown on the right 125

Figure 5.5: ATR-FTIR spectra of BG and BGZ films 126

Figure 5.6: TGA (left) and DSC (right) curves of BG and BGZ films 127

Figure 5.7: Photograph of a PHBV film 128

Figure 5.8: XRD patters of PHBV and PHBV-Z films 129

Figure 5.9: ATR-FTIR pattern of PHBV and PHBV-Z films 129

Figure 5.10: TGA curves for PHBV and PHBV-Z films. 130

Figure 5.11: Swelling ratio of BG and BGZ films in distilled water at different pH values 131

Figure 5.12: Swelling ratio of PHBV and PHBV-Z films in distilled water at different pH values 132

Figure 5.13: Disk diffusion test of (A) BGZ-2, (B) BGZ-4 and (C) BGZ-6 film samples against *S.epidermidis.* C indicates the filter paper control disc. 134

Figure 5.14: Inhibition zone values of BG and BGZ films against *S.epidermids* and *E.coli* 134

Figure 5.15: Inhibition zone values of BG films versus PHBV films against *S.epidermids* 136

Figure 6.1: UV-vis spectra of CMF and CMF-Z films. 150

Figure 6.2: XRD spectra of nZnO, CMF and CMF-Z films. 151

Figure 6.3: ATR-FTIR spectra of nZnO, CMF and CMF-Z films. 152

Figure 6.4: WCA of CMF and CMF-Z films. 153

Figure 6.5: Mechanical properties of CMF and CMF-Z films. 154

Figure 6.6: SEM images and elemental maps of CMF (A1, A2), CMF-Z2 (B1, B2), CMF-Z4 (C1, C2) and CMF-Z6 (D1, D2) films 156

Figure 6.7: Top - SEM images of (A1) CMF-Z4 and (B1) CMF-Z6 samples. Bottom - EDS point analyses of the aggregates on the surface of (A2) CMF-Z4 and (B2) CMF-Z6 samples. 157

Figure 6.8: Swelling ratio of CMF and CMF-Z films in PBS after 2, 24 and 48 hours 158

Figure 6.9: Disk diffusion test of CMF and CMF-Z samples against *S. epidermidis* and *E. coli* 160

Figure 6.10: Inhibition zone of CMF19-Z4, CMF-Z4 and CMC-Z4 against *S. epidermidis.*.....161

Figure 7.1: (left) optical transmittance of bionanocomposites with 4% nZnO content and (right) their inhibition zone against *S. epidermidis*.....168

Figure 7.2: Graphical representation of the experimental set-up used for the hydration test. The semipermeable membrane is comprised by a dialysis membrane supported by a pierced Parafilm® sheet. 169

Figure 7.3: WCA values of WPI and WPZ films up to 10 s (mean values ± s.d.; n = 3). Images of the drop at different times (1, 5, and 10 s) are reported for WPI and WPZ films. 174

Figure 7.4: Variation in time of the swelling ratio % of WPI and WPZ films (mean values ± s.d.; n = 6).....175

Figure 7.5: Storage (G') and loss (G") moduli vs. frequency profiles of WPI and WPZ films upon 24 h-hydration in PBS (mean values ± s.e.; n = 3).....177

Figure 7.6: WPI and WPZ film degradation after 1, 3 and 7 days in two different media - PBS and PBS added with H2O2 - expressed in terms of (A) residual film mass and (B) concentration of proteins released in the medium (mean values ± s.e.; n = 3).....178

Figure 7.7: Optical density values after 24h incubation of NHDF cells with WPI and WPZ extracts, undiluted and diluted 1:2, 1:10, 1:50, 1:100 v/v in CM. Complete culture medium (CM) was considered as control (mean values ± s.e.; n = 6).....182

Figure 7.8: Optical density values after 6 and 24h proliferation of NHDF cells in WPI and WPZ extracts, diluted 1:2 v/v in CM. Complete culture medium (CM) was considered as control (mean values ± s.e.; n = 6).....183

Figure 7.9: H&E (left panel) and PSR (central panel - with bright field images; right panel - with polarized light) sections of (a) lesion treated with saline solution as negative control, (b) intact skin, (c) lesion treated with WPI, (d) lesion treated with WPZ. Original magnification: 5×. Each micrograph frame has a width of 1780 μm and refers to a 18-days old lesion. 184

List of Tables

Table 1.1: Overview of modern wound dressings and their applications 14

Table 2.1: Overview of biomacromolecules for wound dressing. 28

Table 2.2: Effect of nZnO on the elastic modulus (EM) and tensile strength (TS) of biomaterials. 41

Table 2.3: Effect of nZnO presence on the WCA of different biomaterials. .43

Table 3.1: Minimum Inhibitory and Minimum Bactericidal Concentrations of nZnO against *S. epidermidis* and *E. coli*.....90

Table 4.1: A typical composition of WPC and WPI. Source: (Lorenzen et al., 2006). Whey proteins from Milei GmbH were used in the source study. 95

Table 6.1: Amounts of solvents and reagents to prepared CMF with different degrees of substitution. 146

Table 6.2: Bionanocomposite samples prepared.....148

Table 6.3: Comparison of mechanical properties between WPI and CMF films and their bionanocomposites 154

Table 6.4: Inhibition zones of the all the bionanocomposites tested so far..160

Table 7.1: Microbicide effect (ME) of WPZ after 5 and 24h incubation with *S. aureus* and *E. coli*; WPI was used as control (CV % < 12%; n = 3). 179

Chapter 1

Humans against microbes

1.1 Antimicrobial resistance and the quest for the next antibiotic

The history of life on Earth is that of a blind series of evolutionary adaptations, slowly yet relentlessly crafted by the laws of natural selection. This everlasting process continues nowadays, growing more and more intertwined with the actions of one of its most sophisticated products so far: humans.

As a result of the continuous – often competitive – interactions among different species within an ecosystem, early human communities were often disrupted by infectious diseases, i.e. illnesses caused by pathogens such as viruses and bacteria. Modern science and medicine have brought tremendous improvements to human condition by contrasting and eradicating many of such diseases, especially thanks to the use of vaccines and antibiotics.

However, these same barriers we have erected against microbes can also act as sources of evolutionary pressure, ultimately triggering changes in microorganisms that make them insensitive to drugs and medicines, mediated by genetic mutations and stress-induced adaptations. By modifying, acquiring or regulating the activity of their genetic material, microbes have learned how to deactivate drugs, expel them, constrain their uptake, of modify their targets (Gyles & Boerlin, 2014; Reygaert, 2018). This sad yet inevitable side effect of our ingenuity – worsened by our excessive and often inappropriate use of antibiotics – goes by the name of *antimicrobial resistance* (AMR), and today represents one of the biggest threats to

global health and economy, together with cancer and climate change (Roope et al., 2019). Antimicrobial resistance is responsible for hundreds of thousands of deaths every year across the globe, which could become 10 million by 2050 if further interventions are not undertaken, with over $100 T of associated losses in total Gross Domestic Product (The Review on Antimicrobial Resistance, 2014).

AMR is exacerbated by a complex set of factors. One of the preeminent causes is the abuse and misuse of antibiotics in human healthcare, agriculture and livestock, with 73% of global antimicrobials used for food production (van Boeckel et al., 2019). Humans can therefore be exposed to AMR not only in clinical circumstances, but even more likely through environmental transmission mechanisms involving the food and water chains (Samreen et al., 2021). Nevertheless, hospitals represent a critical environment for the development of AMR too: nosocomial infections are contracted at least once by 5.7% of all patients, caused by drug-resistant pathogens selected by the extensive use of broad-spectrum antibiotics (Jenkins, 2021) in the hospital environment. In intensive care units, 9% to 37% of patients are likely to contract one or more infections (Scott et al., 2013). Nosocomial infections translate into prolonged hospital stays, delayed recoveries, impairments, and increased mortality rates. In post-cardiac surgery patients, nosocomial infections have been reported to increase mortality from 3.5% to 16.8% (de la Varga-Martínez et al., 2021). The two most frequent types of infections are urinary tract and surgical wound infections, accounting for 20% and 15% of the total number of cases (Jenkins, 2021).

Over time, AMR has been reported against the most advanced antimicrobials available such as fluoroquinolones, third and fourth generation cephalosporins, and carbapenems (Woolhouse & Ward, 2013). In fact, due to their large populations and extremely fast replication rates, bacteria can build resistance against drugs at a much faster pace than humans can discover, develop and mass-produce new antibiotics (Zaman et al., 2017), a lengthy and high-risk effort which induced a growing number of pharmaceutical companies to withdraw from drug research, development and commercialization due to poor profitability (The Review on Antimicrobial Resistance, 2016).

This requires urgent actions to be undertaken at all scales – from local to international – and levels: social, clinical, political, and scientific.

1.1.1 Approaches to contrast antimicrobial resistance

Every complex problem demands a complex solution. In order to tackle AMR, multiple tactics shall be adopted in order to increase the efficacy of global strategies and their odds of success.

For instance, vaccines and monoclonal antibodies can be a promising solution for certain diseases, as demonstrated with the successful use of the typhoid vaccine against a *Salmonella typhi* outbreak between 2018 and 2019 (*Fighting Antimicrobial Resistance with Vaccines*, n.d.). For their immunostimulatory functions in addition to their intrinsic antimicrobial properties, *antimicrobial peptides* are worth mentioning here as another particularly promising non-conventional treatment against infections (Huan et al., 2020; Mahlapuu et al., 2016). Nanomaterials have recently emerged as a promising novel class of antimicrobial agents. Their use and properties are central for this work and will be further explained later.

More in general, the underlying idea behind every new potential treatment is that bacteria can be killed by adopting alternative routes with respect to those typically employed by the common antibiotics microbes have become resistant to. Ideally, a new treatment would be able to deploy a multitude of different antibacterial mechanisms, thus eliminating single points of failures and raising the barriers to adaptation.

The traditional approach to the discovery of new drugs consists in looking for "new inhibitors of old targets" (Schrader et al., 2020), i.e. new molecules that can attain an inhibitory effect over vital functions of bacterial cells, such as replication, by binding to the same cellular receptors that other drugs used to bind to prior to the insurgence of AMR against them. It is hence suggested that new targets could be found that can lead to bacterial cell death through different inhibition – or event activation – pathways, involving new targets other than those that are essential for *in-vitro* replication.

When the infection is localized on the skin, topical antimicrobial solutions, i.e., solutions administered on a specific site, can also be preferred to tackle the issue more effectively, as opposed to *systemic* solutions, i.e., those solutions that are administered either orally or intravenously, delivering the active substance throughout the entire organism. In fact, the former allows to obtain a higher concentration of antimicrobials in the target zone, which in turn leads to a quicker and more effective eradication of the infection (Stringel et al., 1989).

All in all, the selection and development of better antimicrobial strategies shall follow two key directions: the identification of new antimicrobial mechanisms, and an increasing treatment customization that takes advantage of the peculiarities of the tissues involved.

In this regard, wound infections represent a good and very compelling case due to their high incidence and impact on patient's lifestyle, as well as their inherent complexity deriving from the overlap and mutual influence between infection progression and wound healing physiology. It is therefore very important that solutions in this domain can balance all these delicate and interconnected instances to provide the best treatment to patients. In the broader framework of AMR contrast action, this doctoral thesis revolves around the development of innovative antimicrobial bionanocomposite devices, in an effort to expand the knowledge and push the frontier of wound treatments and biomedical materials.

Prior to venturing into the domain of biomaterials and advanced wound dressings, the following sections will briefly illustrate the main characteristics of the skin and of wounds in order to set the context for subsequent investigations.

1.2 The skin

The skin is the largest organ of the body and its main interface with the external environment, accounting for about 15% of the adult body weight (Mohamed & Hargest, 2021).

Skin possesses several barrier and immunological properties that protect the body from pathogens, harmful substances, ultraviolet radiation, and physical damage. Some important functions of the cutaneous immune system are also the result of the presence of a vast and diverse skin microbiota that colonizes it (Byrd et al., 2018). It also deploys different mechanisms to help maintain body temperature, such as sweating, blood flow regulation through vasodilation or vasoconstriction, and insulation with adipose layers. It possesses sensory functions thanks through the presence of sensory receptors scattered across its surface and the ability to release neurotransmitters and hormones. Skin is also responsible for the synthesis of Vitamin D upon exposure to sunlight. Finally, skin hosts 18-20% of total body water volume and is fundamental in regulating water homeostasis (Abdo et al., 2020; Mohamed & Hargest, 2021).

Anatomically, skin is comprised by three main layers, each divided into sublayers. The innermost layer is called *hypodermis* and is constituted by

connective tissue and fats. Hypodermis also hosts temperature and touch receptors. The middle layer is called *dermis*, and it is mainly formed by fibroblast cells. This layer is in turn subdivided into a bottom *reticular* layer and a top *papillary* layer. Collagen makes up for 70% of the dermis layer followed by elastin. These two proteins endow dermis with robustness and elasticity, so it acts as mechanical support for the skin. The outermost layer is named *epidermis.* This interface with the outer environment consists of a seven-layers architecture. The lowest layer is called *stratum basale.* This is the source of keratinocytes, the epithelial cells that constitute 95% of the epidermis and that are responsible for the production of keratin, and essential fibrous protein of the skin. Keratinocytes differentiate while migrating across the various layers of the epidermis up to the top one, the *stratus corneum.* Here, keratinocytes have the form of squamous, flat dead cells, devoid of nuclei and organelles, and take the name of corneocytes. Corneocytes contain carefully oriented keratin envelopes that confer mechanical resistance to the layer and are surrounded an extracellular environment rich in lipid bilayers that ultimately make the skin impermeable (Mayet et al., 2014). The skin also hosts nerves, blood vessels and several *appendages*, such as hair follicles and glands.

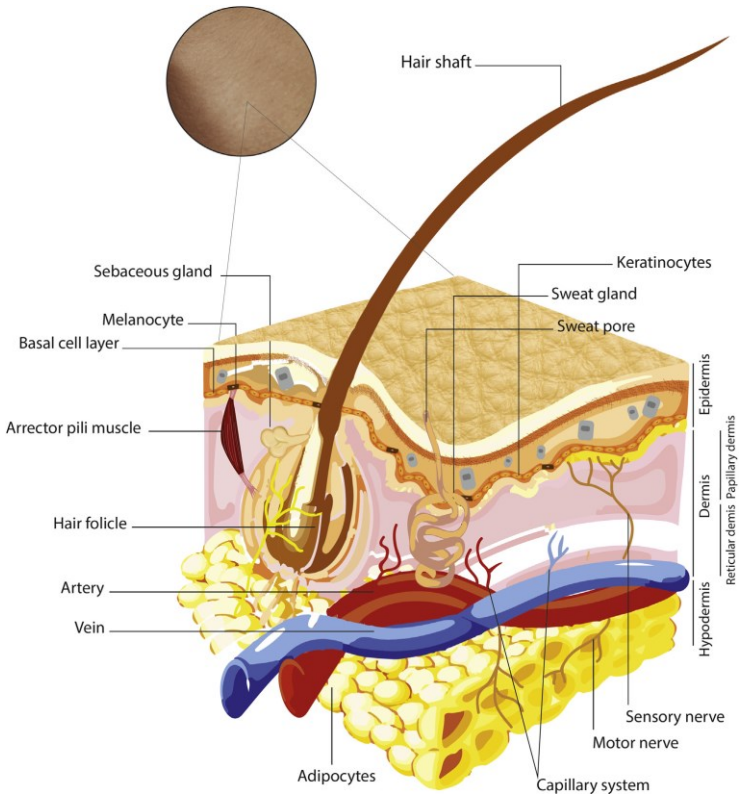


Figure 1.1: Representation of human skin. Source: (Kordestani, 2019a).

1.2.1 Wound types and healing

Wounds are injuries to the body that can be caused by accidents, surgeries or diseases, consisting in the loss of integrity of epithelial tissues and extracellular matrixes (ECM) (Kordestani, 2019a). The ECM is present in every tissue to provide structural support to cells and to regulate tissue health. It is mainly constituted by proteoglycans and fibrous proteins such as collagen and elastin (Frantz et al., 2010). Interruptions in skin continuity typically implies loss of its abovementioned functions and can be accompanied by various extents of damage to underlying tissues, either muscle, connective, or nervous.

The wound healing process consists of four main phases, which are briefly described as follows (Kordestani, 2019b; Lazarus et al., 1994):

- **Hemostasis** starts immediately after the wound occurs. As a consequence of the injury, blood floods the wound space and gets in contact with components of the damaged ECM. This triggers the aggregation of platelets and the formation of a fibrin clot which stops the hemorrhage and offers a preliminary scaffold for cellular migration. Further clot expansion is contained by a process called fibrinolysis, i.e., fibrin dissolution in view of the subsequent healing phases.
- **Inflammation** involves the recruitment of neutrophils and macrophages to eliminate pathogens and debris. Macrophages are also responsible for the secretion of cytokines and other biological regulators that are part of the overall healing process. In the meanwhile, fibrin degradation byproducts attract fibroblasts and epithelial cells.
- During the **Proliferation** phase, granulation tissue is formed, and keratinocytes start restoring the epidermis in a process termed epithelialization. Angiogenesis leads to the formation of new vascular tissue and blood vessels, restoring blood circulation. Collagen fibers are produced by rapidly replicating fibroblasts, which also release other important proteins, growth and angiogenic factors. Fibroblasts are then converted into myofibroblasts, which can pull wound edges towards the center, reducing its area.
- Finally, in the **Remodelling** phase – the longest of the four – collagen is transformed and rearranged along precise directions to ensure maximum mechanical strength to the new tissue.

Wounds can be classified in two main groups: *acute* and *chronic* wounds. The first class involves wounds caused by traumas, burns or surgeries. These wounds typically follow an ordered and predictable healing process going throughout all the four phases described above, ideally resulting into the final restoration of the initial functions and appearance. On the other side, wounds are defined chronic when the normal healing process is impaired at a given stage for some reason, thus determining a longer, improper healing, or its failure. Many factors can hinder correct wound repair, such as age, lifestyle, maceration, necrotic tissue or systemic diseases such as diabetes, obesity, cardiovascular disorders, and cancer (Kordestani, 2019b), which are all on the rise as result of an aging population in most developed countries (Sen et al., 2009). Plus, the co-existence of chronic wounds and disabilities produces a downward spiral where the patient's adverse conditions related to their disability intensify wound chronicity, which in turn amplifies the disability.

Impaired healing can also be caused by bacterial infections. Even when a chronic wound is not infected, the lack of the nominal protective function provided by healthy skin exposes the individual to pathogens and infectious agents. Chronic wounds can therefore be both the result and the cause of infections. In most cases, infection occurs as a consequence of the contamination of the wounded area by bacterial strains which were previously present on the skin. In chronic wounds, bacterial attachment is favored by the presence of cellular debris and necrotic tissue (G. Zhao et al., 2013). Further replication of these bacteria can then cause local or even invasive infections and necrosis, with broader implications for the host's health (Guo & DiPietro, 2010). Infection goes along with a compromised inflammatory response during the healing process, that fails to completely remove the contaminant from the wound bed. This triggers the onset of a persistent inflammatory state with un-inhibited release and accumulation of pro-inflammatory cytokines, reactive oxygen species (ROS) and matrix metalloproteinases (MMPs), resulting in abundant and corrosive exudate fluid (Tottoli et al., 2020) and in the subsequent degradation of ECM and growth factors which are essential for wound healing. In turn, ECM degradation causes new recruiting of inflammatory cells and cytokines, thus amplifying the inflammatory response. Moreover, many chronic wounds are populated by senescent keratinocytes, fibroblasts, endothelial cells and macrophages with degraded secretory and proliferative capabilities, which affect the ability of the wound to heal (Frykberg & Banks, 2015). This scenario is further exacerbated by the formation of bacterial *biofilms*, i.e. the formation of organized aggregates of bacteria within a matrix mainly constituted by extracellular polymeric

substances (EPS) secreted by the bacterial cells (Guo & DiPietro, 2010; Kordestani, 2019b). The biofilm provides superior protection against immune cells and antibiotics (Frykberg & Banks, 2015), which makes treatments less effective, prevents dermal fibroblasts migration and induces cell apoptosis (Johnson et al., 2018). Biofilms have been found in 60% of chronic wounds specimens, as opposed to only 6% in acute wounds (G. Zhao et al., 2013).

All these aspects and implications make wounds a complex, widespread and difficult issue to treat, effectively representing a "silent epidemic" (Järbrink et al., 2016; Tottoli et al., 2020) with profound effects on global health and patient's lifestyle and psychological wellbeing. Figure 1.2 shows the prevalence of different types of wounds registered by US health insurance program Medicare (Nussbaum et al., 2018). In European Union countries, wounds have an annual incidence of 4 million people. (Medtech Europe, n.d.). In a study carried across several countries, 65% of which were European, chronic wound prevalence was found to be 1.67 per 1000 individuals. (EWMA, 2022). A study by Eaglstein and co-workers (Eaglstein et al., 2012) reports that chronic wounds such as diabetic ischemic ulcers, diabetic foot ulcers and lower extremities chronic wounds have mortality rates of 52%, 49% and 28% respectively, comparable with many cancers. Other wounds such as pressure ulcers are also highly exposed to the insurgence of invasive infections such as septicemia. A study by Sen (Sen, 2019) reported how wound infections cause 75% of post-operative deaths. Overall, it has been estimated that chronic wounds alone affect 1-2% of the population in developed countries (Järbrink et al., 2016). The economic implications are also relevant. In developed countries, chronic wound care costs account for 1-6% of total healthcare expenditures (Olsson et al., 2019). In the United States alone, the annual cost of acute and chronic wound care ranged from $28.1 billion to $96.8 billion in 2018 (Sen, 2019), and it is expected to be further inflated by an aging population and by increasingly hard to treat infections. This also implies massive and indirect economic burdens correlated to decreased productivity, early retirement, and wage losses (Sen et al., 2009). A paper by Drew (Drew et al., 2007) provided an interesting cost breakdown for wound care in a local population in England. It emerged how wound dressings and materials account for 17-22% of total costs, while nurse time and inpatient costs account for 33-41% and 37-49% respectively. This suggests that optimal solutions can be those ensuring the best and fastest patient recovery while simultaneously being more cost-efficient to manage.

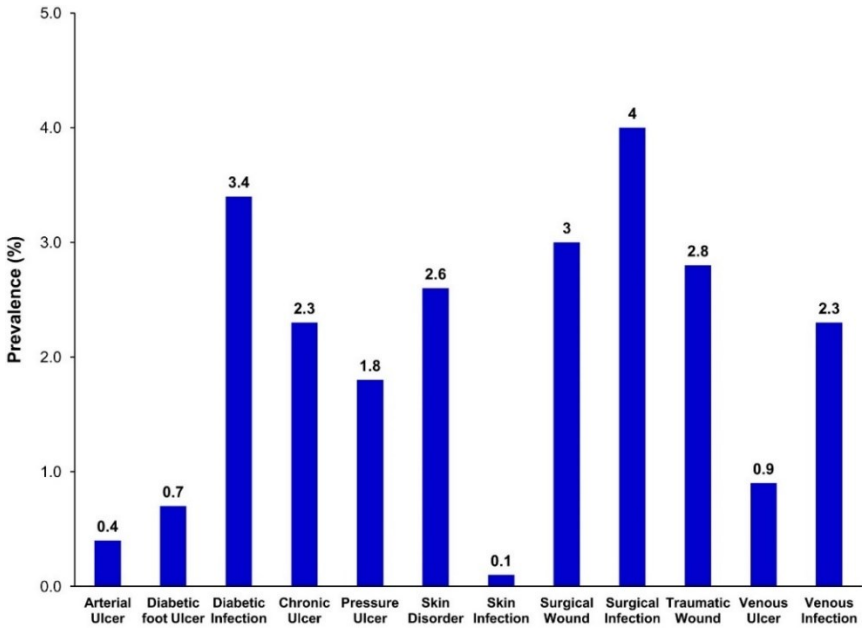


Figure 1.2: Wound prevalence by type in the Medicare population. Source (Nussbaum et al., 2018).

All these facts clearly demonstrate how crucial and important appropriate wound management and treatment solutions are, and how innovation and research in these fields can be instrumental in overcoming the associated challenges.

1.3 Wound treatments and infections

Wound healing, especially in chronic cases, demands appropriate management strategies to ensure expedite restoration of skin functions and aspect. These strategies must take into account a variety of different factors in order to identify the best treatment options and ensure the best possible outcome, and thus require a multidisciplinary and holistic approach.

Chronic wound management starts with a thorough assessment of both the patient and the wound. In fact, as mentioned above, both local and systemic factors – such as diseases – in patient's history and conditions are crucial in determining wound healing. For instance, diabetic ulcers might be treated more effectively by simultaneously addressing the individual's hyperglycemia and renal insufficiency (Frykberg & Banks, 2015). In the clinical practice, chronic wound treatment follows a set of widely adopted and common principles that are commonly referred to under the acronym *T.I.M.E.*, which stands for *Tissue*, *Inflammation/Infection*,

Moisture balance and *Edges* management. As a fundamental first step in proper *Tissue* management, *wound debridement* is considered an effective practice to promote wound healing through the removal of debris, biofilms – which are in many cases found beneath the eschar that is formed above the wound bed (G. Zhao et al., 2013) – and necrotic tissues that constitute the major obstacles to normal skin repair.

Once the wound bed is clean, *Infections* must be prevented or treated. This might involve the use of antiseptics such as iodine or silver sulfadiazine (Tottoli et al., 2020) and topical antibiotics. Topical antibiotics, in the forms of gels and creams, are often considered a better alternative to systemic antibiotics thanks to the possibility of administering high doses of antibiotics only locally, avoiding harmful side effects, even though hypersensitivity reactions and dermatitis are often reported (Tottoli et al., 2020). In fact, biofilm disruption requires much higher concentrations of antimicrobial agents than the Minimum Inhibitory Concentration (MIC) which is effective against the same bacteria in planktonic form (G. Zhao et al., 2013). As mentioned previously, this is due to a more marked resistance to antimicrobials.

One of the main reasons behind this is the failed or retarded penetration of antibiotic molecules throughout the biofilm. In these environments, low molecular weight solutes such as some antibiotics are found to have a reduced diffusion coefficient, down to about 40% of its value in water (Stewart, 2002). This is attributed to interactions with enzymes or with electrically charged groups in the EPS leading to sorption, sequestration, or inactivation of the antibacterial molecule.

Secondly, biofilms can constitute a perfect ground for the spontaneous emergence of mutations and their accelerated spread through gene transfer mechanisms, which are also common mechanisms of conventional AMR (Stewart, 2002). However, dramatic reduction in resistance observed upon dispersion of the biofilm suggests that other mechanisms are involved of adaptive nature. In other words, even non-mutant bacteria are found to be more resistant when aggregated in biofilm (Stewart, 2002). This makes biofilm-based AMR to some extent different than traditional one, with resistance being the result of multiple mechanisms often acting concurrently in the biofilm environment. Other environmental factors can compromise drug efficacy, such as limited oxygen viability or altered pH (Stewart, 2002).

Finally, although this slowed drug diffusion is not sufficient per se in preventing complete antibiotic penetration, it can however give bacterial cells more time to develop stress-induced responses, such as the expression of genes that can protect them from antimicrobials. A study by Whiteley (Whiteley et al., 2001) observed enhanced expression of several efflux-pump transcription genes in *P. aeruginosa* biofilms compared to free-living cells upon exposure to tobramycin.

Another mechanism relies on the alternation of activity states of bacterial cells. In biofilms, microgradients in metabolic substrates and products induce retarded growth or even latency in some cells, which therefore cannot be subject to antibiotics targeting metabolic or proliferation mechanisms of active cells (Stewart, 2002; G. Zhao et al., 2013). In other cases, so-called *persisters* are identified, capable of entering a spore-like state that makes them insusceptible to potent disinfectants like chlorine bleach (Stewart, 2002).

Finally, according to Wolcott (Wolcott et al., 2008), biofilms can also host a *functionally equivalent* polymicrobial community comprising multiple different species instead of one, which explains why many wound infections are hard eradicate with single-treatment-based approaches.

Moisture is the next aspect to be considered in wound management: wounds produce exudates that shall be managed properly to ensure effective healing, especially in chronic wounds. In fact, the exudate of chronic wounds tends to be rich in MMPs and cytokines, which means that excessive exudate retention results into the degradation of surrounding tissues and into the exacerbation of persistent inflammation. On the other side, poor moisture is an obstacle to regenerative cellular activities and therefore healing (Tottoli et al., 2020). The need to maintain this balance is one of the main drivers behind the selection of the most appropriate wound dressing, as will be detailed in the following sections.

Finally, the *E* in the *T.I.M.E.* acronym stands for Edges: the health status and the progressive restriction of wound edges is a significant indicator of an ongoing healing process, thus demanding careful monitoring and attention paid to the removal of potential obstacles along the way. Literature suggests that also an *S* – for Surrounding skin (Ward et al., 2019) – shall be added to the acronym, as it is also important that the wound and the chosen treatment do not compromise the health of the tissues around the injured area.

1.4 Wound dressings

As shown above, wound management is a complex set of practices grounded in the science of complex physiological processes. So far, industry and research have developed numerous devices and dressings to aid wound healing and tissue repair. These devices can be categorized based on their properties and applications. This subsection comprises an overview of the main wound dressing types, as a necessary basis to understand their merits and limitations, and the context for the development of new, advanced solutions.

The selection of the best dressing is obviously dependent on the type of wound, with the goal of accelerating healing and restoration of the skin. However, some overarching functions can be identified that are desirable and beneficial in most of the cases, such as providing a moist environment to maintain tissues hydrated, maintaining the wound area clean by absorbing exudates, being biocompatible, non-toxic and non-allergenic, promoting healing by supporting debridement, proliferation, epithelialization and remodeling processes, protecting the wound and surrounding tissue from stresses and further injury, allowing for painless application and removal, being permeable to oxygen gas, and preventing or contrasting infections (Brown et al., 2018; Dhivya et al., 2015b; Qin, 2009).

1.4.1 Types of wound dressings

Dressings can be classified in different ways, such as according to their physical form, e.g., gauzes, films, foams, hydrogels, hydrocolloids (Dhivya et al., 2015b; Qin, 2009); according to their base materials, e.g., natural versus synthetic polymers (Okur et al., 2020); or based on the nature and time-evolution of their behavior once in contact with the wound, e.g., passive, interactive, advanced and bioactive (Brown et al., 2018). Of all these frameworks, the subdivision by physical form is the most convenient for the purposes of this work. However, distinctions between natural versus synthetic as well as passive versus interactive are also relevant to describe the research drivers and the related findings that will be shown later.

1.4.1.1 Traditional dressings

Sterile gauzes, together with lint, tulle, cotton wools and bandages, belong to the category of traditional dressings. These are typically made by woven or non-woven fibers of cotton or synthetic materials such as polyamide and polyesters. They typically offer some degree of physical protection and exudate absorption but need to be replaced frequently and tend to stick to the wounded area, causing painful removal. (Dhivya et al., 2015b). This major drawback led to the development of

paraffine impregnated dressings, or multilayered dressings with an absorbing core covered by non-adherent faces (Qin, 2009). However, these still failed to maintain a moist environment. For these reasons, traditional dressings are mostly used for dry, superficial wounds, or to support other dressings.

1.4.1.2 Films

Films for wound dressing possess good flexibility and elasticity, which allow an easy application on the injured site and the possibility to model the dressing on the wound morphology. Films can also be chosen based on their permeability to oxygen, water vapor and carbon dioxide to maintain optimal gas exchange. When transparent, films can also allow for wound inspection without removing the dressing. Most typically, films were made of polyurethane with a poor absorption capacity, and used to cover venous accesses, skin graft donor sites and surface wounds in general (Broussard & Powers, 2013a). However, new molecules have been used over time to fabricate novel types of films, both natural and synthetic. Among natural materials, chitosan, hyaluronic acid, starch, gelatin and alginate are the most popular. On the other hand, poly(lactic acid), poly(vinyl alcohol), poly(caprolactone) and poly(vinyl pyrrolidone) are common synthetic polymers used for film fabrication (Savencu et al., 2021).

1.4.1.3 Hydrogels

Hydrogels are porous, three-dimensional networks of chemically or physically crosslinked hydrophilic polymers, such as starches or alginates. This makes hydrogels capable of absorbing large amounts of water, which is a highly desired property for high-exudate wounds and to keep tissues hydrated and cool, as well as to allow painless removal. Injectable hydrogels can also be conveniently accommodated into any type of wound shape. On the other side, the high water uptake can be conductive for bacterial proliferation, wound maceration and consequent bad smell, which in turn demands frequent replacement (Dhivya et al., 2015b).

1.4.1.4 Foams

Foam dressings are typically made by a polyurethane or silicone foam inner layer, covered by an outer water impermeable and gas permeable layer. Foams, similarly to hydrogels, are meant to ensure exudate absorption and moisture maintenance thanks to their porous structure. When provided with adhesive edges, foams can be applied directly and immobilized on the injured area without the need for a secondary dressing. Foams are preferred for their flexibility and strength (Qin,

2009), which makes them particularly suitable for wounds in the proximity of bones (Broussard & Powers, 2013b).

1.4.1.5 Hydrocolloids

When wound exudate is less abundant, hydrocolloids are usually preferred to hydrogels and foams. Hydrocolloids are typically made of hydrophilic, gel-forming phases – most frequently carboxy-methylcellulose or gelatin (Dhivya et al., 2015b) – dispersed in an elastomeric matrix. Upon contact with the wound, the hydrophilic phase absorbs water and exudates. Hydrocolloids can support autolytic debridement (Holloway & Harding, 2022), and have been found to be particularly effective in increasing the healing rate of chronic ulcers compared to other modern dressings (Chaby et al., 2007).

Film, foam, hydrogel, and hydrocolloid dressings have been largely made available commercially over the last decades and today constitute and established set of alternatives for wound care. Table 1.1 below summarizes their main advantages and disadvantages.

Table 1.1: Overview of modern wound dressings and their applications

Dressing	Pros	Cons	Application examples	Ref.
Films	Flexible, gas permeable	Low water absorption	First-degree burns, minor abrasions	(Broussard & Powers, 2013b; Holloway & Harding, 2022)
Foams	Exudate absorption	Difficult to remove	High-exudate wounds	
Hydrogel	High water content	Bacterial proliferation	Dry, necrotic wounds	
Hydrocolloid	Stimulates debridement	Can cause maceration	Ulcers and abrasions	

1.4.1.6 Electrospun dressings

Electrospinning is a modern manufacturing technique that employs an electric potential between two electrodes to stretch polymeric solutions, emulsions or melts

into small-diameter fibers (from micrometers to nanometers), that are subsequently collected to form fiber networks. Thanks to their high surface area and porosity, as well as to the possibility of including drugs and other agents in the spinnable feedstock, electrospun mats can found numerous applications in wound healing. Furthermore, different natural and synthetic polymers can be electrospun independently or in combination, further expanding the variety of devices that can be obtained. A good review work summarizing the recent developments in the field has been done by Liu and co-workers (Y. Liu et al., 2021).

1.4.1.7 Tissue-engineered dressings

These dressings have been conceived to reproduce and replace the skin damaged from the injury. There are two main types available: *epidermal* replacements and *dermal* replacements. The formers involve culturing fibroblasts or keratinocytes, in some cases collected from the patient, and incorporating them into a polymeric matrix that is subsequently apnplied on the wounded area. The others mainly consist in decellularized collagen matrixes and are further broken down into allogeneic or xenogeneic grafts, depending on whether they are from human or animal origin respectively. The main drawback of epidermal replacements is the long time needed to culture the cells, typically in the order of few weeks. On the other hand, dermal replacements may cause rejection and adverse reactions (Broussard & Powers, 2013b; Dhivya et al., 2015b).

1.4.2 Advanced wound dressings properties

Besides the core requirements of biocompatibility, non-allergenicity and non-toxicity, other factors drive the development of wound dressings. These driving factors could be divided in two groups. The first group includes baseline drivers such as cost and properties that are relevant for the particular application, such as gas permeability, water absorption, transparency, strength and flexibility. These can all be improved or tuned with the right selection of materials. The second group includes drivers that have emerged more recently, enabled by the latest findings and breakthroughs in science and engineering. These include biodegradability, environmental sustainability, antimicrobial properties, smart features such as responsiveness to biochemical or physical stimuli, self-healing, monitoring-capability (Dong & Guo, 2021), and *bioactivity*, i.e., the ability of the selected material to interact with the surrounding tissues to enhance or improve the healing process.

All the above-described dressing types have been advanced over the last years following these drivers. This included the use of a growing number of novel materials and their combinations, either of natural or synthetic origin, as well as the introduction in the matrix of dispersed agents with special properties. *Bioactive* dressings have taken advantage of biomacromolecules and biopolymers to mimic the properties and architecture of the extracellular matrix, thus providing a conductive environment of re-epithelialization. This implies using molecules such as proteins and polysaccharides to produce films, hydrogels and fibers, as well as scaffolds for skin tissue engineering (Suarato et al., 2018a). *Medicated* dressings typically incorporate molecules and substances such as antibiotics, growth factors, debriding agents, enzymes (Dhivya et al., 2015b), honey, essential oils (Simões et al., 2018) or plant extracts (Rezvani Ghomi et al., 2019) that are delivered on the target site in a controlled fashion supporting healing. More recently, nanomaterials such as metal and metal oxide nanoparticles have been incorporated into wound dressings thanks to their beneficial properties, most notably their antimicrobial effects (Liang et al., 2022) which make them particularly promising alternatives to antibiotics in contrasting AMR and wound infections. It shall be noted here that the use of nanomaterials in medicine and wound healing does not come without concerns about their cytotoxicity. The effects of nanoparticles on mammal cells and living organism is not yet completely understood and depends not only on their chemical composition but also on physical factors. Features like size, shape, concentration, and administration route have been found to influence their effects, as they determine their ability to penetrate and diffuse across tissues and to interact with cells (Limo et al., 2018; Sruthi et al., 2018). Once internalized by cells – either through direct diffusion or endocytosis – nanoparticles can subsequently induce cell death through a variety of mechanisms. These include dissolution in the cell acidic lysosome compartments, with subsequent production of ions and reactive oxygen species (ROS) causing DNA damage and oxidative stress, interference with the electron transport chain in mitochondria or with redox-active enzymes, and triggering of signaling pathways through interaction with cellular receptors (Espitia et al., 2012; Sruthi et al., 2018). However, as more knowledge is gained on their interaction with cells and organisms, the conditions for their safe utilization begin to emerge. This aspect is crucial for this work and will be further analyzed in Chapter 7.

In the end, the future of advanced wound dressings lies at the intersection between biomacromolecules-based matrixes and safe antimicrobial nanomaterials, which will constitute the focus of the next chapter.

References

Abdo, J. M., Sopko, N. A., & Milner, S. M. (2020). The applied anatomy of human skin: A model for regeneration. *Wound Medicine*, *28*, 100179. https://doi.org/10.1016/J.WNDM.2020.100179

Broussard, K. C., & Powers, J. G. (2013a). Wound dressings: Selecting the most appropriate type. *American Journal of Clinical Dermatology*, *14*(6), 449–459. https://doi.org/10.1007/S40257-013-0046-4/FIGURES/2

Broussard, K. C., & Powers, J. G. (2013b). Wound dressings: Selecting the most appropriate type. *American Journal of Clinical Dermatology*, *14*(6), 449–459. https://doi.org/10.1007/S40257-013-0046-4/FIGURES/2

Brown, M. S., Ashley, B., & Koh, A. (2018). Wearable technology for chronic wound monitoring: Current dressings, advancements, and future prospects. *Frontiers in Bioengineering and Biotechnology*, *6*(APR), 47. https://doi.org/10.3389/FBIOE.2018.00047/BIBTEX

Byrd, A. L., Belkaid, Y., & Segre, J. A. (2018). The human skin microbiome. *Nature Reviews Microbiology 2018 16:3*, *16*(3), 143–155. https://doi.org/10.1038/nrmicro.2017.157

Chaby, G., Senet, P., Vaneau, M., Martel, P., Guillaume, J. C., Meaume, S., Téot, L., Debure, C., Dompmartin, A., Bachelet, H., Carsin, H., Matz, V., Richard, J. L., Rochet, J. M., Sales-Aussias, N., Zagnoli, A., Denis, C., Guillot, B., & Chosidow, O. (2007). Dressings for Acute and Chronic Wounds: A Systematic Review. *Archives of Dermatology*, *143*(10), 1297–1304. https://doi.org/10.1001/ARCHDERM.143.10.1297

de la Varga-Martínez, O., Gómez-Sánchez, E., Muñoz, M. F., Lorenzo, M., Gómez-Pesquera, E., Poves-Álvarez, R., Tamayo, E., & Heredia-Rodríguez, M. (2021). Impact of nosocomial infections on patient mortality following cardiac surgery. *Journal of Clinical Anesthesia*, *69*, 110104. https://doi.org/10.1016/J.JCLINANE.2020.110104

Dhivya, S., Padma, V. V., & Santhini, E. (2015). Wound dressings – a review. *BioMedicine*, *5*(4), 24–28. https://doi.org/10.7603/S40681-015-0022-9

Dong, R., & Guo, B. (2021). Smart wound dressings for wound healing. *Nano Today*, *41*, 101290. https://doi.org/10.1016/J.NANTOD.2021.101290

Drew, P., Posnett, J., & Rusling, L. (2007). The cost of wound care for a local population in England. *International Wound Journal*, *4*(2), 149–155. https://doi.org/10.1111/J.1742-481X.2007.00337.X

Eaglstein, W. H., Kirsner, R. S., & Robson, M. C. (2012). Food and Drug Administration (FDA) drug approval end points for chronic cutaneous ulcer studies. *Wound Repair and Regeneration*, *20*(6), 793–796. https://doi.org/10.1111/J.1524-475X.2012.00849.X

Espitia, P. J. P., Soares, N. de F. F., Coimbra, J. S. dos R., de Andrade, N. J., Cruz, R. S., & Medeiros, E. A. A. (2012). Zinc Oxide Nanoparticles: Synthesis, Antimicrobial Activity and Food Packaging Applications. In *Food and Bioprocess Technology* (Vol. 5, Issue 5, pp. 1447–1464). Springer. https://doi.org/10.1007/s11947-012-0797-6

EWMA. (2022). *The Impact of patient health and lifestyle factors on wound healing*. https://ewma.org/what-we-do/projects/lifestyle-factors

Fighting antimicrobial resistance with vaccines. (n.d.). Retrieved December 29, 2021, from https://www.nature.com/articles/d42473-021-00356-4#ref-CR1

Frantz, C., Stewart, K. M., & Weaver, V. M. (2010). The extracellular matrix at a glance. *Journal of Cell Science*, *123*(24), 4195–4200. https://doi.org/10.1242/JCS.023820

Frykberg, R. G., & Banks, J. (2015). Challenges in the Treatment of Chronic Wounds. *Advances in Wound Care*, *4*(9), 560–582. https://doi.org/10.1089/wound.2015.0635

Guo, S., & DiPietro, L. A. (2010). Factors affecting wound healing. *Journal of Dental Research*, *89*(3), 219–229. https://doi.org/10.1177/0022034509359125

Gyles, C., & Boerlin, P. (2014). Horizontally Transferred Genetic Elements and Their Role in Pathogenesis of Bacterial Disease. *Veterinary Pathology*, *51*(2), 328–340. https://doi.org/10.1177/0300985813511131

Holloway, S., & Harding, K. G. (2022). Wound dressings. *Surgery (Oxford)*, *40*(1), 25–32. https://doi.org/10.1016/J.MPSUR.2021.11.002

Huan, Y., Kong, Q., Mou, H., & Yi, H. (2020). Antimicrobial Peptides: Classification, Design, Application and Research Progress in Multiple Fields. *Frontiers in Microbiology*, *11*, 2559. https://doi.org/10.3389/FMICB.2020.582779/BIBTEX

Järbrink, K., Ni, G., Sönnergren, H., Schmidtchen, A., Pang, C., Bajpai, R., & Car, J. (2016). Prevalence and incidence of chronic wounds and related complications: a protocol for a systematic review. *Systematic Reviews*, *5*(1). https://doi.org/10.1186/S13643-016-0329-Y

Jenkins, D. R. (2021). Nosocomial infections and infection control. *Medicine*, *49*(10), 638–642. https://doi.org/10.1016/J.MPMED.2021.07.007

Johnson, T. R., Gómez, B. I., McIntyre, M. K., Dubick, M. A., Christy, R. J., Nicholson, S. E., & Burmeister, D. M. (2018). The Cutaneous Microbiome and Wounds: New Molecular Targets to Promote Wound Healing. *International Journal of Molecular Sciences*, *19*(9). https://doi.org/10.3390/IJMS19092699

Kordestani, S. S. (2019a). Wound Anatomy. *Atlas of Wound Healing*, 3–9. https://doi.org/10.1016/B978-0-323-67968-8.00002-1

Kordestani, S. S. (2019b). Wound Healing Process. *Atlas of Wound Healing*, 11–22. https://doi.org/10.1016/B978-0-323-67968-8.00003-3

Lazarus, G. S., Cooper, D. M., Knighton, D. R., Margolis, D. J., Pecoraro, R. E., Rodeheaver, G., & Robson, M. C. (1994). *Definitions and Guidelines for Assessment of Wounds and Evaluation of Healing Background: Chronic wounds represent a worldwide*. http://archderm.jamanetwork.com/

Liang, Y., Liang, Y., Zhang, H., & Guo, B. (2022). Antibacterial biomaterials for skin wound dressing. *Asian Journal of Pharmaceutical Sciences*. https://doi.org/10.1016/J.AJPS.2022.01.001

Limo, M. J., Sola-Rabada, A., Boix, E., Thota, V., Westcott, Z. C., Puddu, V., & Perry, C. C. (2018). Interactions between Metal Oxides and Biomolecules: From Fundamental Understanding to Applications. *Chemical Reviews*, *118*(22), 11118–11193.

https://doi.org/10.1021/ACS.CHEMREV.7B00660/ASSET/IMAGES/LARGE/CR-2017-006605_0023.JPEG

Liu, Y., Li, T., Han, Y., Li, F., & Liu, Y. (2021). Recent development of electrospun wound dressing. *Current Opinion in Biomedical Engineering*, *17*, 100247. https://doi.org/10.1016/J.COBME.2020.100247

Mahlapuu, M., Håkansson, J., Ringstad, L., & Björn, C. (2016). Antimicrobial peptides: An emerging category of therapeutic agents. *Frontiers in Cellular and Infection Microbiology*, *6*(DEC), 194. https://doi.org/10.3389/FCIMB.2016.00194/BIBTEX

Mayet, N., Choonara, Y. E., Kumar, P., Tomar, L. K., Tyagi, C., du Toit, L. C., & Pillay, V. (2014). A Comprehensive Review of Advanced Biopolymeric Wound Healing Systems. *Journal of Pharmaceutical Sciences*, *103*(8), 2211–2230. https://doi.org/10.1002/JPS.24068

Medtech Europe. (n.d.). *The Burden of Wounds on EU Healthcare Systems*. Retrieved November 8, 2022, from https://www.medtecheurope.org/wp-content/uploads/2015/10/290902009_MTE_The-Burden-of-Wounds-on-EU-Healthcare-Systems_Brochure.pdf

Mohamed, S. A., & Hargest, R. (2021). Surgical anatomy of the skin. *Surgery (Oxford)*. https://doi.org/10.1016/J.MPSUR.2021.11.021

Nussbaum, S. R., Carter, M. J., Fife, C. E., DaVanzo, J., Haught, R., Nusgart, M., & Cartwright, D. (2018). An Economic Evaluation of the Impact, Cost, and Medicare Policy Implications of Chronic Nonhealing Wounds. *Value in Health*, *21*(1), 27–32. https://doi.org/10.1016/J.JVAL.2017.07.007/ATTACHMENT/A0677023-E1D3-4506-95C9-76C391AD9811/MMC1.DOC

Okur, M. E., Karantas, I. D., Şenyiğit, Z., Üstündağ Okur, N., & Siafaka, P. I. (2020). Recent trends on wound management: New therapeutic choices based on polymeric carriers. *Asian Journal of Pharmaceutical Sciences*, *15*(6), 661–684. https://doi.org/10.1016/J.AJPS.2019.11.008

Olsson, M., Järbrink, K., Divakar, U., Bajpai, R., Upton, Z., Schmidtchen, A., & Car, J. (2019). The humanistic and economic burden of chronic wounds: A systematic review. *Wound Repair and Regeneration*, *27*(1), 114–125. https://doi.org/10.1111/wrr.12683

Qin, Y. (2009). Advanced Wound Dressings. *Https://Doi.Org/10.1080/00405000108659563*, *92*(2), 127–138. https://doi.org/10.1080/00405000108659563

Reygaert, W. C. (2018). An overview of the antimicrobial resistance mechanisms of bacteria. *AIMS Microbiology*, *4*(3), 482. https://doi.org/10.3934/MICROBIOL.2018.3.482

Rezvani Ghomi, E., Khalili, S., Nouri Khorasani, S., Esmaeely Neisiany, R., & Ramakrishna, S. (2019). Wound dressings: Current advances and future directions. *Journal of Applied Polymer Science*, *136*(27), 47738. https://doi.org/10.1002/APP.47738

Roope, L. S. J., Smith, R. D., Pouwels, K. B., Buchanan, J., Abel, L., Eibich, P., Butler, C. C., Tan, P. S., Sarah Walker, A., Robotham, J. v., & Wordsworth, S. (2019). The challenge of antimicrobial resistance: What economics can contribute. *Science*, *364*(6435). https://doi.org/10.1126/SCIENCE.AAU4679/SUPPL_FILE/AAU4679_ROOPE_SM.PDF

Samreen, Ahmad, I., Malak, H. A., & Abulreesh, H. H. (2021). Environmental antimicrobial resistance and its drivers: a potential threat to public health. *Journal of Global Antimicrobial Resistance*, *27*, 101–111. https://doi.org/10.1016/J.JGAR.2021.08.001

Savencu, I., Iurian, S., Porfire, A., Bogdan, C., & Tomuță, I. (2021). Review of advances in polymeric wound dressing films. *Reactive and Functional Polymers*, *168*, 105059. https://doi.org/10.1016/J.REACTFUNCTPOLYM.2021.105059

Schrader, S. M., Vaubourgeix, J., & Nathan, C. (2020). Biology of antimicrobial resistance and approaches to combat it. *Science Translational Medicine*, *12*(549). https://doi.org/10.1126/SCITRANSLMED.AAZ6992

Scott, B. N. V., Roberts, D. J., Robertson, H. L., Kramer, A. H., Laupland, K. B., Ousman, S. S., Kubes, P., & Zygun, D. A. (2013). Incidence, prevalence, and occurrence rate of infection among adults hospitalized after traumatic brain injury: study protocol for a systematic review and meta-analysis. *Systematic Reviews*, *2*, 68. https://doi.org/10.1186/2046-4053-2-68

Sen, C. K. (2019). Human Wounds and Its Burden: An Updated Compendium of Estimates. In *Advances in Wound Care* (Vol. 8, Issue 2, pp. 39–48). Mary Ann Liebert Inc. https://doi.org/10.1089/wound.2019.0946

Sen, C. K., Gordillo, G. M., Roy, S., Kirsner, R., Lambert, L., Hunt, T. K., Gottrup, F., Gurtner, G. C., & Longaker, M. T. (2009). Human skin wounds: A major and snowballing threat to public health and the economy: PERSPECTIVE ARTICLE. *Wound Repair and Regeneration*, *17*(6), 763–771. https://doi.org/10.1111/j.1524-475X.2009.00543.x

Simões, D., Miguel, S. P., Ribeiro, M. P., Coutinho, P., Mendonça, A. G., & Correia, I. J. (2018). Recent advances on antimicrobial wound dressing: A review. *European Journal of Pharmaceutics and Biopharmaceutics*, *127*, 130–141. https://doi.org/10.1016/J.EJPB.2018.02.022

Sruthi, S., Ashtami, J., & Mohanan, P. V. (2018). Biomedical application and hidden toxicity of Zinc oxide nanoparticles. In *Materials Today Chemistry*. https://doi.org/10.1016/j.mtchem.2018.09.008

Stewart, P. S. (2002). Mechanisms of antibiotic resistance in bacterial biofilms. *International Journal of Medical Microbiology*, *292*(2), 107–113. https://doi.org/10.1078/1438-4221-00196

Stringel, G., Bawdon, R., Savrich, M., Guertin, L., & Horton, J. (1989). Topical and systemic antibiotics in the prevention of wound infection. *Journal of Pediatric Surgery*, *24*(10), 1003–1006. https://doi.org/10.1016/S0022-3468(89)80202-7

Suarato, G., Bertorelli, R., & Athanassiou, A. (2018). Borrowing from nature: Biopolymers and biocomposites as smart wound care materials. *Frontiers in Bioengineering and Biotechnology*, *6*(OCT), 1–11. https://doi.org/10.3389/fbioe.2018.00137

The Review on Antimicrobial Resistance. (2014). *Antimicrobial Resistance: Tackling a crisis for the health and wealth of nations*.

The Review on Antimicrobial Resistance. (2016). *Tackling Drug-Resistant Infections Globally: Final Report and Recommendations*.

Tottoli, E. M., Dorati, R., Genta, I., Chiesa, E., Pisani, S., & Conti, B. (2020). Skin wound healing process and new emerging technologies for skin wound care and

regeneration. In *Pharmaceutics* (Vol. 12, Issue 8, pp. 1–30). MDPI AG. https://doi.org/10.3390/pharmaceutics12080735

van Boeckel, T. P., Pires, J., Silvester, R., Zhao, C., Song, J., Criscuolo, N. G., Gilbert, M., Bonhoeffer, S., & Laxminarayan, R. (2019). Global trends in antimicrobial resistance in animals in low- And middle-income countries. *Science*, *365*(6459). https://doi.org/10.1126/SCIENCE.AAW1944/SUPPL_FILE/AAW1944-VAN-BOECKEL-SM.PDF

Ward, J., Holden, J., & Grob, M. (2019). *Management of wounds in the community: five principles Lead Nurse for Plastic Surgery 1 Mark Soldin*.

Whiteley, M., Bangera, M. G., Bumgarner, R. E., Parsek, M. R., Teitzel, G. M., Lory, S., & Greenberg, E. P. (2001). Gene expression in Pseudomonas aeruginosa biofilms. *Nature 2001 413:6858*, *413*(6858), 860–864. https://doi.org/10.1038/35101627

Wolcott, R. D., Rhoads, D. D., & Dowd, S. E. (2008). Biofilms and chronic wound inflammation. *Journal of Wound Care*, *17*(8), 333–341. https://doi.org/10.12968/JOWC.2008.17.8.30796

Woolhouse, M. E. J., & Ward, M. J. (2013). Sources of Antimicrobial Resistance. *Science*, *341*(6153), 1460–1461. https://doi.org/10.1126/SCIENCE.1243444

Zaman, S. bin, Hussain, M. A., Nye, R., Mehta, V., Mamun, K. T., & Hossain, N. (2017). A Review on Antibiotic Resistance: Alarm Bells are Ringing. *Cureus*, *9*(6). https://doi.org/10.7759/CUREUS.1403

Zhao, G., Usui, M. L., Lippman, S. I., James, G. A., Stewart, P. S., Fleckman, P., & Olerud, J. E. (2013). Biofilms and Inflammation in Chronic Wounds. *Advances in Wound Care*, *2*(7), 389. https://doi.org/10.1089/WOUND.2012.0381

Chapter 2

Biopolymers and nanomaterials: next generation healthcare

The contents of this Chapter have been reported in Pino, P., Bosco, F., Mollea, C., & Onida, B. (2023). Antimicrobial Nano-Zinc Oxide Biocomposites for Wound Healing Applications: A Review. *Pharmaceutics* (Under revision)

2.1 Hacking tissue repair

The functions and features of wound dressings and their constituent materials have evolved from passive protection of the injured site from the external environment to an active involvement in the healing process, mediated by the ability of these advanced materials to interact, both physically and biochemically, with the surrounding tissues and environment. These modes of interactions could be classified in two fundamental types. The first one consists in *enhancing* physiological healing mechanisms, for instance by triggering cellular proliferation pathways. The second one consists in *removing* obstacles to those healing mechanisms, for instance by eradicating bacterial infections. Therefore, advanced biomedical materials that combine these two mechanisms of action have the highest potential to achieve a significant impact on human health.

The previous chapter has tried to illustrate the vast complexity that lies behind wound healing and infections. Evolution – of both microorganisms and human societies – has posed new challenges to our collective efforts to preserve the

integrity and the wellbeing of the human body. In fact, phenomena such as the raging antimicrobial resistance (AMR) and the increasing incidence of chronic wounds due to an aging population and diffused comorbidities are merging into a fatal combination that can seriously undermine our health.

This chapter will dive deeper into the latest advancements in this new quest for the next wound dressings. As already mentioned, a critical role will be played by biomacromolecules, i.e., nature-derived molecules with bioactive features and the ability to form structures such as hydrogels and films to be used in the fabrication of wound dressing. In many cases, these molecules are also very abundant and easy to source, which makes them a competitive alternative to petroleum-derived compounds from the economic standpoint too. The following section offers a high-level overview of the most researched biomacromolecules for wound healing applications, grouped into two main categories that ultimately reflect the fundamental constituents of the skin: polysaccharides and proteins.

2.2 Biomacromolecules for wound dressings

2.2.1 Polysaccharides-based polymers

2.2.1.1 Chitosan

Chitin is a natural polycationic polymer typically obtained from the cuticles of crustaceans (Younes & Rinaudo, 2015). Chitin deacetylation produces chitosan, a renown intrinsically antimicrobial material (Abd El-Hack et al., 2020), active also against some resistant strains, such as the methicillin-resistant *Staphylococcus aureus* (E. M. Costa et al., 2017). Chitosan is biocompatible, non-toxic, haemostatic, and thus frequently used in biomedicine, including wound healing (Deng et al., 2021; Miguel et al., 2019; Moeini et al., 2020; Torkaman et al., 2021) and biomolecule and drug delivery (Z. Mohammadi et al., 2021). Due to these properties and thanks to its good processability, it is often mixed with other polymers such as poly(ε-caprolactone) (T. T. P. Ho et al., 2021; Shahrousvand et al., 2021), polyurethane (K., M.P., et al., 2019) or poly(vinyl)alcohol (Hezma et al., 2019) to produce advanced wound dressings, also with new techniques such as electrospinning (R. Ahmed et al., 2018; Zhou et al., 2021).

2.2.1.2 Cellulose

Cellulose is an abundant organic polymer that can be obtained from plants and bacteria (Cacicedo et al., 2016). It is non-toxic, biocompatible, and biodegradable.

It is water insoluble and possesses good thermal stability. It is gaining increasing attention particularly in its nanostructured forms (Dhali et al., 2021; N. A. D. Ho & Leo, 2021; Klemm et al., 2021; Raghav et al., 2021), and extensive research exists exploring drug loading and combination with nanomaterials (A. Gupta et al., 2019; Jin et al., 2021; Q. Wang et al., 2021). Gopi and co-workers offered a wide review of its uses and applications in the medical field, including wound dressing and drug delivery (Gopi et al., 2019). Several derivatives can also be obtained from cellulose by modifying its molecule with different functional moieties, such as carboxyl (Tavakolian et al., 2020) and allyl (S. Lu et al., 2021) groups. This allows to manipulate key properties such as hydrophilicity or to enable the conjugation with drugs or other medical compounds.

2.2.1.3 Hyaluronic acid

Hyaluronic acid is a component of the extracellular matrix. It is typically extracted from animal tissues or produced by fermentation of some *Streptococcus* strains (Cerminati et al., 2021; Sze et al., 2016).

Its biocompatibility and hydrophilicity are valuable for the development of biomedical materials, especially hydrogels (Burdick & Prestwich, 2011). Recently, Graça and coworkes (Graça et al., 2020) offered a review of its applications in wound dressings, underlying its highly beneficial role in wound repair and cell signalling (G. Agarwal et al., 2020; Dovedytis et al., 2020).

2.2.1.4 Alginate

Alginate shares similar properties (Reig-Vano et al., 2021) with hyaluronic acid. Commercial alginate is isolated from brown seaweeds, and its bacterial production has recently traction (Urtuvia et al., 2017). Its high water absorption capacity has been known since a long time, making this biomacromolecule extensively used in the production of wound dressings for high exudate wounds. Alginate stimulates macrophages activation, supporting the healing process (Dhivya et al., 2015a). The abundance of hydroxyl and carboxyl groups in its molecule endows this polymer with high reactivity, which is in turn useful in the design of encapsulation and drug delivery systems (Reig-Vano et al., 2021). Its biocompatibility and printability meet the need of biomaterials for tissue engineering and modern wound dressings (Ahmad Raus et al., 2021; Mallakpour et al., 2021; Tavassoli-Kafrani et al., 2016).

2.2.1.5 Starch

Starch is an abundant, plant-derived polysaccharide which is also widely researched as a substitute for synthetic packaging materials thanks to biodegradability, non-toxicity and film forming ability. It can be manufactured with simple extrusion or solvent casting methods (Cheng et al., 2021), as well as electrospinning, which is a promising technique for biomedical devices (Hemamalini & Giri Dev, 2018).

2.2.1.6 Beta-glucans

β-glucans are typically found in the cell walls of plants, bacteria, fungi, and yeasts. They are known for their immunostimulatory properties (J. Ma & Underhill, 2013) and they have been shown to stimulate collagen deposition, fibroblasts and keratinocytes migration, and overall reepithelialisation (Majtan & Jesenak, 2018a; Seo et al., 2019; Wei et al., 2002). Therefore, these polysaccharides have been recently researched for the production of advanced dressings, such as wet gels and nanofibers for hard-to-treat and chronic diabetic wounds (Grip et al., 2018a; King et al., 2017).

2.2.2. Protein-based polymers

2.2.2.1 Collagen and gelatin

Protein-based biopolymers such as collagen and gelatin (A. v. Thanusha et al., 2018; Yoon et al., 2018) are also very popular. Collagen – the main protein constituent of extracellular matrix, extracted from animal skin and hides and featured by many bioactive peptides – favours tissue regeneration, has good moisture retention properties, and has been used for the controlled release of bioactive molecules (Kalai Selvan et al., 2020), thus representing a very promising solution in wound healing and tissue engineering (Gopinath et al., 2004; Irastorza et al., 2021; Taraballi et al., 2013). Gelatin, a collagen derivative, has also good potential as substitute to petroleum-derived plastics in food packaging materials, thanks to its good film forming ability, transparency and ease of combination with functional and reinforcing additives or other biopolymers (Tavassoli et al., 2021; H. Wang et al., 2021). It has also been used to fabricate scaffolds (Jalaja et al., 2014; Sarika et al., 2014), aerogels (Mao et al., 2021a) and antimicrobial nanofibrous composites (Kwak et al., 2019).

2.2.2.2 Keratin

Keratin is a fibrous protein which has been extensively researched for fabrication of biomaterials with uses in wound healing, drug delivery and tissue engineering, thanks to its biocompatibility, biodegradability and self-assembly properties (Feroz et al., 2020; McLellan et al., 2019). Its combination with citric acid has shown to confer the necessary mechanical properties to be employed for food packaging as well (Ramirez et al., 2017). Keratin is usually extracted from feathers, nails, horns or wool (Chilakamarry et al., 2021), which raised concerns around the extraction methods and the environmental issues related to the accumulation of waste keratin-containing biomasses (Sharma & Gupta, 2016; Suarato et al., 2018b).

2.2.2.3 Whey proteins

Whey proteins are biocompatible and biodegradable byproducts of the dairy industry and are most commonly used as food additives and supplements. Their excellent film forming ability and gelation properties have been extensively investigated and used for the formulation of edible films and particles for the delivery of nutraceuticals. Their combination with nZnO is described in a previous work (Pino et al., 2021).

The above classification captures the wide variety of biomacromolecules investigated in research only partially. Table 2.1 below provides a more extensive list of the numerous alternatives explored in the scientific literature and summarizes some of their most important features.

Table 2.1: Overview of biomacromolecules for wound dressing.

Biopolymer	Properties	Ref.
Alginate	Biocompatible, non-toxic, non-immunogenic, biodegradable, antimicrobial, haemostatic	(Jayakumar et al., 2015; Koehler et al., 2018; H. Wang et al., 2019; Zahran & Marei, 2019a)
Chitosan	Non-toxic, biocompatible, biodegradable, moisture retentive, haemostatic	(Dananjaya et al., 2018; Z. Lu et al., 2017; Priyadarshi & Negi, 2017; Sudheesh

		Kumar et al., 2012; Taghizadeh et al., 2020)
Chitosan oligosaccharide	Antibacterial, anti-inflammatory, immune-stimulating	(Zhang et al., 2021)
Cellulose	Biocompatible, hydrophilic, micro porous, transparent; non-toxic	(Azizi et al., 2014; George et al., 2020a; Khalid et al., 2017; Shahmohammadi Jebel & Almasi, 2016a)
Carboxymethyl -cellulose	Biocompatible and biodegradable	(Hashem et al., 2013; Naserian & Mesgar, 2022; Shankar et al., 2015; Zare-Akbari et al., 2016)
Carboxymethyl -chitosan	Amphoteric and hydrophilic	(T. Hu et al., 2022; Noshirvani et al., 2017; Wahid et al., 2016)
Gum acacia	Biocompatible, nontoxic, water soluble	(Bajpai et al., 2016)
Starch	Low-cost, biocompatible, biodegradable, easy preparation, good film forming properties	(El-Nahhal et al., 2020; Nafchi et al., 2012; Namazi et al., 2019; Peighambardoust et al., 2019)
Carrageenan	Water soluble, good film forming abilities and mechanical properties	(Kanmani & Rhim, 2014; Roy & Rhim, 2019; Saputri et al., 2018)
Cellulose acetate	Water insoluble, high transparency, good mechanical and chemical resistance	(Aly & Ahmed, 2021; Pittarate et al., 2011)
Cellulose acetate phtalate	Hydrophilic, biodegradable	(Indumathi et al., 2019a)

Oxidised starch	Low viscosity, high stability and transparency	(Namazi et al., 2019)
Dextran	Active in wound healing, controls bacterial growth	(Zahran & Marei, 2019a; Zhou et al., 2022)
Chitin	Biodegradable, hemostatic, cytocompatible	(Sudheesh Kumar et al., 2013b)
Gelatin	Biodegradable, biocompatible, cell-recognizable	(Amjadi et al., 2019; Arfat et al., 2016; Shankar et al., 2015; Sherafatkhah Azari et al., 2020; A. V. Thanusha et al., 2018; Zahran & Marei, 2019b)
Keratin	Low-cost, highly suitable for hydrogels, concerns about wastes	(Villanueva et al., 2019; Zhai et al., 2018a)
Fish protein isolate	High film forming ability	(Arfat et al., 2014, 2015, 2016)
Collagen	High biocompatibility and biodegradability. Bioactive	(*New Collagen-Dextran-Zinc Oxide Composites for Wound Dressing*, n.d.)
Hyaluronic Acid	Primary component of connective tissue, long-term safety, reduces bacterial adhesion	(Rao et al., 2019; Shirzaei Sani et al., 2018)
Polylactic acid	Biodegradable, biocompatible, high mechanical strength	(Chu et al., 2017; Mao et al., 2021b)
Betaglucans	Immunostimulatory, biodegradable	(Razzaq et al., 2021)

Soy protein isolate	Biocompatible, non-immunogenic, non-toxic, low cost, biodegradable, highly stable	(Jaberifard et al., 2022)
Silk fibroin	Biocompatible, biodegradable, minimum inflammatory reactions	(Cao et al., 2019)

It shall also be considered how, in the cited reports, these compounds are frequently mixed among themselves or with other synthetic polymers to create synergies and obtain special combinations of desired properties.

With all their beneficial properties and high compatibility with the human tissues, biomacromolecules are most frequently found to serve the *healing enhancement* function mentioned at the beginning of this chapter. The other side of the advanced wound care coin – i.e., the *healing obstacles removal* function – is often offered by nanomaterials. Of course, this is not a rigid distinction: many nanomaterials also serve a healing enhancement function, and several biomacromolecules can act as obstacle removal agents. Considering that infections are the most serious obstacle to healing, however, nanomaterials deserve special consideration for their promising antimicrobial properties, as will be shown in the next section.

2.3 Nano-antimicrobials

Nanomaterials are defined as those materials which have at least one of their dimensions in the nanoscale, i.e., below 100 nm. In this particular condition, new properties are disclosed that enable a variety of unprecedented applications. One of these is the much higher surface-to-volume ratio and specific surface area compared to bulk materials. Since materials interact with the outer environment through their surface, a larger surface means a larger number of interactions and a larger surface energy, and therefore a greater reactivity and efficacy in several applications. Specific surface area can also be largely increased in the presence of pores, which can then be filled with other substances such as drugs or antibiotics for targeted and controlled delivery. Another important property is the reduced size which, in biomedical applications, allows nanoparticles to diffuse more effectively in the extracellular environment and to get in contact – or in some cases to penetrate – the surrounding cells.

During the last years, many nanomaterials have been discovered, designed and studied, and their properties in wound healing have been deeply investigated. Although many questions remain unanswered, there is clear evidence in support of the beneficial role of these nanoplatforms in healthcare.

When it comes to antimicrobial applications, a major parting line can be drawn between *carbon-based* and *metal-based* nanomaterials. The first group includes carbon nanomaterials such as carbon quantum dots, carbon nanotubes, graphene and fullerenes, which have all shown antimicrobial and skin regeneration promotion effects (Pormohammad et al., 2021; Shalaby et al., 2022). Lipid and polymer nanoparticles can also be included in this category, although they are mostly applied as carriers in drug delivery.

The second group includes metal nanoparticles, namely silver and gold nanoparticles, and metal oxide nanoparticles, such as iron, copper, titanium and zinc oxide nanoparticles. These nanoparticles have been proven effective in eradicating multi-drug resistant species and in promoting wound healing and re-epithelialization (Pormohammad et al., 2021; Shalaby et al., 2022).

Among all these interesting alternatives, zinc oxide (ZnO) nanoparticles stand out for a few reasons. Contrary to the other metals previously mentioned, zinc is an essential element for the human body, given its role in the functioning of hundreds of enzymes that are essential for metabolism and gene transcription, with key implications for wound healing and the immune system (M. Gupta et al., 2014; Mishra et al., 2017; Wessels et al., 2017). Moreover, zinc oxide nanoparticles showed lower toxicity compared with gold and silver nanoparticles (Shalaby et al., 2022), while also resulting more effective than TiO_2 and Al_2O_3 nanoparticles in imparting damages to the phospholipid membrane of bacteria (W. Jiang et al., 2010). In some cases, zinc oxide and its nanoparticles are also used as food additives as a more effective way of administering the necessary doses of zinc (J. Jiang et al., 2018), and have shown good therapeutic effects when used in dressings for the treatment of diabetic foot ulcers and post-operative leg wounds (Loera-Valencia et al., 2022; Thompson et al., 2017). However, as mentioned in Chapter 1, many concerns exist around the toxicity of nanoparticles for human health (Sengul & Asmatulu, 2020), and will be further considered later in this work.

For alle these reasons, nanostructured zinc oxide (nZnO) will have a central role in this work, as progresses in its development and application offer some of the best opportunities to positively impact healthcare through nanomedicine.

2.3.1 Nanostructured Zinc Oxide

Nanostructured zinc oxide is an extremely versatile material with applications in a wide variety of sectors. In the biomedical field, nano-ZnO has shown anticancer, antibacterial, antifungal, antidiabetic and anti-inflammatory properties, and used for imaging and drug delivery. Due to the extensive literature and review works available on nZnO (J. Jiang et al., 2018; Mishra et al., 2017; Sirelkhatim et al., 2015), this section aims at briefly recalling its main characteristics, with special attention towards its antimicrobial properties.

2.3.1.1 Preparation methods

Nano-ZnO can be produced with a wide variety of techniques such as thermal evaporation (Zou et al., 2015), sol-gel (M. F. Khan et al., 2016; Paper & Submission, 2016), mechanochemical (Espitia et al., 2012), sonochemical (Ponnamma et al., 2019), and microfluidics methods (Zukas & Gupta, 2017). Microwave-assisted syntheses (Garino, Limongi, et al., 2019; Garino, Sanvitale, et al., 2019; Kajbafvala et al., 2010; Wojnarowicz et al., 2020) are also gaining increasing attention due to the shorter reaction times and better size and morphology control with respect to conventional chemical routes. Wet chemical precipitation is however the most common method for nZnO in nanocomposites preparation, as it is often cheaper, simple, and yields higher amounts of nanoparticles. It involves the reaction of a zinc precursor – usually zinc nitrate (Chittofrati & Matijević, 1990; Wahid et al., 2016), zinc sulphate (Bharathi et al., 2019), zinc chloride (Phan et al., 2020) or zinc acetate (Paper & Submission, 2016; Roy & Rhim, 2019) – with a base solution – such as KOH or NaOH. The reaction takes place in very mild conditions, typically ambient pressure and constant temperatures up to 80°C (Kakiuchi et al., 2006). The precipitate is subsequently collected, washed, and ultimately dried or calcinated (Y. Wang et al., 2010).

Recently, a growing trend in nanomaterials and nZnO synthesis has been represented by the use of green compounds such as plant extracts (H. Agarwal et al., 2019; B. Ahmed et al., 2019; Darvishi et al., 2019; Dhandapani et al., 2020; Elumalai et al., 2015; Gunalan et al., 2012; Happy Agarwal et al., 2018; M. Li et al., 2013; Singhal et al., 2020; Tiwari et al., 2018; Zanni et al., 2016), which are used in substitution of NaOH and KOH as reducing and capping agents, and that can also functionalize the nanoparticles with phytochemicals possessing anti-inflammatory, antioxidant or antimicrobial properties, further mitigating potential toxicity issues.

2.3.1.2 Antimicrobial mechanisms

Nano-ZnO fulfills its antimicrobial action through three main mechanisms:

- **Release of Zn^{2+} ions.** These ions bind to the thiol groups of bacterial respiratory enzymes, compromising their activity (Mishra et al., 2017). They have been also found to inhibit active transport and amino acid metabolism (Sirelkhatim et al., 2015) in bacteria.
- **Production of Reactive Oxygen Species (ROS).** Zinc Oxide is a direct, 3.3 eV bandgap semiconductor. Therefore, electron-hole pairs can be created across its conduction and valence bands upon exposure to UV radiation. In the presence of water and oxygen molecules, these charge carriers subsequently trigger redox reactions at the surface of the material, leading to the production of ROS such as hydroxyl radicals OH·, hydrogen peroxide H_2O_2 and superoxide anion O_2^-. The high reactivity of these species is known to be responsible for fatal oxidative damage and denaturation of DNA, proteins and lipids, ultimately triggering cell apoptosis (J. Jiang et al., 2018; Sirelkhatim et al., 2015).
- **Physical interactions.** ZnO nanoparticles accumulate in the proximity of bacterial cells. The contact is promoted by electrostatic interactions, as cells are negatively charged, while ZnO nanoparticles typically possess a positive charge in aqueous suspension. In turn, this causes membrane depolarization and deformation, as well as abrasion caused by surface edges, ultimately leading to cell death (Sirelkhatim et al., 2015). A graphical representation of these three mechanisms is offered in Figure 2.1.

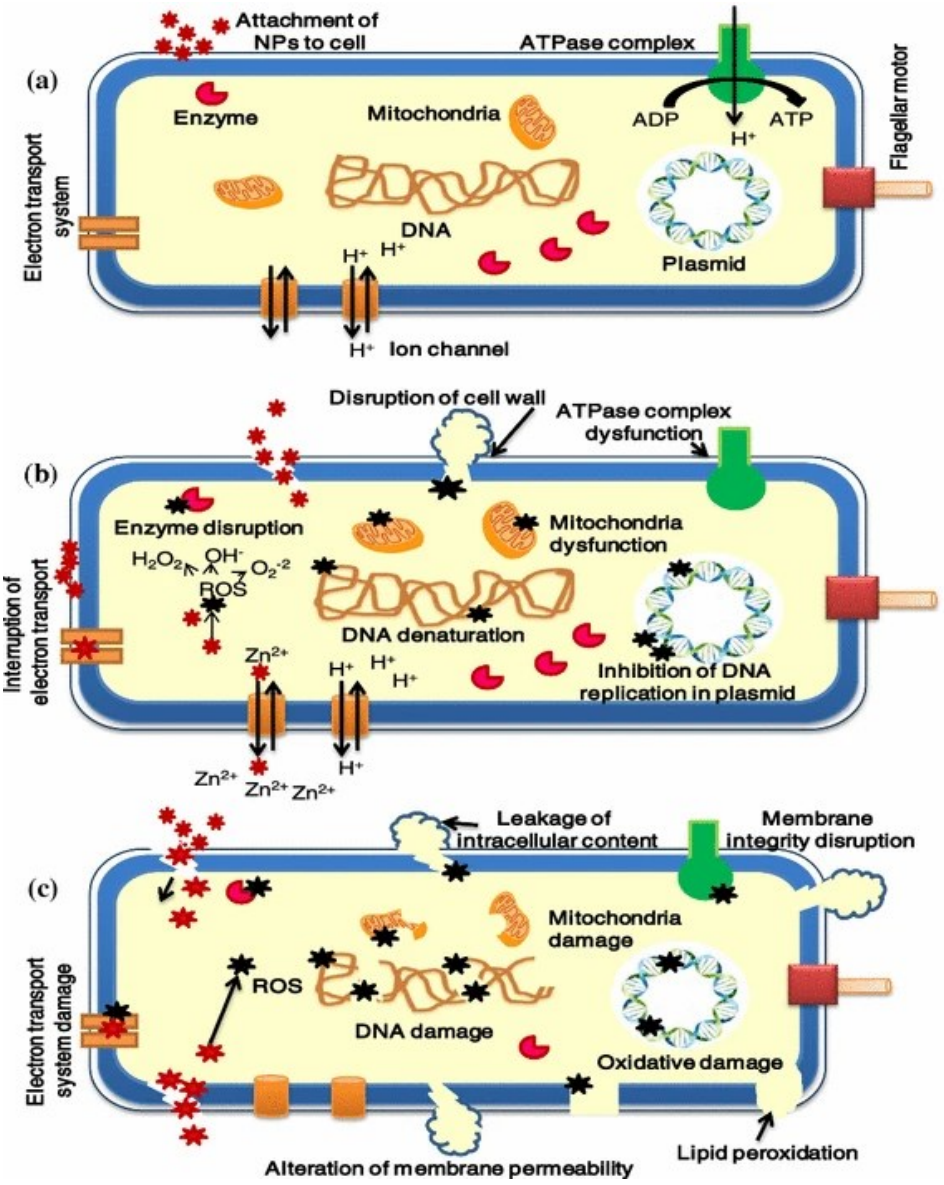


Figure 2.1: Antibacterial mechanisms of nano-ZnO. Source (A. Singh et al., 2018)1.

[1] Reprinted from Journal of Materials Science, Singh et al., Zinc oxide nanoparticles: a review of their biological synthesis, antimicrobial activity, uptake, translocation and biotransformation in plants 185–201 (2018), Copyright © 2017, Springer Science Business Media, LLC

As a rule of thumb emerged over years of experimental studies on the antimicrobial activity of zinc oxide, this nanomaterial tends to be more effective against Gram-positive (Gram(+)) species than on Gram-negative (Gram(-)) ones. This is attributed to the structural differences that characterize the two types of bacteria. Gram-positive bacteria have a thick peptidoglycan wall surrounding their cell membrane. In Gram-negatives, the peptidoglycan wall is thinner, but it is in turn surrounded by an additional phospholipid layer that constitute the outer membrane. This additional layer is often considered responsible for the highest resistance of Gram(-) to nZnO, as it is hypothesized to act as a shield against Zn^{2+} and ROS. It has also been advanced that small concentrations of ZnO can actually enhance the growth of gram-negatives bacteria (Sirelkhatim et al., 2015). A schematic representation is shown in Figure 2.2 below. This is a crucial aspect to be considered: on one side, it restricts the potential use cases of this nanomaterial; on the other side, it offers a clear direction for improvement

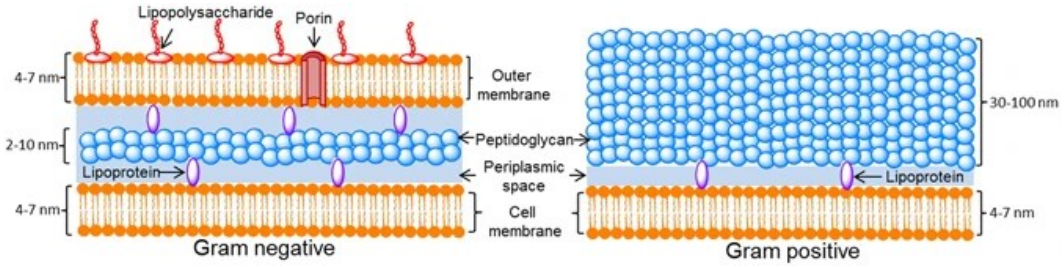


Figure 2.2: Differences in Gram-negative and Gram-positive cell walls. Source: (Berezin et al., 2017).

It's also important to underline that the fact that nZnO can act through three different mechanisms is extremely relevant towards the development of more resilient AMR contrast agents: as mentioned in the first chapter of this work, many conventional antibiotics rapidly lose their efficacy because of their single-mechanisms action, which means that they suffer a single point of failure. What is also very relevant is that this multi-mechanism antimicrobial activity profile can actually be tuned by acting on the synthesis parameters, as these determine the features of nZnO that shape the contribution of each mechanism on the final antimicrobial action. In other words, nZnO – and nanomaterials more in general – can be *designed* to maximize its efficacy.

In fact, things like the selection of reagents as well as the tuning of process parameters such as stirring rate (M. F. Khan et al., 2016), ensure a good degree of control on the final characteristics of the nanoparticles, leading to a wide variety of sizes and shapes, such as nano-spheres (Paper & Submission, 2016), nano-rods (Zanni et al., 2016), nano-platelets (Alwin & Shajan, 2017) and nano-flowers (M. Li et al., 2013). These morphological features, together with the specific surface area (SSA), crystal structure and surface electric charge have all been found to contribute to nZnO antimicrobial activity, as reviewed by several authors (Alavi & Nokhodchi, 2020; Happy Agarwal et al., 2018; Rutherford et al., 2021; Sirelkhatim et al., 2015; Tiwari et al., 2018). For instance, a smaller size and a spherical shape have been found to increase nanoparticle solubility, thus boosting the release of Zn^{2+} ions. Similarly, the type of facets exposed – e.g. (100) versus (111) – have different antimicrobial activity and can thus be factored in developing new types of nZnO (Sirelkhatim et al., 2015). A simplified representation of nano-ZnO preparation processes and their main parameters and outcomes is offered below.

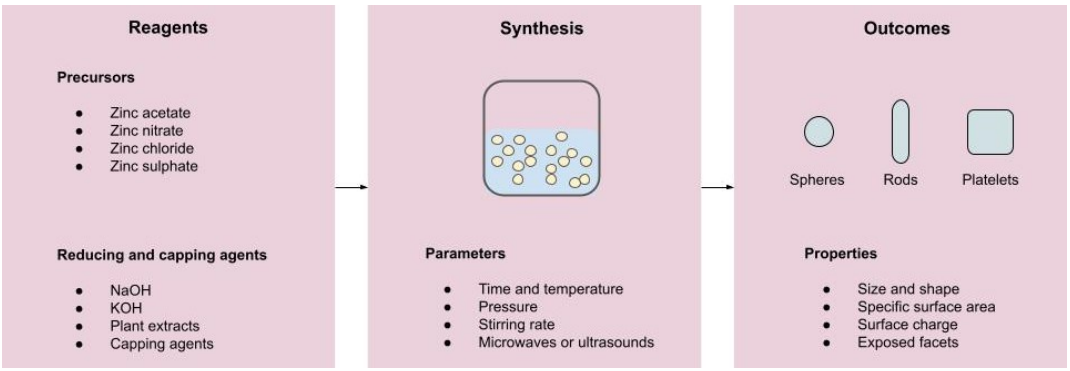


Figure 2.3: Nano-ZnO design through selection of reagents and synthesis parameters

Now that the main features of nZnO and biomacromolecules have been recalled in relation to their antimicrobial and wound healing applications, it is time to explore the intersection between these two types of materials, where they merge to create the next generation of healthcare devices: *bionanocomposites*.

2.4 Biomacromolecules-nZnO composites

What happens to nZnO and biomacromolecules when they are combined to form a bionanocomposite (BNC)? What happens to the antimicrobial mechanisms of nZnO and to the bioactive properties of biomacromolecules? Is there any synergy? Are there any mutual interactions from which new properties and features emerge? This section will try to answer to these questions through a survey of the most recent

advancements and best practices in the preparation, characterization, and applications of BNCs.

2.4.1 Preparation methods

Several preparation processes exist for BNCs. Zahran et al. (Zahran & Marei, 2019b) offered a useful overview of preparation methods for polymer-nanoparticle nanocomposites. Following that classification, two options are found to be most common for nZnO-BNCs, namely *in situ* and *ex situ* methods.

In situ methods consist in mixing a suspension of nZnO with a monomer solution or polymeric chains suspension (Waghmode et al., 2016). After sufficient homogenisation of the two components, the BNCs is obtained by entangling or crosslinking the polymers, or by polymerizing, reticulating or gelling the monomers. This can be achieved through addition of a polymerization initiator or crosslinking agent (Rao et al., 2019), or by solvent evaporation. In this latter case, techniques such as solvent casting (Amjadi et al., 2019; Indumathi et al., 2019a; K., M.P., et al., 2019; Kanmani & Rhim, 2014; Mujeeb Rahman et al., 2018b; Peighambardoust et al., 2019; Priyadarshi & Negi, 2017; Shankar et al., 2015; Shankar & Rhim, 2019), freeze-drying (Jayakumar et al., 2015; Khorasani et al., 2018; Ul-Islam et al., 2014), electrospinning (Augustine et al., 2014; Kim et al., 2018; Pittarate et al., 2011) spin-coating or electrophoretic deposition (Cordero-Arias et al., 2015) can be applied.

In situ methods can be used with low molecular weight, well soluble polymers and facilitates a good dispersion of the filler. They have been successfully used to produce, among the others, gelatin/hyaluronic acid/chitosan (A. V. Thanusha et al., 2018), cellulose (Anagha et al., 2019), starch (Nafchi et al., 2012), and keratin (Villanueva et al., 2019) composite hydrogels containing nZnO. Moreover, they are the most common for polyurethane-ZnO composites, as demonstrated in the dedicated review work done by Rahman (M. M. Rahman, 2020).

Ex situ methods consist in immersing an already formed matrix into a nZnO suspension under agitation, in order for the nanoparticles to migrate inside the matrix and to finally interact with it, either physically or chemically. These methods are relatively simple, but are limited to highly porous matrixes with good affinity for the suspension medium, and capable of significant swelling in that environment. Indeed, poor penetration of NPs in the core region of the matrix is a typical issue. *Ex situ* methods have been applied to craft, for instance, keratin/chitosan (Zhai et al., 2018a) hydrogels or alginate bandages (Jayakumar et al., 2015).

Several variations of both the above-described methods have been adopted by researchers. In some cases (Pandiselvi & Thambidurai, 2015; Rao et al., 2019), for *in situ* methods, the direct addition of pre-synthesised ZnO nanoparticles is replaced with the addition of a zinc oxide precursor. This leads to a solution of monomers and zinc ions which is then brought to basic pH to favour the simultaneous formation of nZnO and polymers. Similarly, in some *ex situ* routes, the preformed matrix is immersed into a zinc oxide precursor solution (Namazi et al., 2019; Wahid et al., 2016). This allows Zn^{2+} ions to diffuse into the polymeric network before formation of ZnO. Figure 2.4 summarizes the main approaches to BNCs fabrication.

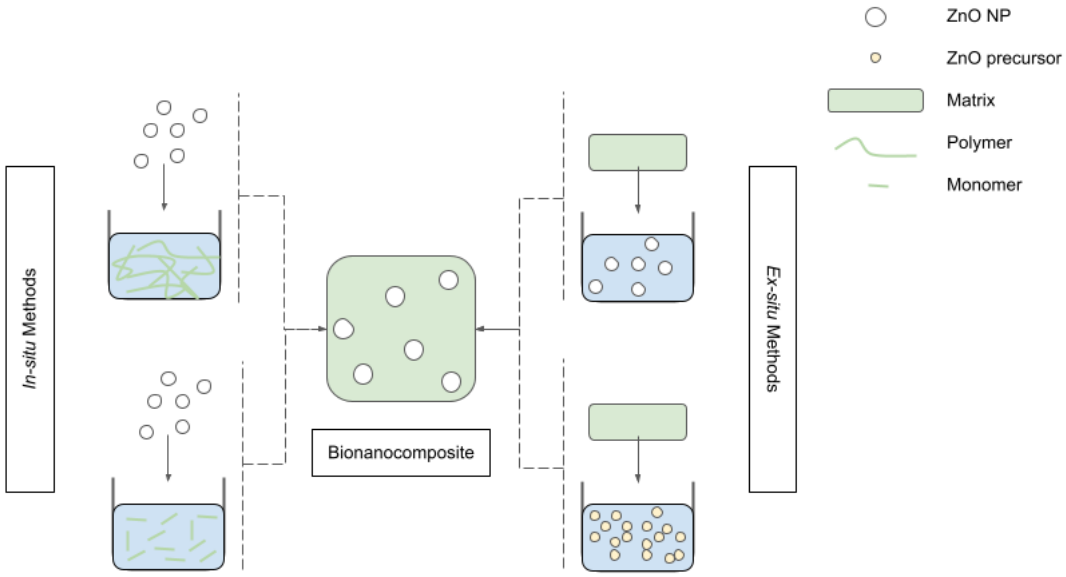


Figure 2.4: Schematic representation of BNCs preparation techniques.

Once together, the interaction between nZnO and the matrix is mostly regulated by hydrogen bonds and by van der Waals interactions (Arfat et al., 2014; Indumathi et al., 2019a; Khorasani et al., 2018; Mujeeb Rahman et al., 2018b; Peighambardoust et al., 2019; Rao et al., 2019; Sudheesh Kumar et al., 2013b; Zanini et al., 2021). This plays a significant role in shaping the final nanocomposite and its properties. For instance, a decrease in matrix crystallinity has been reported in several BNCs made with chitosan or cellulose (Espitia et al., 2012; Hezma et al., 2019; Khalid et al., 2017; L.-H. Li et al., 2010; Mujeeb Rahman et al., 2018b; P. M. Rahman et al., 2017; Shahmohammadi Jebel & Almasi, 2016a; Ul-Islam et al., 2014). This has been ascribed to the disruption of biomacromolecular order caused

by the nanoparticles. In fact, these biomacromolecules are rich in amino and hydroxyl groups, which upon interaction with (or shielding by) nZnO are no longer available to mediate the intermolecular interactions governing the spatial organisation and subsequent crystallization of the macromolecular chains.

It is interesting to note how an increase in crystallinity has been reported for some synthetic poly(vinyl-alcohol)-based nanocomposites (Azizi et al., 2014; Gong et al., 2014; Khorasani et al., 2018) as well as in composites of non-ionic polymers such as cellulose acetate, poly(butylene-succinate) and poly(lactic-acid) (Chu et al., 2017; Petchwattana et al., 2016; Pittarate et al., 2011). In these cases, given the minor contribution of electrostatic phenomena, the stabilizing effect of nanophase might prevail, facilitating molecular organisation and triggering heterogeneous nucleation.

Conversely, when nZnO synthesis is carried out within the NCs preparation process starting from a precursor, either *in situ* or *ex situ*, the resulting nanofiller is affected in several ways. The existence of an already formed matrix or the presence of monomers or macromolecules in the solvent can interfere with nZnO formation by acting as capping agents that constrain the growth of the nanoparticles and regulate their final shape (Rao et al., 2019; Steffy et al., 2018).

2.4.2 Mechanical and functional properties

Following the above description of preparation methods, we shall now dive into how the inclusion of nZnO inside a biomolecular matrix translates into new or modified properties.

2.4.2.1 Mechanical properties

Mechanical properties are critical for antimicrobial BNCs. Inadequate mechanical properties can result in low compliance with the skin and in the inability to stretch or bend according to patients' movements, as well as in poor protection from scratches and punctures. They can also limit the suitable production technologies and drive an increase of the relative costs.

In general, the addition of nZnO typically has a concentration-dependent reinforcing effect translating into an increase of tensile strength and elastic modulus, accompanied by a decrease in elongation at break. A 176% enhancement of tensile strength was reported by Azizi (Azizi et al., 2014) after reinforcing a poly(vinyl-alcohol)/chitosan blend film with nZnO and cellulose nanocrystals. The

polyurethane/chitosan film made by Indumathi (K., Indumathi, et al., 2019) gained a 56% improvement in tensile strength after a 5% w/w nZnO addition. Similarly, a 5% w/w nZnO loading allowed to increase the tensile strength and the Young's modulus of a bacterial cellulose composite film by 42% and 30% respectively, according to Jebel et al. (Shahmohammadi Jebel & Almasi, 2016a). Arfat and co-workers obtained a 36% tensile strength increase by adding 3% w/w nZnO to a fish protein isolate/fish skin gelatin composite film (Arfat et al., 2016). Similar results have been obtained by other researchers as well (Arfat et al., 2014; Espitia et al., 2012; K., M.P., et al., 2019; Khorasani et al., 2018; Peighambardoust et al., 2019; Petchwattana et al., 2016; Pittarate et al., 2011; Prasert et al., 2020; Shankar & Rhim, 2019; Ul-Islam et al., 2014). The reasons underlying this reinforcement are ascribed to the ability of nZnO of limiting the movement of polymeric chains by means of physical, chemical and mechanical interactions. This effect is further enhanced by high degree of dispersion of the filler and by a high surface area, which increases by decreasing the size of the nanoparticles.

On the other side, a worsening of mechanical properties has been reported in some cases, occurring above the initial concentration-dependent improvement, at the highest nZnO contents (Hezma et al., 2019; X. Hu et al., 2019; Indumathi et al., 2019a; Mujeeb Rahman et al., 2018b). In fact, after a critical concentration threshold, the agglomeration of nanoparticles into larger aggregates is triggered, thereby causing a worsened ability of transmitting loads across the composite microstructure. The use of a capping agent wrapped around nZnO has shown to mitigate these side effects by preventing agglomeration and favouring dispersion (Shankar et al., 2015).

Aside from the role of nZnO content, a weak matrix-filler interaction causes a decrease in mechanical properties, where the resulting nanocomposite shows higher elongation at break and decreased tensile strength and elastic modulus, as reported by Kanmani et al. (Kanmani & Rhim, 2014) for carrageenan, carboxymethyl cellulose and agar-based composites obtained *in situ* via solvent casting. Similar results were obtained by other researchers (Chu et al., 2017; Roy & Rhim, 2019; Sudheesh Kumar et al., 2013b). A summary of these findings is offered in Table 2.2.

Table 2.2: Effect of nZnO on the elastic modulus (EM) and tensile strength (TS) of biomaterials.

	EM (MPa)	**TS (Mpa)**	**Ref**

Matrix Type	Pure	Filled	Pure	Filled	nZnO (% wt)	
Agar	1004.9	109.8	34.6	13.0	-	(Kanmani & Rhim, 2014)
Carrageenan	1112.1	130.4	44.6	12.3	-	(Kanmani & Rhim, 2014)
Carboxymethyl-cellulose	20.5	14.0	6.4	5.1	-	(Kanmani & Rhim, 2014)
Gelatin	1451.2	262.5 – 344.4	50.1	29.8-33.4	-	(Shankar et al., 2015)
Chitosan	1821	3304	12.84	41.73	1-2	(Mujeeb Rahman et al., 2018b; Priyadarshi & Negi, 2017)
Starch	7.8	25.44	4.11	12.73	2-3	(X. Hu et al., 2019; Peighambardoust et al., 2019)
Poly(lactic acid)/poly(butyleneadipate-co-terephthalate	800	970-1220	14.5	16.8-26.9	3	(Shankar & Rhim, 2019)
Bacterial cellulose	93.8	132.11	26.3	45.21	5	(Shahmohammadi Jebel & Almasi, 2016a)
Poly(lactic-acid)	3118.8	2610.64	47.78	39.96	3	(Chu et al., 2017)

Poly(caprolactone) nanofibers	3.70	5.25-3.78	1.40	1.60-0.98	1-6	(Augustine et al., 2014)

2.4.2.2 Surface roughness and wettability

Many of the studies examined for this work found that incorporation of nZnO into the matrix usually leads to an increase in the surface roughness due to the presence of nanoparticles in the upper layers of the material and at the interface with the external environment (Arfat et al., 2014; K., M.P., et al., 2019). This has an important impact on another important property, that is *wettability*.

Wettability is defined as the affinity of a given surface for a liquid, typically water. The traditional measure of wettability is the water contact angle (WCA). There is wide agreement in the community that the addition of nZnO to biopolymeric materials causes an increase in WCA, meaning an increase in hydrophobicity (Dhapte et al., 2015; Indumathi et al., 2019a; K., M.P., et al., 2019; Kanmani & Rhim, 2014; Khorasani et al., 2018; Roy & Rhim, 2019; Shankar & Rhim, 2019), (el Saeed et al., 2015). One of the causes is indeed the increase of the surface roughness, which opposes capillary forces to the penetration of water droplets into the material. Another cause is the lower water affinity of nZnO compared to biomacromolecules. A third reason is, in some cases (Khorasani et al., 2018), the enhanced crystallinity of the surrounding matrix: more tightly packed crystalline phases are more difficult to be penetrated by water. A high water affinity – and thus a low WCA – is important for wound dressings as it ensures good adhesion to the underlying tissue. In many cases, it goes in parallel with the ability of the dressing to absorb wound exudate. Given that nZnO increases WCA, it could be argued that its effect is in fact detrimental on this important feature of a good dressing. However, the emergence of a hydrophobic behaviour upon addition of nZnO, i.e., a WCA greater than 90°C, is extremely rare. In the vast majority of cases, hydrophilicity is preserved, as shown in Table 2.3.

Table 2.3: Effect of nZnO presence on the WCA of different biomaterials.

Matrix Type	**WCA (deg)**		**nZnO**	**Ref**
	Pure	**Filled**	**(% wt)**	

Agar	66.5	68.8	-	(Kanmani & Rhim, 2014)
Carrageenan	61.6	84.5	-	(Kanmani & Rhim, 2014)
Carboxymethyl-cellulose	31.6	55.2	-	(Kanmani & Rhim, 2014)
Gelatin	52.4	62.15	-	(Shankar et al., 2015)
Starch	51	43	2-3	(X. Hu et al., 2019; Peighambardoust et al., 2019)
Poly(lactic acid)/poly(butylenea dipate-co-terephthalate	82	78.1-88.3	3	(Shankar & Rhim, 2019)
Chitosan-cellulose acetate phthalate	57	81	5	(Indumathi et al., 2019a)
Cellulose acetate nanofibers	47	124	-	(Anitha et al., 2012)

2.4.2.3 Porosity and swelling

Porosity is influenced by the presence of nZnO too, and both increase (George et al., 2020b; Rao et al., 2019; Zare-Akbari et al., 2016; Zhai et al., 2018a) and decrease (Jayakumar et al., 2015; Shahmohammadi Jebel & Almasi, 2016a; Sudheesh Kumar et al., 2013b) of porosity were reported.

A high porosity may be beneficial for the swelling ratio (SR) – defined as the percentage increase in weight of a specimen after immersion in a liquid medium with respect to the dry weight. SR was reported to increase after addition of nZnO

(George et al., 2020b; Khorasani et al., 2018; Rao et al., 2019; Villanueva et al., 2019; Wahid et al., 2016; Zare-Akbari et al., 2016). In addition to a higher porosity, this was also ascribed to the electrostatic charge on the surface of ZnO nanoparticles which causes ionic osmotic pressure build-up inside the matrix, therefore inducing higher water uptake to counterbalance it. However, high concentrations of nanofiller might too strongly reduce the intermolecular movements at the basis of the swelling phenomenon – the so-called *knot tying function* – thereby lowering the swelling ratio in some cases (Al-Naamani et al., 2016; Anagha et al., 2019; Bajpai et al., 2016; Jayakumar et al., 2015; Namazi et al., 2019; Rath et al., 2016; Sudheesh Kumar et al., 2013b; H. Wang et al., 2019). Another reason for this decrease in swelling ratio of nanocomposites can be an overall lower water affinity of the system, as a result of the diminished net electrostatic charge of the matrix caused by a shielding effect imparted by the nanoparticles.

2.4.2.3 Gas barrier properties

Barrier properties to oxygen and water vapour can also be very important for wound dressings. A very high water permeability might lead to wound dehydration, whereas limiting oxygen afflux can promote angiogenesis through hypoxia (Tan et al., 2019).

The diffusion rates of both water and oxygen have been found to decrease with increasing zinc oxide amount. Priyadarshi and Negi measured the water vapour transmission rate (WVTR) of chitosan/nZnO films (Priyadarshi & Negi, 2017). In their study, the measured WVTR of chitosan films was 0.0067 g/m^2/day, and decreased to 0.0028 and 0.0011 g/m^2/day upon the additon of ZnO nanoparticles in amounts equal to 1% and 2% w/w respectively. The decrease was attributed to the occupation of pore volume by the nanoparticles. Arfat and co-workers studied the properties of fish protein isolate/fish skin gelatin-ZnO NCs (Arfat et al., 2016). The researchers have measured a concentration-dependent decrease of water vapour permeability (WVP) up to a 3% w/w nano-ZnO loading. At 4% loadings, nanoparticle agglomeration determined the loss of matrix integrity, thus causing an increase of WVP. In the gelatin/β-glucan/ZnO nanocomposites prepared by Azari et al. (Sherafatkhah Azari et al., 2020), WVP decreased from 2.15×10^{-8} g m^{-1} h^{-1} Pa^{-1} for neat gelatin films to 1.58×10^{-8} g m^{-1} h^{-1} Pa^{-1} for composite films containing 20% w/w β-glucans and 5% w/w ZnO nanoparticles. The decrease was explained with an increase of matrix compactness induced by the higher number of intermolecular interactions, as well as with the higher tortuosity imposed to the path of water molecules. Peighambardoust et al. (Peighambardoust et al., 2019) found

similar results for starch-based BNCs. Furthermore, the authors have found that ZnO nanoparticles were more efficient in decreasing WVP compared to CuO and Ag nanoparticles thanks to their superior dispersibility, which ultimately translated into maximum path tortuosity. Chu and co-workers (Chu et al., 2017) measured instead an increase in WVP for a polylactic acid matrix upon addition of nZnO. However, a possible explanation to that can be found in the microstructural changes imparted to the continuous polymeric phase by the nano-filler that introduced some voids in the matrix, as shown by SEM images. A higher water vapor permeability was observed also in the study from Shankar et al. (Shankar et al., 2015), and was attributed to the higher porosity of the composite in the proximity of the separation between the gelatin matrix and the filler phases.

As for oxygen permeability, Indumathi et al. (Indumathi et al., 2019a) reported a concentration dependent decrease in oxygen transmission rate (OTR) in chitosan/cellulose acetate phthalate/nZnO, with a minimum of 1490,43 cm^3 m^{-2} d^{-1} in correspondence of the highest nano-ZnO loading of 7.5% w/w. This value is lower than traditional synthetic polymeric films such as polyethylene. The same was observed by Petchwattana et al. in poly(butylene succinate)/nZnO BNCs (Petchwattana et al., 2016). The presence of nZnO constitutes an obstacle to oxygen molecules migration across the material. Similar results have been observed in numerous other studies (Arfat et al., 2014; Espitia et al., 2012; X. Hu et al., 2019; Indumathi et al., 2019a; Kanmani & Rhim, 2014; Khorasani et al., 2018; Nafchi et al., 2012; Roy & Rhim, 2019; Shankar & Rhim, 2019; Vaezi et al., 2019).

2.4.2.4 Ultraviolet light barrier

Wound dressings shall also be capable of protecting the injured area from harmful radiation. As a semiconductor with a band energy gap around 3.3 eV, ZnO has excellent UV blocking properties. Quantum confinement effects at the nanoscale can also increase the energy gap, thereby promoting the absorption of even higher frequencies of the spectrum. This property is always successfully transferred to the nanocomposites (Shankar et al., 2015).

2.5 Biomedical applications

2.5.1 Controlled drug release

The ability to release drugs loaded onto the matrix is also modified by the simultaneous presence of nZnO in the system, as shown by Rath (Rath et al., 2016)

for a cefazolin-loaded nanofibrous gelatin mats for surgical wounds incorporated with zinc oxide nanoparticles. When designing a drug delivery device, a controlled release profile is highly desired, as well as an optimal drug loading capacity. Researchers have found that nZnO content is an active parameter in optimising drug loading capacity (Anagha et al., 2019; George et al., 2019, 2020b), due to its previously discussed ability of influencing water uptake and swelling behaviour of the BNCs. In addition to this, drug release is also found to become slower and more controlled in proportion to the amount of nZnO included in the matrix. This is due to the higher tortuosity that the nanofiller imposes on the path of the drug molecules upon release. As mentioned previously, nanostructured zinc oxide with high specific surface area can be used as a standalone drug delivery system as well (Banchero et al., 2019).

2.5.2 Antimicrobial properties

As mentioned in Section 2.3.1.2, nZnO acts through three main antimicrobial mechanisms. These shall be reconsidered in the context of the BNCs.

The matrix can influence the release kinetics of zinc ions or of the nanoparticles themselves, thus regulating the antimicrobial activity of the BNCs. Jebel et al. (Shahmohammadi Jebel & Almasi, 2016a) and Villanueva and co-workers (Villanueva et al., 2019) examined the release properties of zinc ions or nanoparticles from bacterial cellulose and keratin BNCs, respectively. In the first case, it was found that greater release occurred in a medium with pH = 8 as opposed to a medium at pH = 4. This was attributed to the higher SR achieved in basic conditions, which promoted the diffusion of ions and nanoparticles. In the second case, it was found that two-months old samples showed significantly lower release, presumably due to a slow rearrangement of polymeric molecules that translated into greater hindrance to diffusion.

Release phenomena have been investigated also from other BNCs. Sudheesh Kumar (Sudheesh Kumar et al., 2013b) showed that 12% of the ZnO contained inside a β-chitin hydrogel was released after 1-week immersion in phosphate buffered saline. Azizi and co-workers investigated the release of Zn^{2+} from a poly(vinyl alcohol)-chitosan BNC (Azizi et al., 2014) through the inductively coupled plasma technique, and showed a sustained and ZnO-concentration-dependent release of zinc ions in water throughout a period of 8 days, reaching a final concentration of 0.7 mg/L. In a work from Chu (Chu et al., 2017), the antimicrobial activity of a polylactic-acid/nano-ZnO film against *E. coli* was measured immediately after exposure to the samples and after 12 hours. Inhibition

was only reported after 12 hours and attributed to the gradual release of nanoparticles from the porous matrix.

Reactive Oxygen Species diffusion kinetics can also be affected. Prasert and co-workers (Prasert et al., 2020) observed the photocatalytic degradation of the polypropylene matrix of a nZnO-containing antibacterial nanocomposite after exposure to sunlight. That was explained as the result of the interaction of ROS with the backbone of the polymer molecules, resulting in the formation of alkyl radicals which would subsequently react among themselves causing the crosslinking and subsequent embrittlement of the material.

In general, the antimicrobial efficacy of BNCs usually increases with the content of nanofiller (X. Y. Ma & Zhang, 2009; Siyanbola et al., 2015), although in some cases agglomeration might cause a reduction of the antimicrobial potential of the nanoparticles (Hezma et al., 2019). In some systems, such as for chitosan-based BNCs, the matrix itself possesses antimicrobial properties which can act in synergy with the nanoparticles (Priyadarshi & Negi, 2017).

Figure 2.5 below shows a schematic representation of all these phenomena at work.

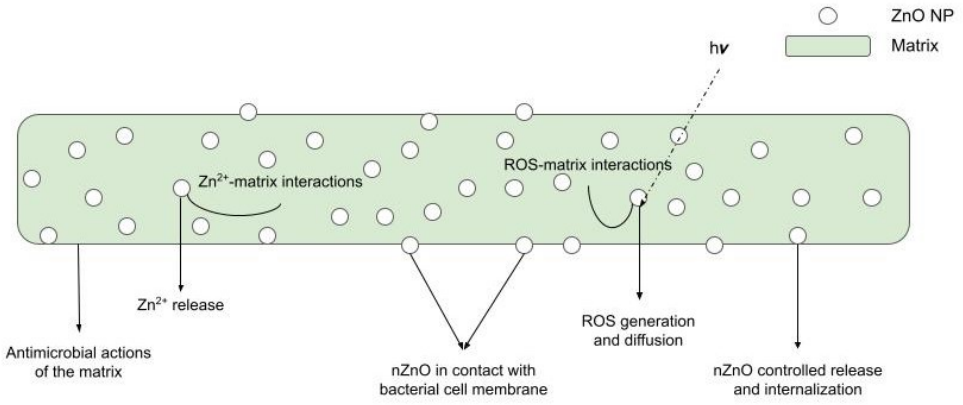


Figure 2.5: Antibacterial action mechanisms of BNCs

All these aspects imply that the final antimicrobial performance of the BNC can actually be different than that displayed by the bare nZnO. For instance, a review of the recent scientific literature from 2010 to present day shows how some BNCs tend to have greater inhibitory activity against gram-positive bacteria, while others result more effective against gram-negatives. Although similar behaviour has been

reported for bare nZnO as well, this is more frequently reported to be more effective against gram-positives, as mentioned in Section 2.3.1.2.

Interestingly, studies reporting a more pronounced effect of gram-positive species than on gram-negative (Anitha et al., 2012; Arfat et al., 2014; Augustine et al., 2014; Dural Erem et al., 2011; El-Nahhal et al., 2020; X. Hu et al., 2019; Khalid et al., 2017; L.-H. Li et al., 2010; Namazi et al., 2019; Priyadarshi & Negi, 2017; Shekh et al., 2018; Sherafatkhah Azari et al., 2020; Sirohi et al., 2017; Taghizadeh et al., 2020; Villanueva et al., 2019; Wahid et al., 2016) attribute this result to the presence, on Gram-negative bacteria, of the negatively charged lipopolysaccharide outer membrane covering their thin peptidoglycan layer, which would be less permeable to potentially harmful species such as ROS.

On the other side, in articles where the nZnO-BNCs resulted more effective against gram-negative species than on gram-positive ones (Bharathi et al., 2019; Hezma et al., 2019; X. Y. Ma & Zhang, 2009; Mujeeb Rahman et al., 2018b; Rao et al., 2019; A. V. Thanusha et al., 2018), the result is attributed to the fact that the thicker peptidoglycan layer which is typical of Gram-positive bacteria is more difficult to penetrate than the Gram-negatives' thinner one, which therefore makes gram-negatives more susceptible to the antimicrobial agents.

Among the studies considered for the present review, around 65% of those employing the disk diffusion method reported a more marked effect on gram positive species. However, no sufficient evidence is found to correlate differences in experimental conditions or in antimicrobial systems to these asymmetric results. One of the main reasons might be found in the use of different bacterial species and strains for testing in these studies, which can therefore show different responses to antimicrobials. Ahmed et al. (R. Ahmed et al., 2018) tested the antimicrobial efficacy of a chitosan-poly(vinyl-alcohol) nanofibrous blend against *E. coli* and *S. aureus*, both in presence and in absence of nZnO. Results of the disk diffusion method for the composite blend showed comparable inhibition zones of 20.2 ± 1 mm and 21.5 ± 0.5 mm respectively, while the inhibition zones of the neat chitosan-poly(vinyl-alcohol) blend were 14 ± 0.5 mm and 5 ± 0.5 mm, suggesting that the matrix may play a role in complementing the weaker effect of nZnO against Gram-negative bacteria. This is supported by several studies on the ability of chitosan to disrupt Gram-negative cell membrane by means of electrostatic interactions (Helander et al., 2001; X. fang Li et al., 2010; H. Liu et al., 2004). Chitosan matrixes are indeed the most frequent among the studies reporting greater activity on Gram-negatives (Bharathi et al., 2019; Hezma et al., 2019; Mujeeb Rahman et al., 2018b;

A. V. Thanusha et al., 2018). Similar results can be found in (L.-H. Li et al., 2010), where it shown how chitosan only films have greater antimicrobial activity on *E. coli* than on *S. aureus*. Data in (Indumathi et al., 2019b) show instead that chitosan only films are more effective on *S. aureus* than on *E. coli*, despite the fact that the chitosan used for film preparation had the same molecular weight in both studies and comparable deacetylation degrees.

In order to elucidate the role played by the matrix, Kanmani and Rhim (Kanmani & Rhim, 2014) prepared three different BNCs via *in situ* method, combining the same type of nZnO with three matrixes, namely agar, carrageenan and carboxymethylcellulose. The matrixes altered the final aggregation and dispersion of the nanofiller. Also, agar/nZnO composite was found less transparent to ROS-inducing UV light. Carrageenan/nZnO composite exhibited the lowest moisture content and water vapour permeability. Despite this, no significant difference was observed in the antimicrobial activity of the three nanocomposites.

On the other side, to evaluate the role of morphologically different ZnO nanostructures coupled with the same matrix, Shankar et al. (Shankar et al., 2015) tested ZnO nanoparticles obtained from different precursors in the same gelatin matrix against *E. coli* (Gram-negative) and *L. monocytogenes* (Gram-positive). Also in this case, no significant difference in antimicrobial efficacy was observed, even though it could be noticed that ZnO nanoparticles synthesised from zinc acetate were slightly more effective against *L. monocytogenes* than those obtained from zinc nitrate.

While all these studies confirm that BNCs are actually effective against a wide variety of bacterial strains, many questions remain open about their actual mechanism of action. Gaining insights into these aspects will therefore be a great contribution towards a more rational design of better solutions. In parallel, research is also advancing to answer another important question: are bionanocomposites effective in healing wounds?

2.5.3 Wound healing properties

In 2013, Kumar et al. (Sudheesh Kumar et al., 2013b) tested the wound healing potential of a β-chitin hydrogel/nZnO composite bandage, as a potential solution for different types of infected wounds with a large volume of exudates. Bandages were tested on Sprague-Dawley rats, allowing a 100% skin wound closure after 3 weeks, together with good antimicrobial activity and collagen deposition.

Rakhshaei and Namazi (Rakhshaei & Namazi, 2017) prepared a nanocomposite hydrogel based on carboxymethyl cellulose filled with ZnO impregnated MCM-41 mesoporous silica, loaded with tetracycline, a broad-spectrum antibiotic. In addition to the enhancement of the antimicrobial properties against *E. coli* brought by nano-ZnO, a cytotoxicity test was carried using adipose tissue-derived stem cells. The tests showed a reduced cell viability of the nZnO-containing hydrogels with respect to the nZnO-free carboxymethyl cellulose hydrogel, 63% versus 81% after 24 h respectively. However, viability continued increasing for the next 7 days. Similar results were obtained by Khorasani et al. (Khorasani et al., 2018) for a heparinised-nanoZnO/poly(vinylalcohol)/carboxymethyl cellulose hydrogel tested on mouse fibroblast cells (L-929). These results led to the conclusions that the BNCs were in fact biocompatible.

Along the same lines, Raguvaran et al. (Raguvaran et al., 2017) demonstrated that embedding nZnO into sodium alginate-gum acacia hydrogels yielded remarkably lower cytotoxicity than the bare nano-oxide while retaining good wound healing properties. In fact, the hydrogel matrix was able to effectively reduce the contact between ZnO nanoparticles and the cells and to control Zn^{2+} release. This is reassuring evidence in consideration of the existing concerns about the toxicity of ZnO nanopowders.

Burn wounds on Bagg's albino (BALB) mice were treated with bacterial cellulose/nZnO composites by Khalid et al. (Khalid et al., 2017), that reported wound healing activity comparable with a commercial silver sulfadiazine cream positive control. Histopathological analyses revealed regenerated epithelium in the wound beds treated with the BNC. After 15 days, the average wound area was 98.3 ± 7.6 mm^2 after treatment with the bionanocomposite, compared to the 143 ± 7.5 of the bacterial cellulose dressing alone, and the 66 ± 5.7 of the positive control.

In a similar study, re-epithelialisation, dense keratinocytes proliferation and organised fibrous connective tissue were observed by Lu and coworkers (Z. Lu et al., 2017) after wound treatment with a chitosan/nZnO composite. The composite performed better than a commercial ZnO ointment gauze. Promising results were also obtained by Amhed and co-workers (R. Ahmed et al., 2018) on diabetic rabbits treated with an electrospun chitosan/poly(vinyl-alcohol) nanofiber mat loaded with nZnO: the bionanocomposite induced a 44.8 ± 4.9 % wound contraction at day 4, whereas the ZnO-free mat only led to a 22.5 ± 3.0 % contraction.

All these findings demonstrate how promising nZnO and BNCs are to address some of the most pressing healthcare issues our society is facing today. Still, the road towards fully understood, broadly available and maximally effective solutions is long. At the present day, the state of the art on nZnO-BNC is characterized by three main challenges.

Firstly, while research has investigated numerous bio- and nano- materials for wound healing applications, the span of potential bionanocomposites that can be designed is not fully explored yet and grows continuously as new materials are developed. In this respect, in this work, six different biomacromolecules have been used to fabricate and test BNCs containing nZnO, providing new evidence to the existing body of knowledge and demonstrating the untapped potential hidden in biomacromolecules that have been poorly considered so far.

Secondly, many aspects remain to be clarified about their working principles and the mechanisms the drive their antibacterial or tissue regeneration activities. A vast portion of the current literature only reports the end results of the tests but does not provide full insights into the mechanisms of action. Gaining deeper understanding of these underlying mechanisms is key to engineer better performing BNCs by investing into enhancing their most useful features. In this sense, this work deepened the characterization of the bionanocomposites and manipulated their preparation processes to better correlate their properties to their final antibacterial activity.

Thirdly, while so many BNCs are being investigated, no clear and established standards exist to systematically assess and compare their properties. This includes not only antibacterial properties, but also cytocompatibility, wound healing, and swelling. Agreeing on a uniform set of recognized characterization protocols is necessary in order to identify the best solutions. To this end, a systematic characterization of all the BNCs prepared in the present work has been conducted using always the same techniques and testing methods, establishing a preliminary framework for a more reliable and productive comparison of these promising materials.

The following chapters of this work will describe into more detail the effort we have made to make this one step further.

References

Abd El-Hack, M. E., El-Saadony, M. T., Shafi, M. E., Zabermawi, N. M., Arif, M., Batiha, G. E., Khafaga, A. F., Abd El-Hakim, Y. M., & Al-Sagheer, A. A. (2020). Antimicrobial and antioxidant properties of chitosan and its derivatives and their applications: A review. In *International Journal of Biological Macromolecules* (Vol. 164, pp. 2726–2744). Elsevier B.V. https://doi.org/10.1016/j.ijbiomac.2020.08.153

Agarwal, G., Agiwal, S., & Srivastava, A. (2020). Hyaluronic acid containing scaffolds ameliorate stem cell function for tissue repair and regeneration. In *International Journal of Biological Macromolecules* (Vol. 165, pp. 388–401). Elsevier B.V. https://doi.org/10.1016/j.ijbiomac.2020.09.107

Agarwal, H., Nakara, A., Menon, S., & Shanmugam, V. (2019). Eco-friendly synthesis of zinc oxide nanoparticles using Cinnamomum Tamala leaf extract and its promising effect towards the antibacterial activity. *Journal of Drug Delivery Science and Technology*, *53*, 101212. https://doi.org/10.1016/J.JDDST.2019.101212

Ahmad Raus, R., Wan Nawawi, W. M. F., & Nasaruddin, R. R. (2021). Alginate and alginate composites for biomedical applications. In *Asian Journal of Pharmaceutical Sciences*. Shenyang Pharmaceutical University. https://doi.org/10.1016/j.ajps.2020.10.001

Ahmed, B., Solanki, B., Zaidi, A., Khan, M. S., & Musarrat, J. (2019). Bacterial toxicity of biomimetic green zinc oxide nanoantibiotic: insights into ZnONP uptake and nanocolloid-bacteria interface. *Toxicology Research*, *8*(2), 246–261. https://doi.org/10.1039/C8TX00267C

Ahmed, R., Tariq, M., Ali, I., Asghar, R., Noorunnisa Khanam, P., Augustine, R., & Hasan, A. (2018). Novel electrospun chitosan/polyvinyl alcohol/zinc oxide nanofibrous mats with antibacterial and antioxidant properties for diabetic wound healing. *International Journal of Biological Macromolecules*, *120*, 385–393. https://doi.org/10.1016/j.ijbiomac.2018.08.057

Alavi, M., & Nokhodchi, A. (2020). An overview on antimicrobial and wound healing properties of ZnO nanobiofilms, hydrogels, and bionanocomposites based on cellulose, chitosan, and alginate polymers. In *Carbohydrate Polymers* (Vol. 227, p. 115349). Elsevier Ltd. https://doi.org/10.1016/j.carbpol.2019.115349

Al-Naamani, L., Dobretsov, S., & Dutta, J. (2016). Chitosan-zinc oxide nanoparticle composite coating for active food packaging applications. *Innovative Food Science and Emerging Technologies*, *38*, 231–237. https://doi.org/10.1016/j.ifset.2016.10.010

Alwin, S., & Shajan, X. S. (2017). Facile synthesis of 3-D nanostructured zinc oxide aerogel and its application as photoanode material for dye-sensitized solar cells. *Surfaces and Interfaces*, *7*(January), 14–19. https://doi.org/10.1016/j.surfin.2017.02.002

Aly, A. A., & Ahmed, M. K. (2021). Nanofibers of cellulose acetate containing ZnO nanoparticles/graphene oxide for wound healing applications. *International Journal of Pharmaceutics*, *598*, 120325. https://doi.org/10.1016/j.ijpharm.2021.120325

Amjadi, S., Emaminia, S., Nazari, M., Davudian, S. H., Roufegarinejad, L., & Hamishehkar, H. (2019). Application of Reinforced ZnO Nanoparticle-Incorporated Gelatin Bionanocomposite Film with Chitosan Nanofiber for Packaging of Chicken Fillet and Cheese as Food Models. *Food and Bioprocess Technology*, *12*(7), 1205–1219. https://doi.org/10.1007/s11947-019-02286-y

Anagha, B., George, D., Maheswari, P. U., & Begum, K. M. M. S. (2019). Biomass Derived Antimicrobial Hybrid Cellulose Hydrogel with Green ZnO Nanoparticles for Curcumin Delivery and its Kinetic Modelling. *Journal of Polymers and the Environment*, *27*(9), 2054–2067. https://doi.org/10.1007/s10924-019-01495-y

Anitha, S., Brabu, B., Thiruvadigal, D. J., Gopalakrishnan, C., & Natarajan, T. S. (2012). Optical, bactericidal and water repellent properties of electrospun nano-composite membranes of cellulose acetate and ZnO. *Carbohydrate Polymers*, *87*(2), 1065–1072. https://doi.org/10.1016/j.carbpol.2011.08.030

Arfat, Y. A., Benjakul, S., Prodpran, T., Sumpavapol, P., & Songtipya, P. (2014). Properties and antimicrobial activity of fish protein isolate/fish skin gelatin film containing basil leaf essential oil and zinc oxide nanoparticles. *Food Hydrocolloids*, *41*, 265–273. https://doi.org/10.1016/j.foodhyd.2014.04.023

Arfat, Y. A., Benjakul, S., Prodpran, T., Sumpavapol, P., & Songtipya, P. (2016). Physico-Mechanical Characterization and Antimicrobial Properties of Fish Protein Isolate/Fish Skin Gelatin-Zinc Oxide (ZnO) Nanocomposite Films. *Food and Bioprocess Technology*, *9*(1), 101–112. https://doi.org/10.1007/s11947-015-1602-0

Arfat, Y. A., Benjakul, S., Vongkamjan, K., Sumpavapol, P., & Yarnpakdee, S. (2015). Shelf-life extension of refrigerated sea bass slices wrapped with fish protein isolate/fish skin gelatin-ZnO nanocomposite film incorporated with basil leaf essential oil. *Journal of Food Science and Technology*, *52*(10), 6182–6193. https://doi.org/10.1007/s13197-014-1706-y

Augustine, R., Malik, H. N., Singhal, D. K., Mukherjee, A., Malakar, D., Kalarikkal, N., & Thomas, S. (2014). Electrospun polycaprolactone/ZnO nanocomposite membranes as biomaterials with antibacterial and cell adhesion properties. *Journal of Polymer Research*, *21*(3), 1–17. https://doi.org/10.1007/s10965-013-0347-6

Azizi, S., Ahmad, M. B., Ibrahim, N. A., Hussein, M. Z., & Namvar, F. (2014). Cellulose nanocrystals/ZnO as a bifunctional reinforcing nanocomposite for poly(vinyl alcohol)/chitosan blend films: Fabrication, characterization and properties. *International Journal of Molecular Sciences*, *15*(6), 11040–11053. https://doi.org/10.3390/ijms150611040

Bajpai, S. K., Jadaun, M., & Tiwari, S. (2016). Synthesis, characterization and antimicrobial applications of zinc oxide nanoparticles loaded gum acacia/poly(SA) hydrogels. *Carbohydrate Polymers*, *153*, 60–65. https://doi.org/10.1016/j.carbpol.2016.07.019

Banchero, M., Mohamed, S. S. Y., Leone, F., Lopez, F., Ronchetti, S., Manna, L., & Onida, B. (2019). Supercritical solvent impregnation of different drugs in mesoporous nanostructured zno. *Pharmaceutics*, *11*(7), 1–14. https://doi.org/10.3390/pharmaceutics11070340

Berezin, S., Aviv, Y., Aviv, H., Goldberg, E., & Tischler, Y. R. (2017). Replacing a Century Old Technique – Modern Spectroscopy Can Supplant Gram Staining. *Scientific Reports 2017 7:1*, *7*(1), 1–7. https://doi.org/10.1038/s41598-017-02212-2

Bharathi, D., Ranjithkumar, R., Chandarshekar, B., & Bhuvaneshwari, V. (2019). Preparation of chitosan coated zinc oxide nanocomposite for enhanced antibacterial

and photocatalytic activity: As a bionanocomposite. *International Journal of Biological Macromolecules*, *129*, 989–996. https://doi.org/10.1016/J.IJBIOMAC.2019.02.061

Burdick, J. A., & Prestwich, G. D. (2011). Hyaluronic acid hydrogels for biomedical applications. *Advanced Materials*, *23*(12), H41–H56. https://doi.org/10.1002/adma.201003963

Cacicedo, M. L., Castro, M. C., Servetas, I., Bosnea, L., Boura, K., Tsafrakidou, P., Dima, A., Terpou, A., Koutinas, A., & Castro, G. R. (2016). Progress in bacterial cellulose matrices for biotechnological applications. In *Bioresource Technology* (Vol. 213, pp. 172–180). Elsevier Ltd. https://doi.org/10.1016/j.biortech.2016.02.071

Cao, F., Zeng, B., Zhu, Y., Yu, F., Wang, M., Song, X., Cheng, X., Chen, L., & Wang, X. (2019). Porous ZnO modified silk sutures with dual light defined antibacterial, healing promotion and controlled self-degradation capabilities. *Biomaterials Science*, *8*(1), 250–255. https://doi.org/10.1039/C9BM01422E

Cerminati, S., Leroux, M., Anselmi, P., Peirú, S., Alonso, J. C., Priem, B., & Menzella, H. G. (2021). Low cost and sustainable hyaluronic acid production in a manufacturing platform based on Bacillus subtilis 3NA strain. *Applied Microbiology and Biotechnology*, *105*(8), 3075–3086. https://doi.org/10.1007/S00253-021-11246-6/FIGURES/4

Cheng, H., Chen, L., McClements, D. J., Yang, T., Zhang, Z., Ren, F., Miao, M., Tian, Y., & Jin, Z. (2021). Starch-based biodegradable packaging materials: A review of their preparation, characterization and diverse applications in the food industry. *Trends in Food Science & Technology*, *114*, 70–82. https://doi.org/10.1016/j.tifs.2021.05.017

Chilakamarry, C. R., Mahmood, S., Saffe, S. N. B. M., Arifin, M. A. bin, Gupta, A., Sikkandar, M. Y., Begum, S. S., & Narasaiah, B. (2021). Extraction and application of keratin from natural resources: a review. *3 Biotech*, *11*(5), 1–12. https://doi.org/10.1007/S13205-021-02734-7/FIGURES/7

Chittofrati, A., & Matijević, E. (1990). Uniform particles of zinc oxide of different morphologies. *Colloids and Surfaces*, *48*(C), 65–78. https://doi.org/10.1016/0166-6622(90)80219-T

Chu, Z., Zhao, T., Li, L., Fan, J., & Qin, Y. (2017). Characterization of Antimicrobial Poly (Lactic Acid)/Nano-Composite Films with Silver and Zinc Oxide Nanoparticles. *Materials*, *10*(6), 659. https://doi.org/10.3390/ma10060659

Cordero-Arias, L., Cabanas-Polo, S., Goudouri, O. M., Misra, S. K., Gilabert, J., Valsami-Jones, E., Sanchez, E., Virtanen, S., & Boccaccini, A. R. (2015). Electrophoretic deposition of ZnO/alginate and ZnO-bioactive glass/alginate composite coatings for antimicrobial applications. *Materials Science and Engineering C*, *55*, 137–144. https://doi.org/10.1016/j.msec.2015.05.034

Costa, E. M., Silva, S., Vicente, S., Neto, C., Castro, P. M., Veiga, M., Madureira, R., Tavaria, F., & Pintado, M. M. (2017). Chitosan nanoparticles as alternative anti-staphylococci agents: Bactericidal, antibiofilm and antiadhesive effects. *Materials Science and Engineering C*, *79*, 221–226. https://doi.org/10.1016/j.msec.2017.05.047

Dananjaya, S. H. S., Kumar, R. S., Yang, M., Nikapitiya, C., Lee, J., & de Zoysa, M. (2018). Synthesis, characterization of ZnO-chitosan nanocomposites and evaluation of its antifungal activity against pathogenic Candida albicans. *International Journal of Biological Macromolecules*. https://doi.org/10.1016/j.ijbiomac.2017.11.046

Darvishi, E., Kahrizi, D., & Arkan, E. (2019). Comparison of different properties of zinc oxide nanoparticles synthesized by the green (using Juglans regia L. leaf extract) and chemical methods. *Journal of Molecular Liquids*, *286*, 110831. https://doi.org/10.1016/J.MOLLIQ.2019.04.108

Deng, P., Jin, W., Liu, Z., Gao, M., & Zhou, J. (2021). Novel multifunctional adenine-modified chitosan dressings for promoting wound healing. *Carbohydrate Polymers*, *260*, 117767. https://doi.org/10.1016/j.carbpol.2021.117767

Dhali, K., Ghasemlou, M., Daver, F., Cass, P., & Adhikari, B. (2021). A review of nanocellulose as a new material towards environmental sustainability. In *Science of the Total Environment* (Vol. 775, p. 145871). Elsevier B.V. https://doi.org/10.1016/j.scitotenv.2021.145871

Dhandapani, K. V., Anbumani, D., Gandhi, A. D., Annamalai, P., Muthuvenkatachalam, B. S., Kavitha, P., & Ranganathan, B. (2020). Green route for the synthesis of zinc oxide nanoparticles from Melia azedarach leaf extract and evaluation of their

antioxidant and antibacterial activities. *Biocatalysis and Agricultural Biotechnology*, *24*, 101517. https://doi.org/10.1016/J.BCAB.2020.101517

Dhapte, V., Gaikwad, N., More, P. v., Banerjee, S., Dhapte, V. v., Kadam, S., & Khanna, P. K. (2015). Transparent ZnO/polycarbonate nanocomposite for food packaging application. *Nanocomposites*, *1*(2), 106–112. https://doi.org/10.1179/2055033215Y.0000000004

Dhivya, S., Padma, V. V., & Santhini, E. (2015). Wound dressings - A review. *BioMedicine (Netherlands)*, *5*(4), 24–28. https://doi.org/10.7603/s40681-015-0022-9

Dovedytis, M., Liu, Z. J., & Bartlett, S. (2020). Hyaluronic acid and its biomedical applications: A review. *Engineered Regeneration*, *1*, 102–113. https://doi.org/10.1016/j.engreg.2020.10.001

Dural Erem, A., Ozcan, G., & Skrifvars, M. (2011). Antibacterial activity of PA6/ZnO nanocomposite fibers. *Textile Research Journal*, *81*(16), 1638–1646. https://doi.org/10.1177/0040517511407380

el Saeed, A. M., El-Fattah, M. A., & Azzam, A. M. (2015). Synthesis of ZnO nanoparticles and studying its influence on the antimicrobial, anticorrosion and mechanical behavior of polyurethane composite for surface coating. *Dyes and Pigments*, *121*, 282–289. https://doi.org/10.1016/j.dyepig.2015.05.037

El-Nahhal, I. M., Salem, J., Anbar, R., Kodeh, F. S., & Elmanama, A. (2020). Preparation and antimicrobial activity of ZnO-NPs coated cotton/starch and their functionalized ZnO-Ag/cotton and Zn(II) curcumin/cotton materials. *Scientific Reports*, *10*(1), 1–10. https://doi.org/10.1038/s41598-020-61306-6

Elumalai, K., Velmurugan, S., Ravi, S., Kathiravan, V., & Adaikala Raj, G. (2015). Bio-approach: Plant mediated synthesis of ZnO nanoparticles and their catalytic reduction of methylene blue and antimicrobial activity. *Advanced Powder Technology*, *26*(6), 1639–1651. https://doi.org/10.1016/J.APT.2015.09.008

Espitia, P. J. P., Soares, N. de F. F., Coimbra, J. S. dos R., de Andrade, N. J., Cruz, R. S., & Medeiros, E. A. A. (2012). Zinc Oxide Nanoparticles: Synthesis, Antimicrobial Activity and Food Packaging Applications. In *Food and Bioprocess Technology* (Vol. 5, Issue 5, pp. 1447–1464). Springer. https://doi.org/10.1007/s11947-012-0797-6

Feroz, S., Muhammad, N., Ranayake, J., & Dias, G. (2020). Keratin - Based materials for biomedical applications. In *Bioactive Materials* (Vol. 5, Issue 3, pp. 496–509). KeAi Communications Co. https://doi.org/10.1016/j.bioactmat.2020.04.007

Garino, N., Limongi, T., Dumontel, B., Canta, M., Racca, L., Laurenti, M., Castellino, M., Casu, A., Falqui, A., & Cauda, V. (2019). *A Microwave-Assisted Synthesis of Zinc Oxide Nanocrystals Finely Tuned for Biological Applications*. https://doi.org/10.3390/nano9020212

Garino, N., Sanvitale, P., Dumontel, B., Laurenti, M., Colilla, M., Izquierdo-Barba, I., Cauda, V., & Vallet-Regì, M. (2019). Zinc oxide nanocrystals as a nanoantibiotic and osteoinductive agent. *RSC Advances*, *9*(20), 11312–11321. https://doi.org/10.1039/C8RA10236H

George, D., Maheswari, P. U., & Begum, K. M. M. S. (2019). Synergic formulation of onion peel quercetin loaded chitosan-cellulose hydrogel with green zinc oxide nanoparticles towards controlled release, biocompatibility, antimicrobial and anticancer activity. *International Journal of Biological Macromolecules*, *132*, 784–794. https://doi.org/10.1016/j.ijbiomac.2019.04.008

George, D., Maheswari, P. U., & Begum, K. M. M. S. (2020a). Chitosan-cellulose hydrogel conjugated with L-histidine and zinc oxide nanoparticles for sustained drug delivery: Kinetics and in-vitro biological studies. *Carbohydrate Polymers*, *236*, 116101. https://doi.org/10.1016/J.CARBPOL.2020.116101

George, D., Maheswari, P. U., & Begum, K. M. M. S. (2020b). Chitosan-cellulose hydrogel conjugated with L-histidine and zinc oxide nanoparticles for sustained drug delivery: Kinetics and in-vitro biological studies. *Carbohydrate Polymers*, *236*, 116101. https://doi.org/10.1016/J.CARBPOL.2020.116101

Gong, X., Tang, C. Y., Pan, L., Hao, Z., & Tsui, C. P. (2014). Characterization of poly(vinyl alcohol) (PVA)/ZnO nanocomposites prepared by a one-pot method. *Composites Part B: Engineering*, *60*, 144–149. https://doi.org/10.1016/J.COMPOSITESB.2013.12.045

Gopi, S., Balakrishnan, P., Chandradhara, D., Poovathankandy, D., & Thomas, S. (2019). General scenarios of cellulose and its use in the biomedical field. In *Materials Today Chemistry* (Vol. 13, pp. 59–78). Elsevier Ltd. https://doi.org/10.1016/j.mtchem.2019.04.012

Gopinath, D., Ahmed, M. R., Gomathi, K., Chitra, K., Sehgal, P. K., & Jayakumar, R. (2004). Dermal wound healing processes with curcumin incorporated collagen films. *Biomaterials*, *25*(10), 1911–1917. https://doi.org/10.1016/S0142-9612(03)00625-2

Graça, M. F. P., Miguel, S. P., Cabral, C. S. D., & Correia, I. J. (2020). Hyaluronic acid—Based wound dressings: A review. In *Carbohydrate Polymers* (Vol. 241, p. 116364). Elsevier Ltd. https://doi.org/10.1016/j.carbpol.2020.116364

Grip, J., Engstad, R. E., Skjæveland, I., Škalko-Basnet, N., Isaksson, J., Basnet, P., & Holsæter, A. M. (2018). Beta-glucan-loaded nanofiber dressing improves wound healing in diabetic mice. *European Journal of Pharmaceutical Sciences*, *121*, 269–280. https://doi.org/10.1016/J.EJPS.2018.05.031

Gunalan, S., Sivaraj, R., & Rajendran, V. (2012). Green synthesized ZnO nanoparticles against bacterial and fungal pathogens. *Progress in Natural Science: Materials International*, *22*(6), 693–700. https://doi.org/10.1016/j.pnsc.2012.11.015

Gupta, A., Keddie, D. J., Kannappan, V., Gibson, H., Khalil, I. R., Kowalczuk, M., Martin, C., Shuai, X., & Radecka, I. (2019). Production and characterisation of bacterial cellulose hydrogels loaded with curcumin encapsulated in cyclodextrins as wound dressings. *European Polymer Journal*, *118*, 437–450. https://doi.org/10.1016/j.eurpolymj.2019.06.018

Gupta, M., Mahajan, V. K., Mehta, K. S., & Chauhan, P. S. (2014). Zinc therapy in dermatology: A review. *Dermatology Research and Practice*, *2014*. https://doi.org/10.1155/2014/709152

Happy Agarwal, Soumya Menon, Venkat Kumar, S., & Rajeshkumar, S. (2018). Mechanistic study on antibacterial action of zinc oxide nanoparticles synthesized using green route. *Chemico-Biological Interactions*, *286*, 60–70. https://doi.org/10.1016/J.CBI.2018.03.008

Hashem, M., Sharaf, S., Abd El-Hady, M. M., & Hebeish, A. (2013). Synthesis and characterization of novel carboxymethylcellulose hydrogels and carboxymethylcellulolse-hydrogel-ZnO-nanocomposites. *Carbohydrate Polymers*, *95*(1), 421–427. https://doi.org/10.1016/j.carbpol.2013.03.013

Helander, I. M., Nurmiaho-Lassila, E. L., Ahvenainen, R., Rhoades, J., & Roller, S. (2001). Chitosan disrupts the barrier properties of the outer membrane of Gram-

negative bacteria. *International Journal of Food Microbiology*, *71*(2–3), 235–244. https://doi.org/10.1016/S0168-1605(01)00609-2

Hemamalini, T., & Giri Dev, V. R. (2018). Comprehensive review on electrospinning of starch polymer for biomedical applications. In *International Journal of Biological Macromolecules* (Vol. 106, pp. 712–718). Elsevier B.V. https://doi.org/10.1016/j.ijbiomac.2017.08.079

Hezma, A. M., Rajeh, A., & Mannaa, M. A. (2019). An insight into the effect of zinc oxide nanoparticles on the structural, thermal, mechanical properties and antimicrobial activity of Cs/PVA composite. *Colloids and Surfaces A: Physicochemical and Engineering Aspects*, *581*, 123821. https://doi.org/10.1016/J.COLSURFA.2019.123821

Ho, N. A. D., & Leo, C. P. (2021). A review on the emerging applications of cellulose, cellulose derivatives and nanocellulose in carbon capture. *Environmental Research*, *197*, 111100. https://doi.org/10.1016/j.envres.2021.111100

Ho, T. T. P., Doan, V. K., Tran, N. M. P., Nguyen, L. K. K., Le, A. N. M., Ho, M. H., Trinh, N. T., van Vo, T., Tran, L. D., & Nguyen, T. H. (2021). Fabrication of chitosan oligomer-coated electrospun polycaprolactone membrane for wound dressing application. *Materials Science and Engineering C*, *120*, 111724. https://doi.org/10.1016/j.msec.2020.111724

Hu, T., Wu, G. P., Bu, H., Zhang, H., Li, W. X., Song, K., & Jiang, G. B. (2022). An injectable, adhesive, and self-healable composite hydrogel wound dressing with excellent antibacterial activity. *Chemical Engineering Journal*, *450*, 138201. https://doi.org/10.1016/J.CEJ.2022.138201

Hu, X., Jia, X., Zhi, C., Jin, Z., & Miao, M. (2019). Improving the properties of starch-based antimicrobial composite films using ZnO-chitosan nanoparticles. *Carbohydrate Polymers*, *210*, 204–209. https://doi.org/10.1016/j.carbpol.2019.01.043

Indumathi, M. P., Saral Sarojini, K., & Rajarajeswari, G. R. (2019a). Antimicrobial and biodegradable chitosan/cellulose acetate phthalate/ZnO nano composite films with optimal oxygen permeability and hydrophobicity for extending the shelf life of black grape fruits. *International Journal of Biological Macromolecules*, *132*, 1112–1120. https://doi.org/10.1016/J.IJBIOMAC.2019.03.171

Indumathi, M. P., Saral Sarojini, K., & Rajarajeswari, G. R. (2019b). Antimicrobial and biodegradable chitosan/cellulose acetate phthalate/ZnO nano composite films with optimal oxygen permeability and hydrophobicity for extending the shelf life of black grape fruits. *International Journal of Biological Macromolecules*, *132*, 1112–1120. https://doi.org/10.1016/j.ijbiomac.2019.03.171

Irastorza, A., Zarandona, I., Andonegi, M., Guerrero, P., & de la Caba, K. (2021). The versatility of collagen and chitosan: From food to biomedical applications. In *Food Hydrocolloids* (Vol. 116, p. 106633). Elsevier B.V. https://doi.org/10.1016/j.foodhyd.2021.106633

Jaberifard, F., Ramezani, S., Ghorbani, M., Arsalani, N., & Mortazavi Moghadam, F. (2022). Investigation of wound healing efficiency of multifunctional eudragit/soy protein isolate electrospun nanofiber incorporated with ZnO loaded halloysite nanotubes and allantoin. *International Journal of Pharmaceutics*, 122434. https://doi.org/10.1016/J.IJPHARM.2022.122434

Jalaja, K., Kumar, P. R. A., Dey, T., Kundu, S. C., & James, N. R. (2014). Modified dextran cross-linked electrospun gelatin nanofibres for biomedical applications. *Carbohydrate Polymers*, *114*, 467–475. https://doi.org/10.1016/j.carbpol.2014.08.023

Jayakumar, R., Sudheesh Kumar, P., Mohandas, A., Lakshmanan, V.-K., & Biswas, R. (2015). Exploration of alginate hydrogel/nano zinc oxide composite bandages for infected wounds. *International Journal of Nanomedicine*, *10*(Supplement 1 Challenges in biomaterials research), 53. https://doi.org/10.2147/IJN.S79981

Jiang, J., Pi, J., & Cai, J. (2018). The Advancing of Zinc Oxide Nanoparticles for Biomedical Applications. In *Bioinorganic Chemistry and Applications*. https://doi.org/10.1155/2018/1062562

Jiang, W., Yang, K., Vachet, R. W., & Xing, B. (2010). Interaction between oxide nanoparticles and biomolecules of the bacterial cell envelope as examined by infrared spectroscopy. *Langmuir*, *26*(23), 18071–18077. https://doi.org/10.1021/LA103738E/SUPPL_FILE/LA103738E_SI_001.PDF

Jin, T., Yan, L., Liu, W., Liu, S., Liu, C., & Zheng, L. (2021). Preparation and physicochemical/antimicrobial characteristics of asparagus cellulose films containing quercetin. *Food Science and Human Wellness*, *10*(2), 251–257. https://doi.org/10.1016/j.fshw.2021.02.015

K., S. S., Indumathi, M. P., & Rajarajeswari, G. R. (2019). Mahua oil-based polyurethane/chitosan/nano ZnO composite films for biodegradable food packaging applications. *International Journal of Biological Macromolecules*, *124*, 163–174. https://doi.org/10.1016/j.ijbiomac.2018.11.195

K., S. S., M.P., I., & G.R., R. (2019). Mahua oil-based polyurethane/chitosan/nano ZnO composite films for biodegradable food packaging applications. *International Journal of Biological Macromolecules*, *124*, 163–174. https://doi.org/10.1016/J.IJBIOMAC.2018.11.195

Kajbafvala, A., Zanganeh, S., Kajbafvala, E., Zargar, H. R., Bayati, M. R., & Sadrnezhaad, S. K. (2010). Microwave-assisted synthesis of narcis-like zinc oxide nanostructures. *Journal of Alloys and Compounds*, *497*(1–2), 325–329. https://doi.org/10.1016/j.jallcom.2010.03.057

Kakiuchi, K., Hosono, E., Kimura, T., Imai, H., & Fujihara, S. (2006). Fabrication of mesoporous ZnO nanosheets from precursor templates grown in aqueous solutions. *Journal of Sol-Gel Science and Technology*, *39*(1 SPEC. ISS.), 63–72. https://doi.org/10.1007/s10971-006-6321-6

Kalai Selvan, N., Shanmugarajan, T. S., & Uppuluri, V. N. V. A. (2020). Hydrogel based scaffolding polymeric biomaterials: Approaches towards skin tissue regeneration. In *Journal of Drug Delivery Science and Technology* (Vol. 55, p. 101456). Editions de Sante. https://doi.org/10.1016/j.jddst.2019.101456

Kanmani, P., & Rhim, J.-W. (2014). Properties and characterization of bionanocomposite films prepared with various biopolymers and ZnO nanoparticles. *Carbohydrate Polymers*, *106*, 190–199. https://doi.org/10.1016/J.CARBPOL.2014.02.007

Khalid, A., Khan, R., Ul-Islam, M., Khan, T., & Wahid, F. (2017). Bacterial cellulose-zinc oxide nanocomposites as a novel dressing system for burn wounds. *Carbohydrate Polymers*, *164*, 214–221. https://doi.org/10.1016/J.CARBPOL.2017.01.061

Khan, M. F., Ansari, A. H., Hameedullah, M., Ahmad, E., Husain, F. M., Zia, Q., Baig, U., Zaheer, M. R., Alam, M. M., Khan, A. M., Alothman, Z. A., Ahmad, I., Ashraf, G. M., & Aliev, G. (2016). Sol-gel synthesis of thorn-like ZnO nanoparticles endorsing mechanical stirring effect and their antimicrobial activities: Potential role

as nano-Antibiotics. *Scientific Reports*, *6*(1), 1–12. https://doi.org/10.1038/srep27689

Khorasani, M. T., Joorabloo, A., Moghaddam, A., Shamsi, H., & MansooriMoghadam, Z. (2018). Incorporation of ZnO nanoparticles into heparinised polyvinyl alcohol/chitosan hydrogels for wound dressing application. *International Journal of Biological Macromolecules*, *114*, 1203–1215. https://doi.org/10.1016/j.ijbiomac.2018.04.010

Kim, J. H., Joshi, M. K., Lee, J., Park, C. H., & Kim, C. S. (2018). Polydopamine-assisted immobilization of hierarchical zinc oxide nanostructures on electrospun nanofibrous membrane for photocatalysis and antimicrobial activity. *Journal of Colloid and Interface Science*, *513*, 566–574. https://doi.org/10.1016/J.JCIS.2017.11.061

King, B., Barrett, S., & Cutting, K. F. (2017). Clinical evaluation of a bioactive beta-glucan gel in the treatment of 'hard-to-heal' wounds. *Https://Doi.Org/10.12968/Jowc.2017.26.2.58*, *26*(2), 58–63. https://doi.org/10.12968/JOWC.2017.26.2.58

Klemm, D., Petzold-Welcke, K., Kramer, F., Richter, T., Raddatz, V., Fried, W., Nietzsche, S., Bellmann, T., & Fischer, D. (2021). Biotech nanocellulose: A review on progress in product design and today's state of technical and medical applications. In *Carbohydrate Polymers* (Vol. 254, p. 117313). Elsevier Ltd. https://doi.org/10.1016/j.carbpol.2020.117313

Koehler, J., Brandl, F. P., & Goepferich, A. M. (2018). Hydrogel wound dressings for bioactive treatment of acute and chronic wounds. In *European Polymer Journal* (Vol. 100, pp. 1–11). Elsevier Ltd. https://doi.org/10.1016/j.eurpolymj.2017.12.046

Kwak, H. W., Kim, J. E., & Lee, K. H. (2019). Green fabrication of antibacterial gelatin fiber for biomedical application. *Reactive and Functional Polymers*, *136*, 86–94. https://doi.org/10.1016/j.reactfunctpolym.2018.12.020

Li, L.-H., Deng, J.-C., Deng, H.-R., Liu, Z.-L., & Li, X.-L. (2010). Preparation, characterization and antimicrobial activities of chitosan/Ag/ZnO blend films. *Chemical Engineering Journal*, *160*(1), 378–382. https://doi.org/10.1016/J.CEJ.2010.03.051

Li, M., Li, G., Jiang, J., Tao, Y., & Mai, K. (2013). Preparation, antimicrobial, crystallization and mechanical properties of nano-ZnO-supported zeolite filled polypropylene random copolymer composites. *Composites Science and Technology*, *81*, 30–36. https://doi.org/10.1016/J.COMPSCITECH.2013.03.020

Li, X. fang, Feng, X. qiang, Yang, S., Fu, G. qing, Wang, T. pu, & Su, Z. xing. (2010). Chitosan kills Escherichia coli through damage to be of cell membrane mechanism. *Carbohydrate Polymers*, *79*(3), 493–499. https://doi.org/10.1016/j.carbpol.2009.07.011

Liu, H., Du, Y., Wang, X., & Sun, L. (2004). Chitosan kills bacteria through cell membrane damage. *International Journal of Food Microbiology*, *95*(2), 147–155. https://doi.org/10.1016/j.ijfoodmicro.2004.01.022

Loera-Valencia, R., Neira, R. E., Urbina, B. P., Camacho, A., & Galindo, R. B. (2022). Evaluation of the therapeutic efficacy of dressings with ZnO nanoparticles in the treatment of diabetic foot ulcers. *Biomedicine & Pharmacotherapy*, *155*, 113708. https://doi.org/10.1016/J.BIOPHA.2022.113708

Lu, S., Zhang, X., Tang, Z., Xiao, H., Zhang, M., Liu, K., Chen, L., Huang, L., Ni, Y., & Wu, H. (2021). Mussel-inspired blue-light-activated cellulose-based adhesive hydrogel with fast gelation, rapid haemostasis and antibacterial property for wound healing. *Chemical Engineering Journal*, *417*, 129329. https://doi.org/10.1016/j.cej.2021.129329

Lu, Z., Gao, J., He, Q., Wu, J., Liang, D., Yang, H., & Chen, R. (2017). Enhanced antibacterial and wound healing activities of microporous chitosan-Ag/ZnO composite dressing. *Carbohydrate Polymers*, *156*, 460–469. https://doi.org/10.1016/j.carbpol.2016.09.051

Ma, J., & Underhill, D. M. (2013). β-glucan signaling connects phagocytosis to autophagy. *Glycobiology*, *23*(9), 1047–1051. https://doi.org/10.1093/GLYCOB/CWT046

Ma, X. Y., & Zhang, W. de. (2009). Effects of flower-like ZnO nanowhiskers on the mechanical, thermal and antibacterial properties of waterborne polyurethane. *Polymer Degradation and Stability*, *94*(7), 1103–1109. https://doi.org/10.1016/j.polymdegradstab.2009.03.024

Majtan, J., & Jesenak, M. (2018). β-Glucans: Multi-Functional Modulator of Wound Healing. *Molecules 2018, Vol. 23, Page 806*, *23*(4), 806. https://doi.org/10.3390/MOLECULES23040806

Mallakpour, S., Azadi, E., & Hussain, C. M. (2021). State-of-the-art of 3D printing technology of alginate-based hydrogels—An emerging technique for industrial applications. *Advances in Colloid and Interface Science*, *293*, 102436. https://doi.org/10.1016/j.cis.2021.102436

Mao, Z., Bai, J., Jin, X., Mao, W., & Dong, Y. (2021a). Construction of a multifunctional 3D nanofiber aerogel loaded with ZnO for wound healing. *Colloids and Surfaces B: Biointerfaces*, *208*, 112070. https://doi.org/10.1016/J.COLSURFB.2021.112070

Mao, Z., Bai, J., Jin, X., Mao, W., & Dong, Y. (2021b). Construction of a multifunctional 3D nanofiber aerogel loaded with ZnO for wound healing. *Colloids and Surfaces B: Biointerfaces*, *208*, 112070. https://doi.org/10.1016/J.COLSURFB.2021.112070

McLellan, J., Thornhill, S. G., Shelton, S., & Kumar, M. (2019). Keratin-Based Biofilms, Hydrogels, and Biofibers. In *Keratin as a Protein Biopolymer* (pp. 187–200). Springer, Cham. https://doi.org/10.1007/978-3-030-02901-2_7

Miguel, S. P., Moreira, A. F., & Correia, I. J. (2019). Chitosan based-asymmetric membranes for wound healing: A review. In *International Journal of Biological Macromolecules* (Vol. 127, pp. 460–475). Elsevier B.V. https://doi.org/10.1016/j.ijbiomac.2019.01.072

Mishra, P. K., Mishra, H., Ekielski, A., Talegaonkar, S., & Vaidya, B. (2017). Zinc oxide nanoparticles: a promising nanomaterial for biomedical applications. *Drug Discovery Today*, *22*(12), 1825–1834. https://doi.org/10.1016/J.DRUDIS.2017.08.006

Moeini, A., Pedram, P., Makvandi, P., Malinconico, M., & Gomez d'Ayala, G. (2020). Wound healing and antimicrobial effect of active secondary metabolites in chitosan-based wound dressings: A review. In *Carbohydrate Polymers* (Vol. 233, p. 115839). Elsevier Ltd. https://doi.org/10.1016/j.carbpol.2020.115839

Mohammadi, Z., Eini, M., Rastegari, A., & Tehrani, M. R. (2021). Chitosan as a machine for biomolecule delivery: A review. In *Carbohydrate Polymers* (Vol. 256, p. 117414). Elsevier Ltd. https://doi.org/10.1016/j.carbpol.2020.117414

Mujeeb Rahman, P., Abdul Mujeeb, V. M., Muraleedharan, K., & Thomas, S. K. (2018). Chitosan/nano ZnO composite films: Enhanced mechanical, antimicrobial and dielectric properties. *Arabian Journal of Chemistry*, *11*(1), 120–127. https://doi.org/10.1016/J.ARABJC.2016.09.008

Nafchi, A. M., Alias, A. K., Mahmud, S., & Robal, M. (2012). Antimicrobial, rheological, and physicochemical properties of sago starch films filled with nanorod-rich zinc oxide. *Journal of Food Engineering*, *113*(4), 511–519. https://doi.org/10.1016/j.jfoodeng.2012.07.017

Namazi, H., Hasani, M., & Yadollahi, M. (2019). Antibacterial oxidized starch/ZnO nanocomposite hydrogel: Synthesis and evaluation of its swelling behaviours in various pHs and salt solutions. *International Journal of Biological Macromolecules*, *126*, 578–584. https://doi.org/10.1016/J.IJBIOMAC.2018.12.242

Naserian, F., & Mesgar, A. S. (2022). Development of antibacterial and superabsorbent wound composite sponges containing carboxymethyl cellulose/gelatin/Cu-doped ZnO nanoparticles. *Colloids and Surfaces B: Biointerfaces*, *218*, 112729. https://doi.org/10.1016/J.COLSURFB.2022.112729

New Collagen-Dextran-Zinc Oxide Composites for Wound Dressing. (n.d.). https://doi.org/10.1155/2016/5805034

Noshirvani, N., Ghanbarzadeh, B., Mokarram, R. R., Hashemi, M., & Coma, V. (2017). Preparation and characterization of active emulsified films based on chitosan-carboxymethyl cellulose containing zinc oxide nano particles. *International Journal of Biological Macromolecules*, *99*, 530–538. https://doi.org/10.1016/j.ijbiomac.2017.03.007

Pandiselvi, K., & Thambidurai, S. (2015). Synthesis, characterization, and antimicrobial activity of chitosan-zinc oxide/polyaniline composites. *Materials Science in Semiconductor Processing*, *31*, 573–581. https://doi.org/10.1016/j.mssp.2014.12.044

Paper, N., & Submission, P. (2016). *Synthesis of Zinc Oxide Nanoparticles via Sol – Gel Route and Their Characterization Synthesis of Zinc Oxide Nanoparticles via Sol – Gel Route and Their Characterization Synthesis of Zinc Oxide Nanoparticles via Sol – Gel Route and Their Characterization*. *5*(2009), 2010–2014. https://doi.org/10.5923/j.nn.20150501.01

Peighambardoust, S. J., Peighambardoust, S. H., Mohammadzadeh Pournasir, N., & Pakdel, P. (2019). Properties of active starch-based films incorporating a combination of Ag, ZnO and CuO nanoparticles for potential use in food packaging applications. *Food Packaging and Shelf Life*, *22*. https://doi.org/10.1016/j.fpsl.2019.100420

Petchwattana, N., Covavisaruch, S., Wibooranawong, S., & Naknaen, P. (2016). Antimicrobial food packaging prepared from poly(butylene succinate) and zinc oxide. *Measurement*, *93*, 442–448. https://doi.org/10.1016/J.MEASUREMENT.2016.07.048

Phan, D.-N., Rebia, R. A., Saito, Y., Kharaghani, D., Khatri, M., Tanaka, T., Lee, H., & Kim, I.-S. (2020). Zinc oxide nanoparticles attached to polyacrylonitrile nanofibers with hinokitiol as gluing agent for synergistic antibacterial activities and effective dye removal. *Journal of Industrial and Engineering Chemistry*. https://doi.org/10.1016/J.JIEC.2020.02.008

Pino, P., Ronchetti, S., Mollea, C., Sangermano, M., Onida, B., & Bosco, F. (2021). Whey Proteins–Zinc Oxide Bionanocomposite as Antibacterial Films. *Pharmaceutics 2021, Vol. 13, Page 1426*, *13*(9), 1426. https://doi.org/10.3390/PHARMACEUTICS13091426

Pittarate, C., Yoovidhya, T., Srichumpuang, W., Intasanta, N., & Wongsasulak, S. (2011). Effects of poly(ethylene oxide) and ZnO nanoparticles on the morphology, tensile and thermal properties of cellulose acetate nanocomposite fibrous film. *Polymer Journal*, *43*(12), 978–986. https://doi.org/10.1038/pj.2011.97

Ponnamma, D., Cabibihan, J. J., Rajan, M., Pethaiah, S. S., Deshmukh, K., Gogoi, J. P., Pasha, S. K. K., Ahamed, M. B., Krishnegowda, J., Chandrashekar, B. N., Polu, A. R., & Cheng, C. (2019). Synthesis, optimization and applications of ZnO/polymer nanocomposites. *Materials Science and Engineering: C*, *98*, 1210–1240. https://doi.org/10.1016/J.MSEC.2019.01.081

Pormohammad, A., Monych, N. K., Ghosh, S., Turner, D. L., & Turner, R. J. (2021). Nanomaterials in Wound Healing and Infection Control. *Antibiotics 2021, Vol. 10, Page 473*, *10*(5), 473. https://doi.org/10.3390/ANTIBIOTICS10050473

Prasert, A., Sontikaew, S., Sriprapai, D., & Chuangchote, S. (2020). Polypropylene/ZnO Nanocomposites: Mechanical Properties, Photocatalytic Dye Degradation, and Antibacterial Property. *Materials*, *13*(4). https://doi.org/10.3390/ma13040914

Priyadarshi, R., & Negi, Y. S. (2017). Effect of Varying Filler Concentration on Zinc Oxide Nanoparticle Embedded Chitosan Films as Potential Food Packaging Material. *Journal of Polymers and the Environment*, *25*(4), 1087–1098. https://doi.org/10.1007/s10924-016-0890-4

Raghav, N., Sharma, M. R., & Kennedy, J. F. (2021). Nanocellulose: A mini-review on types and use in drug delivery systems. *Carbohydrate Polymer Technologies and Applications*, *2*, 100031. https://doi.org/10.1016/j.carpta.2020.100031

Raguvaran, R., Manuja, B. K., Chopra, M., Thakur, R., Anand, T., Kalia, A., & Manuja, A. (2017). Sodium alginate and gum acacia hydrogels of ZnO nanoparticles show wound healing effect on fibroblast cells. *International Journal of Biological Macromolecules*, *96*, 185–191. https://doi.org/10.1016/J.IJBIOMAC.2016.12.009

Rahman, M. M. (2020). Polyurethane/zinc oxide (PU/ZnO) composite-synthesis, protective property and application. In *Polymers* (Vol. 12, Issue 7, p. 1535). MDPI AG. https://doi.org/10.3390/polym12071535

Rahman, P. M., Mujeeb, V. M. A., & Muraleedharan, K. (2017). Flexible chitosan-nano ZnO antimicrobial pouches as a new material for extending the shelf life of raw meat. *International Journal of Biological Macromolecules*, *97*, 382–391. https://doi.org/10.1016/j.ijbiomac.2017.01.052

Rakhshaei, R., & Namazi, H. (2017). A potential bioactive wound dressing based on carboxymethyl cellulose/ZnO impregnated MCM-41 nanocomposite hydrogel. *Materials Science and Engineering: C*, *73*, 456–464. https://doi.org/10.1016/J.MSEC.2016.12.097

Ramirez, D. O. S., Carletto, R. A., Tonetti, C., Giachet, F. T., Varesano, A., & Vineis, C. (2017). Wool keratin film plasticized by citric acid for food packaging. *Food Packaging and Shelf Life*, *12*, 100–106. https://doi.org/10.1016/j.fpsl.2017.04.004

Rao, K. M., Suneetha, M., Zo, S., Duck, K. H., & Han, S. S. (2019). One-pot synthesis of ZnO nanobelt-like structures in hyaluronan hydrogels for wound dressing applications. *Carbohydrate Polymers*, *223*, 115124. https://doi.org/10.1016/J.CARBPOL.2019.115124

Rath, G., Hussain, T., Chauhan, G., Garg, T., & Goyal, A. K. (2016). Development and characterization of cefazolin loaded zinc oxide nanoparticles composite gelatin

nanofiber mats for postoperative surgical wounds. *Materials Science and Engineering C*, *58*, 242–253. https://doi.org/10.1016/j.msec.2015.08.050

Razzaq, H. A. A., Gomez d'Ayala, G., Santagata, G., Bosco, F., Mollea, C., Larsen, N., & Duraccio, D. (2021). Bioactive films based on barley β-glucans and ZnO for wound healing applications. *Carbohydrate Polymers*, *272*, 118442. https://doi.org/10.1016/J.CARBPOL.2021.118442

Reig-Vano, B., Tylkowski, B., Montané, X., & Giamberini, M. (2021). Alginate-based hydrogels for cancer therapy and research. In *International Journal of Biological Macromolecules* (Vol. 170, pp. 424–436). Elsevier B.V. https://doi.org/10.1016/j.ijbiomac.2020.12.161

Roy, S., & Rhim, J.-W. (2019). Carrageenan-based antimicrobial bionanocomposite films incorporated with ZnO nanoparticles stabilized by melanin. *Food Hydrocolloids*, *90*, 500–507. https://doi.org/10.1016/J.FOODHYD.2018.12.056

Rutherford, D., Jíra, J., Kolářová, K., Matolínová, I., Mičová, J., Remeš, Z., & Rezek, B. (2021). Growth Inhibition of Gram-Positive and Gram-Negative Bacteria by Zinc Oxide Hedgehog Particles. *International Journal of Nanomedicine*, *16*, 3541. https://doi.org/10.2147/IJN.S300428

Saputri, A. E., Praseptiangga, D., Rochima, E., Panatarani, C., & Joni, I. M. (2018). Mechanical and solubility properties of bio-nanocomposite film of semi refined kappa carrageenan/ZnO nanoparticles. *AIP Conference Proceedings*, *1927*(1), 030040. https://doi.org/10.1063/1.5021233

Sarika, P. R., Cinthya, K., Jayakrishnan, A., Anilkumar, P. R., & James, N. R. (2014). Modified gum arabic cross-linked gelatin scaffold for biomedical applications. *Materials Science and Engineering C*, *43*, 272–279. https://doi.org/10.1016/j.msec.2014.06.042

Sengul, A. B., & Asmatulu, E. (2020). Toxicity of metal and metal oxide nanoparticles: a review. *Environmental Chemistry Letters 2020 18:5*, *18*(5), 1659–1683. https://doi.org/10.1007/S10311-020-01033-6

Seo, G., Hyun, C., Choi, S., Kim, Y. M., & Cho, M. (2019). The wound healing effect of four types of beta-glucan. *Applied Biological Chemistry*, *62*(1), 1–9. https://doi.org/10.1186/S13765-019-0428-2/FIGURES/5

Shahmohammadi Jebel, F., & Almasi, H. (2016). Morphological, physical, antimicrobial and release properties of ZnO nanoparticles-loaded bacterial cellulose films. *Carbohydrate Polymers*, *149*, 8–19. https://doi.org/10.1016/j.carbpol.2016.04.089

Shahrousvand, M., Haddadi-Asl, V., & Shahrousvand, M. (2021). Step-by-step design of poly (ε-caprolactone) /chitosan/Melilotus officinalis extract electrospun nanofibers for wound dressing applications. *International Journal of Biological Macromolecules*, *180*, 36–50. https://doi.org/10.1016/j.ijbiomac.2021.03.046

Shalaby, M. A., Anwar, M. M., & Saeed, H. (2022). Nanomaterials for application in wound Healing: current state-of-the-art and future perspectives. *Journal of Polymer Research 2022 29:3*, *29*(3), 1–37. https://doi.org/10.1007/S10965-021-02870-X

Shankar, S., & Rhim, J.-W. (2019). Effect of types of zinc oxide nanoparticles on structural, mechanical and antibacterial properties of poly(lactide)/poly(butylene adipate-co-terephthalate) composite films. *Food Packaging and Shelf Life*, *21*, 100327. https://doi.org/10.1016/J.FPSL.2019.100327

Shankar, S., Teng, X., Li, G., & Rhim, J. W. (2015). Preparation, characterization, and antimicrobial activity of gelatin/ZnO nanocomposite films. *Food Hydrocolloids*, *45*, 264–271. https://doi.org/10.1016/j.foodhyd.2014.12.001

Sharma, S., & Gupta, A. (2016). Sustainable Management of Keratin Waste Biomass: Applications and Future Perspectives. *Brazilian Archives of Biology and Technology*, *59*(0). https://doi.org/10.1590/1678-4324-2016150684

Shekh, M. I., Patel, K. P., & Patel, R. M. (2018). Electrospun ZnO Nanoparticles Doped Core–Sheath Nanofibers: Characterization and Antimicrobial Properties. *Journal of Polymers and the Environment*, *26*(12), 4376–4387. https://doi.org/10.1007/s10924-018-1310-8

Sherafatkhah Azari, S., Alizadeh, A., Roufegarinejad, L., Asefi, N., & Hamishehkar, H. (2020). Preparation and characterization of gelatin/β-glucan nanocomposite film incorporated with ZnO nanoparticles as an active food packaging system. *Journal of Polymers and the Environment*, 1–10. https://doi.org/10.1007/s10924-020-01950-1

Shirzaei Sani, E., Portillo-Lara, R., Spencer, A., Yu, W., Geilich, B. M., Noshadi, I., Webster, T. J., & Annabi, N. (2018). Engineering Adhesive and Antimicrobial Hyaluronic Acid/Elastin-like Polypeptide Hybrid Hydrogels for Tissue

Engineering Applications. *ACS Biomaterials Science and Engineering*, *4*(7), 2528–2540. https://doi.org/10.1021/acsbiomaterials.8b00408

Singh, A., Singh, N. B., Afzal, S., Singh, T., & Hussain, I. (2018). Zinc oxide nanoparticles: a review of their biological synthesis, antimicrobial activity, uptake, translocation and biotransformation in plants. *Journal of Materials Science*, *53*(1), 185–201. https://doi.org/10.1007/S10853-017-1544-1/TABLES/4

Singhal, U., Pendurthi, R., & Khanuja, M. (2020). Prunus: A natural source for synthesis of zinc oxide nanoparticles towards photocatalytic and antibacterial applications. *Materials Today: Proceedings*. https://doi.org/10.1016/J.MATPR.2020.01.606

Sirelkhatim, A., Mahmud, S., Seeni, A., Kaus, N. H. M., Ann, L. C., Bakhori, S. K. M., Hasan, H., & Mohamad, D. (2015). Review on zinc oxide nanoparticles: Antibacterial activity and toxicity mechanism. *Nano-Micro Letters*, *7*(3), 219–242. https://doi.org/10.1007/s40820-015-0040-x

Sirohi, S., Singh, R., Jain, N., Pani, B., Dutt, K., & Nain, R. (2017). Synthesis and characterization of multifunctional ZnO/polyester green composite films. *Journal of Polymer Research*, *24*(11), 1–10. https://doi.org/10.1007/s10965-017-1355-8

Siyanbola, T. O., Sasidhar, K., Rao, B. V. S. K., Narayan, R., Olaofe, O., Akintayo, E. T., & Raju, K. V. S. N. (2015). Development of functional polyurethane-ZnO hybrid nanocomposite coatings from thevetia peruviana seed oil. *JAOCS, Journal of the American Oil Chemists' Society*, *92*(2), 267–275. https://doi.org/10.1007/s11746-014-2587-y

Steffy, K., Shanthi, G., Maroky, Anson. S., & Selvakumar, S. (2018). Potential bactericidal activity of S. nux-vomica–ZnO nanocomposite against multidrug-resistant bacterial pathogens and wound-healing properties. *Journal of Trace Elements in Medicine and Biology*, *50*, 229–239. https://doi.org/10.1016/J.JTEMB.2018.07.009

Suarato, G., Bertorelli, R., & Athanassiou, A. (2018). Borrowing from nature: Biopolymers and biocomposites as smart wound care materials. In *Frontiers in Bioengineering and Biotechnology* (Vol. 6, Issue OCT, p. 137). Frontiers Media S.A. https://doi.org/10.3389/fbioe.2018.00137

Sudheesh Kumar, P. T., Lakshmanan, V. K., Anilkumar, T. v., Ramya, C., Reshmi, P., Unnikrishnan, A. G., Nair, S. v., & Jayakumar, R. (2012). Flexible and microporous

chitosan hydrogel/nano ZnO composite bandages for wound dressing: In vitro and in vivo evaluation. In *ACS Applied Materials and Interfaces*. https://doi.org/10.1021/am300292v

Sudheesh Kumar, P. T., Lakshmanan, V. K., Raj, M., Biswas, R., Hiroshi, T., Nair, S. v., & Jayakumar, R. (2013). Evaluation of wound healing potential of β-chitin hydrogel/nano zinc oxide composite bandage. *Pharmaceutical Research*, *30*(2), 523–537. https://doi.org/10.1007/s11095-012-0898-y

Sze, J. H., Brownlie, J. C., & Love, C. A. (2016). Biotechnological production of hyaluronic acid: a mini review. *3 Biotech*, *6*(1), 1–9. https://doi.org/10.1007/S13205-016-0379-9/FIGURES/5

Taghizadeh, M. T., Siyahi, V., Ashassi-Sorkhabi, H., & Zarrini, G. (2020). ZnO, AgCl and AgCl/ZnO nanocomposites incorporated chitosan in the form of hydrogel beads for photocatalytic degradation of MB, E. coli and S. aureus. *International Journal of Biological Macromolecules*, *147*, 1018–1028. https://doi.org/10.1016/J.IJBIOMAC.2019.10.070

Tan, S. T., Winarto, N., Dosan, R., & Aisyah, P. B. (2019). The Benefits Of Occlusive Dressings In Wound Healing. *The Open Dermatology Journal*, *13*(1), 27–33. https://doi.org/10.2174/1874372201913010027

Taraballi, F., Zanini, S., Lupo, C., Panseri, S., Cunha, C., Riccardi, C., Marcacci, M., Campione, M., & Cipolla, L. (2013). Amino and carboxyl plasma functionalization of collagen films for tissue engineering applications. *Journal of Colloid and Interface Science*, *394*(1), 590–597. https://doi.org/10.1016/j.jcis.2012.11.041

Tavakolian, M., Munguia-Lopez, J. G., Valiei, A., Islam, M. S., Kinsella, J. M., Tufenkji, N., & van de Ven, T. G. M. (2020). Highly Absorbent Antibacterial and Biofilm-Disrupting Hydrogels from Cellulose for Wound Dressing Applications. *ACS Applied Materials and Interfaces*, *12*(36), 39991–40001. https://doi.org/10.1021/ACSAMI.0C08784/SUPPL_FILE/AM0C08784_SI_001.PDF

Tavassoli, M., Sani, M. A., Khezerlou, A., Ehsani, A., & McClements, D. J. (2021). Multifunctional nanocomposite active packaging materials: Immobilization of quercetin, lactoferrin, and chitosan nanofiber particles in gelatin films. *Food Hydrocolloids*, *118*, 106747. https://doi.org/10.1016/j.foodhyd.2021.106747

Tavassoli-Kafrani, E., Shekarchizadeh, H., & Masoudpour-Behabadi, M. (2016). Development of edible films and coatings from alginates and carrageenans. In *Carbohydrate Polymers* (Vol. 137, pp. 360–374). Elsevier Ltd. https://doi.org/10.1016/j.carbpol.2015.10.074

Thanusha, A. V., Amit Kumar, D., & Veena, K. (2018). Evaluation of nano hydrogel composite based on gelatin/HA/CS suffused with Asiatic acid/ZnO and CuO nanoparticles for second degree burns. *Materials Science and Engineering: C*, *89*, 378–386. https://doi.org/10.1016/J.MSEC.2018.03.034

Thanusha, A. v., Dinda, A. K., & Koul, V. (2018). Evaluation of nano hydrogel composite based on gelatin/HA/CS suffused with Asiatic acid/ZnO and CuO nanoparticles for second degree burns. *Materials Science and Engineering C*, *89*, 378–386. https://doi.org/10.1016/j.msec.2018.03.034

Thompson, C. B., Wiemken, T. L., & Brown, T. S. (2017). Effect of postoperative dressing on excisions performed on the leg: A comparison between zinc oxide compression dressings versus standard wound care. *Dermatologic Surgery*, *43*(11), 1379–1384. https://doi.org/10.1097/DSS.0000000000001209

Tiwari, V., Mishra, N., Gadani, K., Solanki, P. S., Shah, N. A., & Tiwari, M. (2018). Mechanism of anti-bacterial activity of zinc oxide nanoparticle against Carbapenem-Resistant Acinetobacter baumannii. *Frontiers in Microbiology*, *9*(JUN). https://doi.org/10.3389/fmicb.2018.01218

Torkaman, S., Rahmani, H., Ashori, A., & Najafi, S. H. M. (2021). Modification of chitosan using amino acids for wound healing purposes: A review. In *Carbohydrate Polymers* (Vol. 258, p. 117675). Elsevier Ltd. https://doi.org/10.1016/j.carbpol.2021.117675

Ul-Islam, M., Khattak, W. A., Ullah, M. W., Khan, S., & Park, J. K. (2014). Synthesis of regenerated bacterial cellulose-zinc oxide nanocomposite films for biomedical applications. *Cellulose*, *21*(1), 433–447. https://doi.org/10.1007/s10570-013-0109-y

Urtuvia, V., Maturana, N., Acevedo, F., Peña, C., & Díaz-Barrera, A. (2017). Bacterial alginate production: an overview of its biosynthesis and potential industrial production. *World Journal of Microbiology and Biotechnology*, *33*(11), 1–10. https://doi.org/10.1007/S11274-017-2363-X/TABLES/4

Vaezi, K., Asadpour, G., & Sharifi, H. (2019). Effect of ZnO nanoparticles on the mechanical, barrier and optical properties of thermoplastic cationic starch/montmorillonite biodegradable films. *International Journal of Biological Macromolecules*, *124*, 519–529. https://doi.org/10.1016/j.ijbiomac.2018.11.142

Villanueva, M. E., Cuestas, M. L., Pérez, C. J., Campo Dall′ Orto, V., & Copello, G. J. (2019). Smart release of antimicrobial ZnO nanoplates from a pH-responsive keratin hydrogel. *Journal of Colloid and Interface Science*, *536*, 372–380. https://doi.org/10.1016/J.JCIS.2018.10.067

Waghmode, B. J., Husain, Z., Joshi, M., Sathaye, S. D., Patil, K. R., & Malkhede, D. D. (2016). Synthesis and study of calixarene-doped polypyrrole-TiO2/ZnO composites: Antimicrobial activity and electrochemical sensors. *Journal of Polymer Research*, *23*(2), 1–11. https://doi.org/10.1007/s10965-016-0921-9

Wahid, F., Yin, J.-J., Xue, D.-D., Xue, H., Lu, Y.-S., Zhong, C., & Chu, L.-Q. (2016). Synthesis and characterization of antibacterial carboxymethyl Chitosan/ZnO nanocomposite hydrogels. *International Journal of Biological Macromolecules*, *88*, 273–279. https://doi.org/10.1016/J.IJBIOMAC.2016.03.044

Wang, H., Ding, F., Ma, L., & Zhang, Y. (2021). Edible films from chitosan-gelatin: Physical properties and food packaging application. In *Food Bioscience* (Vol. 40, p. 100871). Elsevier Ltd. https://doi.org/10.1016/j.fbio.2020.100871

Wang, H., Gong, X., Guo, X., Liu, C., Fan, Y.-Y., Zhang, J., Niu, B., & Li, W. (2019). Characterization, release, and antioxidant activity of curcumin-loaded sodium alginate/ZnO hydrogel beads. *International Journal of Biological Macromolecules*, *121*, 1118–1125. https://doi.org/10.1016/J.IJBIOMAC.2018.10.121

Wang, Q., Barnes, L. M., Maslakov, K. I., Howell, C. A., Illsley, M. J., Dyer, P., & Savina, I. N. (2021). In situ synthesis of silver or selenium nanoparticles on cationized cellulose fabrics for antimicrobial application. *Materials Science and Engineering C*, *121*, 111859. https://doi.org/10.1016/j.msec.2020.111859

Wang, Y., Zhang, C., Bi, S., & Luo, G. (2010). Preparation of ZnO nanoparticles using the direct precipitation method in a membrane dispersion micro-structured reactor. *Powder Technology*, *202*(1–3), 130–136. https://doi.org/10.1016/j.powtec.2010.04.027

Wei, D., Zhang, L., Williams, D. L., & Browder, W. (2002). Glucan stimulates human dermal fibroblast collagen biosynthesis through a nuclear factor-1 dependent mechanism. *Wound Repair and Regeneration*, *10*(3), 161–168. https://doi.org/10.1046/J.1524-475X.2002.10804.X

Wessels, I., Maywald, M., & Rink, L. (2017). Zinc as a Gatekeeper of Immune Function. *Nutrients 2017, Vol. 9, Page 1286*, *9*(12), 1286. https://doi.org/10.3390/NU9121286

Wojnarowicz, J., Chudoba, T., & Lojkowski, W. (2020). A review of microwave synthesis of zinc oxide nanomaterials: Reactants, process parameters and morphoslogies. In *Nanomaterials* (Vol. 10, Issue 6, p. 1086). MDPI AG. https://doi.org/10.3390/nano10061086

Yoon, D., Yoon, D., Cha, H. J., Lee, J. S., & Chun, W. (2018). Enhancement of wound healing efficiency mediated by artificial dermis functionalized with EGF or NRG1. *Biomedical Materials (Bristol)*, *13*(4), 045007. https://doi.org/10.1088/1748-605X/aaac37

Younes, I., & Rinaudo, M. (2015). Chitin and Chitosan Preparation from Marine Sources. Structure, Properties and Applications. *Marine Drugs*, *13*(3), 1133. https://doi.org/10.3390/MD13031133

Zahran, M., & Marei, A. H. (2019a). Innovative natural polymer metal nanocomposites and their antimicrobial activity. In *International Journal of Biological Macromolecules* (Vol. 136, pp. 586–596). Elsevier B.V. https://doi.org/10.1016/j.ijbiomac.2019.06.114

Zahran, M., & Marei, A. H. (2019b). Innovative natural polymer metal nanocomposites and their antimicrobial activity. *International Journal of Biological Macromolecules*, *136*, 586–596. https://doi.org/10.1016/J.IJBIOMAC.2019.06.114

Zanini, N. C., Souza, A. G., Barbosa, R. F. S., Rosa, D. S., & Mulinari, D. R. (2021). A novel hybrid polyurethane composites with ZnO particles and sheath palm residues: Synergistic effect. *Polymer Composites*, *42*(1), 532–542. https://doi.org/10.1002/pc.25845

Zanni, E., Chandraiahgari, C., de Bellis, G., Montereali, M., Armiento, G., Ballirano, P., Polimeni, A., Sarto, M., & Uccelletti, D. (2016). Zinc Oxide Nanorods-Decorated Graphene Nanoplatelets: A Promising Antimicrobial Agent against the Cariogenic

Bacterium Streptococcus mutans. *Nanomaterials*, *6*(10), 179. https://doi.org/10.3390/nano6100179

Zare-Akbari, Z., Farhadnejad, H., Furughi-Nia, B., Abedin, S., Yadollahi, M., & Khorsand-Ghayeni, M. (2016). PH-sensitive bionanocomposite hydrogel beads based on caborboxymethyl cellulose/ZnO nanoparticle as drug carrier. *International Journal of Biological Macromolecules*, *93*(Pt A), 1317–1327. https://doi.org/10.1016/j.ijbiomac.2016.09.110

Zhai, M., Xu, Y., Zhou, B., & Jing, W. (2018). Keratin-chitosan/n-ZnO nanocomposite hydrogel for antimicrobial treatment of burn wound healing: Characterization and biomedical application. *Journal of Photochemistry and Photobiology B: Biology*, *180*, 253–258. https://doi.org/10.1016/J.JPHOTOBIOL.2018.02.018

Zhang, M., Qiao, X., Han, W., Jiang, T., Liu, F., & Zhao, X. (2021). Alginate-chitosan oligosaccharide-ZnO composite hydrogel for accelerating wound healing. *Carbohydrate Polymers*, *266*, 118100. https://doi.org/10.1016/J.CARBPOL.2021.118100

Zhou, L., Cai, L., Ruan, H., Zhang, L., Wang, J., Jiang, H., Wu, Y., Feng, S., & Chen, J. (2021). Electrospun chitosan oligosaccharide/polycaprolactone nanofibers loaded with wound-healing compounds of Rutin and Quercetin as antibacterial dressings. *International Journal of Biological Macromolecules*. https://doi.org/10.1016/j.ijbiomac.2021.05.031

Zhou, L., Zhou, L., Wei, C., & Guo, R. (2022). A bioactive dextran-based hydrogel promote the healing of infected wounds via antibacterial and immunomodulatory. *Carbohydrate Polymers*, *291*, 119558. https://doi.org/10.1016/J.CARBPOL.2022.119558

Zou, C., Liang, F., & Xue, S. (2015). Synthesis and oxygen vacancy-related photocatalytic properties of ZnO nanotubes grown by thermal evaporation. *Research on Chemical Intermediates*, *41*(8), 5167–5176. https://doi.org/10.1007/s11164-014-1620-y

Zukas, B. G., & Gupta, N. R. (2017). Interphase Synthesis of Zinc Oxide Nanoparticles in a Droplet Flow Reactor. *Industrial and Engineering Chemistry Research*, *56*(25), 7184–7191. https://doi.org/10.1021/acs.iecr.7b00407

Chapter 3

Big problems, small solutions: nanostructured zinc oxide

3.1 Introduction

Nanostructured zinc oxide (nZnO) is a promising nanomaterial with multiple applications in the biomedical field. Its main features and applications have been already described in Chapter 2. This Chapter will be focused on the nZnO that has been prepared, characterized and used for this work as an antimicrobial agent for the development of new bionanocomposite materials.

3.2 Experimental

3.2.1 Materials

Zinc acetate di-hydrate (≥98%), potassium hydroxide (≥85%), absolute ethanol and commercial zinc oxide powder (average size 230 nm) were purchased from Sigma-Aldrich (St. Louis, MO, USA) and used as received. Mueller Hinton Broth (MHB) and Mueller Hinton Agar (MHA) were supplied by OXOID Ltd (Basingstoke, United Kingdom). Phosphate Buffered Saline (PBS) tablets were purchased from Sigma-Aldrich (St. Louis, MO, USA).

3.2.2 Synthesis of nanostructured zinc oxide

Nanostructured zinc oxide (nZnO) was obtained through a slightly modified wet chemical precipitation method previously described (Banchero et al., 2019), based on the work of Mitra and co-workers (Mitra et al., 2012). Briefly, 29.50 g of zinc acetate dihydrate and 14.8 g of potassium hydroxide were dissolved in 120 mL and 64 mL of ethanol respectively. The two solutions were then mixed and kept at 60 °C for 72 h under constant stirring and reflux. This induced the precipitation of a white powder (about 8.5 g) that was recovered by means of a 30 min centrifugation cycle at 4000 rpm and subsequently washed three times with ethanol.

3.2.3 Characterization of nanostructured zinc oxide

The obtained nZnO was characterized through X-ray diffraction (XRD) using a PANalytical X'Pert Diffractometer (Cu Kα radiation, Almelo, The Netherlands). Field Emission Scanning Electron Microscopy (FESEM) was carried out with a ZEISS Merlin instrument (Oxford Instruments, Abingdon-on-Thames, UK) on both nZnO and commercial ZnO (cZnO). Before measurement, the zinc oxide samples were coated with a 4 nm Pt layer. ImageJ software (open source, https://imagej.net/, accessed 26 August 2021) was used to measure particle size distribution by analyzing 62 particles. Transmission Electron Microscopy (TEM) was carried out with a LVEM5 Benchtop Electron Microscope (Delong America, Montreal, CA) with maximum accelerating voltage of 5 kV. A droplet of 0.2 wt% nZnO suspension previously sonicated for one hour was deposited on a Cu-300HD copper 300 mesh grid with a holey carbon film (Pacific Grid Techgrid, San Francisco, CA, USA) and left for 10 minutes. Excess liquid was removed with a filter paper. Absorbance in the UV-visible spectrum was measured using a a Lambda 465 UV/Vis spectrophotometer (PerkinElmer, Waltham, MA, US) in the 250-800 nm range. For the measurement, a 0,125 mg/mL nZnO suspension in distilled water was prepared and ultrasonicated for 1h. The optical bandgap E_g was established using the equation:

$$E_g = \frac{hc}{\lambda}$$

Where h is the Planck constant, c is the speed of light, and λ is the wavelength of maximum absorption. Nitrogen physisorption measurements were performed using a ASAP2020 Plus Micromeritics apparatus (Norcross, GA, USA). Prior to the measurements, samples were outgassed at 70°C for 2 h. Specific Surface Area

(SSA) was determined based on the Brunauer–Emmet–Teller (BET) model in the relative pressure p/p0 range of 0.01-0.1. Zeta potential and particle size distribution were obtained through Dynamic Light Scattering by means of a Malvern Instruments DLS Zetasizer Nanoseries ZS90 instrument (Malvern, UK). For these measurements, aqueous 0.5 mg/mL nZnO suspensions were prepared at pH of 3, 5 and 7 and sonicated in an Elmasonic ultrasonic bath (Elma Schmidbauer GmbH, Singen, Germany) for 1 h before testing. All measurements were repeated three times. Fourier-Transform Infrared Spectroscopy (FTIR) was performed on nZnO dispersed in potassium bromide using a Bruker Equinox 55 spectrometer (Bruker, Billerica, MA, USA) operating at 2 cm^{-1} resolution. Samples were outgassed at room temperature for 1 h (residual pressure equal to 0.1 Pa) before measurements.

3.2.4 Antibacterial activity

The antibacterial activity of zinc oxide powders was assessed against Gram-positive *Staphylococcus epidermidis*, LMG 10474 and Gram-negative *Escherichia coli*, LMG 08063 bacteria. Mueller Hinton Broth (MHB) and Mueller Hinton Agar (MHA) were used as test media in accordance with standard procedures, as described below.

3.2.4.1 Disk diffusion test

The antibacterial activity of nZnO was tested by means of a modified Kirby–Bauer agar diffusion test following the standard "EUCAST disk diffusion method" (2021) (*EUCAST: Disk Diffusion Methodology*, n.d.) with some adaptations. A standardized inoculum, corresponding to 10^6 CFU/mL, was obtained by dispersing three microbial colonies from an overnight culture at 37 °C on MHA into 5 mL of sterile 0.85% w/v NaCl solution (10^8 CFU/mL) and diluting (1:100) the suspension with MHB. ZnO samples were prepared, in sterile conditions, by dispersing the nZnO in distilled water (pH=6) inside microcentrifuge tubes (capacity 2 mL). The following nZnO concentrations were tested: 25, 20, 17.5, 15, 10, 7.5, 6, 5, 3.75, and 1.92 mg/mL. All the suspensions were sonicated for 60 min at 35 kHz to break down agglomerates and to further disperse ZnO nanoparticles.

A standardized 100 µL inoculum was spread over the surface of MHA Petri dishes. Subsequently, 20 µL of each nZnO suspension was deposited as single droplets equally spaced around the circumference of the Petri dish, while a 20 µL droplet of sterile distilled water was deposited in the center of the dish as a negative control. Petri dishes were incubated at 37 °C for 24 h. All experiments were performed in triplicate. At the end of the incubation, samples were observed, and

inhibition halos were measured as the average distance between the drop outline and that of the bacterial growth, at the two perpendicular diameters (mm). A minimum inhibitory concentration (MIC) value was identified as the lowest concentration where an inhibition halo could be observed.

In order to further assess the effects of particle size and surface area on antimicrobial activity, the same disk diffusion test was repeated with the commercial ZnO powder (cZnO).

3.2.4.2 Broth micro-dilution test

The minimum inhibitory concentration (MIC) and the minimum bactericidal concentration (MBC) of nZnO were determined applying the EUCAST broth microdilution method with some modifications (*EUCAST Reading Guide for Broth Microdilution*, 2022). A standardized inoculum, corresponding to $5x10^5$ CFU/mL, was obtained by dispersing three colonies, taken from an overnight culture grown on MHA at 37°C, into 5 mL of sterile 0.85% w/v NaCl solution and opportunely diluting the suspension with MHB. 96-well plates were filled with 10 µL of inoculum, 50 µL of MHB, and 50 µL of nZnO suspensions with oxide concentrations ranging from 30 to 20000 µg/mL. In the biotic controls the nZnO suspensions were substituted with 50 µL of MHB, while in the abiotic ones the inoculum was substituted with 10 µL of MHB.

MIC was established as the lowest nZnO concentration capable of completely inhibiting the growth of the bacteria as detected by the unaided eye. MBC was determined subculturing, on MHA, 10 µL of the broth dilutions that inhibited bacterial growth (those at or above the MIC); the MBC was the lowest broth dilution of nZnO that prevented the bacterial growth on MHA after 24 hours of incubation at 37°C.

3.3 Results and discussion

3.3.1 Characterization of nZnO

FESEM image shows that nZnO (Figure 3.1A) is obtained in the form of spherical and ovoidal nanoparticles with an average diameter of 30 nm, measured using the ImageJ software (Figure 3.2). The commercial zinc oxide (Figure 3.1B) is instead constituted by larger prismatic particles with hexagonal cross section and sizes ranging from 200 to 500 nm. The TEM picture in Figure 3.3 offers a better visualization of the individual particles further confirming their size and shape.

Figure 3.4 shows the absorption spectrum in the UV-visible spectrum. Maximum absorption is observed at 355 nm, which corresponds to an optical bangap of 3.49 eV.

Figure 3.5 reports the XRD pattern of the powder, revealing that nZnO is characterized by a hexagonal, wurtzite-type crystalline structure (JCPDS ICDD 36-1451 card).

The nitrogen adsorption isotherm is shown in Figure 3.6. The isotherm is type IV.with an hysteresis loop ascribed to interparticles porosity. BET specific surface area (SSA_{BET}) results to be 49,5 m^2/g. This is a relatively high SSA for zinc oxides (G. Dutta & Sugumaran, 2021; T. A. Singh et al., 2021) , and, coupled with the nanometric particles size, is an important factor in view of its final application as antimicrobial agent (Sirelkhatim et al., 2015). The SSA_{BET} measured for cZnO (hysotherm not reported) was only 8 m^2/g.

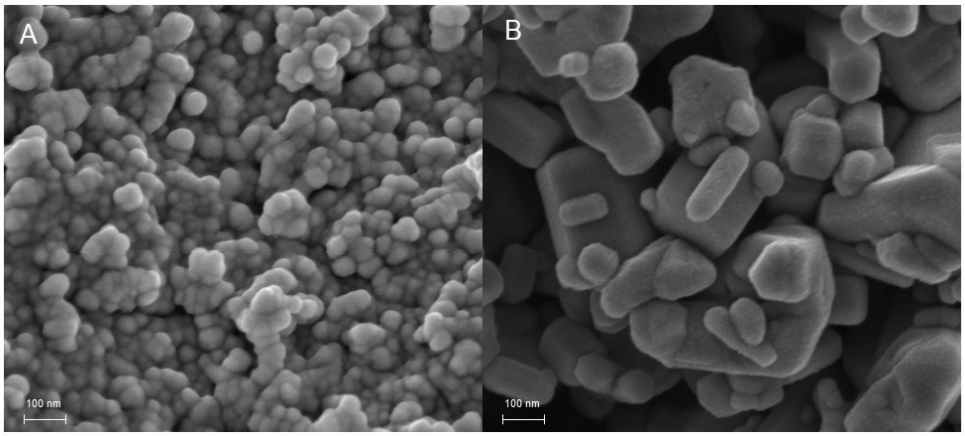


Figure 3.1: FESEM image of nZnO (A) and cZnO (B)

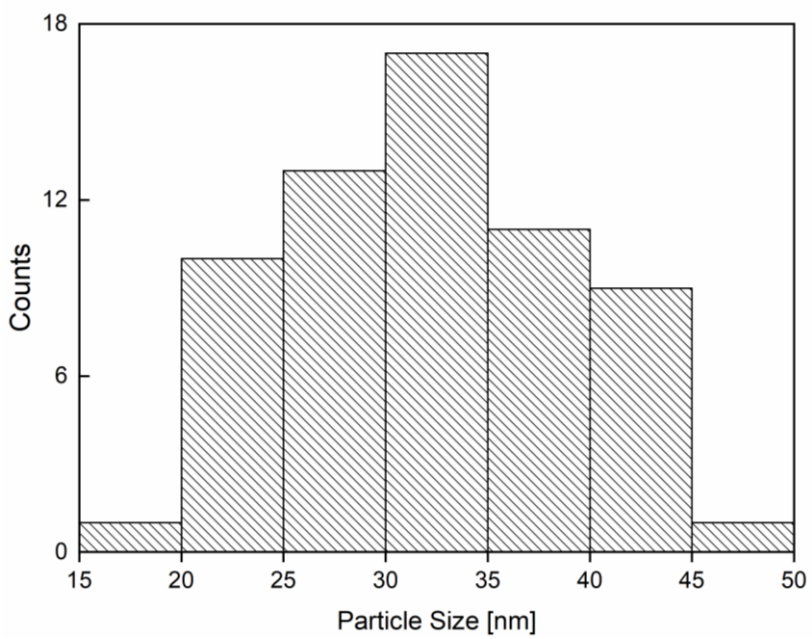


Figure 3.2: nZnO particle size distribution.

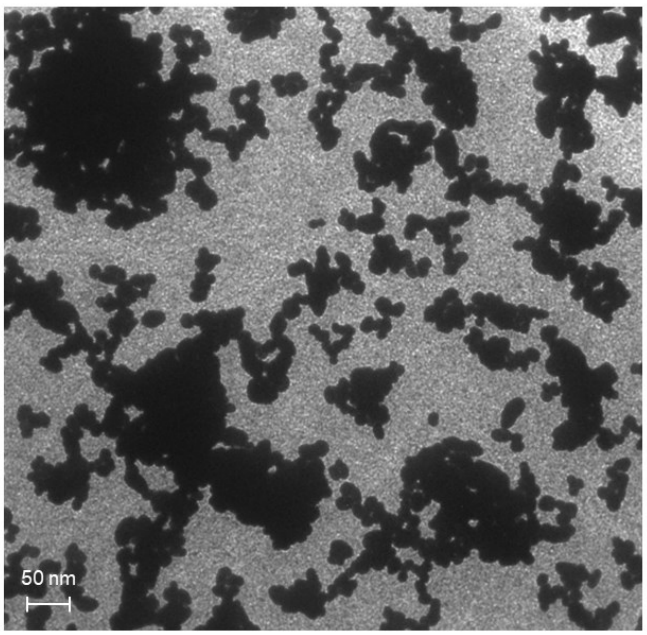


Figure 3.3: TEM image of nZnO

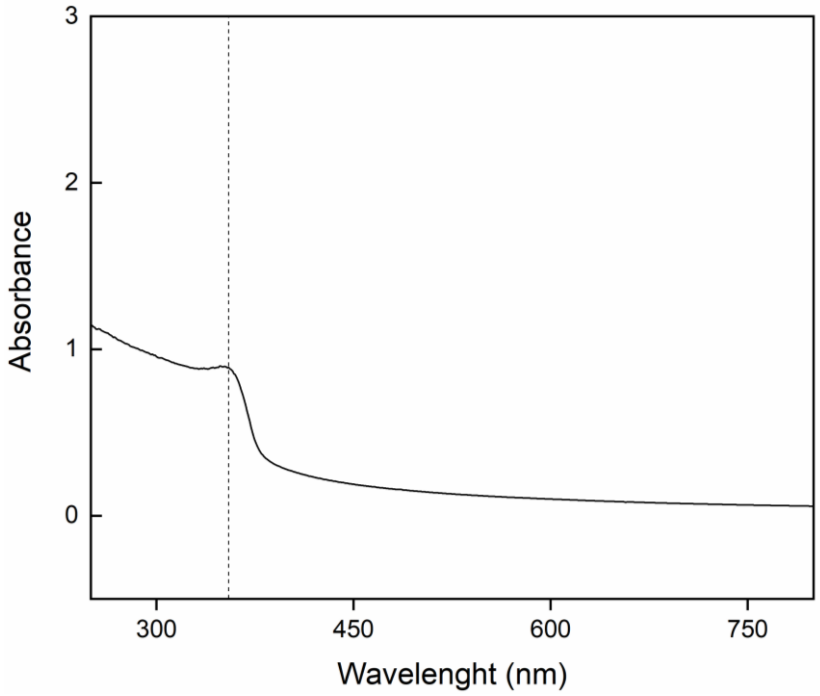


Figure 3.4: UV-visible absorbance spectrum of nZnO

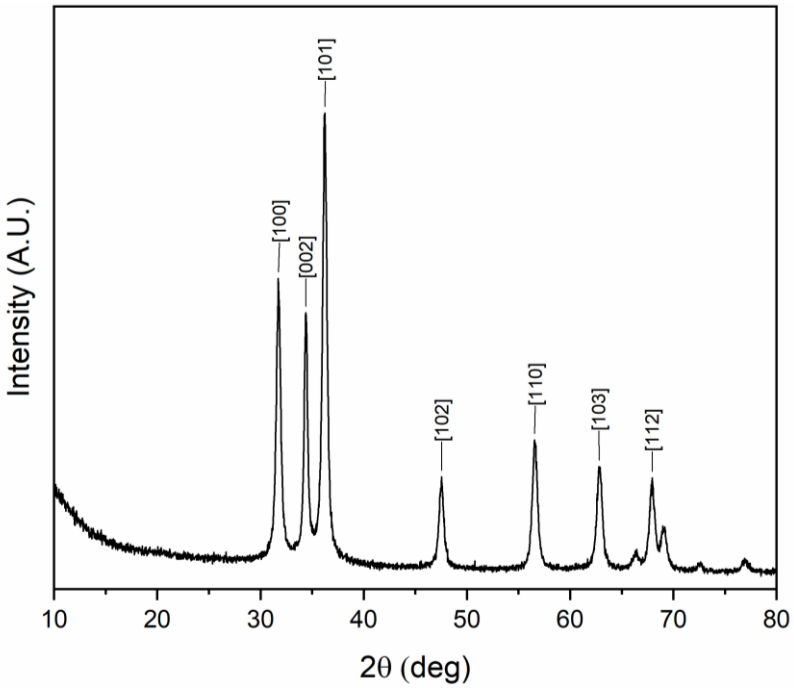


Figure 3.5: X-rays diffraction pattern of nZnO corresponding to a wurtzite-type crystalline structure.

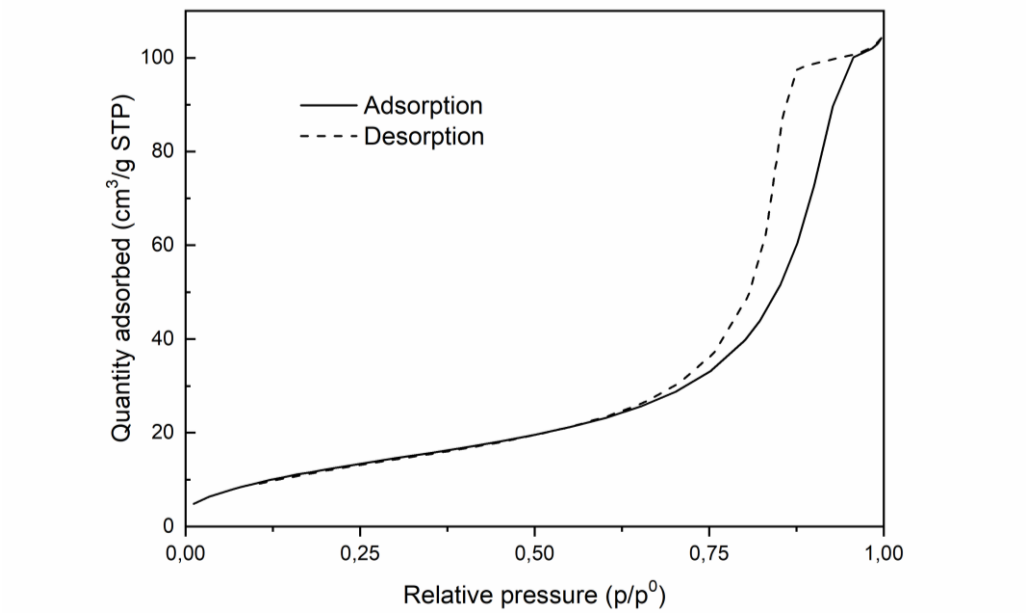


Figure 3.6: Nitrogen adsorption-desorption isotherms of nZnO.

Figure 3.7 shows the FTIR spectrum of nZnO. The broad band around 3390 cm^{-1} as associated to the stretching of hydroxyl groups on the surface of the oxide, whereas bands in the 1700-1300 cm-1 region are attributed to surface carbonate species (Socratres, 2001)

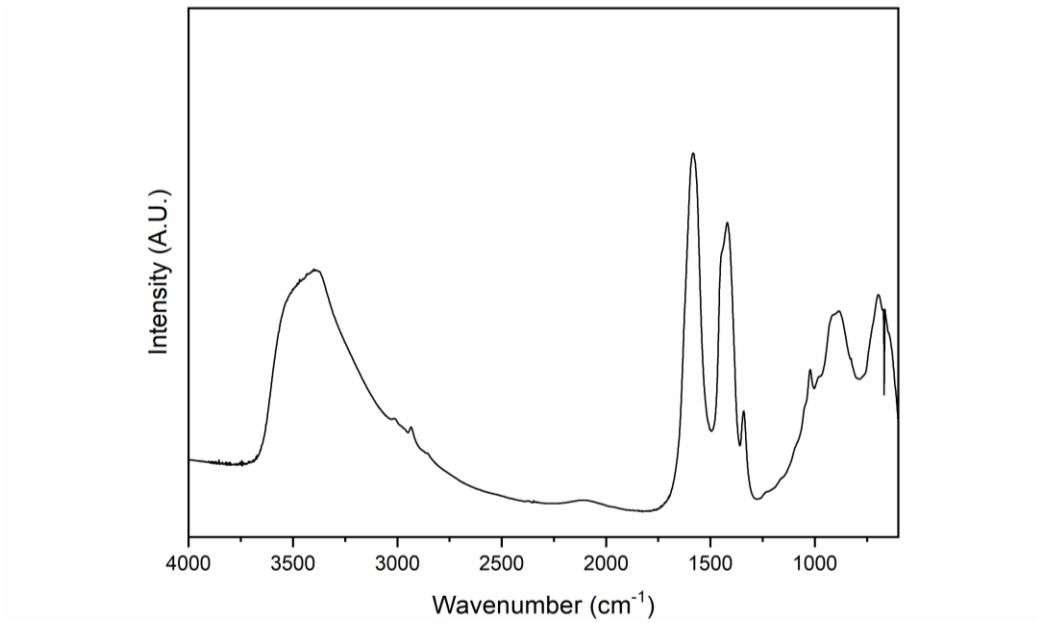


Figure 3.7: FTIR spectrum of nZnO.

The particle size distribution curves obtained by means of DLS of nZnO suspensions at different pH values are shown in Figure 3.8. The curves show the occurrence of aggregation of nZnO depending on the pH of the aqueous nanoparticle suspension. As can be seen in the figure, pH 3 is the condition in which n-ZnO are less aggregated, as revealed by the sharp and intense peak registered at 48 nm. This is in good agreement with the nanoparticles size provided by FESEM imaging if the hydrodynamic radius is considered (J. M. Berg et al., 2009). At higher pH values, the peak shifts towards larger size, reaching a maximum width at pH 7. This is justified by the results obtained by Berg and co-workers (J. M. Berg et al., 2009) locating the isoelectric point of 30-nm ZnO nanoparticles at pH equal to 7. In fact, at the isoelectric point the lack of electrostatic repulsion may favor nanoparticles aggregation, determining a wider particle size distribution and a larger average size. Nanoparticles have a zeta potential of 31.9 mV at pH 7. A positive surface charge is considered crucial for the antimicrobial activity thanks to the interaction with the negatively charged bacterial cell membrane (Mendes et al., 2022).

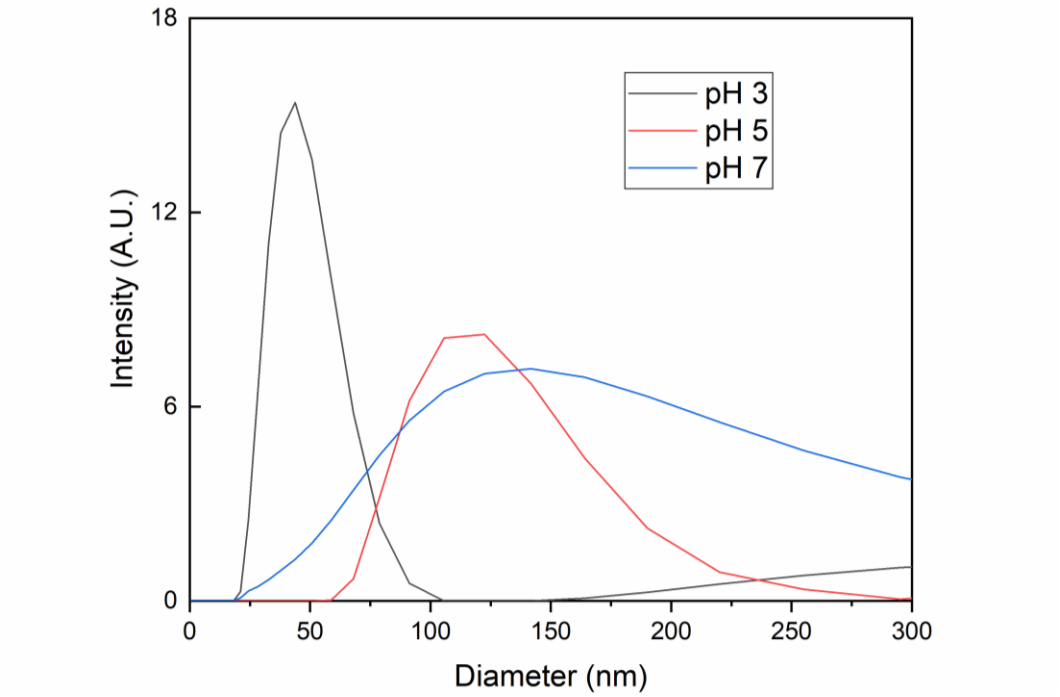


Figure 3.8: Particle size distribution for different pH values.

3.3.2 Antibacterial activity

3.3.2.1 Disk diffusion test

The antimicrobial activity of n-ZnO against *S. epidermidis* and *E. coli* was preliminarily assessed by means of a modified Kirby-Bauer agar diffusion test and the results are shown in Figure 3.9.

As *S. epidermidis* is concerned, at the lowest tested concentration, 1.92 mg/mL, a growth reduction was observed, while at 3.75 mg/mL and above the complete growth inhibition was obtained in the area where the drop was deposited. On the contrary, for *E. coli*, it is necessary a nZnO concentration of 6 mg/mL to inhibit the bacterial growth. Considering the lower sensibility of *E. coli*, the concentrations below 5 mg/mL were not tested, while the concentration of 25 mg/mL has also been evaluated as the highest one. On the basis of the obtained results, the MIC values are 3.75 and 6 mg/mL for *S. epidermidis* and *E. coli*, respectively. Different nZnO concentrations also determined different inhibition zone sizes, which are reported in the bar chart in Figure 3.10. It is interesting to note that the largest inhibition zones were not obtained for the highest concentrations. For *S. epidermidis*, the peak inhibition was reported at 7.5 mg/mL, while for *E. coli* it has been observed at 10 mg/mL. Higher concentrations achieved instead lower inhibition. This could be attributed to aggregation phenomena between oxide nanoparticles becoming prominent at those concentrations, which impair the overall antimicrobial effects by reducing the effective active contact interface with the bacteria (Sirelkhatim et al., 2015).

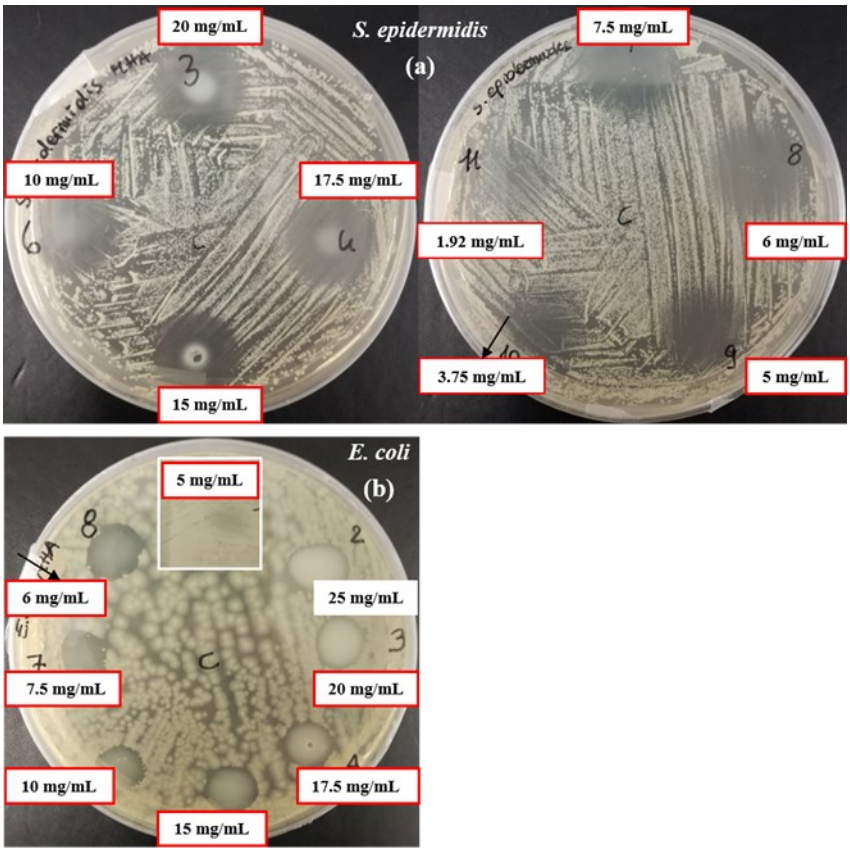


Figure 3.9: Modified Kirby-Bauer agar diffusion test against *S. epidermidis* (a) and E. coli (b). Red frames indicate the nZnO concentrations tested against both microorganisms. Black arrows indicate the MIC values, 3.75 and 6 mg/mL, for S. epidermidis and *E. coli* respectively.

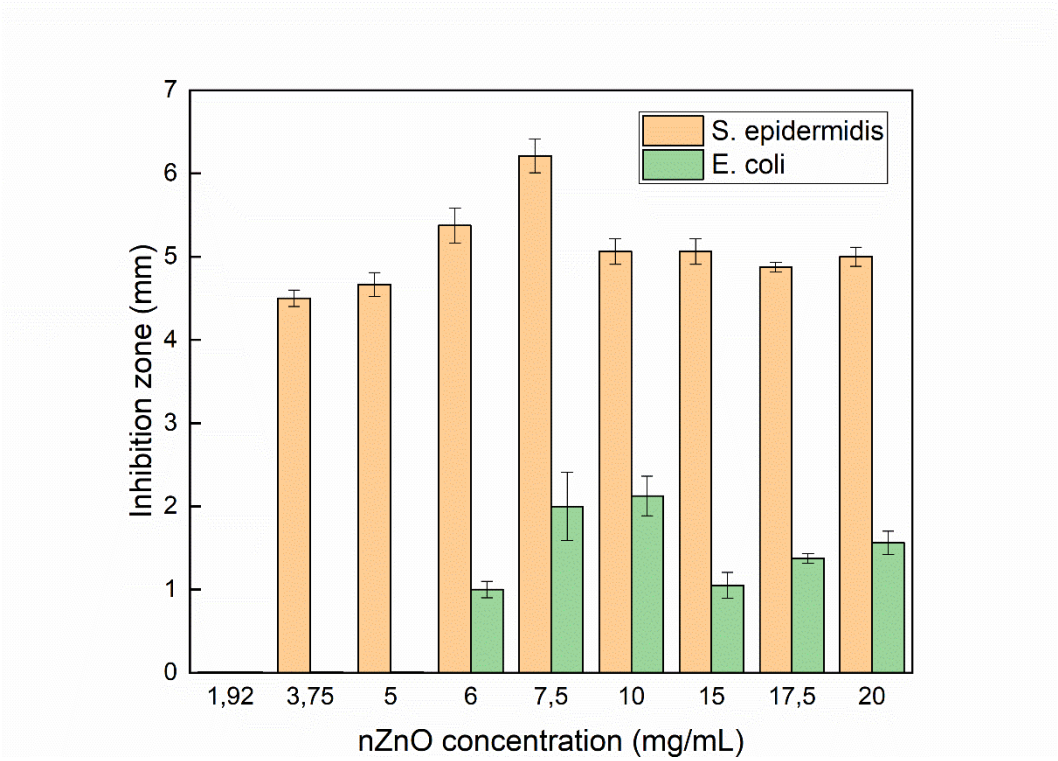


Figure 3.10: Inhibition zones for different nZnO concentrations against *S.epidermidis* and *E.coli*.

Conversely, the micro-sized, low surface area cZnO did not show any inhibitory activity against none of the strains. This is evident from the pictures in Figure 3.11 for the highest cZnO concentrations. Thus, as already proven extensively by previous research (Álvarez-Chimal et al., 2022), it can be reaffirmed that nanostructuring the oxide is a key to maximize its antibacterial effectiveness.

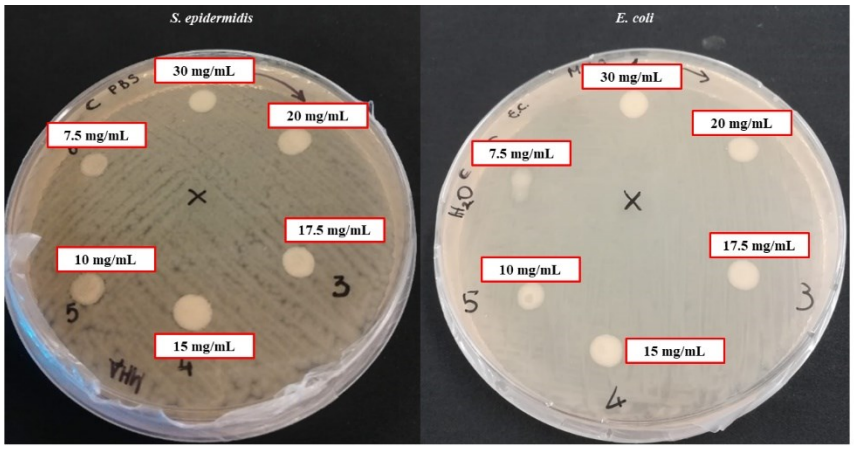


Figure 3.11: Modified Kirby-Bauer agar diffusion test against *S. epidermidis* (left) and *E. coli* (right) using cZnO. Red frames indicate the concentrations tested against both microorganisms.

3.3.2.2 Micro-broth dilution test

For this test, aqueous nZnO suspensions were tested having the following nanoparticles content: 30, 60, 120, 240, 480, 960, 1920, 3750, 7500, 15000, 17500 and 20000 μg/mL.

The MIC and MBC values of nZnO against the tested bacteria are reported in Table 3.1. The MIC value found for *E. coli* was four-fold higher than that for *S. epidermidis;* moreover, the MBC related to the Gram-negative bacterium was more than 7 times higher than that of the Gram-positive one. These results confirm that nanostructured zinc oxide is more effective against *S. epidermidis* than against *E. coli*, in agreement with the literature [37].

Table 3.1: Minimum Inhibitory and Minimum Bactericidal Concentrations of nZnO against *S. epidermidis* and *E. coli*.

	MIC [μg/mL]	**MBC [μg/mL]**
S. epidermidis	120	480
E. coli	480	3750

MIC values of 64 and 300 μg/mL for ZnO nanorods were found by Jain and co-workers (Jain et al., 2013) against *S. aureus* (ATCC 2592) and *E. coli* (ATCC 25922) respectively, using a spread plate method in which the nanorods were dispersed in the agar medium prior to the addition of the bacterial inoculum. The same study also showed how the presence of nano-zinc oxide in liquid cultures induces a concentration-dependent delay in the onset of the log phase of bacterial growth.

Premanathan et al. (Premanathan et al., 2011) tested 30-nm acicular ZnO nanoparticles using the micro-broth dilution method against Gram-negative *E. coli* (MTCC 739), Gram-negative *P. aeruginosa* (MTCC 1688) and Gram-positive *S. aureus* (MTCC 96), finding MICs of 500 μg/mL, 500 μg/mL, and 125 μg/mL, respectively.

It is also important to note here that the MIC values obtained from the two tests – disk diffusion and micro-broth dilution – are different for the same bacterial strain. In other words, the nZnO concentration required to inhibit the growth of either *S. epidermidis* or *E. coli* via disk diffusion is one order of magnitude larger than that required in the micro-broth dilution test. This gives insights into the antimicrobial mechanism of nZnO. In fact, one of the main differences between the two tests was the dispersion conditions of the nanoparticles in the medium. In the micro-broth dilution test, nanoparticles are suspended and then incubated with the bacterium under constant agitation, whereas for the disk diffusion test the nanoparticles are suspended and then simply deposited onto a plated dish, ultimately depositing and aggregating on its surface. The dynamic conditions provided by agitation in the former test method might therefore prevent aggregation and promote better contact between the nanoparticles and the bacterial cells as well as greater dissolution and diffusion of Zn^{2+} ions and ROS, which translates into higher antimicrobial efficacy (Rutherford et al., 2021). In turn, this suggests that nZnO wound dressings shall be optimized to prevent nanoparticle aggregation and to favor controlled dissolution to reap the maximum benefits of the oxide (Rutherford et al., 2021).

3.4 Conclusions

In this chapter, the preparation and characterization of nanostructured zinc oxide was described, and its antimicrobial properties tested against two different strains using two different testing protocols. In the disk diffusion test, the antibacterial activity was compared with that of a commercial, bulk zinc oxide powder. While this was found to be ineffective, nanostructured zinc oxide showed antimicrobial activity against both *S. epidermidis* and *E. coli*, with greater effects on the Gram positive strain. Antimicrobial activity was higher when nanoparticles were kept in agitation with the bacterial cells. Overall, this confirmed the importance of size and surface area in driving the antibacterial capacity of nanomaterials, as well as the role played by aggregation in limiting their potential effects. Moving from this solid body of evidence on this promising nano-platform, the following chapters will describe the path from nanoparticles to bionanocomposites through the use of six different and promising biomacromolecules.

References

Álvarez-Chimal, R., García-Pérez, V. I., Álvarez-Pérez, M. A., Tavera-Hernández, R., Reyes-Carmona, L., Martínez-Hernández, M., & Arenas-Alatorre, J. Á. (2022). Influence of the particle size on the antibacterial activity of green synthesized zinc oxide nanoparticles using Dysphania ambrosioides extract, supported by molecular docking analysis. *Arabian Journal of Chemistry*, *15*(6), 103804. https://doi.org/10.1016/J.ARABJC.2022.103804

Banchero, M., Mohamed, S. S. Y., Leone, F., Lopez, F., Ronchetti, S., Manna, L., & Onida, B. (2019). Supercritical solvent impregnation of different drugs in mesoporous nanostructured zno. *Pharmaceutics*, *11*(7), 1–14. https://doi.org/10.3390/pharmaceutics11070340

Berg, J. M., Romoser, A., Banerjee, N., Zebda, R., & Sayes, C. M. (2009). The relationship between pH and zeta potential of ~ 30 nm metal oxide nanoparticle suspensions relevant to in vitro toxicological evaluations. *Nanotoxicology*, *3*(4), 276–283. https://doi.org/10.3109/17435390903276941

Dutta, G., & Sugumaran, A. (2021). Bioengineered zinc oxide nanoparticles: Chemical, green, biological fabrication methods and its potential biomedical applications. *Journal of Drug Delivery Science and Technology*, *66*, 102853. https://doi.org/10.1016/J.JDDST.2021.102853

EUCAST: Disk diffusion methodology. (n.d.). Retrieved November 25, 2020, from https://www.eucast.org/ast_of_bacteria/disk_diffusion_methodology/

EUCAST reading guide for broth microdilution. (2022). www.eucast.org

Jain, A., Bhargava, R., & Poddar, P. (2013). Probing interaction of Gram-positive and Gram-negative bacterial cells with ZnO nanorods. *Materials Science and Engineering C*, *33*(3), 1247–1253. https://doi.org/10.1016/j.msec.2012.12.019

Mendes, C. R., Dilarri, G., Forsan, C. F., Sapata, V. de M. R., Lopes, P. R. M., de Moraes, P. B., Montagnolli, R. N., Ferreira, H., & Bidoia, E. D. (2022). Antibacterial action and target mechanisms of zinc oxide nanoparticles against

bacterial pathogens. *Scientific Reports*, *12*(1), 2658. https://doi.org/10.1038/S41598-022-06657-Y

Mitra, S., B, S., Patra, P., Chandra, S., Debnath, N., Das, S., Banerjee, R., Kundu, S. C., Pramanik, P., & Goswami, A. (2012). Porous ZnO nanorod for targeted delivery of doxorubicin: In vitro and in vivo response for therapeutic applications. *Journal of Materials Chemistry*, *22*(45), 24145–24154. https://doi.org/10.1039/c2jm35013k

Premanathan, M., Karthikeyan, K., Jeyasubramanian, K., & Manivannan, G. (2011). Selective toxicity of ZnO nanoparticles toward Gram-positive bacteria and cancer cells by apoptosis through lipid peroxidation. *Nanomedicine: Nanotechnology, Biology and Medicine*, *7*(2), 184–192. https://doi.org/10.1016/J.NANO.2010.10.001

Rutherford, D., Jíra, J., Kolářová, K., Matolínová, I., Mičová, J., Remeš, Z., & Rezek, B. (2021). Growth Inhibition of Gram-Positive and Gram-Negative Bacteria by Zinc Oxide Hedgehog Particles. *International Journal of Nanomedicine*, *16*, 3541. https://doi.org/10.2147/IJN.S300428

Singh, T. A., Sharma, A., Tejwan, N., Ghosh, N., Das, J., & Sil, P. C. (2021). A state of the art review on the synthesis, antibacterial, antioxidant, antidiabetic and tissue regeneration activities of zinc oxide nanoparticles. *Advances in Colloid and Interface Science*, *295*, 102495. https://doi.org/10.1016/J.CIS.2021.102495

Sirelkhatim, A., Mahmud, S., Seeni, A., Kaus, N. H. M., Ann, L. C., Bakhori, S. K. M., Hasan, H., & Mohamad, D. (2015). Review on zinc oxide nanoparticles: Antibacterial activity and toxicity mechanism. *Nano-Micro Letters*, *7*(3), 219–242. https://doi.org/10.1007/s40820-015-0040-x

Socratres, G. (2001). Infrared and Raman Characteristic Group Frequencies. In *Endeavour* (Third, Vol. 5, Issue 2). Wiley. https://doi.org/10.1016/0160-9327(81)90159-9

Chapter 4

Upcycling food by-products: whey proteins as bionanocomposite matrix

The contents of this Chapter have been reported in Pino, P., Ronchetti, S., Mollea, C., Sangermano, M., Onida, B., & Bosco, F. (2021). Whey Proteins–Zinc Oxide Bionanocomposite as Antibacterial Films. *Pharmaceutics*, Vol. 13, Page 1426, 13(9), 1426. https://doi.org/10.3390/pharmaceutics13091426

4.1 Introduction

Whey proteins (WP) are biocompatible and biodegradable biomolecules abundantly available as by-products of dairy production. In particular, whey proteins are obtained by concentrating the whey that is co-produced during the cheesemaking process. According to the protein concentration in the final product, the purity and the composition, Whey Protein Concentrate (WPC, protein content 65-80%) or Whey Protein Isolate (WPI, protein content ≥ 90%) can be obtained. Table 4.1 shows the typical compositions of WPI and WPC. The major constituents of whey proteins are β-lactoglobulins and α-lactalbumins, followed by bovine serum albumins and immunoglobulins, and by small fractions of other glycoproteins (Mehra et al., 2021). The non-protein part in WPC and WPI is mainly comprised by fats and lactose.

Table 4.1: A typical composition of WPC and WPI. Source: (Lorenzen et al., 2006). Whey proteins from Milei GmbH were used in the source study.

	WPC	**WPI**
Protein (%)	70.5	92.6
Lactose (%)	14.8	1.1
Fat (%)	5.2	traces
Moisture (%)	4.9	4.1
Ash (%)	3.3	1.9
Ca, Mg, K, Na, Cl, P (g·100 g^{-1} of product)	1.36	0.86

Thanks to their numerous beneficial properties, WP have been extensively used and researched for the formulation of functional foods, as well as for pharmaceutical and therapeutic applications like drug encapsulation and controlled delivery of nutraceuticals (Abaee et al., 2017; Gunasekaran et al., 2007; Mehra et al., 2021).

WP have also been found to possess excellent gelling and film-forming properties without requiring the use of toxic crosslinkers and with good mechanical, water absorption and gas barrier properties useful in food packaging (McHugh et al., 1994; Ramos et al., 2013; Shaw et al., 2002). The formation of gels and films is mainly driven by the disulfide bonds and sulfhydryl groups of β-lactoglobulins. Upon protein denaturation, the globular conformation of the protein is lost, allowing for the formation of intermolecular disulfide bridges, as well as of hydrogen bonds and hydrophobic interactions (Gounga et al., 2010). This results into strong yet brittle structures, often requiring the use of plasticizers to obtain flexible films and gels (Gounga et al., 2007a).

All these characteristics also make WP excellent candidates for the development of new wound dressing films. In this chapter, the fabrication, characterization and antibacterial testing of WP-ZnO bionanocomposites will be illustrated.

4.2 Experimental

4.2.1 Materials

Whey Protein Isolate (WPI) and Whey Protein Concentrate (WPC) powders were kindly supplied by Milei GmbH (Leutkirch im Allgäu, Germany). Potassium hydroxide (≥85%), potassium phosphate monobasic (≥99%), magnesium sulfate (≥99.5%), sodium chloride and glycerol (≥99%) were purchased from Sigma-Aldrich (St. Louis, MO, USA) and used as received. Calcium chloride was obtained from Merck. Mueller Hinton Broth (MHB) and Mueller Hinton Agar (MHA) were supplied by OXOID Ltd (Basingstoke, United Kingdom). Phosphate Buffered Saline (PBS) tablets were purchased from Sigma-Aldrich (St. Louis, MO, USA).

4.2.2 Preparation of Whey Protein films

Whey protein-based films were fabricated by means of a simple solvent casting technique. An aqueous WPI or WPC film forming suspension (FFS) was prepared with a 10% (w/w) protein concentration by dispersing WP powder in distilled water at room temperature under constant agitation. The pH of the suspension was adjusted to 7 with the addition of 1 M NaOH solution. The suspension was then placed inside a Huber 112A-E thermostatic bath (Huber, Offenburg, Germany) under continuous magnetic stirring to induce protein denaturation. For WPC, thermal treatment was carried at 90°C for 40 min. For WPI, the treatment was carried at 70°C for 20 min in order to avoid premature gelling. Subsequently, the FFS was cooled down to ambient temperature and 60% (w/w) of glycerol was added on a dry basis as a plasticizing agent. A volume of suspension was then casted into circular non-stick moulds such that the volume-to-surface ratio was kept equal to 0.135 m, and finally dried in an ISCO 900 oven for 2.5 h at 60 °C.

4.2.3 Preparation of WP-ZnO films

For the fabrication of composite films, aqueous suspensions of nZnO prepared as described in Chapter 3 were and sonicated in an Elmasonic ultrasonic bath (Elma Schmidbauer GmbH, Singen, Germany) for 60 min and subsequently vigorously

mixed with a magnetic stirrer with the whey protein FFS obtained as illustrated above, prior to casting.

Films with nZnO mass fraction of 2%, 4% and 6% with respect to the dry weight of WP were thus obtained and labelled as the type of protein used – WPI or WPC – followed by the amount of oxide contained, expressed as ZnO-2, ZnO-4, or ZnO-6. For instance, 2% nZnO WPI films were labelled as WPI-ZnO-2, et cetera. An additional film with 7.5% nZnO content was also prepared for antibacterial testing.

4.2.4 Characterization of the films

Composite and non-composite films were characterised by means of X-Ray Diffraction using a PANalytical X'Pert Diffractometer (Cu Kα radiation, Almelo, The Netherlands). Spectroscopic characterization was carried out by means of UV–Visible spectroscopy, using a Lambda 465 UV/Vis spectrophotometer (PerkinElmer, Waltham, MA, US), as well as Attenuated Total Reflectance Fourier-Transform Infrared Spectroscopy (ATR-FTIR), using a Nicolet iS50 FTIR Spectrometer equipped with Smart iTX optics and diamond crystal (Thermo Fischer Scientific, Waltham, MA, USA). Mechanical properties were assessed using an Instron 3366 Universal Testing System (Norwood, MA, USA). Samples were cut into rectangular 3 × 10 mm specimens and placed in the apparatus. Grip separation speed was set at 2 mm/min.

4.2.5 Swelling tests

Swelling tests were carried to assess the ability of the composites to absorb water and PBS (pH = 7.4). All films were cut into 1.8 cm diameter disks and weighed. Disks were then dried at 60 °C inside an oven until stabilization of mass on a constant value. Dry samples were hence immersed in 20 mL of either PBS or distilled water at different pH values, namely 3, 5, 7, 9 and 11. Water pH was titrated with 1M NaOH and HCl solutions. After 30 min intervals, samples were collected, blotted from excess water and weighed. The procedure was repeated until stabilization of the measured mass. The swelling ratio (SR) of the samples was determined as:

$$SR = \frac{m_w - m_d}{m_d} \cdot 100$$

Where m_w is the wet mass of each sample and m_d is the dry mass. Each experiment was repeated in triplicate.

4.2.6 Degradation tests

The degradation of bionanocomposites was assessed in PBS (pH = 7.4) and artificial sweat (AF) to simulate the types of fluid a dressing might be exposed to when applied to the skin. Artificial sweat (pH = 4.5) was prepared as an aqueous solution containing 5.49 g/L of sodium chloride, 13.28 g/L of calcium chloride, 0.24 g/L of magnesium sulphate and 1.36 g/L of potassium phosphate monobasic (Marques et al., n.d.). Samples was cut in 18 mm diameter disks, dried as described in Section 4.2.5 above, and immersed in 20 mL of either PBS or AF. For control, film disks were also immersed in distilled water at pH 4.5 and 7.4. The samples were kept at 32°C for 24h under continuous agitation at 150 rpm. After 24h, films were extracted from the fluids and dried as described in Section 4.2.5. The amount of degraded mass was determined as:

$$DM = \frac{m_i - m_f}{m_i} \cdot 100$$

Where m_i is the initial dry mass of each sample and m_f is the final dry mass after degradation. Each experiment was repeated in triplicate.

4.2.7 Antibacterial tests

The antibacterial activity of bionanocomposite films was assessed through a standard "EUCAST disk diffusion method" (2021) with some variations (*EUCAST: Disk Diffusion Methodology*, n.d.). A WP film without nZnO was tested as well to assess the antibacterial effects of the matrix. Both the top and the bottom face of each film were tested against *S. epidermidis* (LMG 10474) and *E. coli* (LMG 08063) to assess the influence of potential different nZnO surface concentrations induced by the film preparation process. Films were cut into 18 mm diameter disks and gently placed onto the surface of MHA Petri dishes, previously inoculated with 100 µL of a standardised bacterial inoculum prepared as described in Chapter 3. Samples were subsequently incubated at 37 °C for 24 h. All experiments were performed in triplicate. At the end of the incubation period, the inhibition zone was measured as the average distance between the edge of the disk and that of the bacterial growth, at the two perpendicular diameters.

4.3 Results

4.3.1 Characterization of the films

Figure 4.1 shows WPI and WPC films and their UV-visible spectrum. WPC films are characterized by a much lower transparency and by a yellowish coloration brought by the higher content of impurities, lactose and fats (Ramos et al., 2013). Transparency is a very important feature of a wound dressing as it allows for better wound inspection and monitoring. Furthermore, WPC films integrity appears generally lower due to the lower concentration of β-lactoglobulins, which are responsible for film strength (Lorenzen et al., 2006). For these reasons, WPC were set aside in favour of WPI for the subsequent characterization and testing of the bionanocomposites.

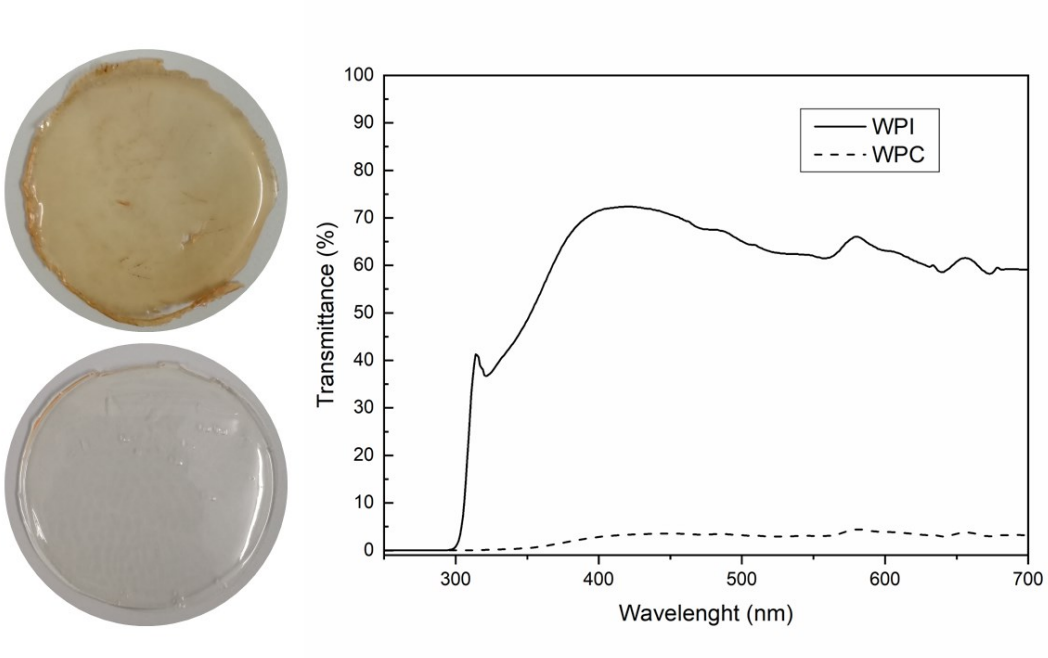


Figure 4.1: A WPC film sample (top left) and a WPI film sample (bottom left) and their UV-visible spectra.

Figure 4.2 shows the appearance of WPI and WPI-ZnO films. The oxide-free films are highly transparent, while opacity increases with increasing nZnO content, as demonstrated by the UV-Vis spectra shown in the same Figure. It is also worth noting how the introduction of nZnO provides significant barrier against UV light (250-400 nm), which is very desirable for skin health.

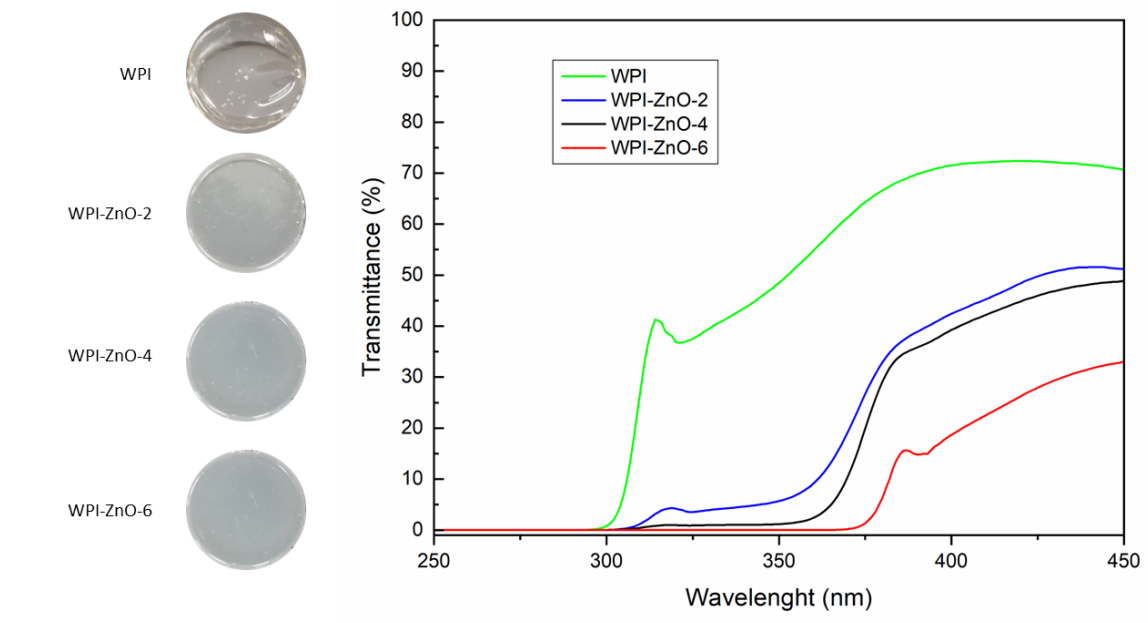


Figure 4.2: WPI and WPI-ZnO film samples (left) and their UV-visible spectra.

Figure 4.3 below shows the XRD spectra of WPI and WPI-ZnO films. WPI films (represented by the green curve) are amorphous, while WPI-ZnO samples show the crystalline features of the oxide overlapped on the amorphous background. No other phases are observable, suggesting that the introduction of nanoparticles did not induce crystallization phenomena in the protein matrix.

The ATR-FTIR spectra are instead shown in Figure 4.4. The sharp peaks at 1640 cm^{-1} and 1540 cm^{-1} where attributed to the Amide I (υ C=O; υ C–N) and Amide II (δ N–H; υ C–N) groups of the peptide bonds of proteins respectively. Evidence of residual fatty acids and carbohydrates can be found in the peaks around 1500 cm^{-1} and 700 cm^{-1} (Andrade et al., 2019). The presence of nZnO did not result in shifts of these bands or in the -OH region, as the result of what has been in other cases considered an effect of the interaction between the nanomaterial and the biopolymer (Jayakumar et al., 2015; Saedi et al., 2021).

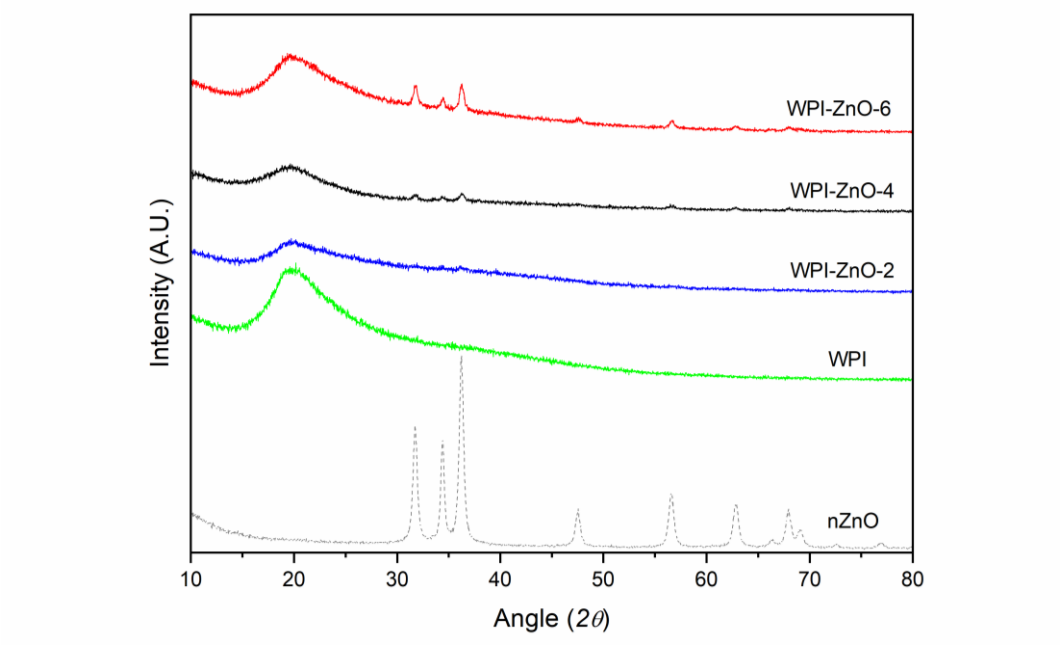


Figure 4.3: XRD spectra of WPI and WPI-ZnO films.

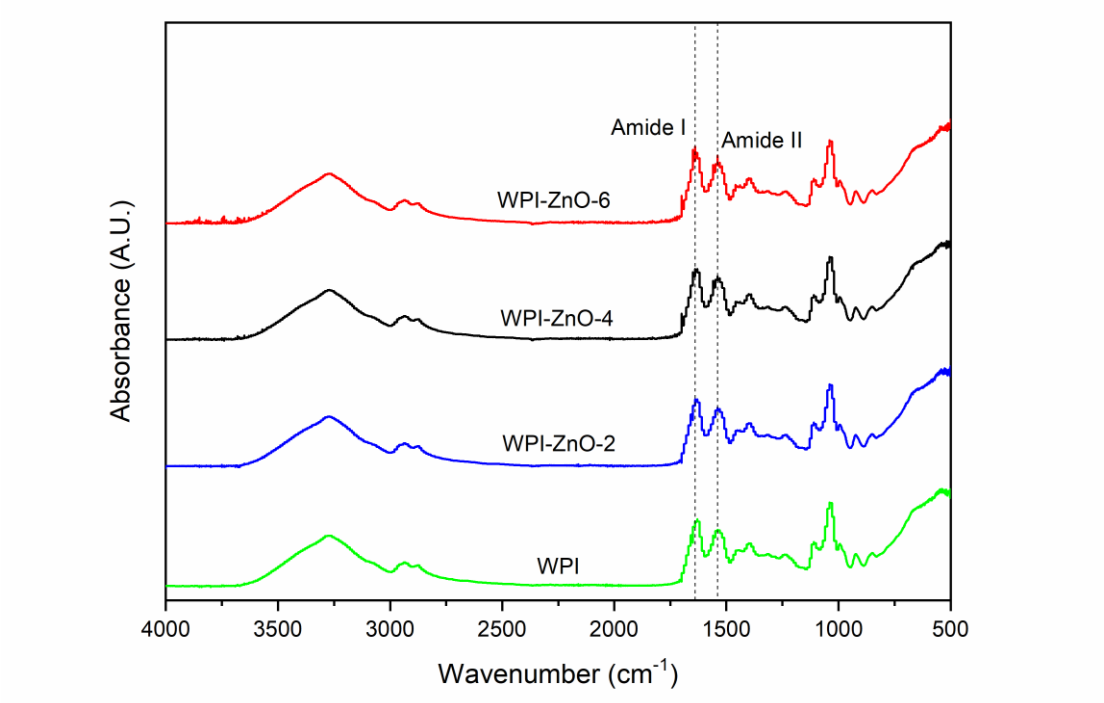


Figure 4.4: ATR-FTIR spectra of WPI and WPI-ZnO films.

The mechanical properties of WPI and WPI-ZnO films are reported in the charts of Figure 4.5 below.

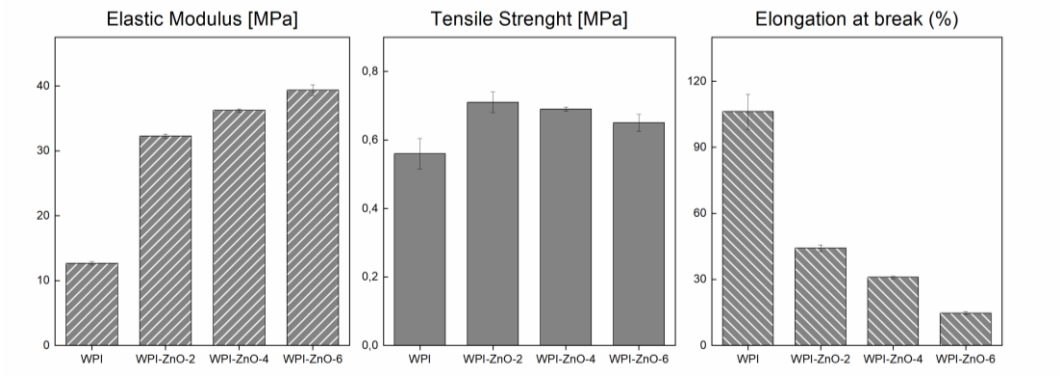


Figure 4.5: Mechanical properties of WPI and WPI-ZnO films.

The addition of nZnO produced a concentration-dependent increase in the elastic modulus. This effect is commonly reported as a consequence of the physical interaction between the two phases (Khorasani et al., 2018; Shahmohammadi Jebel & Almasi, 2016a). On the other side, tensile strength reached a maximum for nZnO concentration of 2% w/w and was lower for higher filler content, while elongation at break immediately fell after zinc oxide addition and kept decreasing with increasing nanoparticles content. This can be ascribed to the increased amount of discontinuities and aggregates in the material, which promote nucleation and propagation of cracks by creating localised stress concentrations (Hezma et al., 2019; Mujeeb Rahman et al., 2018a). This makes the material more brittle.

Considering the future uses as wound dressings, it is here worth noting that the measured elastic modulus and elongation at break values fall within the range of human skin, which are 83.3 ± 38.9 MPa and 54 ± 17% respectively (Annaidh et al., 2010). This compliance can eliminate patient discomfort and improve the duration and effectiveness of the treatments. Elastic modulus has also implications on the swelling ability of biopolymers (Koehler et al., 2017), as will be shown briefly.

4.3.2 Swelling tests

Figure 4.6 shows the swelling ratio of WPI and WPI-ZnO films in water at different pH levels and in PBS (pH = 7.4).

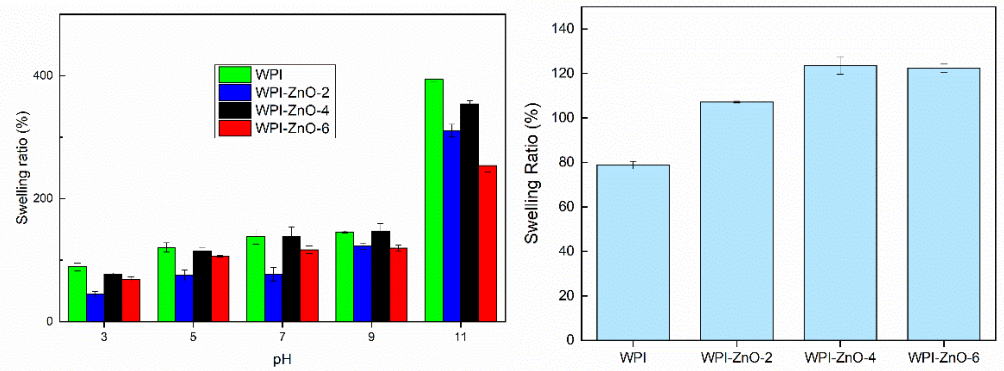


Figure 4.6: Swelling ratio of WPI and WPI-ZnO composites in water (left) and in PBS (right).

For both WPI and WPI–ZnO films, the swelling ratio increased slowly as pH increased from 3 to 9 and then increased rapidly at pH 11. The analogous behavior observed for WPI and WPI–ZnO films suggested that the swelling process was mostly governed by the protein matrix. At pH values close to the isoelectric point of whey proteins (~5) (Abaee et al., 2017), the effect of reciprocal electrostatic repulsion forces is absent, and interaction is dominated by hydrogen bonds. This promoted the contraction of the matrix and prevented water molecules from being absorbed, thereby determining a small SR. The further SR reduction observed at pH 3 might be the consequence of the acid-induced denaturation of a residual non-denatured and non-gelled protein fraction in the film (Quevedo et al., 2021; W. Wang et al., 2020), which might have favored the formation of new intermolecular bonds.

At high pH (above 9), full deprotonation of carboxylic moieties occurred, thus maximizing electrostatic repulsion and promoting water uptake (Gunasekaran et al., 2007; Livney, 2010). This can be very useful to absorb chronic wound exudate, which typically ranges from pH 7.5 to 8.9 (Muthuramalingam et al., 2019). In a study by Sharpe (Sharpe et al., 2013), the pH of the skin burns of 30 patients was measured every time that the wound dressing was replaced starting from hospital admission until healing. The average pH at the beginning was 8.1 ± 0.57, and gradually decreased to more neutral values as time passed. What is most interesting is that the pH of non-healing wounds and that of full-thickness wounds was reported to remain higher than that of healing or superficial burns. This indicates that a WPI-based dressing like the one here described can be better suited to treat deep, hard-to-heal wounds. It also implies that the small SR registered at pH 3 should not be of concern, as these pH levels are not found in the use case of interest.

The effect of nZnO was an overall decrease in SR, which could be appreciated especially at high pH values (>9). This can be due to physical interactions between the matrix and the nZnO, with the nanoparticles increasing the elastic modulus of the composite (Figure 4.5) and hindering the expansion of the matrix by limiting the required structural rearrangement of the biomacromolecules (Koehler et al., 2017; Namazi et al., 2019; Villanueva et al., 2019).

It is also interesting to note that the WPI–ZnO-4 sample showed a higher SR compared to its WPI–ZnO-2 and WPI–ZnO-6 counterparts, more markedly at pH 7, 9 and 11. This may be explained by considering the effect of the osmotic pressure. A small nZnO content (2%) may not be sufficient to generate sufficient osmotic pressure to promote water uptake by the hydrogel (Namazi et al., 2019), which instead may occur at higher nanoparticle contents (4%). However, when additional nZnO is introduced (6%), the stronger hindrance to expansion and the occupation of free space by the more abundant nanoparticles become a major constraint to swelling. Beyond just influencing swelling and exudate absorption, the pH can also have an impact on the antibacterial effects of the dressing (Wiegand et al., 2015), as it governs the aggregation kinetics of the nanoparticles or their dissolution rates. As reported in Chapter 3, ZnO nanoparticles were found to undergo maximum aggregation at pH around 7. Aggregation phenomena should therefore be less significant at more basic pH values like those encountered in the wounds, and the increased swelling of the matrix reported at alkaline pH can further allow for higher release of nanoparticles, ROS and Zn^{2+} ions, in turn supporting a stronger antimicrobial activity. It is here worth noting that ZnO is maximally soluble at acidic pH. However, this can be partially compensated by the increase in solubility brought by the nanometric size (Mudunkotuwa et al., 2012).

Considering the observed SR values, we can compare the one at neutral pH with data reported in the literature. The value of the WPI film (~140%) was lower than those reported by Wahid and co-workers (Wahid et al., 2016) for a carboxymethyl–chitosan hydrogel (~600%) and by Namazi (Namazi et al., 2019) for an oxidised-starch (~2400%) matrix, while it was higher than that reported for β-chitin (~22%) by Kumar (Sudheesh Kumar et al., 2013a) and for keratin–chitosan (~23%) by Zhai (Zhai et al., 2018b). For the keratin–chitosan hydrogel, addition of ZnO caused a reduction in the SR at the same neutral pH, similarly to what was herein observed for WPI–ZnO films. The carboxymethyl–chitosan and the oxidised-starch hydrogels showed instead an SR increase upon addition of ZnO, which was attributed to the buildup of osmotic pressure inside the matrix. However, also in these cases, SR decreased above a ZnO content threshold, due to the

abovementioned hindrance to the swelling. In these two latter cases, moreover, SR decreased with increasing pH value, conversely to the WPI case. Figure 4.7 below offers instead a graphical comparison of the swelling ratio of WPI films with that of other commercial alginate-based wound dressings.

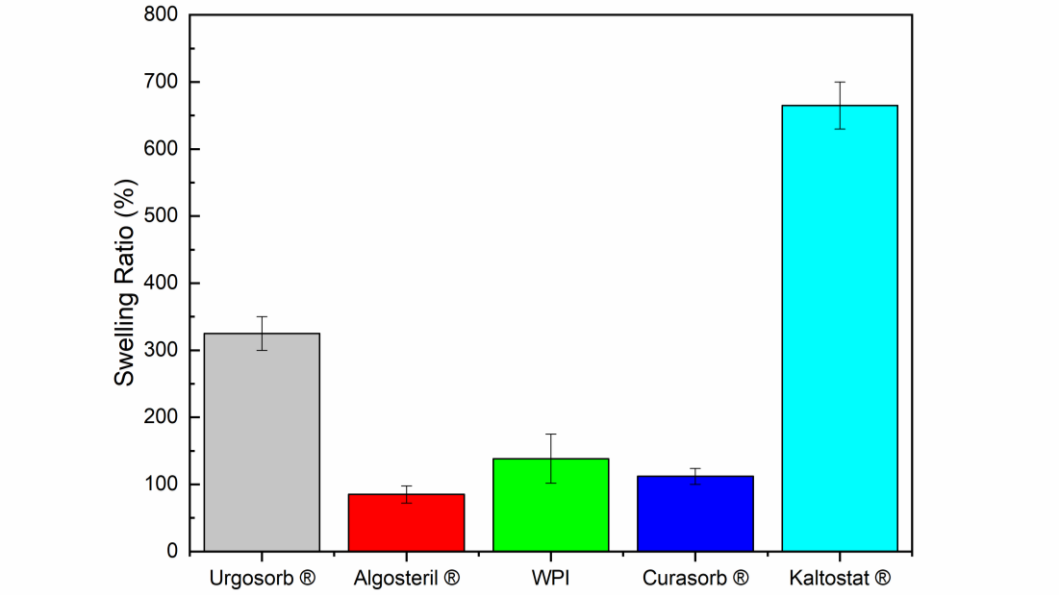


Figure 4.7: Swelling ratio in water of WPI films versus commercial wound dressings at neutral pH

To further probe composite behavior in physiological environments, swelling ratios of WPI and WPI–ZnO films were measured in PBS and results are reported in Figure 4.6 (on the right). The value for WPI films (79 ± 5%) was lower than the corresponding value in water at neutral pH (138 ± 12%, Figure 4.6 on the left). This can be ascribed to the higher ionic strength of the PBS solution, which reduced the range of repulsive electrostatic interactions within the matrix network (Namazi et al., 2019; Tee et al., 2020). The addition of nZnO was instead found to cause an increase in the swelling ratio (Jayakumar et al., 2015), presumably due to the abovementioned buildup of osmotic pressure. This is a positive feature, in that a higher content of nZnO can therefore lead to both higher wound exudate absorption as well as more significant antibacterial effects, as will be shown in the following sections.

4.3.3 Degradation tests

The results of the degradation tests are illustrated in Figure 4.8. When samples are immersed in water, the amount of degraded mass does not seem to be strongly influenced by nor the nZnO content nor the pH value. It is maximum for WPI at pH = 4.5 (66.88% ± 0.67%) and minimum for WPI-ZnO-6 at pH = 7.4 (58,95% ± 0,29%). The difference might be ascribed to presence of nZnO inside the matrix that constraints the swelling, as explained in Section 4.3.2 above. If less water is uptaken, matrix dissolution is hindered. A larger and constant decrease can instead be observed for degradation in AF and in PBS. In the simulated sweat the degraded mass goes from 57,85% ± 0,88% for the WPI sample down to 45,30% ± 0,88% for the WPI-ZnO-6 sample. This more marked resistance to degradation can now be considered the effect of nZnO presence, summed to higher ionic strength of the AF solution, which further reduces swelling.

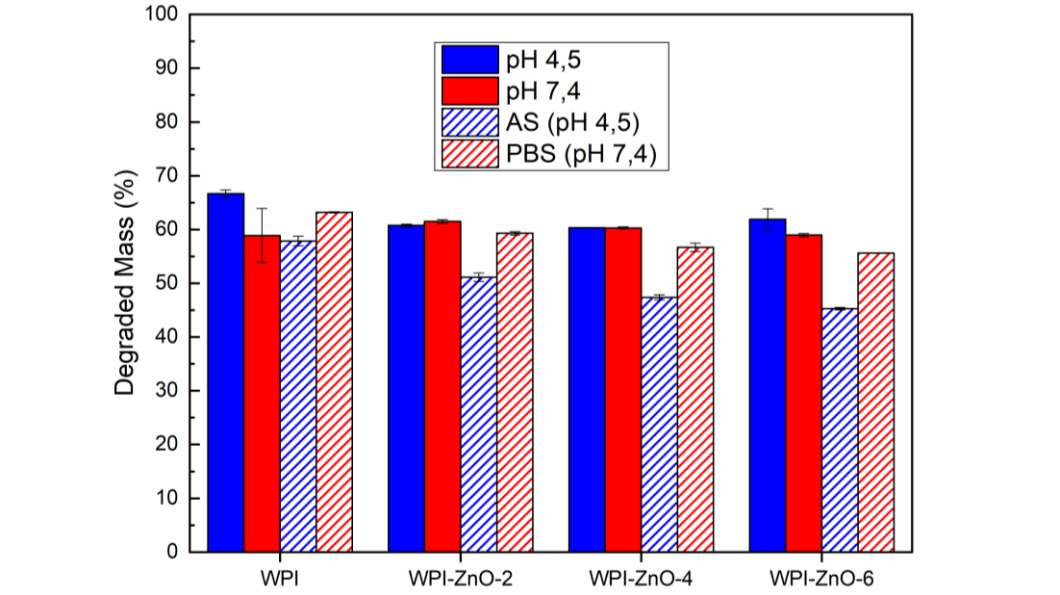


Figure 4.8: Percentage of degraded mass in different fluids versus nZnO content

These findings are quite positive, as they demonstrate how nZnO improves film stability in simulated physiological fluids, which can allow for prolonged and more effective therapeutic use.

4.3.4 Antibacterial tests

In the present study, *S. epidermidis* was chosen for being very common in the human skin microbiota, and often responsible for skin wounds infections, especially nosocomial and surgical ones (Amato et al., 2018). Moreover, this strain has been poorly investigated in the literature on ZnO bionanocomposite wound dressings.

Figure 4.9 shows the inhibition halo values measured for WPI and WPI-ZnO films against *S. epidermidis* and *E. coli*. A nZnO concentration dependent antibacterial activity can be observed, with the WPI control showing no intrinsic antimicrobial properties. The antibacterial activity against *E. coli* was null for WPI–ZnO-2, WPI–ZnO-4 and WPI–ZnO-6. This reflects the different antibacterial effect shown by nZnO against the two bacterial species as shown in the previous Chapter.

This therefore induced to prepare and test WPI-ZnO films with a 7.5% nZnO content. These were able to obtain a net yet modest inhibition against *E. coli*. However, the elevated oxide content inside the WPI-ZnO-7.5 samples severely affected their structural integrity and subsequent use, which is the reason why these have not been considered for the characterization studies.

However, although the highest inhibition was obtained with these WPI–ZnO-7.5 film (4.97 ± 0.06 mm), for the Gram-positive it was not too far from that achieved for oxide contents as low as for WPI–ZnO-4 (4.19 ± 0.05 mm), which could thus be an optimal compromise between nanoparticles concentration and antibacterial efficacy. As shown before in this chapter, very high nZnO contents lead to reduced swelling, low transparency, and worse mechanical properties. An optimised ZnO nanoparticle content can also help avoid potential cytotoxic effects on skin cells, which are still debated in the literature (Soares & Soares, 2021; Sruthi et al., 2018; Vinardell et al., 2017).

Inhibition halos against *S. epidermidis* were comparable with those reported for other Gram-positive species in other studies. Azari (Sherafatkhah Azari et al., 2021) obtained inhibition zones of 18.0 ± 1.53 mm against *S. aureus* around a 12-mm diameter disk of a gelatin/beta-glucan film containing 5% of ZnO nanoparticles. Arfat (Arfat et al., 2014) applied 10-mm fish protein isolate/fish skin gelatin disks containing 3% nano-ZnO on agar plates inoculated with *L. monocytogenes*, reporting zones of inhibition of ~22 mm.

The antibacterial activity obtained in the present work against the Gram-positive bacterium was also comparable with that of other WPI-based nanocomposites. Sani et al. (Alizadeh Sani et al., 2017; Alizadeh-Sani et al., 2018) developed WPI films embedded with TiO_2 nanoparticles (1% w/w) and cellulose nanofibers, obtaining inhibition halos of 4.00 ± 0.55 and 4.10 ± 0.68 mm against *L. monocytogenes* and *S. aureus* respectively for 10-mm diameter samples. Karimi and co-workers (Karimi et al., 2020) obtained inhibition halos of 0 and 3.5 ± 1.0 mm against the same species for 7-mm WPI/polydextrose films incorporated with cellulose nanofibers and *L. plantarum*, a Gram-positive bacterium employed for its antagonistic effect against the growth of other pathogens. Mohammadi (M. Mohammadi et al., 2020) obtained an inhibition halo of 2.00 ± 0.61 mm against *S. aureus* with a 6-mm WPI film disk containing chitosan nanofibers and nanostructured lipid carriers loaded with cinnamon essential oil.

In contrast with these results, Hezma (Hezma et al., 2019) and Thanusha (A. v. Thanusha et al., 2018) obtained a greater effect on Gram-negatives than on Gram-positive bacteria using nano-ZnO-incorporated chitosan/poly(vinylalcohol) and gelatin/hyaluronic acid/chitosan matrixes respectively. Some of the previously cited studies on WPI-based nanocomposites also reported higher effects against *E. coli* (Alizadeh Sani et al., 2017; Alizadeh-Sani et al., 2018; Karimi et al., 2020; M. Mohammadi et al., 2020).

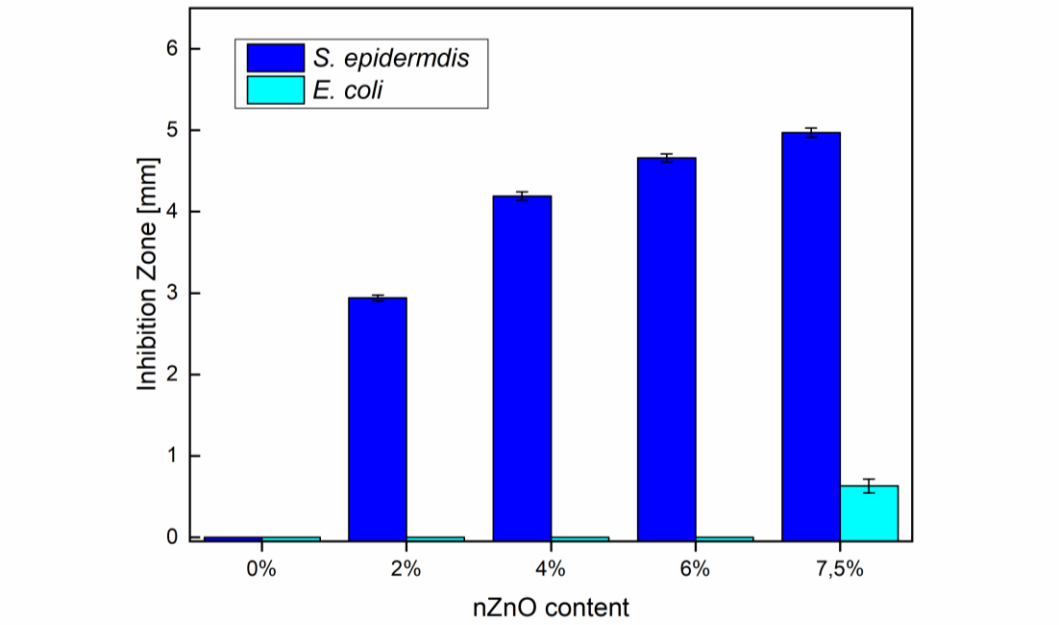


Figure 4.9: Inhibition zones of WPI and WPI-ZnO films with different nZnO contents against *S. epidermidis* and *E. coli*

Finally, Figure 4.10 reports the inhibition zones obtained by testing the top and the bottom film sides of the bionanocomposites against *S. epidermidis*. In general, it was not possible to identify a significant difference between the two film sides, which could suggest that nZnO is well dispersed across the thickness of the film and can thus provide sustained and effective antibacterial activity as the dressing degrades during the usage. However, an exception is found in WPI-ZnO-6. This suggests that nZnO maintains good dispersion across the thickness of the film until a critical threshold is reached, at which point agglomerates form and more easily sediment at the bottom.

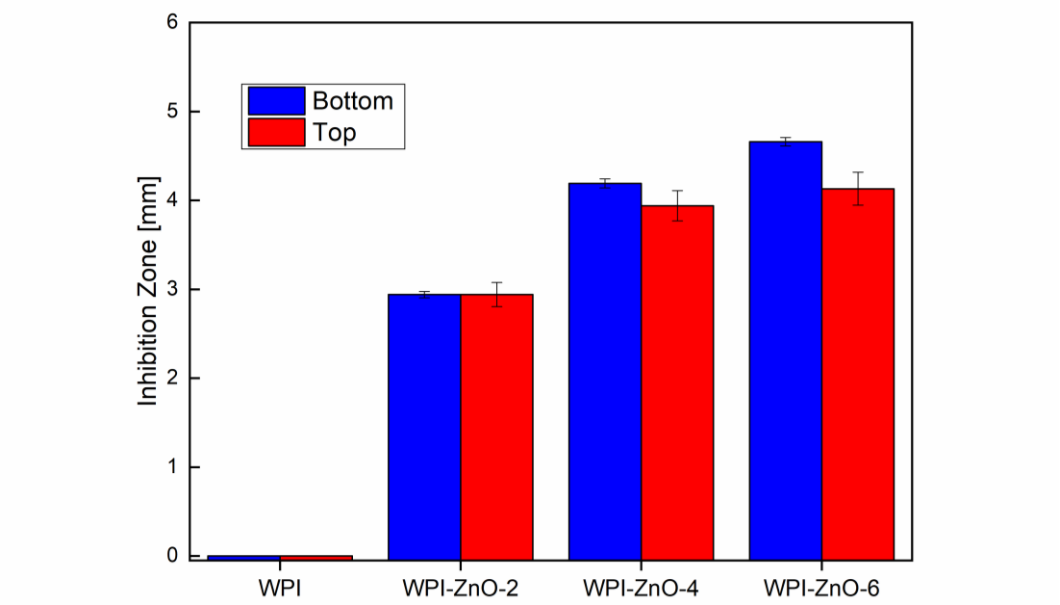


Figure 4.10: Inhibition zones of WPI and WPI-ZnO films top and bottom faces against *S. epidermidis*

4.4 Conclusions

In this chapter, the preparation, characterization and antibacterial testing of bionanocomposites made of whey proteins were illustrated. Whey proteins – especially whey protein isolate – possess very good film forming abilities and yield flexible and transparent films. Nano-zinc oxide can be easily incorporated to enhance mechanical and UV-barrier properties, resistance to degradation and antibacterial activity, especially against *S. epidermidis.* WPI films also showed

swelling ratios comparable to those of alginate-based commercial wound dressings, although high nZnO contents can reduce it. Overall, these preliminary findings are very promising towards the development of novel bionanocomposite wound dressings. Are there other promising biomacromolecules that can be exploited as successfully? The next chapters will tell.

References

Abaee, A., Mohammadian, M., & Jafari, S. M. (2017). Whey and soy protein-based hydrogels and nano-hydrogels as bioactive delivery systems. In *Trends in Food Science and Technology* (Vol. 70, pp. 69–81). Elsevier Ltd. https://doi.org/10.1016/j.tifs.2017.10.011

Alizadeh Sani, M., Ehsani, A., & Hashemi, M. (2017). Whey protein isolate/cellulose nanofibre/TiO2 nanoparticle/rosemary essential oil nanocomposite film: Its effect on microbial and sensory quality of lamb meat and growth of common foodborne pathogenic bacteria during refrigeration. *International Journal of Food Microbiology*, *251*, 8–14. https://doi.org/10.1016/J.IJFOODMICRO.2017.03.018

Alizadeh-Sani, M., Khezerlou, A., & Ehsani, A. (2018). Fabrication and characterization of the bionanocomposite film based on whey protein biopolymer loaded with TiO2 nanoparticles, cellulose nanofibers and rosemary essential oil. *Industrial Crops and Products*, *124*, 300–315. https://doi.org/10.1016/j.indcrop.2018.08.001

Amato, A., Migneco, L. M., Martinelli, A., Pietrelli, L., Piozzi, A., & Francolini, I. (2018). Antimicrobial activity of catechol functionalized-chitosan versus Staphylococcus epidermidis. *Carbohydrate Polymers*, *179*, 273–281. https://doi.org/10.1016/j.carbpol.2017.09.073

Andrade, J., Pereira, C. G., Almeida Junior, J. C. de, Viana, C. C. R., Neves, L. N. de O., Silva, P. H. F. da, Bell, M. J. V., & Anjos, V. de C. dos. (2019). FTIR-ATR determination of protein content to evaluate whey protein concentrate adulteration. *LWT*, *99*, 166–172. https://doi.org/10.1016/j.lwt.2018.09.079

Annaidh, A. N., Ottenio, M., Bruyère, K., Destrade, M., & Gilchrist, M. D. (2010). Mechanical Properties of Excised Human Skin. *IFMBE Proceedings*, *31 IFMBE*, 1000–1003. https://doi.org/10.1007/978-3-642-14515-5_255

Arfat, Y. A., Benjakul, S., Prodpran, T., Sumpavapol, P., & Songtipya, P. (2014). Properties and antimicrobial activity of fish protein isolate/fish skin gelatin film containing basil leaf essential oil and zinc oxide nanoparticles. *Food Hydrocolloids*, *41*, 265–273. https://doi.org/10.1016/j.foodhyd.2014.04.023

EUCAST: Disk diffusion methodology. (n.d.). Retrieved November 25, 2020, from https://www.eucast.org/ast_of_bacteria/disk_diffusion_methodology/

Gounga, M. E., Xu, S. Y., & Wang, Z. (2007). Whey protein isolate-based edible films as affected by protein concentration, glycerol ratio and pullulan addition in film formation. *Journal of Food Engineering*, *83*(4), 521–530. https://doi.org/10.1016/j.jfoodeng.2007.04.008

Gounga, M. E., Xu, S. Y., & Wang, Z. (2010). Film forming mechanism and mechanical and thermal properties of whey protein isolate-based edible films as affected by protein concentration, glycerol ratio and pullulan content. *Journal of Food Biochemistry*, *34*(3), 501–519. https://doi.org/10.1111/j.1745-4514.2009.00294.x

Gunasekaran, S., Ko, S., & Xiao, L. (2007). Use of whey proteins for encapsulation and controlled delivery applications. *Journal of Food Engineering*, *83*(1), 31–40. https://doi.org/10.1016/j.jfoodeng.2006.11.001

Hezma, A. M., Rajeh, A., & Mannaa, M. A. (2019). An insight into the effect of zinc oxide nanoparticles on the structural, thermal, mechanical properties and antimicrobial activity of Cs/PVA composite. *Colloids and Surfaces A: Physicochemical and Engineering Aspects*, *581*, 123821. https://doi.org/10.1016/J.COLSURFA.2019.123821

Jayakumar, R., Sudheesh Kumar, P., Mohandas, A., Lakshmanan, V.-K., & Biswas, R. (2015). Exploration of alginate hydrogel/nano zinc oxide composite bandages for infected wounds. *International Journal of Nanomedicine*, *10*(Supplement 1 Challenges in biomaterials research), 53. https://doi.org/10.2147/IJN.S79981

Karimi, N., Alizadeh, A., Almasi, H., & Hanifian, S. (2020). Preparation and characterization of whey protein isolate/polydextrose-based nanocomposite film

incorporated with cellulose nanofiber and L. plantarum: A new probiotic active packaging system. *LWT*, *121*, 108978. https://doi.org/10.1016/j.lwt.2019.108978

Khorasani, M. T., Joorabloo, A., Moghaddam, A., Shamsi, H., & MansooriMoghadam, Z. (2018). Incorporation of ZnO nanoparticles into heparinised polyvinyl alcohol/chitosan hydrogels for wound dressing application. *International Journal of Biological Macromolecules*, *114*, 1203–1215. https://doi.org/10.1016/j.ijbiomac.2018.04.010

Koehler, J., Wallmeyer, L., Hedtrich, S., Goepferich, A. M., & Brandl, F. P. (2017). pH-Modulating Poly(ethylene glycol)/Alginate Hydrogel Dressings for the Treatment of Chronic Wounds. *Macromolecular Bioscience*, *17*(5), 1600369. https://doi.org/10.1002/MABI.201600369

Livney, Y. D. (2010). Milk proteins as vehicles for bioactives. In *Current Opinion in Colloid and Interface Science* (Vol. 15, Issues 1–2, pp. 73–83). Elsevier. https://doi.org/10.1016/j.cocis.2009.11.002

Lorenzen, P. C., Schrader, K., Lorenzen, P. C., & Schrader, K. (2006). A comparative study of the gelation properties of whey protein concentrate and whey protein isolate. *Le Lait*, *86*(4), 259–271. https://doi.org/10.1051/LAIT:2006008

Marques, M. R. C., Loebenberg, R., & Almukainzi, M. (n.d.). *Simulated Biological Fluids with Possible Application in Dissolution Testing*. https://doi.org/10.14227/DT180311P15

McHugh, T. H., Aujard, J.-F., & Krochta, J. M. (1994). Plasticized Whey Protein Edible Films: Water Vapor Permeability Properties. *Journal of Food Science*, *59*(2), 416–419. https://doi.org/10.1111/j.1365-2621.1994.tb06980.x

Mehra, R., Kumar, H., Kumar, N., Ranvir, S., Jana, A., Buttar, H. S., Telessy, I. G., Awuchi, C. G., Okpala, C. O. R., Korzeniowska, M., & Guiné, R. F. P. (2021). Whey proteins processing and emergent derivatives: An insight perspective from constituents, bioactivities, functionalities to therapeutic applications. *Journal of Functional Foods*, *87*, 104760. https://doi.org/10.1016/J.JFF.2021.104760

Mohammadi, M., Mirabzadeh, S., Shahvalizadeh, R., & Hamishehkar, H. (2020). Development of novel active packaging films based on whey protein isolate incorporated with chitosan nanofiber and nano-formulated cinnamon oil.

International Journal of Biological Macromolecules, *149*, 11–20. https://doi.org/10.1016/j.ijbiomac.2020.01.083

Mudunkotuwa, I. A., Rupasinghe, T., Wu, C. M., & Grassian, V. H. (2012). Dissolution of ZnO nanoparticles at circumneutral pH: A study of size effects in the presence and absence of citric acid. *Langmuir*, *28*(1), 396–403. https://doi.org/10.1021/LA203542X/SUPPL_FILE/LA203542X_SI_001.PDF

Mujeeb Rahman, P., Abdul Mujeeb, V. M., Muraleedharan, K., & Thomas, S. K. (2018). Chitosan/nano ZnO composite films: Enhanced mechanical, antimicrobial and dielectric properties. *Arabian Journal of Chemistry*, *11*(1), 120–127. https://doi.org/10.1016/j.arabjc.2016.09.008

Muthuramalingam, K., Choi, S. I., Hyun, C., Kim, Y. M., & Cho, M. (2019). β-Glucan-Based Wet Dressing for Cutaneous Wound Healing. *Advances in Wound Care*, *8*(4), 125–135. https://doi.org/10.1089/WOUND.2018.0843/ASSET/IMAGES/LARGE/FIGURE5.JPEG

Namazi, H., Hasani, M., & Yadollahi, M. (2019). Antibacterial oxidized starch/ZnO nanocomposite hydrogel: Synthesis and evaluation of its swelling behaviours in various pHs and salt solutions. *International Journal of Biological Macromolecules*, *126*, 578–584. https://doi.org/10.1016/J.IJBIOMAC.2018.12.242

Quevedo, M., Karbstein, H. P., & Emin, M. A. (2021). Influence of thermomechanical treatment and pH on the denaturation kinetics of highly concentrated whey protein isolate. *Journal of Food Engineering*, *292*, 110294. https://doi.org/10.1016/j.jfoodeng.2020.110294

Ramos, Ó. L., Reinas, I., Silva, S. I., Fernandes, J. C., Cerqueira, M. A., Pereira, R. N., Vicente, A. A., Poças, M. F., Pintado, M. E., & Malcata, F. X. (2013). Effect of whey protein purity and glycerol content upon physical properties of edible films manufactured therefrom. *Food Hydrocolloids*, *30*(1), 110–122. https://doi.org/10.1016/j.foodhyd.2012.05.001

Saedi, S., Shokri, M., Kim, J. T., & Shin, G. H. (2021). Semi-transparent regenerated cellulose/ZnONP nanocomposite film as a potential antimicrobial food packaging material. *Journal of Food Engineering*, *307*, 110665. https://doi.org/10.1016/j.jfoodeng.2021.110665

Shahmohammadi Jebel, F., & Almasi, H. (2016). Morphological, physical, antimicrobial and release properties of ZnO nanoparticles-loaded bacterial cellulose films. *Carbohydrate Polymers*, *149*, 8–19. https://doi.org/10.1016/j.carbpol.2016.04.089

Sharpe, J. R., Booth, S., Jubin, K., Jordan, N. R., Lawrence-Watt, D. J., & Dheansa, B. S. (2013). Progression of Wound pH During the Course of Healing in Burns. *Journal of Burn Care & Research*, *34*(3), e201–e208. https://doi.org/10.1097/BCR.0B013E31825D5569

Shaw, N. B., Monahan, F. J., O'Riordan, E. D., & O'Sullivan, M. (2002). Physical Properties of WPI Films Plasticized with Glycerol, Xylitol, or Sorbitol. *Journal of Food Science*, *67*(1), 164–167. https://doi.org/10.1111/j.1365-2621.2002.tb11377.x

Sherafatkhah Azari, S., Alizadeh, A., Roufegarinejad, L., Asefi, N., & Hamishehkar, H. (2021). Preparation and characterization of gelatin/β-glucan nanocomposite film incorporated with ZnO nanoparticles as an active food packaging system. *Journal of Polymers and the Environment*, *29*(4), 1143–1152. https://doi.org/10.1007/s10924-020-01950-1

Soares, E. v., & Soares, H. M. V. M. (2021). Harmful effects of metal(loid) oxide nanoparticles. *Applied Microbiology and Biotechnology 2021 105:4*, *105*(4), 1379–1394. https://doi.org/10.1007/S00253-021-11124-1

Sruthi, S., Ashtami, J., & Mohanan, P. V. (2018). Biomedical application and hidden toxicity of Zinc oxide nanoparticles. In *Materials Today Chemistry*. https://doi.org/10.1016/j.mtchem.2018.09.008

Sudheesh Kumar, P. T., Lakshmanan, V. K., Raj, M., Biswas, R., Hiroshi, T., Nair, S. v., & Jayakumar, R. (2013). Evaluation of wound healing potential of β-chitin hydrogel/nano zinc oxide composite bandage. *Pharmaceutical Research*, *30*(2), 523–537. https://doi.org/10.1007/s11095-012-0898-y

Tee, H. T., Zipp, R., Koynov, K., Tremel, W., & Wurm, F. R. (2020). Poly(methyl ethylene phosphate) hydrogels: Degradable and cell-repellent alternatives to PEG-hydrogels. *European Polymer Journal*, *141*, 110075. https://doi.org/10.1016/j.eurpolymj.2020.110075

Thanusha, A. v., Dinda, A. K., & Koul, V. (2018). Evaluation of nano hydrogel composite based on gelatin/HA/CS suffused with Asiatic acid/ZnO and CuO

nanoparticles for second degree burns. *Materials Science and Engineering C*, *89*, 378–386. https://doi.org/10.1016/j.msec.2018.03.034

Villanueva, M. E., Cuestas, M. L., Pérez, C. J., Campo Dall′ Orto, V., & Copello, G. J. (2019). Smart release of antimicrobial ZnO nanoplates from a pH-responsive keratin hydrogel. *Journal of Colloid and Interface Science*, *536*, 372–380. https://doi.org/10.1016/J.JCIS.2018.10.067

Vinardell, M. P., Llanas, H., Marics, L., & Mitjans, M. (2017). In vitro comparative skin irritation induced by nano and non-nano zinc oxide. *Nanomaterials*, *7*(3), 56. https://doi.org/10.3390/nano7030056

Wahid, F., Yin, J.-J., Xue, D.-D., Xue, H., Lu, Y.-S., Zhong, C., & Chu, L.-Q. (2016). Synthesis and characterization of antibacterial carboxymethyl Chitosan/ZnO nanocomposite hydrogels. *International Journal of Biological Macromolecules*, *88*, 273–279. https://doi.org/10.1016/J.IJBIOMAC.2016.03.044

Wang, W., Sheng, H., Zhou, J., Yuan, P., Zhang, X., Lu, M., & Gu, R. (2020). The effect of a variable initial pH on the structure and rheological properties of whey protein and monosaccharide gelation via the Maillard reaction. *International Dairy Journal*, 104896. https://doi.org/10.1016/j.idairyj.2020.104896

Wiegand, C., Abel, M., Ruth, P., Elsner, P., & Hipler, U. C. (2015). In vitro assessment of the antimicrobial activity of wound dressings: influence of the test method selected and impact of the pH. *Journal of Materials Science: Materials in Medicine*, *26*(1), 1–13. https://doi.org/10.1007/S10856-014-5343-9/FIGURES/5

Zhai, M., Xu, Y., Zhou, B., & Jing, W. (2018). Keratin-chitosan/n-ZnO nanocomposite hydrogel for antimicrobial treatment of burn wound healing: Characterization and biomedical application. *Journal of Photochemistry and Photobiology B: Biology*, *180*, 253–258. https://doi.org/10.1016/j.jphotobiol.2018.02.018

Chapter 5

Macromolecules from microorganisms: polysaccharides and polyesters

Part of the contents of this Chapter have been reported in Pino, P., Pellegrino, G., Ronchetti, S., Mollea, C., Sangermano, M., Bosco, F., & Onida, B. (2023). Antibacterial β-glucan/zinc oxide nanocomposite films for wound healing. *BioNanoScience* (Accepted for publication)

5.1 Introduction

As mentioned at the end of the previous chapter, other biomacromolecules exist that can be sourced from nature and engineered to formulate new, advanced wound dressing materials.

Among these, β-glucans (BG) are gaining increasing attention in the fabrication of wound dressings thanks to their immunostimulatory properties. B-glucans are natural polysaccharides that can be found in the cell wall of many plants and yeasts (Q. Wang et al., 2017). The innate immune receptor Dectine-1 recognizes BG as Pathogen-Associated Molecular Patterns (PAMPs), thus triggering immune response (J. Ma & Underhill, 2013) and proliferation of keratinocytes in humans (L. M. van den Berg et al., 2014), as well as other skin health promotion effects (Du

et al., 2014). Beta-glucans have been used as additives for the fabrication of nanofibrous (Grip et al., 2018b) and sprayable wound dressings (Grip et al., 2017), and blended with gelatin (Sherafatkhah Azari et al., 2021), poly(vinyl alcohol) (Huang & Yang, 2008), starch (Sagnelli et al., 2017) and pullulan (Chang et al., 2019). Different types of beta-glucan *gels* for wound healing have also been reported in the literature (Elg et al., 2019; Hunt, 2018).

However, very little research exists on the fabrication of β-glucan *films* – especially bionanocomposite ones – which would constitute another important contribution to the development of wound dressings based on natural biomacromolecules. In fact, we ought to explore all the possible forms these molecules can be engineered into to make sure that we unlock their highest potential. So far, only a study by Razzaq et al. demonstrated the antimicrobial properties of ZnO-containing films exclusively made of β-glucans obtained from barley (Razzaq et al., 2021).

However, the ZnO used in that study was 500 nm in size, i.e. it did not possess the same antibacterial properties that are available at the nanoscale, as explained in Chapters 1 and 3 (Sirelkhatim et al., 2015). Furthermore, there is a large body of scientific evidence suggesting that β-glucans from *Saccharomyces cerevisiae* – as opposed to those obtained from other sources, like barley – promote wound healing and skin repair processes by stimulating fibroblasts proliferation and growth factors expression (Majtan & Jesenak, 2018b), which would be highly desirable properties for innovative wound dressings. In fact, the biological activity of β-glucans is dependent on their source and structural conformation (Q. Wang et al., 2017). However, β-glucans from *S. cerevisiae* are not water soluble, contrary to cereal-derived ones, thus making the fabrication of medical devices more difficult.

Overcoming this limitation would be a significant progress towards the development of multi-functional, advanced wound dressings, and that's what this chapter is about. Firstly, a simple preparation route for the fabrication of flexible β-glucans and β-glucans/nZnO (BGZ) films is presented, using commercial *S. cerevisiae* β-glucans. Secondly, both BG and BGZ films are characterized to investigate their microstructure and the interaction between glucans and nanoparticles. Finally, their antibacterial properties are assessed.

But β-glucans are not the only molecule that microorganisms can provide us with in our quest for novel wound dressings and biomaterials.

Poly(3-hydroxybutyrate-co-3-hydroxyvalerate) (PHBV) is a linear copolymer produced by Gram-positive and Gram-negative bacteria (Antonio et al., 2021). This biopolymer belongs to the family of the polyhydroxyalkanoates (PHAs), i.e. polyesters produced by bacteria and stored as granules inside cytoplasm. Here, they serve as energy source to be exploited whenever the carbon sources from the outer environment are depleted or not available. PHBV is renowned for its non-toxicity, biocompatibility and high biodegradability (Kaniuk et al., 2020). For these reasons, it is one of the best candidates to replace petroleum-derived plastics, for instance as a packaging material (Figueroa-Lopez et al., 2020; Melendez-Rodriguez et al., 2018) but has many biomedical applications too, for instance for the fabrication of stents, scaffolds for tissue engineering (Rivera-Briso & Serrano-Aroca, 2018) and drug delivery nano-devices (Tebaldi et al., 2019). Given its ability to promote the attachment and proliferation of fibroblasts (Kaniuk et al., 2020), PHBV is a promising material for wound healing applications as well. So far, antibacterial nanomaterials such as nanostructured zinc oxide have been repeatedly combined with PHBV, but with principal focus on composite scaffolds or electrospun membranes (Naphade & Jog, 2012a; Râpă et al., 2021; Zare et al., 2019). Thus, there is an opportunity to explore nanocomposite films.

Same as with β-glucan-nZnO films, PHBV-nZnO (PHBV-Z) films have therefore been prepared, characterized and tested against *S. epidermidis* and *E. coli*. In this way, an initial comparison could be made between these two biomacromolecules produced by microorganisms, in preparation for a broader comparative assessment involving a larger set of biopolymers.

5.2 Experimental

5.2.1 Materials

Potassium hydroxide (≥85%) and glycerol (≥99%) were purchased from Sigma-Aldrich (St. Louis, MO, USA) and used as received. Chloroform (≥99%) was obtained from Honeywell (Seelze, Germany) and used as received. Beta-glucan powder (70%) was purchased from ACEF S.p.A. (Fiorenzuola d'Arda, Piacenza, Italy). Commercial ENMAT™ Y1000P PHBV was obtained from Tianan Biologic Materials (Ningbo, China). Mueller Hinton Broth CM0405 (MHB) and Mueller Hinton Agar CM0337 (MHA) were supplied by OXOID Ltd (Basingstoke, United Kingdom).

5.2.2 Preparation of BG and BGZ films

Beta-glucan films have been prepared following a procedure previously described by Sagnelli and co-workers (Sagnelli et al., 2017) with some modifications. Briefly, 2% (w/v) BG suspension in distilled water was prepared and heated at 95°C for 40 min to facilitate beta-glucan dispersion. After the thermal treatment, glycerol was added in an amount equal to 25% of the dry weight of BG powder. After stirring, the suspension was poured onto 9-cm diameter polypropylene Petri dishes, maintaining a volume to surface ratio equal to 0.200 m. The dishes were placed in an oven for 3 h at 60°C for solvent evaporation and film formation, and films were subsequently peeled off and used for further characterization and testing.

For the preparation of composite films, an aqueous suspension of nZnO obtained as described in Chapter 3 was prepared and sonicated in an ultrasonic bath for 1 h. The suspension was then added to a film-forming BG suspension prepared as described above, subsequent to the heat treatment and glycerol addition steps. The mixture was then casted and dried, and composite films were eventually obtained. Three different types of composite films were prepared, based on the nZnO content introduced in the matrix, namely 2%, 4% and 6% of the dry BG mass. Samples were therefore labelled BGZ-2, BGZ-4 and BGZ-6, respectively.

5.2.3 Preparation of PHBV and PHBV-Z films

PHBV films were produced through a simple solvent casting technique. PHBV is dissolved in chloroform and stirred for 15 minutes at room temperature to obtain a 3% (w/v) solution. The solution is then casted onto a glass dish preheated at 90°C and in an amount equal to obtain a volume-to-surface ratio equal to 0.135 m. The film is eventually peeled off upon complete solvent evaporation.

For the preparation of PHBV-Z films, a suspension of nZnO in chloroform is prepared and sonicated for 1h, and then added to the PHBV solution in chloroform before casting. The amount of nZnO is chose in order to finally obtain bionanocomposites where the quantity of oxide is equal to 2%, 4% or 6% of the initial dry mass of PHBV in the solution. The composite films that are obtained are thus labelled PHBV-Z2, PHBV-Z4 and PHBV-Z6.

5.2.4 Characterization of BG and BGZ films

BG and BGZ films were characterised by means of X-Ray Diffraction using a PANalytical X'Pert Diffractometer (Cu K radiation, Almelo, The Netherlands) and scanning electron microscopy done via ZEISS Supra 40 Field Emission Scanning Electron Microscope (ZEISS, Oberkochen, Germany). Cross sections of the films were imaged after immersing and subsequently fracturing samples in liquid nitrogen. Before the analysis, samples were coated with a 8-nm thick Pt layer. Energy-dispersive X-ray spectroscopy (EDS) was carried with an Oxford EDS Microanalysis (liquid N_2 cooled Si(Li) detector) instrument (Oxford Instruments, Abingdon, UK). X-ray photoelectron spectroscopy (XPS) was performed with a Physical Electronics VersaProbe apparatus (Physical Electronics, Lake Drive, MN, USA), using Al radiation ($h\upsilon$ = 1248 eV). The C1s component at 284.8 eV was taken as a reference for the energy scale. Spectroscopic characterization was carried out by means of UV–Vis spectroscopy, using a Lambda 465 UV/Vis spectrophotometer (PerkinElmer, Waltham, MA, US), as well as Attenuated Total Reflectance Fourier-Transform Infrared Spectroscopy (ATR-FTIR), using a Nicolet iS50 FTIR Spectrometer equipped with Smart iTX optics and diamond crystal (Thermo Fischer Scientific, Waltham, MA, USA). Thermal properties were investigated through Differential Scanning Calorimetry (DSC) and Thermogravimetric Analysis (TGA) using a Linseis STA PT 1600 apparatus (Linseis Messgeraete GmbH, Selb, Germany) in inert argon atmosphere in the 25-800°C temperature range, with a 10°C/min heating rate. Glass transition temperature T_g was determined through the first derivative method.

5.2.5 Characterization of PHBV and PHBV-Z films

PHBV and PHBVZ films were characterised by means of X-Ray Diffraction using a PANalytical X'Pert Diffractometer (Cu K radiation, Almelo, The Netherlands) Attenuated Total Reflectance Fourier-Transform Infrared Spectroscopy (ATR-FTIR) was carried using a Nicolet iS50 FTIR Spectrometer equipped with Smart iTX optics and diamond crystal (Thermo Fischer Scientific, Waltham, MA, USA). Thermal properties were investigated via Thermogravimetric Analysis (TGA) using a Linseis STA PT 1600 apparatus (Linseis Messgeraete GmbH, Selb, Germany) in inert argon atmosphere in the 25-800°C temperature range, with a 10°C/min heating rate.

5.2.6 Swelling tests

Swelling tests have been performed as for the WPI-ZnO films described in the previous Chapter. BG, BGZ, PHBV and PHBV-Z films have been cut into 18-mm diameter discs, weighted and dried in oven at 60°C until stabilization of the dry mass. Discs were then immersed in 20 mL of distilled water at different pH values, namely 3, 5, 7, 9 and 11. Films were extracted from the liquid at 30 minutes time intervals, freed from excess water, and weighted until stabilization of the wet mass. Finally, the swelling ratio (SR) was determined as:

$$SR = \frac{m_w - m_d}{m_d} \cdot 100$$

Where m_w is the wet mass of each sample and m_d is the dry mass. Each experiment was repeated in triplicate.

5.2.7 Antibacterial tests

The antibacterial activity of bionanocomposite films was assessed through a standard "EUCAST disk diffusion method" (2021) with some variations (*EUCAST: Disk Diffusion Methodology*, n.d.), as for the samples in the previous Chapter. As for all the previous experiments, the tested microorganisms have been *S. epidermidis* LMG 10474 and *E. coli* LMG 08063.

A standardised inoculum was prepared using the direct colony suspension method as described before. 100 µL of the inoculum were spread on MHA plates (Ø 90 mm) and 18 mm diameter discs of all samples were gently deposited on the agar surface. Filter paper discs were used as negative controls. Plates were then incubated at 37°C for 24h. At the end of the incubation period, the antibacterial activity was measured as the average distance between the edge of the film disc and the end of the inhibition zone across two perpendicular disc diameters. Each experiment was done in triplicate.

5.3 Results

5.3.1 Characterization of BG and BGZ films

The film formation procedure described above led to the formation of flexible films. FESEM images in Figure 5.1 showed that films have a compact microstructure. BG films (Figure 5.1.A1) have a continuous and irregular surface. Addition of ZnO (Figure 5.1.B1) seems to cause an increase in surface roughness. This is caused by the presence of ZnO nanoparticles and their aggregates, as revealed by the EDS analysis. Figure 5.1.B2.1 shows that nZnO is homogeneously distributed in the composite film. Moreover, Figure 5.1.B2.2 shows a several-microns-large nZnO aggregate, as confirmed by the overlap between the oxygen and zinc elemental maps and by the corresponding lack of carbon presence in the same area. In order to verify that nZnO was also dispersed across the thickness of the film, cross section images and elemental maps were taken. The inner part of the film is featured by micrometric pores, as shown in Figure 5.1.A3 for the BG matrix. When nZnO is dispersed, porosity is preserved, but the nanoparticles and their aggregates become visible in the cross section as well (Figure 5.1.B3). As a further confirmation, zinc was detected across the lateral section by EDS, as shown in Figure 5.1.B4.

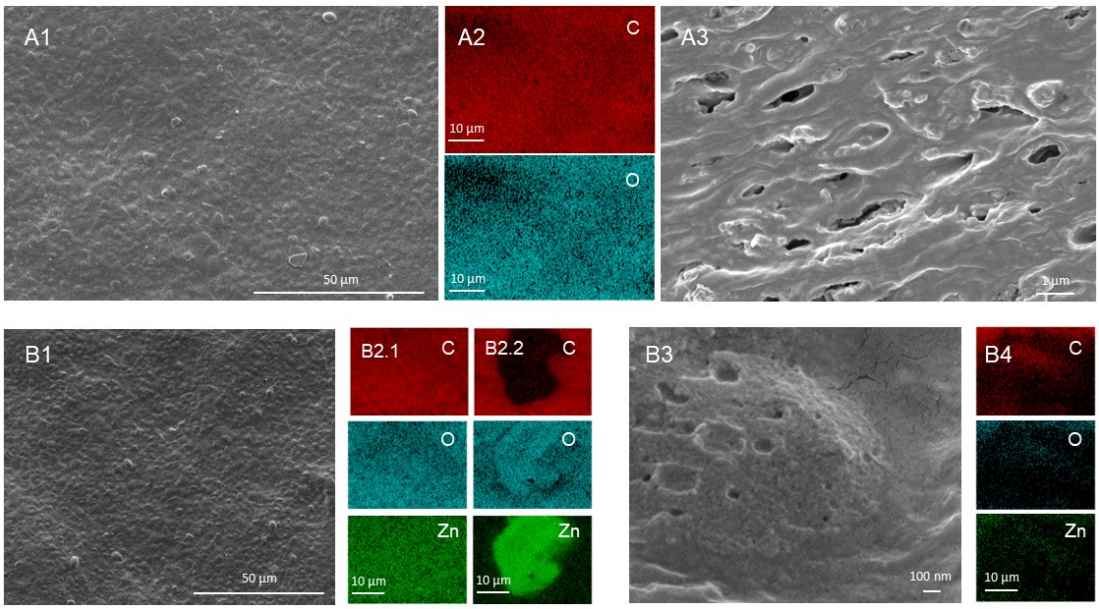


Figure 5.1: A1) FESEM image of BG film surface; A2) EDS carbon and oxygen distribution map of BG film surface; A3) FESEM image of BG film cross section; B1) FESEM image of BGZ-6 film surface; B2) Elemental maps of C, O and Zn of BGZ-6 film surface in a generic point of the sample (1) and in correspondence of a nZnO aggregate (2); B3) Close-up FESEM image of a nZnO aggregate in the BGZ-6 film cross section; B4) Elemental maps of C, O and Zn in the BGZ-6 film cross section.

Figure 5.2 shows the results of the XPS analysis. A survey carried out on the four samples confirmed that nZnO was successfully included in the composite samples (Figure 5.2A). The binding energy of Zn2p3 between 1022.13 and 1022.25 eV (Figure 5.2B) in the four samples is between that reported for zinc hydroxide and zinc carbonate (Winiarski et al., 2018). This suggests that a layer of hydroxylated and carbonate species was formed on the surface of the nanoparticles, as previously reported for a similar nanostructured zinc oxide (Banchero et al., 2019) and in accordance with the nZnO FTIR spectrum shown in Chapter 3 (Figure 3.7).

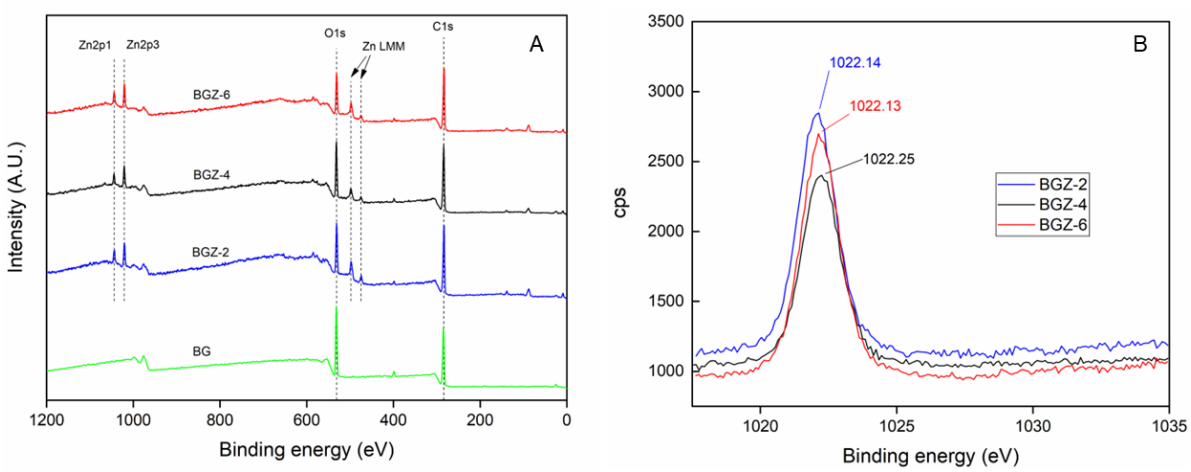


Figure 5.2: A) XPS survey of the samples and B) high-resolution XPS peaks of Zn2p3.

The bulk phase of the nanoparticles is however not affected, as revealed by the XRD spectrum shown in Figure 5.3, where the XRD patterns of the nZnO powder and of the four films are reported. They reveal an amorphous structure in all cases, with a broad reflection at approximately 2θ=20° which is consistent with literature data (Chang et al., 2019; Sagnelli et al., 2017). The amorphous pattern is indicative of the formation of a dense molecular network, as proposed by Chang et al. (Chang et al., 2019), in agreement with the evidence obtained by FESEM analysis. Diffraction peaks attributable to nZnO are observed in the BGZ-4 and in the BGZ-

6 samples thanks to the higher amount of oxidic phase. The presence of nZnO does not appear to affect the amorphous nature of the beta-glucan matrix.

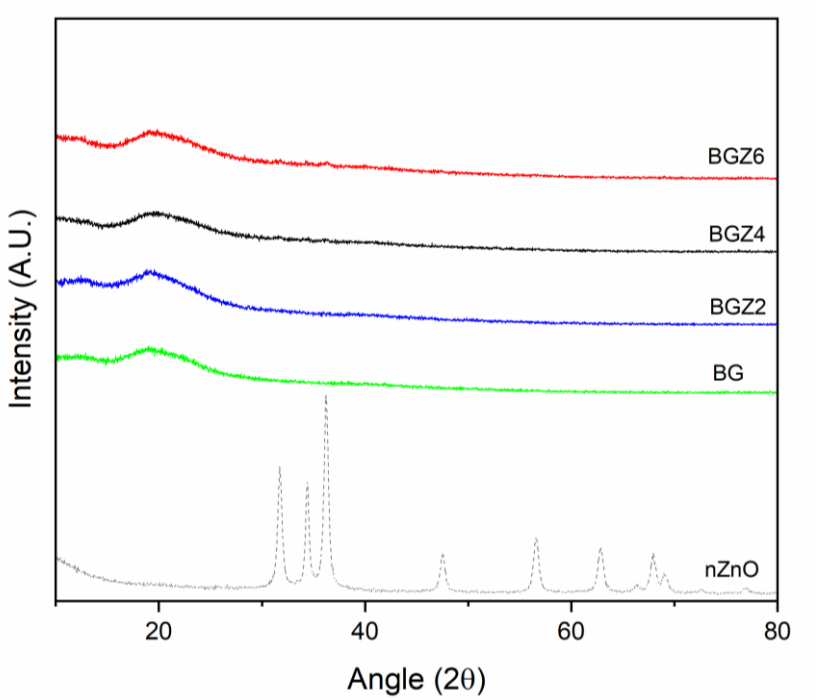


Figure 5.3: XRD pattern of BG and BGZ films.

The optical properties of the films were characterized by UV-visible spectroscopy and spectra are presented in Figure 5.4. While transmittance of the films is low, the addition of nZnO further increases opacity both in the UV and in the visible range. This is widely reported for ZnO-containing composites (Vaezi et al., 2019) and has been found for WPI-ZnO films as well.

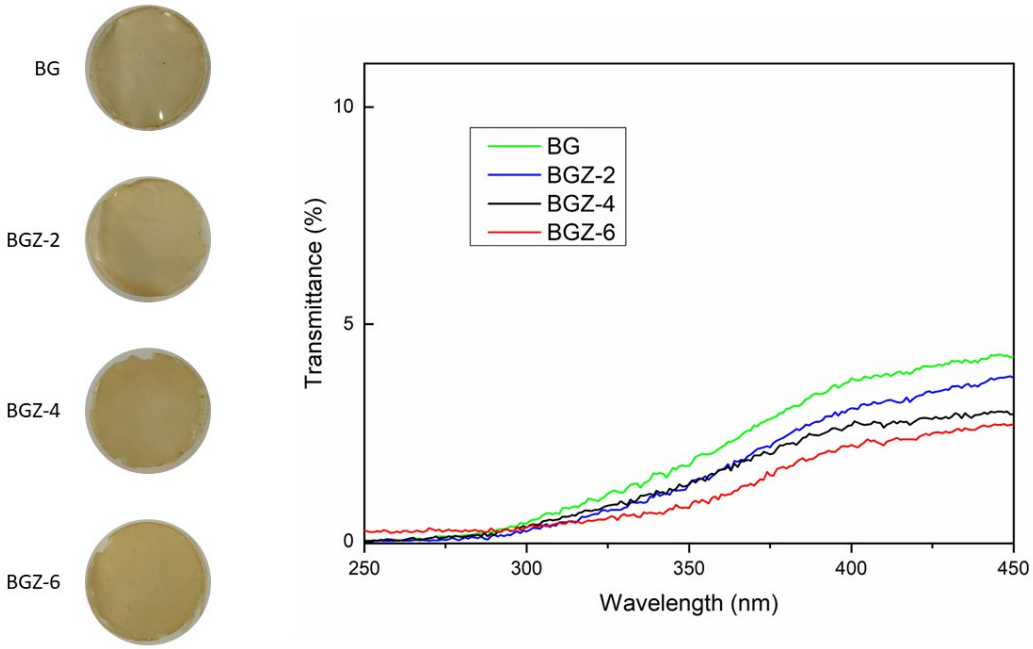


Figure 5.4: UV-Visible spectra of BG and BGZ films. Sample photographs are shown on the right.

ATR-FTIR spectra of BG and BGZ films are shown in Figure 5.5. The broad band at about 3290 cm^{-1} is due to -OH groups, whereas the two peaks at about 2920 cm^{-1} and 2860 cm^{-1} are attributed to the asymmetric and symmetric -CH_2 group stretching respectively (Socratres, 2001). Two weak bands are a at 1635 cm^{-1} and 1560 cm^{-1}, which may be ascribed to amide groups, which might be retained in the BG extraction process (Nováka et al., 2012). The very strong bands in the 1010-1050 cm^{-1} range are typically found in glucans (Kacuráková et al., 2000; Nováka et al., 2012). The presence of nZnO does not result in any changes of the BGZ spectra with respect to the bare BG film.

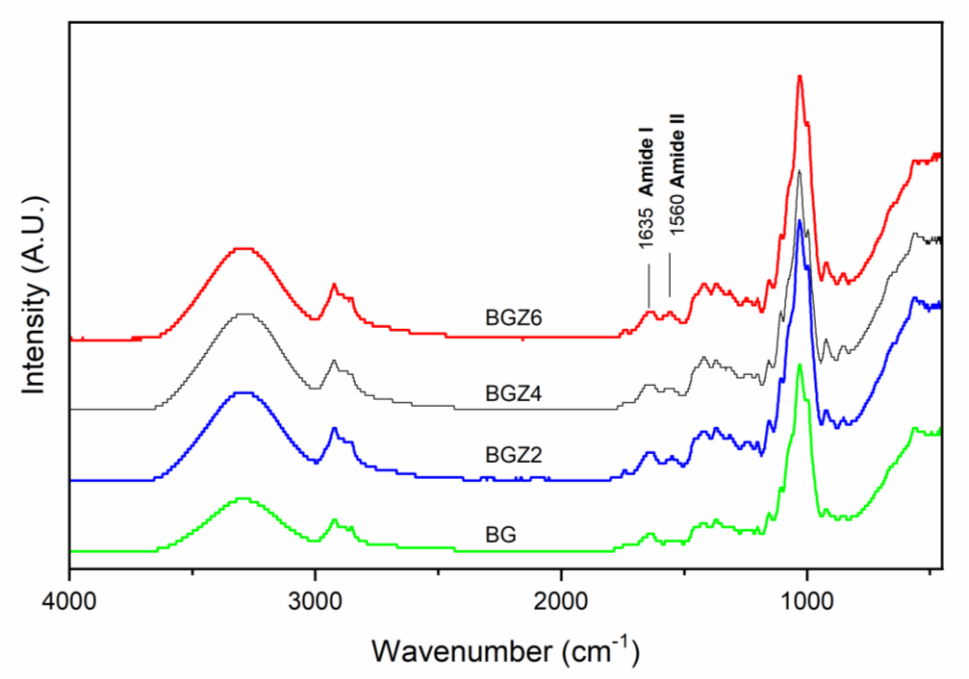


Figure 5.5: ATR-FTIR spectra of BG and BGZ films

Results of thermogravimetric analyses are shown in Figure 5.6 (left side). After an initial weight loss due to evaporation of water, a second mass reduction onsets at approximately 200°C due to the thermal decomposition of β-glucans (Razzaq et al., 2021), followed by a steeper mass loss step starting in the proximity of 300°C, assigned to glycerol removal in addition to polysaccharides decomposition. The corresponding mass loss results to be around 25%, which are in agreement with the glycerol content from the preparation procedure.

In the last portion of the curves, between 400°C and 800 °C, a further mass loss, of about 10%, is observed for BG and BGZ-2, whereas only a minor mass loss is observed for BGZ-4 and BGZ-6 in the same temperature range. The higher amount of residual mass in BGZ-4 and BGZ-6 can be attributed to the effect of ZnO nanoparticles, which absorb heat, stabilize the carbonaceous structure, and limit the diffusion of decomposition species (Arfat et al., 2014).

The right side of Figure 5.6 reports the DSC curves of the films. T_g of pure β-glucan films is around 90°, whereas it increases up to approximately 80°C for the nanocomposite films. These values for the BG films are in agreement with literature data (Razzaq et al., 2016). For BGZ films, a plasticizing effect of ZnO on the films was suggested in the previous study (Razzaq et al., 2021) as the cause of the

decrease of the glass transition temperature. Here, the nZnO with a smaller size might have acted in the same capacity, promoting molecular mobility.

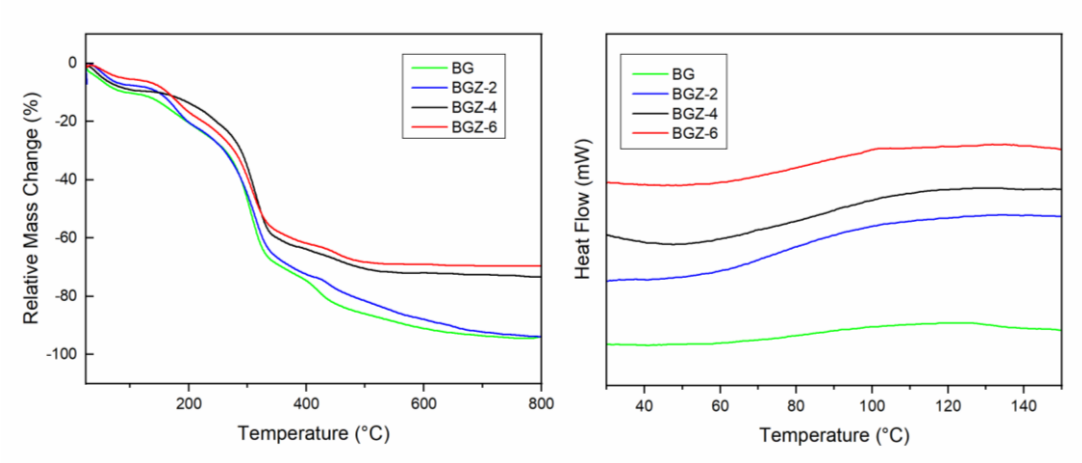


Figure 5.6: TGA (left) and DSC (right) curves of BG and BGZ films

5.3.2 Preparation and characterization of PHBV and PHBV-Z films

The procedure described in Sec. 5.2.3 below leads to the obtainment of flexible yet inhomogeneous films, as shown in Figure 5.7 below.

The film appears opaque and with an irregular surface, presumably as a result of the rapid evolution of gaseous chloroform upon casting on the pre-heated plate. This also had repercussions on the possibility to homogeneously disperse nZnO in the matrix and to gather information on the optical properties in the UV-Visible region. It is also worth mentioning that the choice of chloroform as a solvent was made after numerous efforts to find and employ an alternative yet less toxic solvent. A suitable substitute could be found in formic acid, but it was eventually discarded due to its reactivity towards zinc oxide. Despite this, characterization and testing of PHBV and PHBV-Z films continued for the sake of comparison with the promising β-glucan-based counterparts.



Figure 5.7: Photograph of a PHBV film

Figure 5.8 below shows the XRD pattern of PHBV and PHBV-Z films. PHBV is notoriously a semicrystalline polymer. The peaks at 13.5° and 16.9° are associated to the (020) and (110) planes of the orthorhombic α phase of the polymer (de Almeida Neto et al., 2019; Naphade & Jog, 2012b). The typical peaks of nZnO were not detectable in the pattern of bionanocomposite samples, nor the addition of the nanoparticles induced changes in the pattern of the matrix.

Figure 5.9 shows instead the FTIR spectrum of the samples. The sharp peak at 1719 cm^{-1} is attributed to the C=O bond stretching, while the peaks in the 1226 cm^{-1} and 1276 cm^{-1} region are associated to the C-O-C stretching vibration (M. J. Costa et al., 2021). C-H stretching bands can be found at 2974 cm^{-1} and in the 825–980 cm^{-1} interval (Kaniuk et al., 2021). In PHBV-Z4 and PHBV-Z6 samples, a broad peak around 1584 cm^{-1} appears that might be linked to the carbonate species on the surface of the nZnO, as previously explained in Chapter 3.

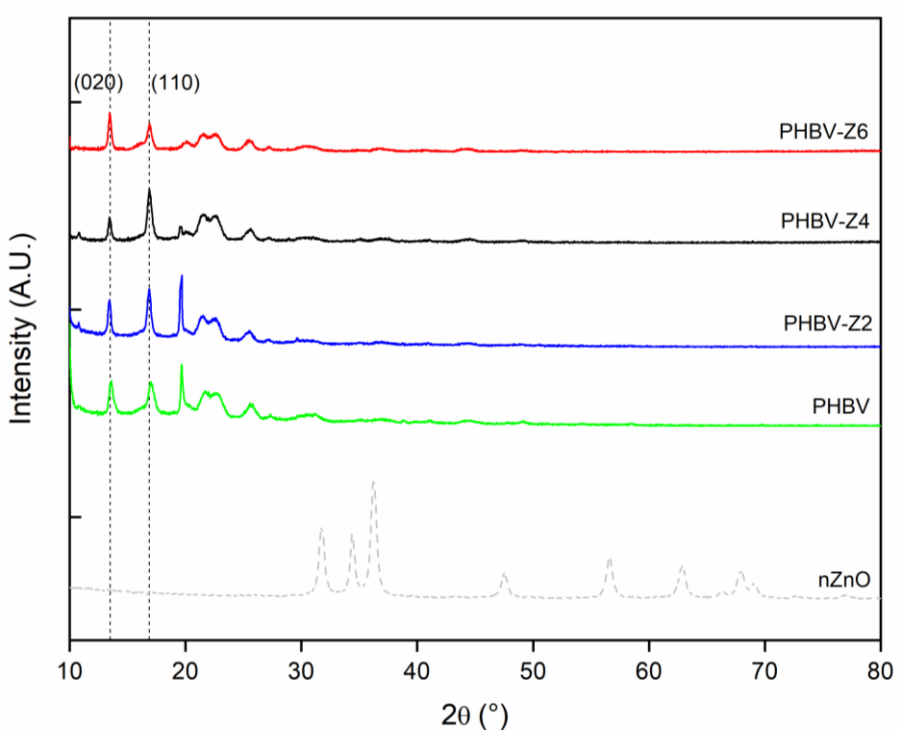


Figure 5.8: XRD patters of PHBV and PHBV-Z films

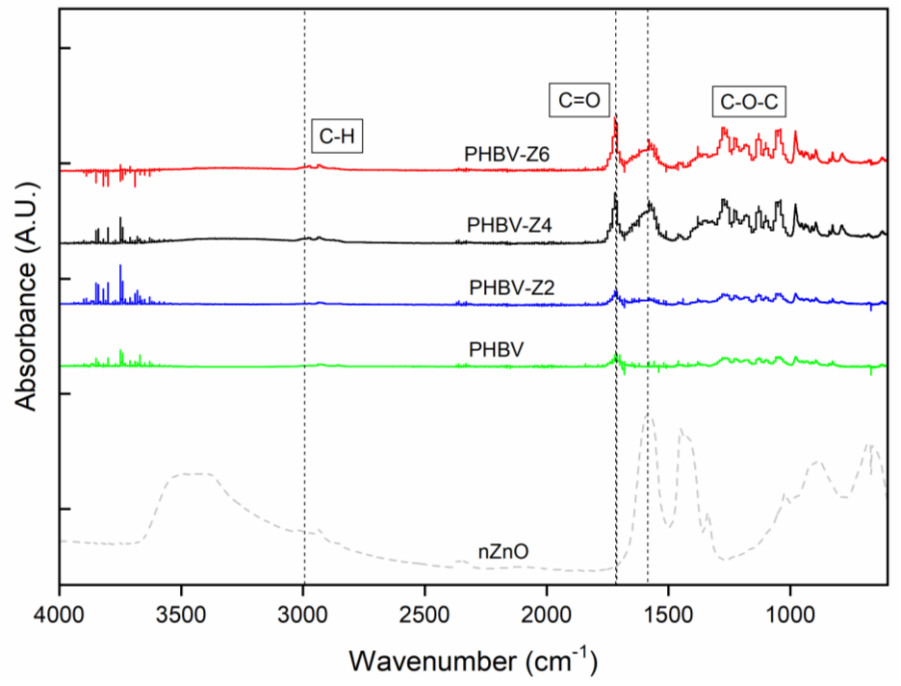


Figure 5.9: ATR-FTIR pattern of PHBV and PHBV-Z films

Figure 5.10 shows the TGA curves of PHBV and PHBV-Z films. All the curves show the typical single-step degradation (M. J. Costa et al., 2021). In accordance with the literature, the addition of nZnO produced a reduction in the onset of the degradation. The T_{50} temperature for PHBV sample was equal to 279°C, while T_{50} for PHBV-Z samples was 271°C. This was ascribed to the higher thermal conductivity and catalytic activity of nZnO (Castro-Mayorga et al., 2017).

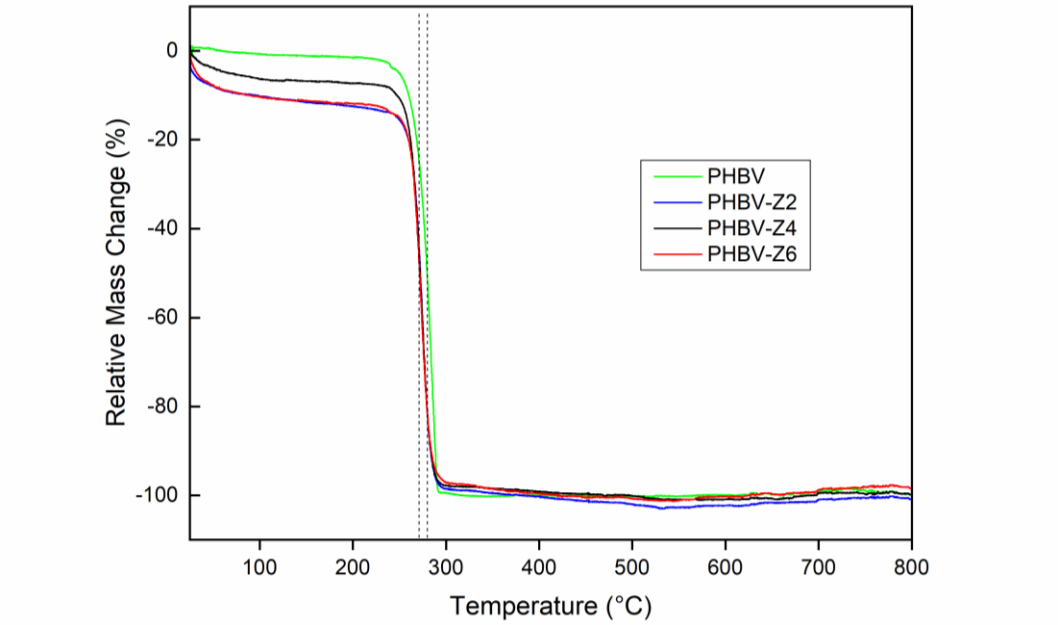


Figure 5.10: TGA curves for PHBV and PHBV-Z films.

5.3.3 Swelling tests

Swelling ratios of BG and BGZ films are show in Figure 5.11. The average SR of the samples is 80%. This value is comparable to the swelling ratios reported in the literature for crosslinked β-glucan hydrogels (Matsumoto et al., 2021) and PVA/β-glucan hydrogels (Muthuramalingam et al., 2019), as well as to the water absorption capacity of commercial hydrogels (Lee et al., 2016; *Neoheal - KIKGEL*, n.d.).

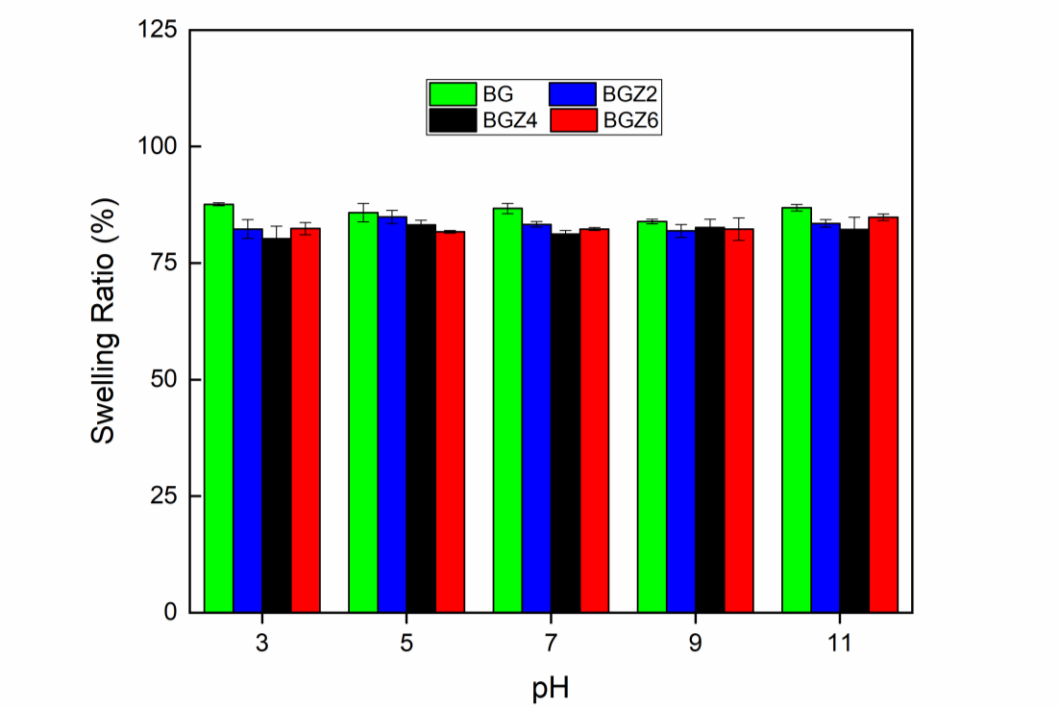


Figure 5.11: Swelling ratio of BG and BGZ films in distilled water at different pH values

Interestingly, neither nZnO content nor pH showed effects on the SR. Swelling of beta-glucan hydrogels is constrained by a multitude of intermolecular hydrogen bonds (Matsumoto et al., 2021). The lack of pH effect of SR suggests that the hydroxyl groups of the β-glucan macromolecules do not exhibit a strong tendency towards dissociation even at high pH values or that the dissociation of hydroxyl moieties at high pH, if any, may be not sufficient to generate enough negative charges to cause electrostatic repulsion among molecules, and to ultimately induce the expansion and swelling of the biopolymeric matrix.

This appears in contrast with the findings of Muthuramalingam and co-workers (Muthuramalingam et al., 2019), who reported a four-fold increase in swelling ratio of PVA/β-glucan hydrogels at pH 9. However, this effect could be attributed to the prevalent content of PVA, which has been shown to exhibit enhanced swelling in alkaline environments (Minhas et al., 2013).

Overall, this can be a positive aspect, as the insensitivity of BGZ films to pH and nZnO content allows their application in the presence of physiological fluids with very different acidity, such as sweat (around 4.5) and wound exudate (typically

between 7.5 and 9). Moreover, nZnO content can be tuned to optimize other key properties without affecting the swelling ratio.

Figure 5.12 shows instead the SR of the PHBV and PHBV-Z films, which are on average lower than in β-glucan films. In fact, PHBV is generally poorly hydrophilic (Kaniuk et al., 2021). No clear behaviour can be identified across the tested pH range, although a pattern seems to emerge at pH > 3. Here, the addition of nZnO produces an initial decrease of the SR compared to the PHBV film, followed by a concentration-dependent increase. As suggested by Zare (Zare et al., 2019), nanoparticles increase tortuosity and water barrier properties, thus reducing water uptake. With higher nZnO concentrations, however, the formation of nanoparticle clusters might create preferential diffusion pathway that enhance the swelling ratio. This effect seems to be more evident at pH 5 and 11, which is further from the isoelectric point of ZnO NPs (~7, see Ch. 3). This would therefore enhance the already mentioned build-up of osmotic pressure promoted by the charged nanoparticles.

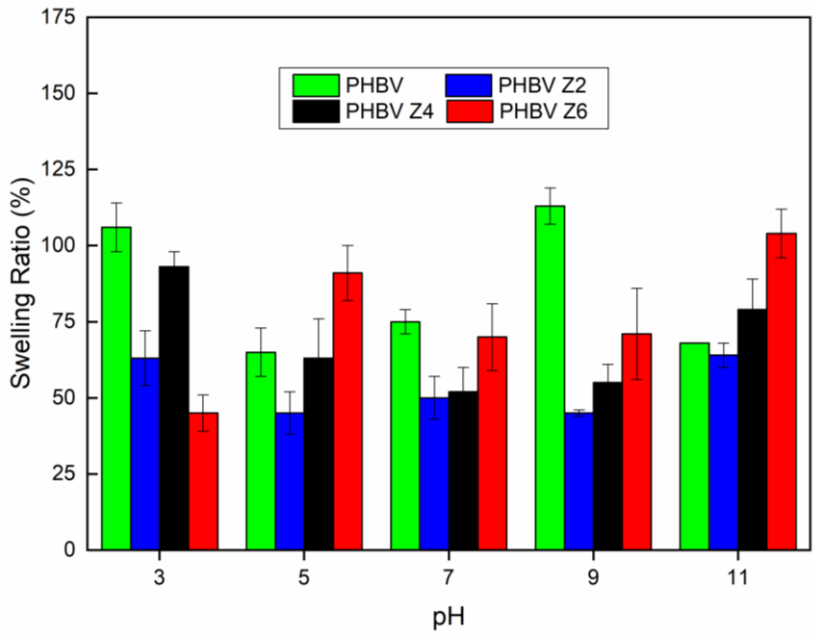


Figure 5.12: Swelling ratio of PHBV and PHBV-Z films in distilled water at different pH values

5.3.4 Antibacterial tests

The antimicrobial activity of the BG, BGZ-2, BGZ-4 and BGZ-6 films has been tested against both *S.epidermids* and *E.coli* and the results are shown in Figures 5.13 and 5.14. Beta-glucans film did not show intrinsic antimicrobial activity. Beta-glucans have been frequently tested in the literature against different microbial strains. Song and Chamidah reported antimicrobial activity of β-glucans from naked barley bran and *Sargassum crassifolium* respectively (Chamidah et al., 2017; Song et al., 2020). Khan and co-workers demonstrated the antimicrobial activity of β-glucans derived from *S. cerevisiae* too (A. A. Khan et al., 2016). β-glucans are found to penetrate bacterial cells interfering with their metabolism and inducing cellular lysis (Chamidah et al., 2017). However, β-glucans antimicrobial effects vary quite widely depending on their purity, origin, molecular weight, structural conformation and chemical modification, as well as on the microbial strains (Chamidah et al., 2017; A. A. Khan et al., 2016; Song et al., 2020). Moreover, the abovementioned studies tested β-glucans in liquid suspensions, which might be substantially different from β-glucans in the form of solid films. In fact, as the polysaccharide molecules are immobilized as part of the film structure, it can be envisaged that their diffusion and consequent penetration of the bacterial cells would be prevented. As an additional consequence, a large fraction of potentially bioactive functional groups would be masked or engaged in intermolecular interactions.

All BGZ films show an antibacterial activity against *S. epidermidis* (Figure 5.13), which appear to be nZnO concentration dependent (Figure 5.14), whereas no activity against *E.coli* was observed. The higher activity of BGZ films on *S. epidermidis* than on *E.coli* is in agreement with the results of antimicrobial tests on nZnO as such, previously discussed. Moreover, the higher activity of the nanocomposite films on the Gram-positive is in accordance with the results of Razzaq et al. on barley BG-ZnO composite films (Razzaq et al., 2021). Azari et al. (Sherafatkhah Azari et al., 2021) reported the preparation of gelatin/β-glucan/ZnO composite films which shown antibacterial properties against *P. aeruginosa, S. typhimorium, S. aureus, E. coli*. Also in their study, antimicrobial effects were more marked on the Gram-positive and could be correlated to the concentration of ZnO nanoparticles, whereas increases in the β-glucan content did not produce any corresponding improvement in antibacterial effects.

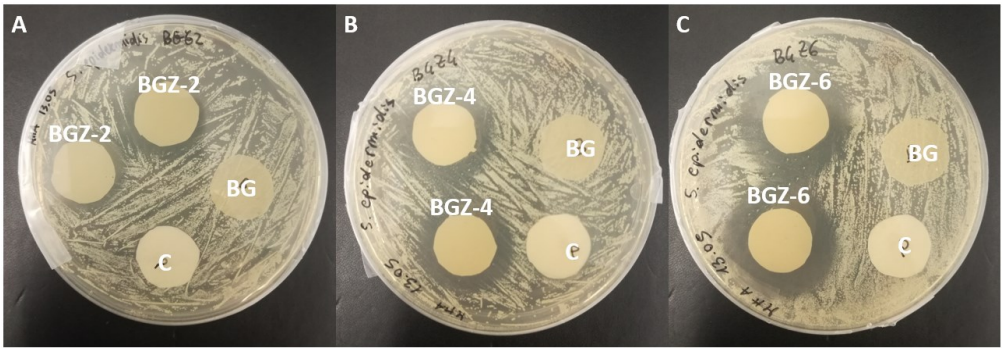


Figure 5.13: Disk diffusion test of (A) BGZ-2, (B) BGZ-4 and (C) BGZ-6 film samples against *S.epidermidis.* C indicates the filter paper control disc.

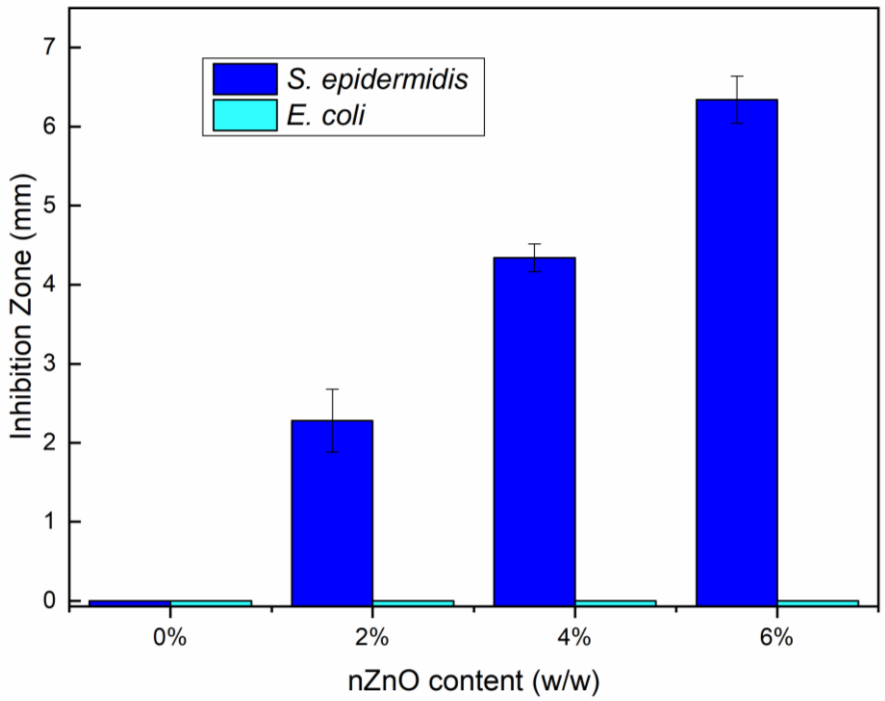


Figure 5.14: Inhibition zone values of BG and BGZ films against *S.epidermids* and *E.coli*

On the other side, PHBV and PHBV-Z films proved much less effective compared to the β-glucan nanocomposites. Figure 5.15 below shows the inhibition zone of the polyester-based films compared to the polysaccharide-based ones. Only samples with a 6% nZnO content could achieve a measurable antibacterial activity, and only limited to *S. epidermidis.* Conversely, the electrospun PLA/PHBV/ZnO NPs composite mats prepared by (Râpă et al., 2021) revealed effective against the

Gram-negative *P. aeruginosa*. Zare and co-workers (Zare et al., 2019) reported significant inhibition of both *S. aureus* and *E. coli* with a PHBV/Chitosan film incorporate with ZnO-Ag nanoparticles obtained through a green hydrothermal method. Similar results were obtained by Ibrahim on the same bacteria for a PHBV/ZnO-Ag bionanocomposite (Ibrahim et al., 2022).

Antibacterial activity in liquid medium against *L. monocytogenes* was also reported by Castro-Mayorga and co-workers (Castro-Mayorga et al., 2017) for PHBV incorporated with 6% w/w 25-nm hexagonal pyramid ZnO nanoparticles. In their study, bionanocomposites were prepared in three different ways. In the first case, ZnO NPs were mixed with molten PHBV pellets and powders, and the mix was subsequently compression moulded to obtain films. In a second case, ZnO-incorporated PHBV nanofibers were produced first, mixed with molten PHBV, and the mix was then compression moulded. In a third case, a compression moulded PHBV film was coated with ZnO-incorporated PHBV nanofibers. These differences in the preparation process of the bionanocomposite translated into different antibacterial performances. In the first case – i.e., film obtained by pure mixing and moulding – antibacterial activity was lowest. In the second case – i.e., film obtained by moulding a mix of PHBV and ZnO NPs-containing PHBV nanofibers – antibacterial activity was higher. This was attributed to the better dispersion of nano zinc oxide achieved through its previous incorporation in the nanofibers. In the third case – i.e., moulded film coated with composite nanofibers – antibacterial activity was the highest and the longest lasting. In fact, in this case nZnO was well disperse *and* widely available at the surface at the same time. This maintained the antibacterial activity constant even after the bionanocomposites were washed for 15 times, each time by immersing them for 5 minutes in Milli-Q water, contrary to the other two samples, for which antibacterial efficacy would gradually decrease with increasing number of washings.

This suggests that the low antibacterial activity reported in the present work for PHBV-Z samples can be attributed to the inhomogeneous structure of the film, as visible in Figure 5.7 above. On one side, this might have led to poor dispersion of nZnO and consequent formation of aggregates, which would reduce its antibacterial action. On another side, the poor wettability of the film and its irregular surface might have considerably reduced the contact area with the MHA plate, further diminishing its final activity. It is also worth highlighting here that PHBV-Z films actually contained *more* nZnO than BGZ ones, as nZnO is added in proportion to the dry biopolymer mass fraction in the film forming solution. This dry mass fraction is 2% for BG and 3% for PHBV.

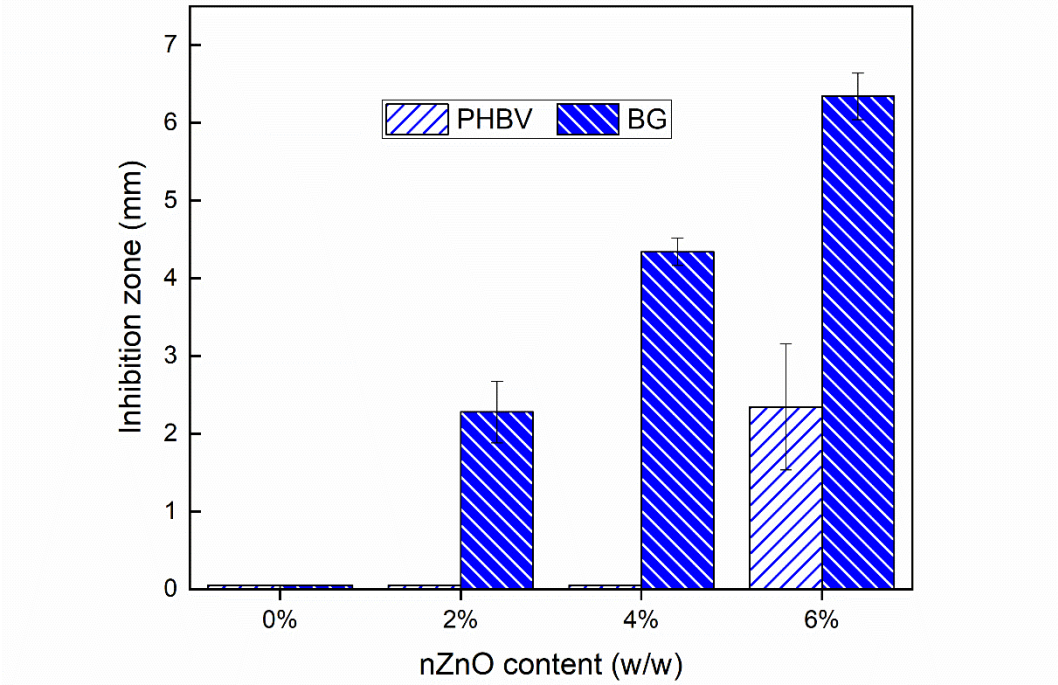


Figure 5.15: Inhibition zone values of BG films versus PHBV films against *S.epidermids*

5.4 Conclusions

Antibacterial bionanocomposite films have been developed for the first time by combining β-glucans from *S. cerevisiae* and nanostructured zinc oxide, using glycerol as a plasticizer. The adopted procedure led good solubilization of the β-glucans in water and to the subsequent formation of a flexible polysaccharide-based material, thus eliminating the need for crosslinking substances and toxic solvents. Addition of nZnO determined a decrease of film transparency but did not affect key functional properties such as the swelling ratio, that is comparable with existing wound dressing solutions, both commercial and reported in the literature. The antibacterial activity was particularly evident against the Gram-positive *S. epidermidis* and it was directly dependent to the nZnO concentration. On the contrary, the effect against the Gram-negative *E. coli* wasn't significative.

In parallel, another biopolymer obtained from microorganisms, PHBV, was used to fabricate bionanocomposites. PHBV is not water soluble, and the selection of different solvents must consider their potential effects on nZnO as well. This led

to the adoption of chloroform, which came however at the expense of film homogeneity. In turn, this affected the optical and antibacterial properties of bionanocomposite films.

All things considered, β-glucans-based films proved more promising on these fronts and established themselves as a point of reference in the domain of microorganisms-derived biopolymers. But there is another domain where biopolymers can be sourced from, waiting to be investigated for the development of next-generation biomedical materials: plants.

References

Antonio, G. P., Fabbricino, P. M., Policastro, G., Fabbricino, Á. M., Fabbricino, M., & Panico, A. (2021). Improving biological production of poly(3-hydroxybutyrate-co-3-hydroxyvalerate) (PHBV) co-polymer: a critical review. *Reviews in Environmental Science and Bio/Technology 2021 20:2*, *20*(2), 479–513. https://doi.org/10.1007/S11157-021-09575-Z

Arfat, Y. A., Benjakul, S., Prodpran, T., Sumpavapol, P., & Songtipya, P. (2014). Properties and antimicrobial activity of fish protein isolate/fish skin gelatin film containing basil leaf essential oil and zinc oxide nanoparticles. *Food Hydrocolloids*, *41*, 265–273. https://doi.org/10.1016/j.foodhyd.2014.04.023

Banchero, M., Mohamed, S. S. Y., Leone, F., Lopez, F., Ronchetti, S., Manna, L., & Onida, B. (2019). Supercritical solvent impregnation of different drugs in mesoporous nanostructured zno. *Pharmaceutics*, *11*(7), 1–14. https://doi.org/10.3390/pharmaceutics11070340

Castro-Mayorga, J. L., Fabra, M. J., Pourrahimi, A. M., Olsson, R. T., & Lagaron, J. M. (2017). The impact of zinc oxide particle morphology as an antimicrobial and when incorporated in poly(3-hydroxybutyrate-co-3-hydroxyvalerate) films for food packaging and food contact surfaces applications. *Food and Bioproducts Processing*, *101*, 32–44. https://doi.org/10.1016/J.FBP.2016.10.007

Chamidah, A., Hardoko, & Prihanto, A. A. (2017). Antibacterial activities of β-glucan (laminaran) against gram-negative and gram-positive bacteria. *AIP Conference Proceedings*, *1844*(May). https://doi.org/10.1063/1.4983422

Chang, J., Li, W., Liu, Q., Zhou, Y., Chen, X., Lyu, Q., & Liu, G. (2019). Preparation, properties, and structural characterization of β-glucan/pullulan blend films. *International Journal of Biological Macromolecules*, *140*, 1269–1276. https://doi.org/10.1016/j.ijbiomac.2019.08.208

Costa, M. J., Pastrana, L. M., Teixeira, J. A., Sillankorva, S. M., & Cerqueira, M. A. (2021). Characterization of PHBV films loaded with FO1 bacteriophage using polyvinyl alcohol-based nanofibers and coatings: A comparative study. *Innovative Food Science & Emerging Technologies*, *69*, 102646. https://doi.org/10.1016/J.IFSET.2021.102646

de Almeida Neto, G. R., Barcelos, M. V., Ribeiro, M. E. A., Folly, M. M., & Rodríguez, R. J. S. (2019). Formulation and characterization of a novel PHBV nanocomposite for bone defect filling and infection treatment. *Materials Science and Engineering: C*, *104*, 110004. https://doi.org/10.1016/J.MSEC.2019.110004

Du, B., Bian, Z., & Xu, B. (2014). Skin Health Promotion Effects of Natural Beta-Glucan Derived from Cereals and Microorganisms: A Review. *Phytotherapy Research*, *28*(2), 159–166. https://doi.org/10.1002/PTR.4963

Elg, F., Posnett, J., & Hunt, S. (2019). Cost-effectiveness of soluble beta-glucan gel in hard-to-heal wounds: An evaluation. *Journal of Wound Care*, *28*(7), 454–460. https://doi.org/10.12968/jowc.2019.28.7.454

EUCAST: Disk diffusion methodology. (n.d.). Retrieved November 25, 2020, from https://www.eucast.org/ast_of_bacteria/disk_diffusion_methodology/

Figueroa-Lopez, K. J., Enescu, D., Torres-Giner, S., Cabedo, L., Cerqueira, M. A., Pastrana, L., Fuciños, P., & Lagaron, J. M. (2020). Development of electrospun active films of poly(3-hydroxybutyrate-co-3-hydroxyvalerate) by the incorporation of cyclodextrin inclusion complexes containing oregano essential oil. *Food Hydrocolloids*, *108*, 106013. https://doi.org/10.1016/J.FOODHYD.2020.106013

Grip, J., Engstad, R. E., Skjæveland, I., Škalko-Basnet, N., & Holsæter, A. M. (2017). Sprayable Carbopol hydrogel with soluble beta-1,3/1,6-glucan as an active ingredient for wound healing – Development and in-vivo evaluation. *European*

Journal of Pharmaceutical Sciences, *107*, 24–31. https://doi.org/10.1016/J.EJPS.2017.06.029

Grip, J., Engstad, R. E., Skjæveland, I., Škalko-Basnet, N., Isaksson, J., Basnet, P., & Holsæter, A. M. (2018). Beta-glucan-loaded nanofiber dressing improves wound healing in diabetic mice. *European Journal of Pharmaceutical Sciences*, *121*, 269–280. https://doi.org/10.1016/J.EJPS.2018.05.031

Huang, M. H., & Yang, M. C. (2008). Evaluation of glucan/poly(vinyl alcohol) blend wound dressing using rat models. *International Journal of Pharmaceutics*, *346*(1–2), 38–46. https://doi.org/10.1016/j.ijpharm.2007.06.021

Hunt, S. D. (2018). A clinical observation evaluation of bioactive soluble beta-glucan gel compared with standard care. *Journal of Wound Care*, *27*(9), 620–630. https://doi.org/10.12968/jowc.2018.27.9.620

Ibrahim, M. I., Alsafadi, D., Alamry, K. A., Oves, M., Alosaimi, A. M., & Hussein, M. A. (2022). A promising antimicrobial bionanocomposite based poly(3-hydroxybutyrate-co-3-hydroxyvalerate) reinforced silver doped zinc oxide nanoparticles. *Scientific Reports 2022 12:1*, *12*(1), 1–10. https://doi.org/10.1038/s41598-022-17470-y

Kacuráková, M., Capek, P., Sasinková, V., Wellner, N., & Ebringerová, A. (2000). FT-IR study of plant cell wall model compounds: pectic polysaccharides and hemicelluloses. *Carbohydrate Polymers*, *43*(2), 195–203. https://doi.org/10.1016/S0144-8617(00)00151-X

Kaniuk, Ł., Ferraris, S., Spriano, S., Luxbacher, T., Krysiak, Z., Berniak, K., Zaszczynska, A., Marzec, M. M., Bernasik, A., Sajkiewicz, P., & Stachewicz, U. (2021). Time-dependent effects on physicochemical and surface properties of PHBV fibers and films in relation to their interactions with fibroblasts. *Applied Surface Science*, *545*, 148983. https://doi.org/10.1016/J.APSUSC.2021.148983

Kaniuk, Ł., Krysiak, Z. J., Metwally, S., & Stachewicz, U. (2020). Osteoblasts and fibroblasts attachment to poly(3-hydroxybutyric acid-co-3-hydrovaleric acid) (PHBV) film and electrospun scaffolds. *Materials Science and Engineering: C*, *110*, 110668. https://doi.org/10.1016/J.MSEC.2020.110668

Khan, A. A., Gani, A., Masoodi, F. A., Amin, F., Wani, I. A., Khanday, F. A., & Gani, A. (2016). Structural, thermal, functional, antioxidant & antimicrobial properties of

β-d-glucan extracted from baker's yeast (Saccharomyces cereviseae)—Effect of γ-irradiation. *Carbohydrate Polymers*, *140*, 442–450. https://doi.org/10.1016/J.CARBPOL.2016.01.003

Lee, O. J., Kim, J. H., Moon, B. M., Chao, J. R., Yoon, J., Ju, H. W., Lee, J. M., Park, H. J., Kim, D. W., Kim, S. J., Park, H. S., & Park, C. H. (2016). Fabrication and characterization of hydrocolloid dressing with silk fibroin nanoparticles for wound healing. *Tissue Engineering and Regenerative Medicine*, *13*(3), 218–226. https://doi.org/10.1007/s13770-016-9058-5

Ma, J., & Underhill, D. M. (2013). β-glucan signaling connects phagocytosis to autophagy. *Glycobiology*, *23*(9), 1047–1051. https://doi.org/10.1093/GLYCOB/CWT046

Majtan, J., & Jesenak, M. (2018). β-Glucans: Multi-Functional Modulator of Wound Healing. *Molecules 2018, Vol. 23, Page 806*, *23*(4), 806. https://doi.org/10.3390/MOLECULES23040806

Matsumoto, Y., Enomoto, Y., Kimura, S., & Iwata, T. (2021). Highly deformable and recoverable cross-linked hydrogels of 1,3-α-D and 1,3-β-D-glucans. *Carbohydrate Polymers*, *251*(July 2020), 116794. https://doi.org/10.1016/j.carbpol.2020.116794

Melendez-Rodriguez, B., Castro-Mayorga, J. L., Reis, M. A. M., Sammon, C., Cabedo, L., Torres-Giner, S., & Lagaron, J. M. (2018). Preparation and Characterization of Electrospun Food Biopackaging Films of Poly(3-hydroxybutyrate-co-3-hydroxyvalerate) Derived From Fruit Pulp Biowaste. *Frontiers in Sustainable Food Systems*, *2*, 38. https://doi.org/10.3389/FSUFS.2018.00038/XML/NLM

Minhas, M. U., Ahmad, M., Ali, L., & Sohail, M. (2013). Synthesis of chemically cross-linked polyvinyl alcohol-co-poly (methacrylic acid) hydrogels by copolymerization; A potential graft-polymeric carrier for oral delivery of 5-fluorouracil. *DARU, Journal of Pharmaceutical Sciences*, *21*(1), 1–9. https://doi.org/10.1186/2008-2231-21-44/TABLES/3

Muthuramalingam, K., Choi, S. I., Hyun, C., Kim, Y. M., & Cho, M. (2019). β-Glucan-Based Wet Dressing for Cutaneous Wound Healing. *Advances in Wound Care*, *8*(4), 125–135. https://doi.org/10.1089/WOUND.2018.0843/ASSET/IMAGES/LARGE/FIGURE5.JPEG

Naphade, R., & Jog, J. (2012a). Electrospinning of PHBV/ZnO membranes: Structure and properties. *Fibers and Polymers 2012 13:6*, *13*(6), 692–697. https://doi.org/10.1007/S12221-012-0692-9

Naphade, R., & Jog, J. (2012b). Electrospinning of PHBV/ZnO membranes: Structure and properties. *Fibers and Polymers 2012 13:6*, *13*(6), 692–697. https://doi.org/10.1007/S12221-012-0692-9

Neoheal - KIKGEL. (n.d.). Retrieved November 10, 2021, from https://kikgel.com.pl/en/products/neoheal/#advantages-of-neoheal--hydrogel-dressing

Nováka, M., Synytsyaa, A., Gedeonb, O., Slepičkac, P., Procházkab, V., Synytsyad, A., Blahovece, J., Hejlovác, A., & Čopíkováa, J. (2012). Yeast β(1-3),(1-6)-d-glucan films: Preparation and characterization of some structural and physical properties. *Carbohydrate Polymers*, *87*(4), 2496–2504. https://doi.org/10.1016/j.carbpol.2011.11.031

Râpă, M., Stefan, M., Popa, P. A., Toloman, D., Leostean, C., Borodi, G., Vodnar, D. C., Wrona, M., Salafranca, J., Nerín, C., Barta, D. G., Suciu, M., Predescu, C., & Matei, E. (2021). Electrospun Nanosystems Based on PHBV and ZnO for Ecological Food Packaging. *Polymers 2021, Vol. 13, Page 2123*, *13*(13), 2123. https://doi.org/10.3390/POLYM13132123

Razzaq, H. A. A., Gomez d'Ayala, G., Santagata, G., Bosco, F., Mollea, C., Larsen, N., & Duraccio, D. (2021). Bioactive films based on barley β-glucans and ZnO for wound healing applications. *Carbohydrate Polymers*, *272*, 118442. https://doi.org/10.1016/J.CARBPOL.2021.118442

Razzaq, H. A. A., Pezzuto, M., Santagata, G., Silvestre, C., Cimmino, S., Larsen, N., & Duraccio, D. (2016). Barley β-glucan-protein based bioplastic film with enhanced physicochemical properties for packaging. *Food Hydrocolloids*, *58*, 276–283. https://doi.org/10.1016/j.foodhyd.2016.03.003

Rivera-Briso, A. L., & Serrano-Aroca, Á. (2018). Poly(3-Hydroxybutyrate-co-3-Hydroxyvalerate): Enhancement Strategies for Advanced Applications. *Polymers*, *10*(7). https://doi.org/10.3390/POLYM10070732

Sagnelli, D., Kirkensgaard, J. J. K., Giosafatto, C. V. L., Ogrodowicz, N., Kruczał, K., Mikkelsen, M. S., Maigret, J. E., Lourdin, D., Mortensen, K., & Blennow, A.

(2017). All-natural bio-plastics using starch-betaglucan composites. *Carbohydrate Polymers*, *172*, 237–245. https://doi.org/10.1016/j.carbpol.2017.05.043

Sherafatkhah Azari, S., Alizadeh, A., Roufegarinejad, L., Asefi, N., & Hamishehkar, H. (2021). Preparation and characterization of gelatin/β-glucan nanocomposite film incorporated with ZnO nanoparticles as an active food packaging system. *Journal of Polymers and the Environment*, *29*(4), 1143–1152. https://doi.org/10.1007/s10924-020-01950-1

Sirelkhatim, A., Mahmud, S., Seeni, A., Kaus, N. H. M., Ann, L. C., Bakhori, S. K. M., Hasan, H., & Mohamad, D. (2015). Review on zinc oxide nanoparticles: Antibacterial activity and toxicity mechanism. *Nano-Micro Letters*, *7*(3), 219–242. https://doi.org/10.1007/s40820-015-0040-x

Socratres, G. (2001). Infrared and Raman Characteristic Group Frequencies. In *Endeavour* (Third, Vol. 5, Issue 2). Wiley. https://doi.org/10.1016/0160-9327(81)90159-9

Song, J., Chen, H., Wei, Y., & Liu, J. (2020). Synthesis of carboxymethylated β-glucan from naked barley bran and its antibacterial activity and mechanism against Staphylococcus aureus. *Carbohydrate Polymers*, *242*, 116418. https://doi.org/10.1016/J.CARBPOL.2020.116418

Tebaldi, M. L., Maia, A. L. C., Poletto, F., de Andrade, F. V., & Soares, D. C. F. (2019). Poly(-3-hydroxybutyrate-co-3-hydroxyvalerate) (PHBV): Current advances in synthesis methodologies, antitumor applications and biocompatibility. *Journal of Drug Delivery Science and Technology*, *51*, 115–126. https://doi.org/10.1016/J.JDDST.2019.02.007

Vaezi, K., Asadpour, G., & Sharifi, H. (2019). Effect of ZnO nanoparticles on the mechanical, barrier and optical properties of thermoplastic cationic starch/montmorillonite biodegradable films. *International Journal of Biological Macromolecules*, *124*, 519–529. https://doi.org/10.1016/j.ijbiomac.2018.11.142

van den Berg, L. M., Zijlstra-Willems, E. M., Richters, C. D., Ulrich, M. M. W., & Geijtenbeek, T. B. H. (2014). Dectin-1 activation induces proliferation and migration of human keratinocytes enhancing wound re-epithelialization. *Cellular Immunology*, *289*(1–2), 49–54. https://doi.org/10.1016/J.CELLIMM.2014.03.007

Wang, Q., Sheng, X., Shi, A., Hu, H., Yang, Y., Liu, L., Fei, L., & Liu, H. (2017). β-Glucans: Relationships between Modification, Conformation and Functional Activities. *Molecules 2017, Vol. 22, Page 257*, *22*(2), 257. https://doi.org/10.3390/MOLECULES22020257

Winiarski, J., Tylus, W., Winiarska, K., Szczygieł, I., & Szczygieł, B. (2018). XPS and FT-IR Characterization of Selected Synthetic Corrosion Products of Zinc Expected in Neutral Environment Containing Chloride Ions. *Journal of Spectroscopy*, *2018*. https://doi.org/10.1155/2018/2079278

Zare, M., Namratha, K., Ilyas, S., Hezam, A., Mathur, S., & Byrappa, K. (2019). Smart Fortified PHBV-CS Biopolymer with ZnO-Ag Nanocomposites for Enhanced Shelf Life of Food Packaging. *ACS Applied Materials and Interfaces*, *11*(51), 48309–48320. https://doi.org/10.1021/ACSAMI.9B15724/ASSET/IMAGES/LARGE/AM9B15724_0004.JPEG

Chapter 6

Wound healing made green: cellulose-based dressings

6.1 Introduction

Cellulose is the most abundant biopolymer on Earth. It is a linear polymer of D-glucose units that constitutes a large fraction of plants cell wall, where it is typically derived from, although also bacteria can synthesize it – in which case it is referred to as *bacterial* cellulose.

Cellulose is non-toxic, biocompatible, biodegradable, and highly stable thanks to its strong intermolecular hydrogen bonds. It has been shown that cellulose can support cell adhesion and tissue regeneration (S. D. Dutta et al., 2019). Carboxymethyl-cellulose (CMC) is a common cellulose derivative that has been widely employed in the fabrication of commercial wound dressings thanks to its high solubility and water absorption properties, as illustrated in the first chapter (Kanikireddy et al., 2020). When produced from bacteria, cellulose naturally comes in the form of a three-dimensional porous fibrous network, which therefore lends itself very well to tissue engineering, and is indeed frequently researched for applications in wound healing (Naomi et al., 2020). However, bacterial cellulose is not as easy to source as plant-derived cellulose, which is a barrier against the diffusion of affordable and easily available healthcare devices (Buldum & Mantalaris, 2021). On the other side, traditional cellulose from plant origin is less hydrophilic, and the production process of cellulose films or other products often

involves the use of toxic chemicals, such as the carbon disulfide employed to obtain dissolvable cellulose in the form of cellulose xanthate (Dawson, 2012).

Therefore, the key to sustainable, cellulose-based wound dressing materials lies in novel types of plant-derived cellulose obtainable through greener routes.

Recently, a research team at McGill University's Pulp and Paper Research Center (Moradian, Alam, et al., 2021) described a procedure to obtain flexible and transparent films from carboxymethyl-cellulose fiber (CMF) i.e., the product of mild carboxymethylation of cellulose pulp with a degree of substitution (DS) of carboxyl groups comprised between 0.1 and 0.4. This allows to dissolve CMF in alkaline solutions, thus removing toxic substances and ultimately resulting into a viscous dope that can be cast and regenerated in a coagulation bath. Additionally, the presence of a certain degree of substitution (DS) of carboxyl groups improves water vapor permeability and moisture absorption (Moradian, Alam, et al., 2021), without however making the final product water soluble as CMC, to the benefit of a much longer utilization. This represents a breakthrough in the path towards the abovementioned sustainable cellulose-based dressings.

This chapter will illustrate the work conducted at McGill's Pulp and Paper Research Center in an endeavor to incorporate nZnO in CMF films in order to make them antibacterial. This work also proven helpful to gain insights into the antibacterial mechanisms of nZnO thanks to the tuneability of the cellulose matrix.

6.2 Experimental

6.2.1 Materials

Bleached softwood kraft pulp was sourced from FPInnovations, (Pointe Claire, Quebec, Canada). Sodium monochloroacetate, sodium hydroxide, sulfuric acid, ethanol, and isopropyl alcohol were purchased from Sigma-Aldrich. Sodium sulfate anhydrous was obtained from Fisher Scientific. All reagents were of analytical grade and used without further purification.

6.2.2 Preparation of CMF dope

Dopes for film production were prepared as described in (Moradian, Islam, et al., 2021) with few modifications. Dopes with two different carboxyl group degrees of substitution were prepared, namely 0.09 and 0.19, in order to ascertain the role

of negatively charged carboxyl groups in affecting the release of antibacterial Zn^{2+} ions.

Briefly, ground pulp was mixed with isopropyl alcohol and a sodium hydroxide solution according to the proportions reported in Table 6.1. The mixture was placed into a 50°C water bath and kept under stirring for 60 min.

Then, an aqueous sodium monochloroacetate (MCA) solution was added, the temperature raised to 60°C, and the mixture left under stirring for additional 120 min. Subsequently, the mixture was vacuum filtered using a 20 μm screen, washed with 800 mL of a 30% (w/w) ethanol aqueous solution for 10 min and filtered again. The washing and filtering step was repeated two times, and the obtained CMF was air dried overnight. After drying, the CMF was finely grinded and dispersed in 250 g of 50% ethanol solution (w/w) for every 10 g of dry CMF. The pH of the dispersion was brought to 3.5 by adding HCl 37% for 10 minutes and subsequently raised to the initial level of 11-12 by adding NaOH 2M. Doing so allows to eliminate the unstable -COOH groups that would otherwise tend to form unwanted CO_2 bubbles inside the final film. The mixture was vacuum filtered, dried overnight in air at room temperature, and grinded.

The degree of substitution was measured through solid-state ^{13}C NMR carried with a Varian/Agilent VNMRS-400 spectrometer at a 100.5 MHz frequency. The DS was determined as the ratio of the integral of C=O/C1.

Finally, CMFs were dissolved in DI water with an equal amount of sodium hydroxide to obtain viscous dopes. Water content was adjusted to have a final CMF concentration of 10% (w/w). The dopes were homogenized for 2 minutes at 10.000 rpm and subsequently degassed by centrifugation for 5 min at 1000 rpm.

Table 6.1: Amounts of solvents and reagents to prepared CMF with different degrees of substitution.

	Degree of substitution	
	0.09	0.19
Reagent	**Mass [g]**	
Pulp	15	15

Isopropyl alcohol	142.5	165
Sodium hydroxide in 9 g of H2O	4.875	4.5
Sodium chloroacetate in 7.5 g of H2O	2.25	4.125

6.2.3 Preparation of CMF films

For film production, a 1-mm thick dope layer was casted on a Teflon mold and then immersed in a 15% (w/w) Na_2SO_4 aqueous regeneration bath for 15 minutes at room temperature. The procedure described in (Moradian, Islam, et al., 2021) employed a H_2SO_4, which however dissolves nZnO. Na_2SO_4 was therefore adopted as an alternative to ensure nZnO integration (S. Wang et al., 2016). Once formed, the films were detached from the mold and then left in DI water overnight for complete washing and neutralization. Wet films were air-dried overnight on a glass plate and used for subsequent characterization. Films obtained from dopes with a degree of substitution of 0.09 have been simply labelled CMF, whereas those with a 0.19 degree of substitution have been labelled CMF19.

For preparation of CMF-nZnO films, nZnO was suspended in DI water, sonicated for 1 hour in a Processor UP200H ultrasonic bath (Hielscher Ultrasonic GmbH, Teltow, Germany), and subsequently mixed with the CMF dope in order to obtain films with a nZnO fraction equal to 2%, 4% and 6% of the dry CMF mass in the dope. These films have been labelled CMF-Z2, CMF-Z4 and CMF-Z6 respectively. To investigate the influence of DS on antibacterial activity, CMF19-Z4 films were made as well.

6.2.3 Preparation of CMC films

In order to further explore the role of DS on bactericidal performances, CMC films were prepared as described in (X. Hu et al., 2022). Briefly, a 2% (w/w) CMC solution in DI water was prepared, and glycerol was added in an amount equal to 25% of the dry CMC mass. For CMC-nZnO films, an aqueous nZnO suspension prepared as described above was added to obtain films with a nZnO content equal to 4% of the dry CMC mass. The mixture was stirred vigorously for 15 minutes, and 30 mL of the so-obtained film forming solution were casted in 15-cm

polypropylene containers and placed in an oven at 50°C for 12 hours, after which films were peeled off and characterized. Films with and without nZnO were labelled CMC-Z4 and CMC respectively. Table 6.2 below summarizes all the samples prepared for the present study.

Table 6.2: Bionanocomposite samples prepared

Matrix type	Dry biomacromolecule mass in the film-forming solution (% w/w)	nZnO (% w/w with respect to the dry biomacromolecule mass)	Label
Carboxymethyl-cellulose fiber with DS = 0.09	8	0	CMF
		2	CMF-Z2
		4	CMF-Z4
		6	CMF-Z6
Carboxymethyl-cellulose fiber with DS = 0.19	8	0	CMF19
		4	CMF19-Z4
Carboxymethyl-cellulose	2	0	CMC
		4	CMC-Z4

6.2.4 Films characterization

The crystalline structure of CMF, CMC, CMF-Z and CMC-Z films was assessed in the 5° to 80° 2θ range using a Bruker D8 Advance X-Ray diffractometer with a Cu Kα radiation source, operated at 40 kV voltage and 40 mA current, with a step size of 0.020°. Films morphology was investigated using a FEI Quanta 450 Environmental Field Emission Scanning Electron Microscope (FESEM) (FEI, Hillsboro, OR, United States). Elemental mapping to ascertain nZnO inclusion and

dispersion was carried via a EDAX TEAM EDS Analysis System (EDAX, Pleasanton, CA, USA). For these analyses, films were previously covered with a 4-nm Pt layer using a Leica EM ACE600 sputtering machine (Leica Microsystems, Wetzlar, Germany). UV-visible spectra were acquired using a Cary 60 UV-Vis Spectrophotometer (Agilent, Santa Clara, CA, United States). FTIR spectroscopy was carried using a Spectrum II instrument equipped with attenuated total reflectance (ATR) accessory, in the 400-4000 cm^{-1} range, with a 1 cm^{-1} resolution. Water contact angle (WCA) measurements were recorded with a Dataphysics Contact Angle System OCA (Future Digital Scientific, Co., NY, USA). Elastic modulus, tensile strength and elongation at break were measured with an Ingstron Mini 44 testing machine with a 500 N load cell. Films were cut in 5x50 mm specimens and positioned in the instrument. Grip separation speed was set at 2 mm/min.

6.2.5 Swelling tests

Swelling tests were carried as described in the previous Chapters.

Briefly, 18-mm diameter disks of CMF and CMF-Z film were cut, weighed, and dried in an oven at 60° until stabilization of the mass. Then, samples were immersed in 20 mL of phosphate buffered saline solution (pH = 7.4). At regular 20-minutes intervals, disks were extracted, excess solution was removed, and wet mass was measured until a constant value was reached. Given that CMF films are insoluble in water, wet mass was also measured after 24h and 48h. The swelling ratio (SR) was determined as:

$$SR = \frac{m_w - m_d}{m_d} \cdot 100$$

Where m_w is the wet mass of each sample and m_d is the dry mass. Each experiment was repeated in triplicate.

6.2.6 Antibacterial tests

The antibacterial activity of CMF and CMC films was assessed through a standard “EUCAST disk diffusion method” (2021) with some variations (EUCAST: Disk Diffusion Methodology, n.d.), as in all the previous Chapters, against *S. epidermidis* LMG 10474 and *E. coli* LMG 08063.

A standardized inoculum was prepared using the direct colony suspension method as described before. 100 µL of the inoculum were spread on MHA plates (Ø 90 mm) and 18 mm diameter discs of all samples were gently deposited on the agar surface. Plates were then incubated at 37°C for 24h. At the end of the incubation period, the antibacterial activity was measured as the average distance between the edge of the film disc and the end of the inhibition zone across two perpendicular disc diameters. Each experiment was done in triplicate.

6.3 Results

6.3.1 Films characterization

Figure 6.1 below shows the UV-visible spectrum of CMF and CMF-Z films.

CMF films have a good transparency, oscillating between roughly 40% and 70% across the visible spectrum. This transparency is decreased upon addition of nZnO, as commonly observed in ZnO-containing bionanocomposites as well as with all the bionanocomposite previously investigated in this work. The presence of nZnO mostly affects UV transmittance, which falls quickly with increasing oxide content. As already mentioned, protecting skin and damaged tissues from harmful UV-radiation is a valuable feature of advanced wound dressings.

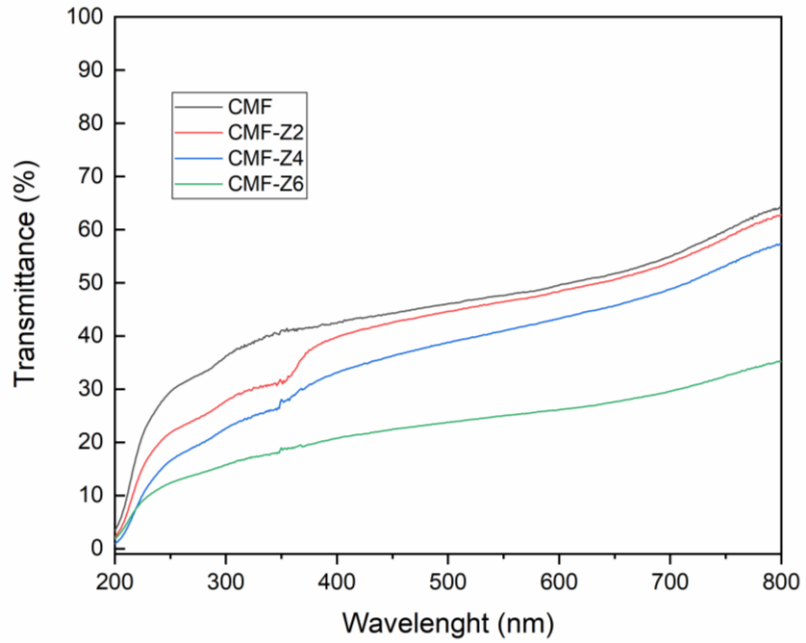


Figure 6.1: UV-vis spectra of CMF and CMF-Z films.

Figure 6.2 shows instead the diffractograms of CMF and CMF-Z films. Two broad peaks can be observed around 11° and 20° that are attributable to the cellulose II structure, representing (110) and $(1\bar{1}0)$ crystal planes respectively (Langan et al., 2001; Moradian & van de Ven, 2022). From the pattern, the presence of an amorphous phase can also be inferred. The addition of nZnO does not modify the diffraction pattern of the matrix. Furthermore, the typical nZnO peaks cannot be detected in the composite samples, presumably due to the relatively small contents of oxide that have been included.

The same applies to the FTIR spectra reported in Figure 6.3. All samples show absorption bands in the ranges around 3330 and 2900 cm^{-1}, assigned to the O–H and C–H stretching vibrations respectively. The peak at 1590 cm^{-1} is associated to the carboxyl group, which demonstrates the successful carboxymethylation reaction described in Sec. 6.2.2 (Moradian, Alam, et al., 2021). The presence of nZnO did not induce any significant shift in peak position.

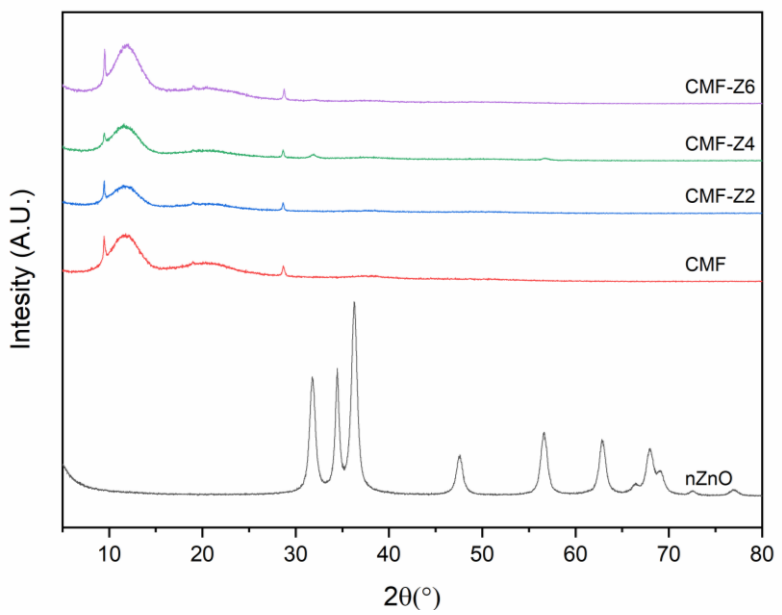


Figure 6.2: XRD spectra of nZnO, CMF and CMF-Z films.

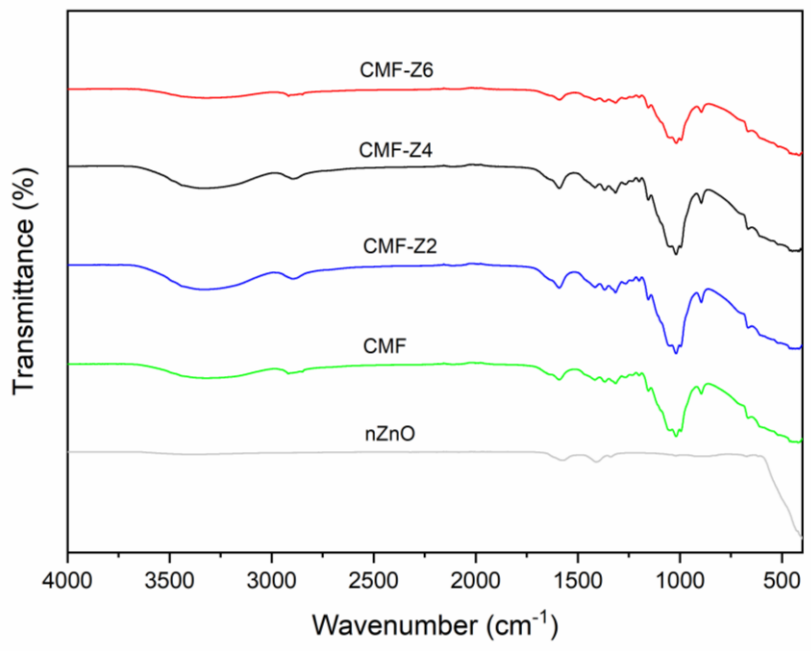


Figure 6.3: ATR-FTIR spectra of nZnO, CMF and CMF-Z films.

Figure 6.4 shows how nZnO content influences the water contact angle of CMF films. A concentration-dependent increase of WCA can be observed across the range of tested nZnO amounts, which brings the initial WCA of 36,00° ± 0,47° of CMF samples to the highest value of 64,89° ± 0,87° in CMF-Z6 samples. This can be attributed to the lower hydrophilicity of nZnO compared to cellulose, but also to an increase of film surface roughness. The increase in WCA, however, does not culminate into hydrophobicity, and wettability properties are maintained that are still relevant for the use of this material for wound dressing applications (Kalantari et al., 2020a; X. Liu et al., 2010a).

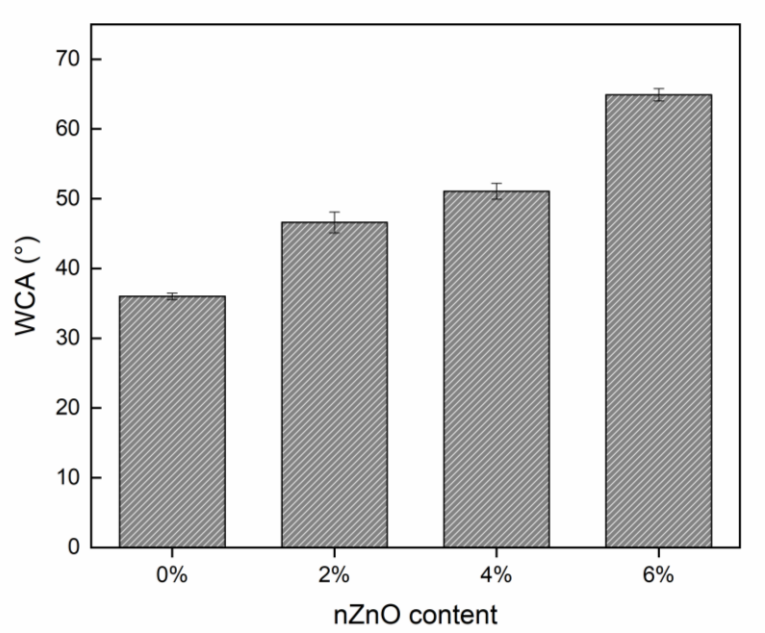


Figure 6.4: WCA of CMF and CMF-Z films.

The mechanical properties of CMF and CMF-Z films are reported in Figure 6.5 below. A 2% nZnO addition produces an increase in tensile strength and elastic modulus, and a corresponding decrease in elongation at break, in line with the reinforcing effect of nZnO in biopolymers (Shahmohammadi Jebel & Almasi, 2016b). Elongation at break always remain around 6% for all nZnO contents, whereas tensile strength falls for nZnO concentrations of 4% and 6%. On the other side, elastic modulus initially drops from 4341,58 ± 227,43 MPa at 2% nZnO content down to 3272,75 ± 314,20 MPa at 4% nZnO, and then increases again 4018,61 ± 418,36 MPa at nZnO contents equal to 6%. This can be explained by several phenomena. As just mentioned, it is known that the introduction of a nanofiller typically induces a stronger yet more brittle behavior in bionanocomposites. This is due both to the superior mechanical properties of nanoparticles and to their physicochemical bonds with the matrix, which oppose and constrain macromolecular motion and overall sample deformation. The decrease in tensile strength and elasticity that is observed above a certain nZnO content threshold shall be attributed to the formation of small aggregates of nZnO. In fact, when too much oxide is added to the film forming dope, achieving homogeneous dispersion becomes increasingly harder, and particles tend to form clusters that act as discontinuities and stress concentrators, thus causing a loss of

mechanical properties. For the same principle, a rough surface – like that of nZnO-rich bionanocomposites, as will be shown soon – is in fact a source of defects where a crack can propagate from.

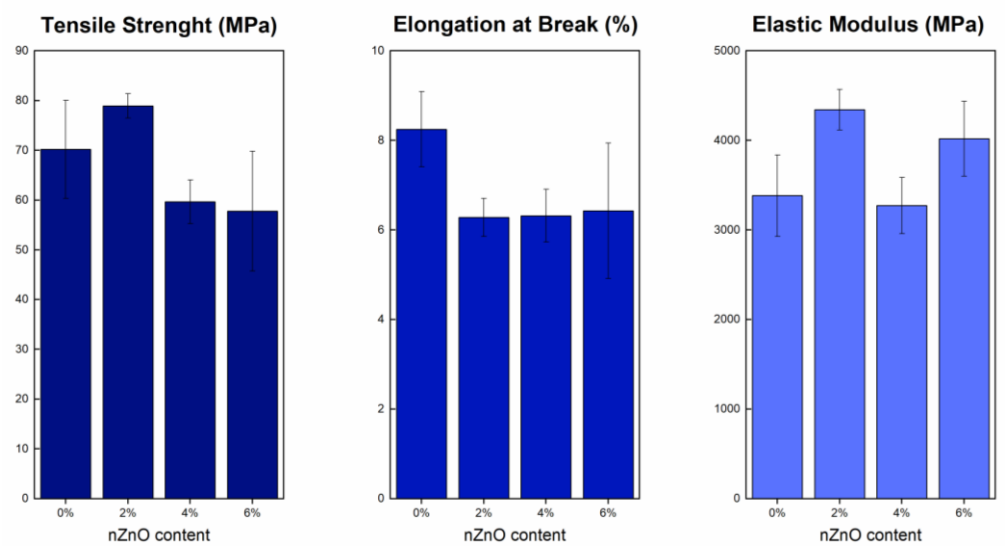


Figure 6.5: Mechanical properties of CMF and CMF-Z films.

It is also interesting here to compare these results with those of the whey protein isolate films and their nZnO-bionanocomposites described in Chapter 4. Table 6.3 below shows the mechanical properties of the WPI and CMF matrixes, together with the WPI-Z4 and CMF-Z4 films, taken here as a reference for the respective bionanocomposites.

CMF films tend to have elastic modulus and tensile strength values two orders of magnitude higher than their WPI counterparts, which in turn show a much higher elongation at break. As already mentioned in the Chapter 4 dedicated to WPI nanocomposites, their mechanical properties are better suited to comply with epithelial tissues, which makes them preferrable as wound dressings under these respects.

Table 6.3: Comparison of mechanical properties between WPI and CMF films and their bionanocomposites

	Elastic Modulus [MPa]	**Tensile Strength [MPa]**	**Elongation at break [%]**

WPI	12.65 ± 0.25	0.56 ± 0.04	106.16 ± 7.99
WPI-Z4	36.25 ± 0.24	0.69 ± 0.01	30.9 ± 0.45
CMF	3383.03 ± 453.60	70.19 ± 9.87	8.25 ± 0.84
CMF-Z4	3272.75 ± 314.20	59.65 ± 4.37	6.32 ± 0.59

In order to characterize film morphology and verify the successful nZnO incorporation and dispersion, CMF and CMF-Z samples were imaged through Scanning Electron Microscopy and subsequently analyzed through energy-dispersive X-Ray spectroscopy. As shown in Figure 6.6 A1, CMF film surface is relatively smooth and homogeneous. The addition of nZnO (Figure 6.6 B1, C1 and D1) induces a gradual evolution towards a more compact morphology with sharper surface features. These images also allow to observe the undissolved fibers that are typically present in CMF dopes and films. Figure 6 also shows the elemental maps of the CMF and CMF-Z samples. The baseline elemental composition of the matrix – carbon, oxygen, and sodium – is reported only for the CMF sample (Figure 6.6 A2) for simplicity. For CMF-Z samples, elemental mapping revealed the presence and distribution of zinc across the surface, showing good dispersion of nZnO for all the three tested nZnO contents (Figure 6.6 B2, C2 and D2).

In order to further characterize nZnO integration in the matrix, CMF-Z4 and CMF-Z6 images at higher magnifications are reported in Figure 6.7. CMF-Z4 samples showed surface aggregates of a few microns in size, which were confirmed to be ZnO via EDS point analysis (Figure 6.7 A1 and A2). These aggregates were not present in the CMF-Z2 sample, which is not reported here for simplicity. Their presence shall therefore be the consequence of the higher nZnO concentration, which favors nanoparticle agglomeration, as mentioned in the previous section. What is perhaps more interesting is that CMF-Z6 samples, despite containing more nZnO, did not show many large aggregates as CMF-Z4. Instead, a multitude of smaller, sub-micrometric clusters could be observed, scattered across the surface of the sample. This might suggest that when nZnO content is increased further, i) nanoparticles tend to emerge at the surface more easily, and ii) more clustering events can occur, which would explain the more numerous yet smaller aggregates that are present. Both these phenomena observed in CMF-Z4 and CMF-Z6 can explain the worsening of their mechanical properties as seen in Figure 6.5.

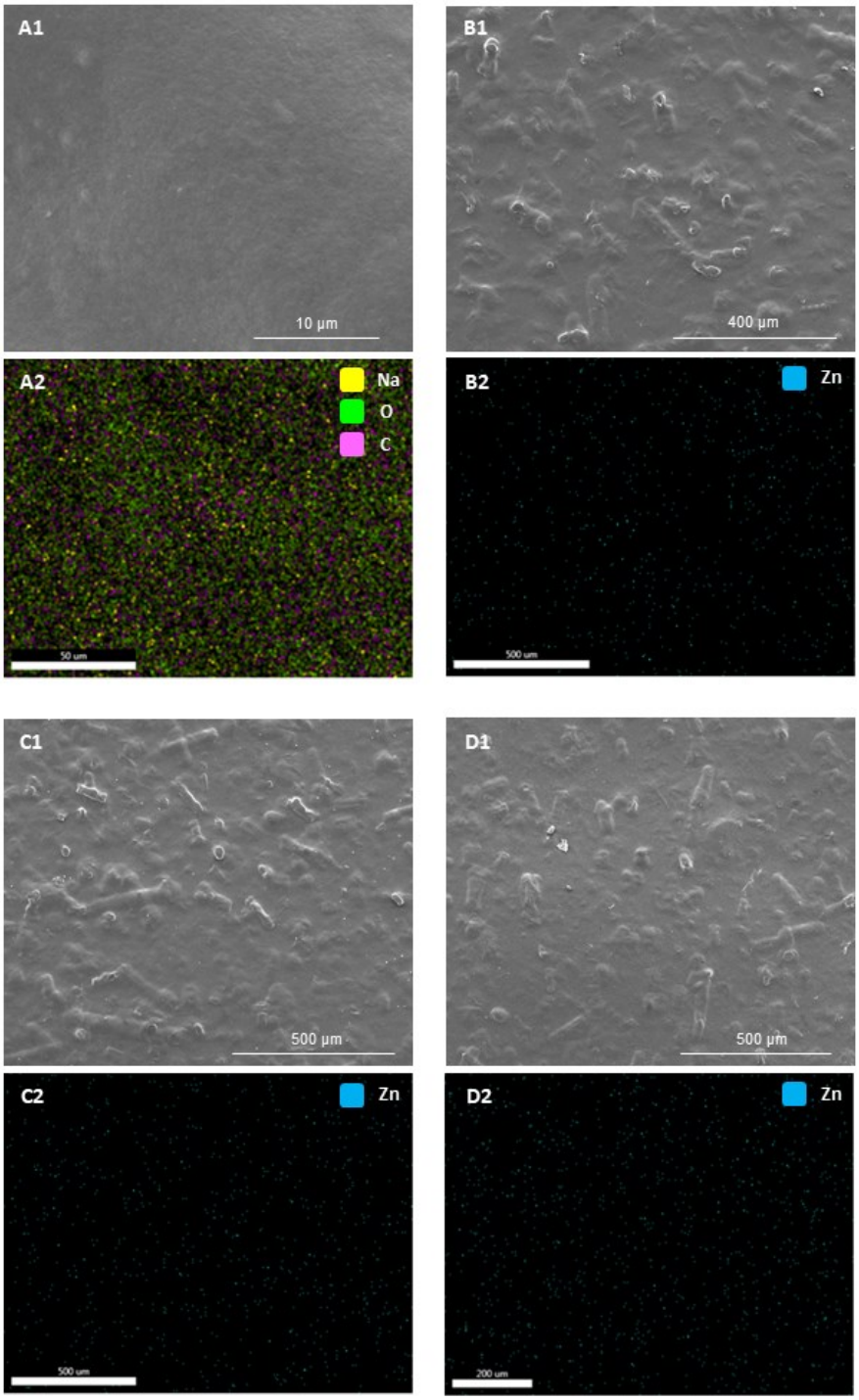


Figure 6.6: SEM images and elemental maps of CMF (A1, A2), CMF-Z2 (B1, B2), CMF-Z4 (C1, C2) and CMF-Z6 (D1, D2) films.

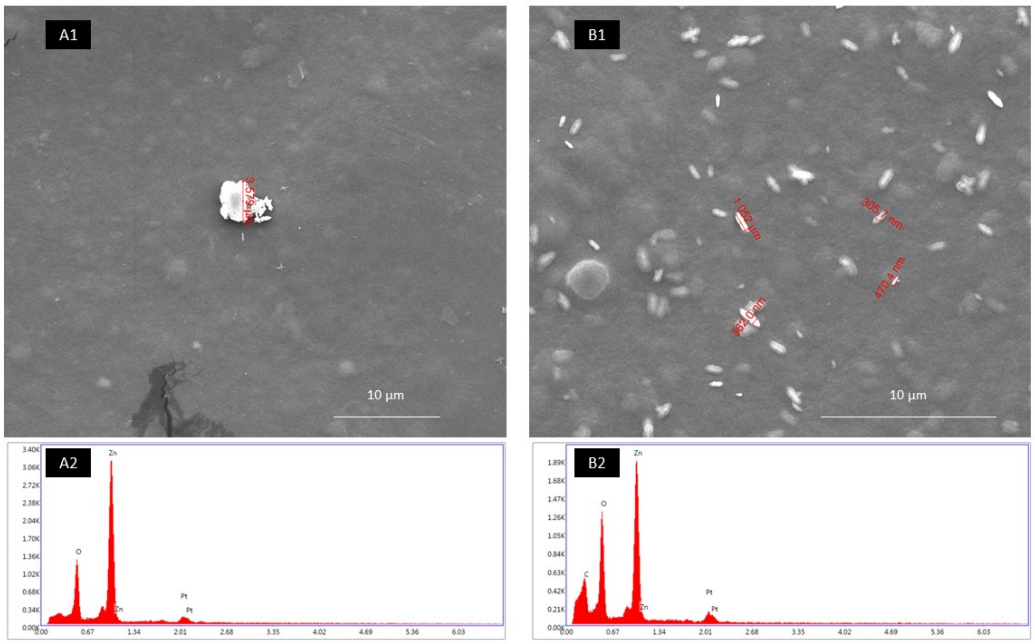


Figure 6.7: Top - SEM images of (A1) CMF-Z4 and (B1) CMF-Z6 samples. Bottom - EDS point analyses of the aggregates on the surface of (A2) CMF-Z4 and (B2) CMF-Z6 samples.

6.3.2 Swelling test

The results of the swelling test are shown in Figure 6.8.

The CMF matrix shows a remarkable 604% ± 59% swelling ratio within two hours, much larger than all the other films assessed in the previous chapters. A concentration-dependent increase is observed up to a 4% nZnO content, where SR peaks at 732% ± 24%. In CMF-Z6, SR goes down again to 640 % ± 70%. This behavior has been frequently reported in the scientific literature on bionanocomposites (Anagha et al., 2019; Sudheesh Kumar et al., 2013a). The addition of nZnO produces an increase in matrix porosity and contributes to water uptake through the build-up of osmotic pressure, as previously explained in Chapter 4. However, a critical concentration of nZnO can be reached that produces the opposite effect, i.e., a lower SR. In fact, very high nZnO contents can constrain water absorption by opposing a physical barrier to water molecules and by increasing the tortuosity of the diffusion path, in addition to reducing the ability of the macromolecules to move to accommodate additional volume.

A small increase in the SR of CMF-Z6 seems to occur after 24h and 48h. This can simply indicate that the additional time spent in the fluid allowed water molecules to fully diffuse into the harder-to-penetrate CMF-Z6 samples, although the final achievable SR still remains constrained by the abundant oxide inclusions. These SRs are similar to the 717% value reported in PBS by (Pei et al., 2015) for regenerated cellulose sponges for wound healing.

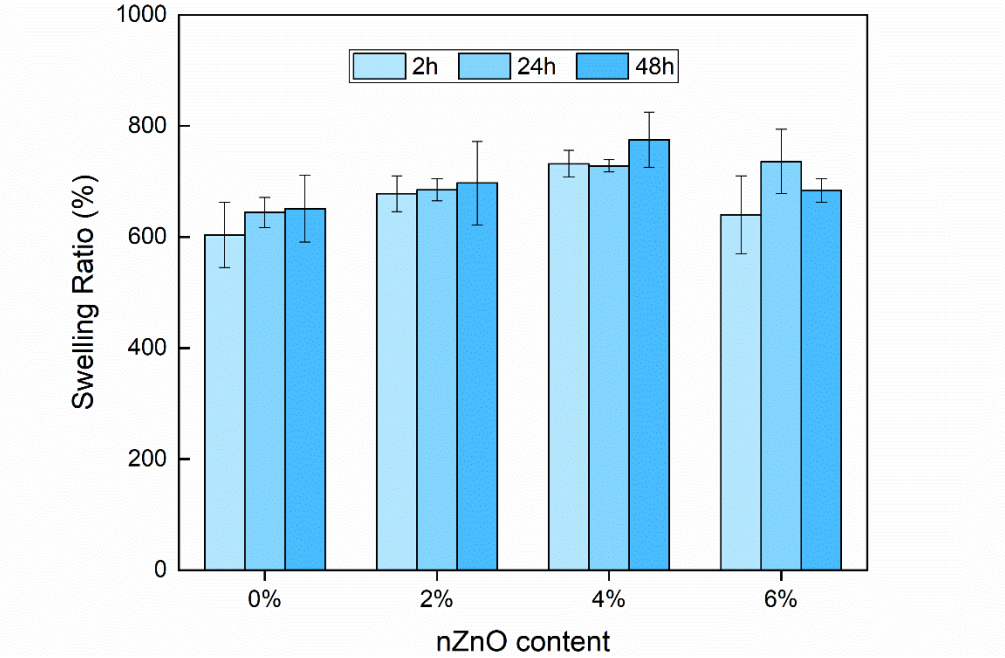


Figure 6.8: Swelling ratio of CMF and CMF-Z films in PBS after 2, 24 and 48 hours.

6.3.3 Antibacterial tests

Results of the antibacterial test are shown in Figure 6.9 below.

CMF films alone did not show any intrinsic antimicrobial activity. A concentration-dependent inhibition could instead be observed against *S. epidermidis* in CMF-Z samples, for 4% and 6% nZnO content. CMF-Z2 films did not induce any inhibition. On the other hand, none of the samples could inhibit the growth of *E. coli*, which confirms the lower effectiveness of nZnO against the Gram-negative.

Similar results were observed by Janpetch and co-workers (Janpetch et al., 2016) for bacterial cellulose/nano-ZnO composites tested against *E. coli* and *S.*

aureus with the disk diffusion method. In 5-mm samples with the highest ZnO content, obtained *ex-situ* after immersion of the cellulose membranes in a 20 % w/v $Zn(NO_3)_2$ solution in methanol and subsequent application of solution plasma process, inhibition halos of 5.33 ± 0.29 mm and 3.33 ± 0.29 mm were reported against *S. aureus* and *E. coli* respectively.

Shahmohammadi Jebel and Almasi (Shahmohammadi Jebel & Almasi, 2016b)prepared bacterial cellulose films containing 5 wt% nano-zinc oxide and carried an agar diffusion test against *S. aureus* and *E. coli* using 5-mm diameter samples. Inhibition halos resulted equal to 11.8 ± 0.04 and 5.6 ± 0.01 mm respectively.

In a review by Zhao et al. (S. W. Zhao et al., 2018) of antibacterial cellulose/ZnO composites with ZnO contents ranging from 2.7 to 37.3 wt%, the inhibition zones reported in the examined studies resulted larger for *S. aureus* than for *E. coli* in 11 out of 12 cases.

It is worth here comparing these antibacterial performances with those of the bionanocomposites tested in the previous chapters. For the sake of comparison, the inhibition zones obtained against *S. epidermidis* by whey protein isolate, beta-glucan, poly(3-hydroxybutyrate-co-3-hydroxyvalerate) and carboxymethyl fiber films with 6% nZnO content are listed in Table 6.4. CMF-Z films are more effective than PHBV films, but less effective than WPI and BG bionanocomposites.

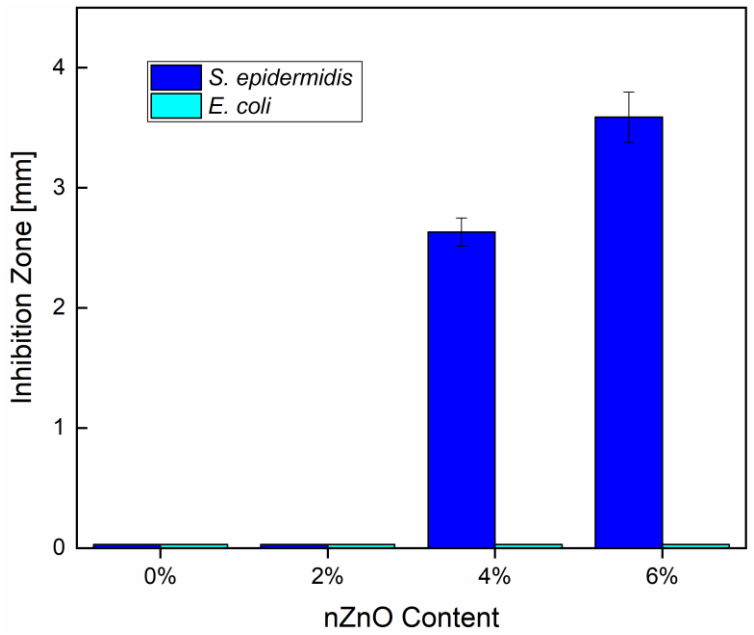


Figure 6.9: Disk diffusion test of CMF and CMF-Z samples against *S. epidermidis* and *E. coli*

Table 6.4: Inhibition zones of the all the bionanocomposites tested so far.

	WPI-Z6	**BG-Z6**	**PHBV-Z6**	**CMF-Z6**
Dry biomacromolecule mass in the film-forming solution (% w/w)	10	2	3	10
nZnO (% w/w with respect to the dry biomacromolecule mass)	6	6	6	6
Inhibition Zone [mm]	4,66 ±0,77	6,34 ±0,59	2,34 ±1,62	3,58 ±0,21

Figure 6.10 shows instead the inhibition activities of CMF-Z4 films compared with CMF19-Z4 and CMC-Z4 samples, i.e., the two bionanocomposites in which the matrix possesses a higher degree of substitution. Compared to CMF, the DS is just slightly higher in the CMF19 matrix, and is highest in CMC. The inhibition

zone values that are reported refer to *S. epidermidis* only, as no inhibition was observed on *E. coli*.

Perhaps not surprisingly, CMF19-Z4 did not show any antimicrobial activity compared to their CMF-Z4 counterpart with a lower DS. In fact, the larger number of negatively charged carboxyl groups in CMF19 might be responsible for the electrostatic sequestration of the antibacterial Zn^{2+} ions, which are therefore prevented from migrating outside the matrix and from ultimately mediating the antibacterial activity. However, when the DS is such that cellulose becomes *carboxymethyl* cellulose, antimicrobial activity becomes more than three-times higher than in the lower-DS CMF. Moreover, as nZnO is added on a dry biopolymer mass basis (which is 8% for CMF and 2% for CMC), the CMC-Z4 samples contain a far lower nZnO mass than CMF-Z4 films. In other words, a much smaller quantity of nZnO achieves a much larger effect when embedded in CMC instead of CMF.

These different antibacterial activities reported demonstrate the key role played by Zn^{2+} diffusion in driving the antibacterial activity of nZnO. As the CMC matrix dissolves upon contact with water, the carboxyl groups can no longer keep the zinc ions sequestered. Instead, matrix dissolution can be leveraged to boost ion transport and diffusion, resulting in the highest antibacterial activity. To the best of our knowledge, this is the first time that the degree of substitution of cellulose is used to probe the influence of Zn^{2+}.

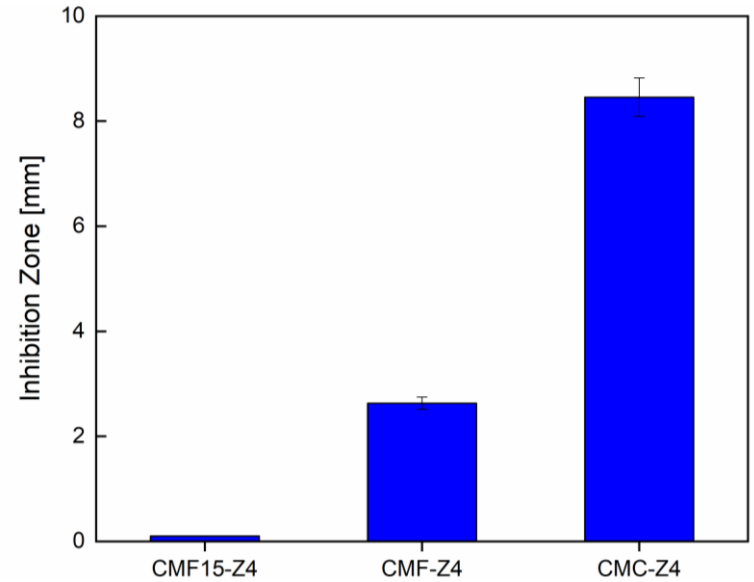


Figure 6.10: Inhibition zone of CMF19-Z4, CMF-Z4 and CMC-Z4 against *S. epidermidis*.

6.4 Conclusions

In this chapter, the use of the novel CMF films for the fabrication of nZnO-bionanocomposites has been explored for the first time, and the peculiar properties of cellulose have been leveraged to shed light on the highly debated antibacterial mechanism of nanostructured zinc oxide.

Carboxymethylated fiber films are a breakthrough in the search for green and affordable cellulose-based materials, and their properties and applications remain yet to be fully discovered. Given their simple fabrication route, they lend themselves very well for integration with other materials that can further extend their capabilities and use cases. In this case, a process was crafted to successfully disperse nZnO and to finally obtain antibacterial cellulose-based bionanocomposites. These have been extensively characterized, showing how nZnO increases water contact angle, swelling ratio and UV-barrier properties while inducing brittleness. Their antibacterial properties proved lower than the whey protein or beta-glucan based composite films, but higher effectiveness can be achieved by manipulating the degree of substitution of carboxyl groups. However, this comes at the expense of film stability in aqueous solution, as carboxymethyl cellulose is in fact completely soluble. This implies that a wound dressing would be extremely short-lasting and hard to maintain firmly positioned on the wounded area. Possible future solutions might be researched in the combination of CMF with CMC into hybrid, cellulose-based dressings.

At this point in our journey, advanced bionanocomposite wound dressings have been developed and investigated using biomacromolecules coming from four different biological sources: animals, yeasts, bacteria, and plants. While all of them possessed promising characteristic and features, whey protein isolate/nZnO bionanocomposites showed the best compromise among physicochemical, functional and antibacterial properties. For this reason, their study has been taken to the next level. This will be the objective of the next Chapter.

References

Anagha, B., George, D., Maheswari, P. U., & Begum, K. M. M. S. (2019). Biomass Derived Antimicrobial Hybrid Cellulose Hydrogel with Green ZnO Nanoparticles for Curcumin Delivery and its Kinetic Modelling. *Journal of Polymers and the Environment*, *27*(9), 2054–2067. https://doi.org/10.1007/s10924-019-01495-y

Buldum, G., & Mantalaris, A. (2021). Systematic Understanding of Recent Developments in Bacterial Cellulose Biosynthesis at Genetic, Bioprocess and Product Levels. *International Journal of Molecular Sciences 2021, Vol. 22, Page 7192*, *22*(13), 7192. https://doi.org/10.3390/IJMS22137192

Dawson, T. (2012). Progress towards a greener textile industry. *Coloration Technology*, *128*(1), 1–8. https://doi.org/10.1111/J.1478-4408.2011.00346.X

Dutta, S. D., Patel, D. K., & Lim, K. T. (2019). Functional cellulose-based hydrogels as extracellular matrices for tissue engineering. *Journal of Biological Engineering 2019 13:1*, *13*(1), 1–19. https://doi.org/10.1186/S13036-019-0177-0

Hu, X., Liu, Y., Zhu, D., Jin, Y., Jin, H., & Sheng, L. (2022). Preparation and characterization of edible carboxymethyl cellulose films containing natural antibacterial agents: Lysozyme. *Food Chemistry*, *385*, 132708. https://doi.org/10.1016/J.FOODCHEM.2022.132708

Janpetch, N., Saito, N., & Rujiravanit, R. (2016). Fabrication of bacterial cellulose-ZnO composite via solution plasma process for antibacterial applications. *Carbohydrate Polymers*, *148*, 335–344. https://doi.org/10.1016/J.CARBPOL.2016.04.066

Kalantari, K., Mostafavi, E., Saleh, B., Soltantabar, P., & Webster, T. J. (2020). Chitosan/PVA hydrogels incorporated with green synthesized cerium oxide nanoparticles for wound healing applications. *European Polymer Journal*, *134*, 109853. https://doi.org/10.1016/J.EURPOLYMJ.2020.109853

Kanikireddy, V., Varaprasad, K., Jayaramudu, T., Karthikeyan, C., & Sadiku, R. (2020). Carboxymethyl cellulose-based materials for infection control and wound healing: A review. *International Journal of Biological Macromolecules*, *164*, 963–975. https://doi.org/10.1016/J.IJBIOMAC.2020.07.160

Langan, P., Nishiyama, Y., & Chanzy, H. (2001). X-ray Structure of Mercerized Cellulose II at 1 Å Resolution. *Biomacromolecules*, *2*(2), 410–416. https://doi.org/10.1021/BM005612Q

Liu, X., Lin, T., Fang, J., Yao, G., Zhao, H., Dodson, M., & Wang, X. (2010). In vivo wound healing and antibacterial performances of electrospun nanofibre membranes. *Journal of Biomedical Materials Research Part A*, *94A*(2), 499–508. https://doi.org/10.1002/JBM.A.32718

Moradian, M., Alam, M. N., & van de Ven, T. G. M. (2021). Influence of Carboxyl Charge Density on Properties of Extruded Cellulose Films. *Industrial and Engineering Chemistry Research*, *60*(38), 13756–13763. https://doi.org/10.1021/ACS.IECR.1C01716/ASSET/IMAGES/MEDIUM/IE1C01716_0009.GIF

Moradian, M., Islam, M. S., & van de Ven, T. G. M. (2021). Insoluble Regenerated Cellulose Films Made from Mildly Carboxylated Dissolving and Kraft Pulps. *Industrial and Engineering Chemistry Research*, *60*(15), 5385–5393. https://doi.org/10.1021/ACS.IECR.1C00485/ASSET/IMAGES/MEDIUM/IE1C00485_0012.GIF

Moradian, M., & van de Ven, T. G. M. (2022). Formation of cellulose microspheres and nanocrystals from mildly carboxylated fibers. *Cellulose*, *29*(6), 3225–3237. https://doi.org/10.1007/S10570-022-04486-W/FIGURES/7

Naomi, R., Idrus, R. B. H., & Fauzi, M. B. (2020). Plant- vs. Bacterial-Derived Cellulose for Wound Healing: A Review. *International Journal of Environmental Research and Public Health*, *17*(18), 1–25. https://doi.org/10.3390/IJERPH17186803

Pei, Y., Ye, D., Zhao, Q., Wang, X., Zhang, C., Huang, W., Zhang, N., Liu, S., & Zhang, L. (2015). Effectively promoting wound healing with cellulose/gelatin sponges constructed directly from a cellulose solution. *Journal of Materials Chemistry B*, *3*(38), 7518–7528. https://doi.org/10.1039/C5TB00477B

Shahmohammadi Jebel, F., & Almasi, H. (2016). Morphological, physical, antimicrobial and release properties of ZnO nanoparticles-loaded bacterial cellulose films. *Carbohydrate Polymers*, *149*, 8–19. https://doi.org/10.1016/J.CARBPOL.2016.04.089

Sudheesh Kumar, P. T., Lakshmanan, V. K., Raj, M., Biswas, R., Hiroshi, T., Nair, S. v., & Jayakumar, R. (2013). Evaluation of wound healing potential of β-chitin hydrogel/nano zinc oxide composite bandage. *Pharmaceutical Research*, *30*(2), 523–537. https://doi.org/10.1007/s11095-012-0898-y

Wang, S., Lu, A., & Zhang, L. (2016). Recent advances in regenerated cellulose materials. *Progress in Polymer Science*, *53*, 169–206. https://doi.org/10.1016/J.PROGPOLYMSCI.2015.07.003

Zhao, S. W., Guo, C. R., Hu, Y. Z., Guo, Y. R., & Pan, Q. J. (2018). The preparation and antibacterial activity of cellulose/ZnO composite: A review. *Open Chemistry*, *16*(1), 9–20. https://doi.org/10.1515/CHEM-2018-0006/ASSET/GRAPHIC/J_CHEM-2018-0006_FIG_003.JPG

Chapter 7

Taken to the next level: a biopharmaceutical characterization of Whey Protein Isolate-nZnO bionanocomposites

7.1 Introduction

So far, the experimental activity carried for this work spanned across four different biomacromolecular matrixes, exploring their properties and unique features, in an effort to understand what is the most promising as a wound dressing.

Poly(3-hydroxybutyrate-co-3-hydroxyvalerate), or PHBV, although utilized in tissue engineering, is poorly suitable for the fabrication of wound dressing films. Firstly, its poor water affinity largely affects the ability of PHBV films to adhere to wet surfaces, which resulted into smaller bacterial inhibition zones compared to other bionanocomposites. Secondly, their inhomogeneous aspect worsens their transparency. Thirdly, different solvents than chloroform would be more preferable for its preparation. Beta-glucans, despite being able to support very well the antibacterial activity of nZnO, showed poor optical properties and swelling abilities. Carboxymethyl fiber demonstrated an excellent swelling ability, but a smaller antibacterial activity and a more complex production process compared to other alternatives. In the end, whey protein isolate-based bionanocomposites

showed the best combination of swelling ability, transparency, mechanical properties and antibacterial activity. Figure 7.1 below compares the optical properties and inhibition zones of the four bionanocomposites examined so far, taking those containing 4% nZnO as a reference. This summary view of the antibacterial performance of the bionanocomposites developed and tested for this work also gives a good opportunity to compare them with current commercial wound dressings. Nano-zinc oxide has not made its way through commercial use in wound dressings yet. Zinc oxide is only present in wound care products such as pastes and bandages containing from 9.25% to 20% of oxide, and for which antibacterial test reports could not be found (Lansdown et al., 2007a). Majority of the most advanced wound dressings today use silver as antimicrobial agent instead, and therefore represent the main alternative to benchmark the bionanocomposites here described against. Agar disk diffusion tests were done by Wiegand and co-workers (Wiegand et al., 2015) on Ag-containing commercial dressings, namely alginate-based Suprasorb® A + Ag and Acticoat®, sodium carboxymethylcellulose-based Aquacel® Ag, and polyurethane-based UrgoCell® Silver. The composites were cut in 6-mm disks and tested against Gram-positive *S. aureus* ATCC 6538 and Gram-negative *P. aeruginosa* ATCC 27853. All the inhibition halos around the film samples reported in the study were between 6 and 12 mm for the Gram-positive, and between 6 and 9 mm for the Gram-negative. Similarly, Yunoki et al. (Yunoki et al., 2015) conducted disk diffusion tests against *S. aureus* ATCC 12783 and *P. aeruginosa* ATCC 3080 of the following Ag-containing dressings: hydrocolloid Biohesive® Ag, nonwoven fabrics Aquacel® Ag and Algisite™, and foams Mepilex® Ag and PolyMem® Ag. The inhibition halos around 20-mm disks were between 0 and 1.0 ± 0.2 mm for the Gram-positive and between 0 and 1.5 ± 0.1 mm for the Gram-negative.

Albeit the bacterial strains used in the cited reports are different from those tested in the present study, it can cautiously be suggested that the bionanocomposites developed in this work may hold some potential to be as good as – if not better – at inhibiting bacterial growth than today's products.

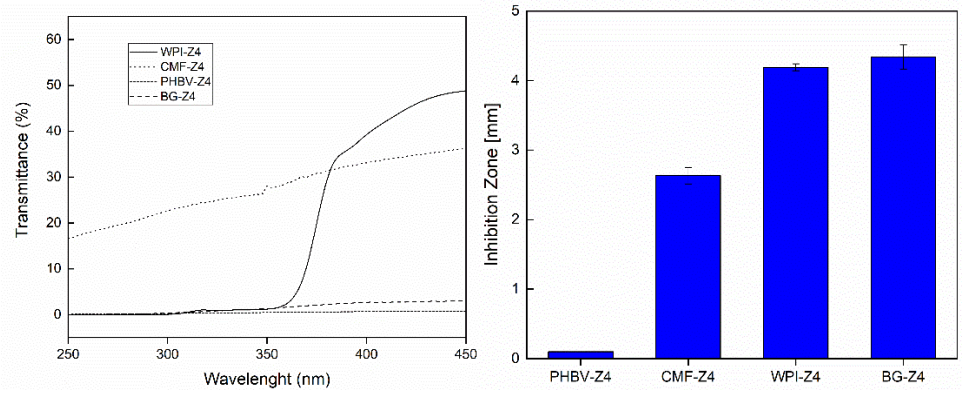


Figure 7.1: (left) optical transmittance of bionanocomposites with 4% nZnO content and (right) their inhibition zone against *S. epidermidis*.

For all these reasons, WPI-nZnO composites were chosen to bring the research of the next-generation wound dressing material to the next level. This chapter will illustrate the work done in collaboration with the University of Pavia's Department of Drug Sciences to deepen the research on WPI-nZnO with a complete biopharmaceutical study, that culminated with *in-vivo* wound healing studies. Of all the WPI-nZnO tested, WPI-Z4 were selected for the study, as the best compromise between antibacterial activity, optical and mechanical properties, and swelling abilities. Unless otherwise specified, WPI-Z4 samples will thus be referred to simply as WPZ.

7.2 Experimental

7.2.1 Water Contact Angle Measurements

Water Contact Angle (WCA) was measured using a DMe-211 Plus Contact Angle Meter (Kyowa Interface Science Co Ltd., Saitama, Japan) according to the $\theta/2$ method. For the test, a 10 μl drop of Phosphate Buffer Solution (PBS, pH 7.4; Biosolve Chimie, Dieuze, France) was deposited onto the surface of WPI and WPZ samples and the contact angle was measured over time at 1 second intervals using FAMAS Dropmaster Software. The experiment was repeated five times.

7.2.2 Hydration test

A hydration test was carried out to monitor water uptake of the film over time. In fact, as wound exudate is gradually secreted, the wound dressing needs to be capable of absorbing and retaining it, preventing tissue maceration.

An experimental set-up has been crafted to better replicate the contact conditions between the films and an exuding wound area. The wells of a polypropylene plate (Corning® 12 Well TC-Treated Microplates, New York, NY, USA) have been filled to the brim with PBS. Subsequently, a layer of Parafilm® has been applied over the plate and pierced in correspondence of the PBS-filled wells, allowing the liquid to surface, forming a thin wet layer on the Parafilm®. WPI and WPZ films have been cut in circles with equal diameter to the wells and dried in an oven at 60°C until stabilization of the mass. Samples were then placed on disks of dialysis membrane of equal size. This allowed to safely manipulate the films across the entire duration of the experiment without compromising their integrity. Membrane-supported film specimens have thus been placed on the wet Parafilm®, and the entire set-up was placed inside an incubator at 32°C to simulate the temperature of the skin. A schematic representation of the set-up is shown in Figure 7.2. To finally measure the swelling ratio (SR), specimens were collected, blotted away of excess water with filter paper, and weighted. The SR was then determined as follows:

$$SR = \frac{m_w - m_d}{m_d} \cdot 100$$

Where m_w is the wet mass and m_d is the dry initial mass. The swelling ratio has been calculated after 1, 3, 6 and 24 h. The experiment has been done in triplicate.

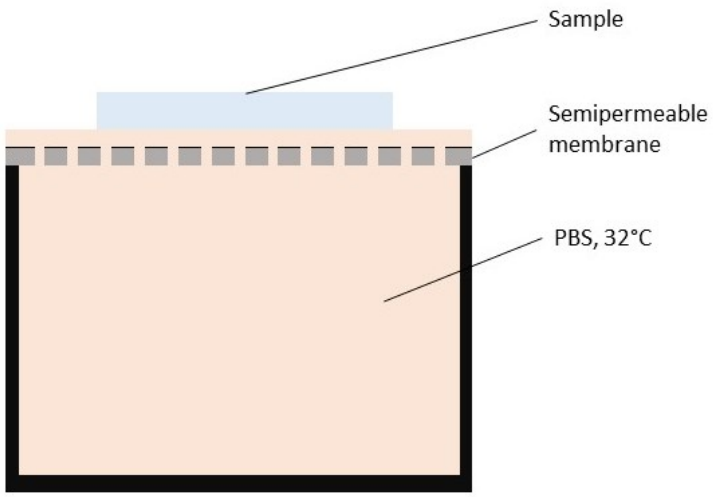


Figure 7.2: Graphical representation of the experimental set-up used for the hydration test. The semipermeable membrane is comprised by a dialysis membrane supported by a pierced Parafilm® sheet.

7.2.3 Viscoelastic Properties after Hydration

Dynamic oscillatory measurements were performed on samples hydrated for 24 hours by means of a rotational rheometer (MCR102, Anton Paar, Turin, Italy), using a parallel plate combination (PP25, 25 mm diameter) as measuring system. In the oscillation test, a 1 Pa shear stress was applied at rising frequencies (1 to 10 Hz) and G' (storage modulus) and G" (loss modulus) profiles were recorded. Measurements were performed at 32°C and repeated three times for each sample.

7.2.4 Degradation test

Time-dependent degradation of WPI and WPZ films was investigated by soaking the samples in two different degradation media: PBS (Kumar et al., 2022) and H_2O_2 500 μM in PBS (Ransy et al., 2020)

WPI and WPZ discs have been dried at 60°C until stabilization of the weight (30 ± 5 mg) and subsequently immersed in 5 mL of PBS or H_2O_2 500 μM in PBS to simulate the oxidative stress in the early inflammatory phase of the healing process (Schäfer & Werner, 2008; Vigani et al., 2019). Immersed films have been kept at 32°C for the entire duration of the experiment.

After 1, 3 and 7 days, sample degradation was assessed in terms of (i) proteins dissolved in the degradation media and (ii) film residual mass. In particular, the concentration of proteins dissolved in each medium as a consequence of film degradation was derived from optical absorbance measurements at $\boldsymbol{\lambda}$ = 280 nm against a calibration curve obtained by measuring the absorbance of WPI suspensions of known concentration, using a UV-vis Lamba 25 spectrophotometer (Perkin Elmer, Milan, Italy).

To determine the film residual mass, samples have been collected and dried in an oven at 60°C until stabilization of the weight. The residual mass (R) has been determined as:

$$R = \frac{m_f}{m_0} \cdot 100$$

where m_f is the final residual dry mass and m_0 is the dry initial mass. The experiment has been repeated three times.

7.2.5 Antimicrobial test

The antibacterial activity of WPI and WPZ films was investigated against pathogen *Staphylococcus aureus* ATCC 6538 (Gram+) and *Escherichia coli* ATCC 10356 (Gram-) following the Japanese Industrial Standard (JIS Z 2811) protocol (ISO, n.d.; JIS, 99 C.E.).

Before testing, the microorganisms were grown overnight in Tryptone Soya Broth (Oxoid; Basingstoke, Hampshire, England) at 37°C. Washed cells were resuspended in Dulbecco's PBS and optical density (OD) at 650 nm was adjusted to 0.3, i.e., approximately to $1x10^8$ Colony Forming Units (CFU/ml).

10 µl of inoculum was deposited on a standard glass slide (76 x 26 mm), and then covered with WPI or WPZ film samples (20 x 20 mm). The glasses were introduced in a Falcon test-tube (50 ml) with 1 ml of PBS to maintain a damp environment and then maintained at room temperature for either 6 or 24 hours. Subsequently, 9 ml of PBS were added to each Falcon tube and gently shaken to detach the WPZ and WPI samples from the glass slides. Bacterial suspensions were then grown in Tryptone Soya Agar to count viable cells. The decimal-log reduction rate, microbicidal effect (ME), was calculated as:

$$ME = \log NC - \log NE$$

where NC is the number of CFU/ml grown on the control glasses (WPI film), and NE is the number of CFU/ml counted after exposure to WPZ films, expressed as the average of three equivalent determinations (Fraise et al., 2013; Grisoli et al., 2021).

7.2.6 *In vitro* cytocompatibility test

A cytocompatibility test has been conducted using Normal Human Dermal Fibroblasts (NHDF) from juvenile foreskin (PromoCell GmbH, VWR, Milan, Italy) from 6^{th} to 12^{th} passage.

Cells were cultured in polystyrene flasks in Dulbecco's Modified Eagle's Medium (DMEM), supplemented with 10% v/v heat-inactivated Fetal Bovine Serum (FBS) (VWR International S.r.l, Milan, Italy), and with 1% v/v antibiotic-antimycotic solution (Merk Life Science S.r.l., Milan, Italy), at 37°C in 5% CO_2 atmosphere.

Extraction dilution method was performed to investigate the cytotoxic effect of WPI and WPZ films (Baek et al., 2005; Podgórski et al., 2022). In particular, WPI

and WPZ specimens (0.32 cm²), previously sterilized for 1 h through UVC irradiation, were soaked in 600 µL of complete culture medium (CM) for 24 h at 37°C to obtain film *extracts*; then, the extracts were collected and serially diluted (1:2, 1:10, 1:50, 1:100 v/v) by adding fresh CM.

NHDF cell line was seeded at a density of 1.0 x 10^5 cells/well into a 96-well plate and incubated (37°C and 5% CO_2) for 24 h to reach semi-confluence. After the medium had been replaced with the extracts, as such or diluted, the cells were incubated for further 24 h. Cells in CM were used as a reference. After incubation, an MTT (3-(4,5-dimethylthiazol-2-yl)-2,5-diphenyltetrazolium bromide) assay was performed. Here, extracts and reference were removed from the 96-well plate and cell monolayers were washed with Phosphate Buffer Solution (PBS); subsequently, 50 µl of MTT 7.5 µM in 100 µl of DMEM without phenol red were added to each well and incubated for 3 h (37°C and 5% CO_2). Finally, 100 µl of DMSO was added to each well to allow for the complete dissolution of formazan crystals originating from MTT dye reduction by mitochondrial dehydrogenases of living cells. The solution absorbance was measured with an iMark® Microplate reader (Bio-Rad Laboratories S.r.l.) at a wavelength of 570 nm and 690 nm (reference wavelength) after 60 s of mild shaking.

7.2.7 *In vitro* proliferation test

Film extracts obtained as described above, this time after conditioning the CM with WPI and WPZ specimens for 6 and 24h, were also used to assess their potential ability to enhance NHDF proliferation.

Cells were seeded into a 96-well plate at a density of 2.0 x 10^4 cells/50 µL of CM/well and immediately added with 150 µL extracts diluted 1:2 v/v with fresh CM. CM was used as a reference. Finally, an MTT test was performed as described in the previous paragraph.

7.2.8 *In vivo* studies

7.2.8.1 Evaluation of wound healing-enhancing properties on rat model

All animal experiments were carried out as described in (Tenci et al., 2016) in full compliance with standard international ethical guidelines (European Parliament, 2013) approved by the Italian Health Ministry (D.L. 228/2021). The study protocol was approved by the Local Institutional Ethics Committee of the University of Pavia for the use of animals.

In brief, four male rats (Wistar 200–250 g) were anesthetized with equitensine (3 mL/kg) and shaved to remove all hair from the injury site. Three full-thickness circular burns were produced on the animal's back by contact with a brass rod (105°C for 40 s), each having a 4-mm diameter. After 24 h, three 6-mm full-thickness excisional wounds were outlined using a punch biopsy tool on each animal back. Wounds were photographed with a digital camera and then treated with i) WPI film (0.32 cm^2) moistened with 25 µL of saline (NaCl 0.9% w/v), ii) WPZ film (0.32 cm^2) moistened with 25 µL of saline and iii) 25 µL of saline as control. Subsequently, each wound was covered with a sterile gauze and the rat's back was wrapped with a surgery stretch (Safety, Monza, Italy), to keep the films or the physiological solution into the wound bed. At predetermined intervals after treatment (3, 7, 10, 14, and 18 days), the three lesions were photographed with a digital camera in order to monitor wound closure. Wound size was measured using the image analysis software ImageJ 2.0. A wound healing >70% was considered the endpoint.

7.2.8.2 Histological analysis

After 18-day treatment, the animals were sacrificed.

After euthanasia, the area around the scar or residual wound was harvested and wound bed tissue specimens were immediately immersed in fixative solution (4% neutral buffered formaldehyde), embedded in paraffin and sectioned at a thickness of 5 µm. Some sections were stained with hematoxylin and eosin (H&E), others with picrosirius red (PSR).

Picrosirius red stain was applied as follows: deparaffinized sections were hydrated, faintly stained with Weigert's hematoxylin for nuclei and then stained with PSR (1 hour). Finally, all sections were dehydrated, cleared in xylene and mounted with DPX (dibutyl phthalate in xylene).

Stained slices were observed with a Carl Zeiss Axiophot microscope (Oberkochen, Germany) equipped with suitable filters in the condenser stage and in the microscope tube for circular polarizing microscopy. Images were recorded through a microscope digital 5 megapixels CCD camera Nikon DS - Fi2.

7.2.9 Statistical analysis

Whenever possible, a one-way ANOVA multiple range test was done on the experimental values from the various measurements, using the Statgraphics 5.0 statistical package (Statistical Graphics Corporation, Rockville, MD, USA).

7.3 Results

7.3.1 Water Contact Angle

The results of the WCA measurements on WPI and WPZ films are shown in Figure 7.3.

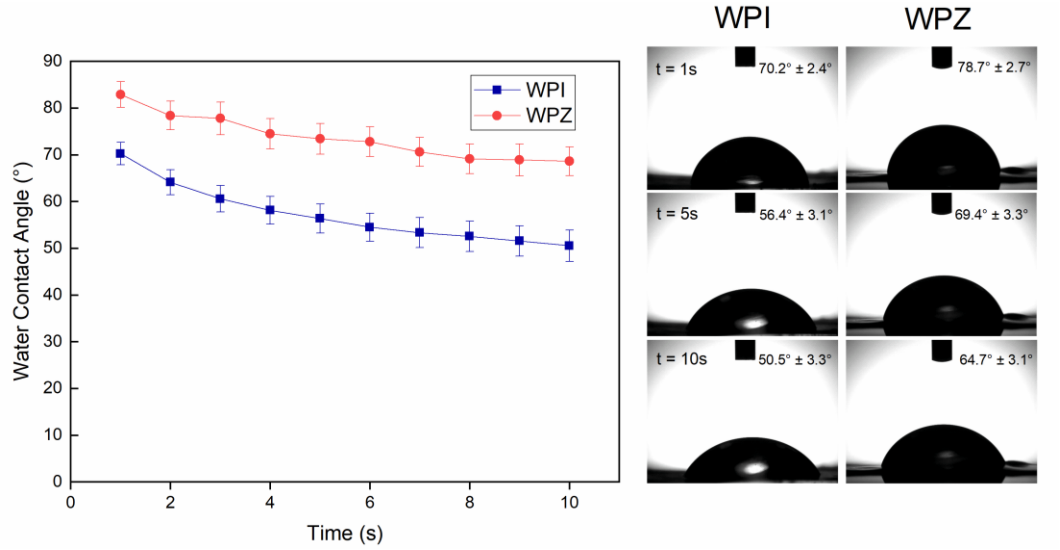


Figure 7.3: WCA values of WPI and WPZ films up to 10 s (mean values ± s.d.; n = 3). Images of the drop at different times (1, 5, and 10 s) are reported for WPI and WPZ films.

As shown by the WCA values, both samples are hydrophilic. The addition of nZnO causes an increase in WCA. This is frequently observed in other biopolymer/nZnO composites described in the literature (Kanmani & Rhim, 2014; Khorasani et al., 2018; Roy & Rhim, 2019). This is the result of the lower water affinity of ZnO with respect to the matrix (L. Y. Lin et al., 2008) and can also be attributed to a higher surface roughness of WPZ samples, as also observed in the CMF-Z films described in Chapter 6.

The chart also shows how the value of WCA decreases over time in both samples. Thanks to the good water affinity for the material, the droplet tends to spread across the surface of the films, thus determining a decrease of WCA. After 10 s, the surface of both samples starts deforming due to the absorption of the liquid droplet, which prevents longer-duration measurements of the contact angle.

Hydrophilicity is a fundamental property for primary dressings, i.e., those dressings that are placed in direct contact with the wound, as it favors exudate

absorption and good adhesion to the site. Using hydrophilic dressings therefore ensures support and protection to the wound, reducing the risk of complications and accelerating the healing process.

The results obtained are in line with the literature; generally, the WCA on an ideal wound dressing should be around 50-70° (Kalantari et al., 2020b; X. Liu et al., 2010b).

7.3.2 Hydration test

The swelling ratio for WPI and WPZ films was monitored across a 24 h span (Figure 7.4) to evaluate the ability of the film to absorb a medium simulating wound exudate (PBS) over time.

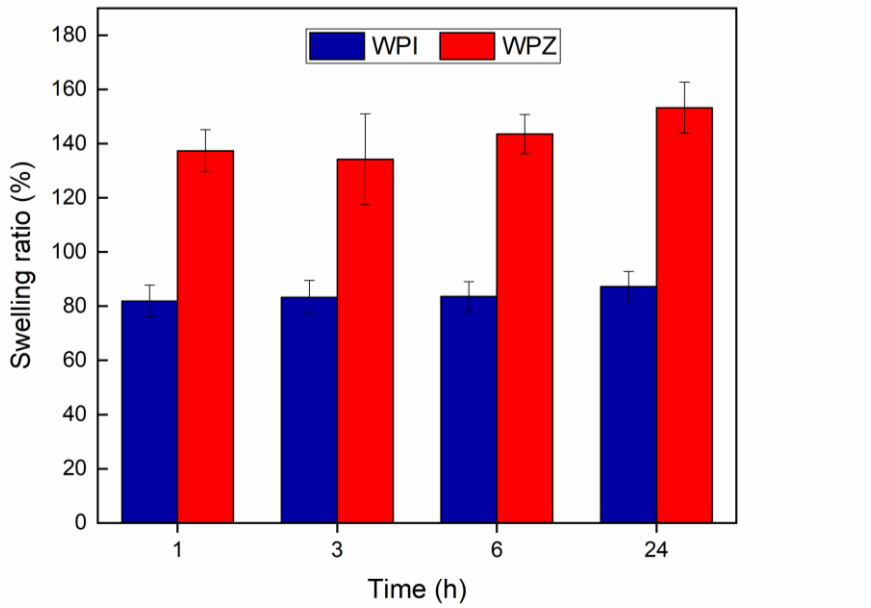


Figure 7.4: Variation in time of the swelling ratio % of WPI and WPZ films (mean values ± s.d.; n = 6).

WPZ samples showed a higher (almost twofold) SR than WPI films. This is in agreement with the results showed in Chapter 4 as well as with other scientific reports (George et al., 2020a; Villanueva et al., 2019). As previously mentioned, the increased SR is attributed to the electrostatically charged surface of nZnO, which attracts ions in the liquid inducing a build-up of osmotic pressure inside the WPI matrix, in turn causing a higher PBS uptake.

Secondly, water uptake is rapid and occurs within the first hour, and then remains relatively stable or slightly increasing throughout the whole experiment.

For WPI films, SR is 81,88% ± 5,85% after the first hour and becomes 87,25% ± 5,52% after 24h. In WPZ, SR has an initial value of 137,36% ± 7,83%, which goes up to 153,26% ± 9,38% after 24h.

Based on this evidence, it is here worth repeating how important fluid uptake capacity is for wound dressings (Chopra et al., 2022). In fact, a wound dressing should preserve a moist environment while preventing the accumulation of exudate, which could impair the healing process and be responsible for the maceration of the healthy surrounding tissue (Gonçalves et al., 2021; Mori et al., 2016). Typically, an ideal wound dressing shall have SR values ranging between 100% and 900% (W. C. Lin et al., 2013; Morgado et al., 2015). The SR values obtained for WPZ fall within this range, revealing another important benefit on nZnO addition besides the antibacterial effects. Moreover, the fluid is effectively retained within the film for the entire duration of the experiment, suggesting that wound exudate would not be released back into the wound bed after an initial absorption.

7.3.3 Viscoelastic Properties after Hydration

After 24h hydration, WPI and WPZ films were subjected to viscoelastic measurements. As shown in Figure 7.5, both samples were characterized by higher G' (elastic storage modulus) values than G'' (viscous loss modulus) in the whole range of frequencies considered. Hence, the amount of PBS absorbed by both films reached an equilibrium without compromising their structural integrity.

Such behavior is highly desirable for a wound dressing, as it shall remain able to stretch and subsequently recover the deformation caused by external shear stresses to effectively protect the injured area even after hydration (Mori et al., 2016; Vigani et al., 2021).

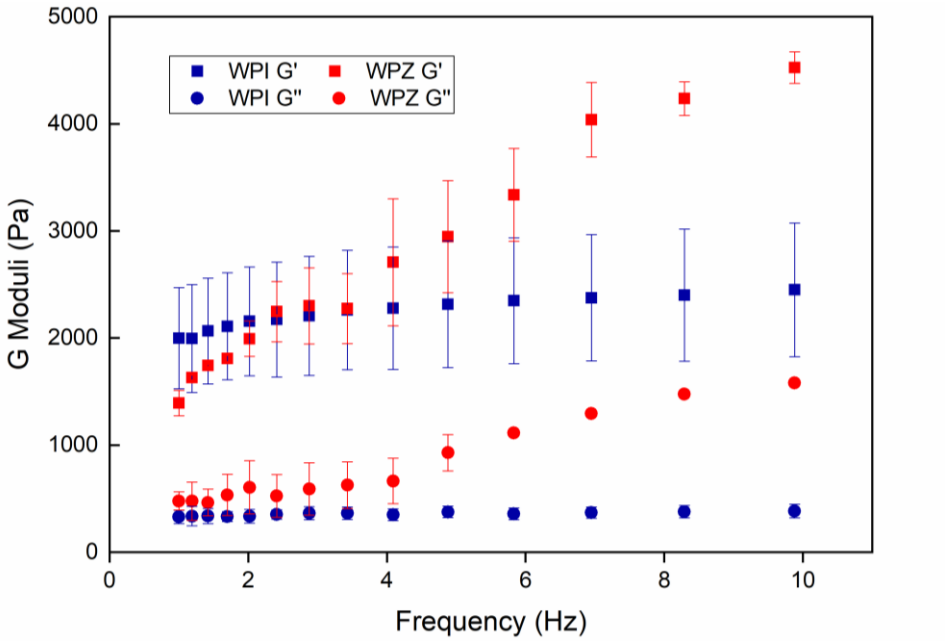


Figure 7.5: Storage (G') and loss (G") moduli vs. frequency profiles of WPI and WPZ films upon 24 h-hydration in PBS (mean values ± s.e.; n = 3).

7.3.4 Degradation Test

The extent of the degradation of WPI and WPZ films over 7 days are shown below, expressed as film residual mass (Figure 7.6A) and protein concentration dissolved in the degradation media (Figure 7.6B).

All the films degraded in either PBS or PBS + H_2O_2, but WPZ samples were notably less impacted. This shall be attributed to the presence of nZnO, which stabilizes the film matrix through its interactions with the whey proteins, preventing or slowing down their diffusion and dissolution in the medium (Khorasani et al., 2018). It shall also be noted how the majority of the degradation occurred within the first day, while the further permanence of the samples in the medium (until 7 days) produced no significant additional mass losses.

It can therefore be hypothesized that the large mass loss occurring at the beginning is linked to the out-diffusion of weakly bonded molecules, such as glycerol or other impurities such ashes, trace fats and lactose which are commonly present in WPI (Table 4.1), as well as of proteins that have not taken part to the formation of the film or that are less strongly integrated in the protein network, as

testified by the proteins detected in the degradation medium (Figure 7.6B). After 7 days, what remains could therefore be the insoluble intermolecular network composed of WPI proteins held together by more disulfide bridges (Gounga et al., 2007b). The addition of H_2O_2 to PBS did not accelerate the degradation process, suggesting that both WPI and WPZ films are resistant to these oxidative conditions. These results are reflected by the protein concentration assessed in the degradation media, where higher protein content is observed in correspondence of those samples where lower residual mass was reported. It is here worth noting that, if complete film degradation was achieved, given the 30 ± 5 mg average mass of the sample, the protein concentration in the degradation medium would be equal to 0.6 mg/mL.

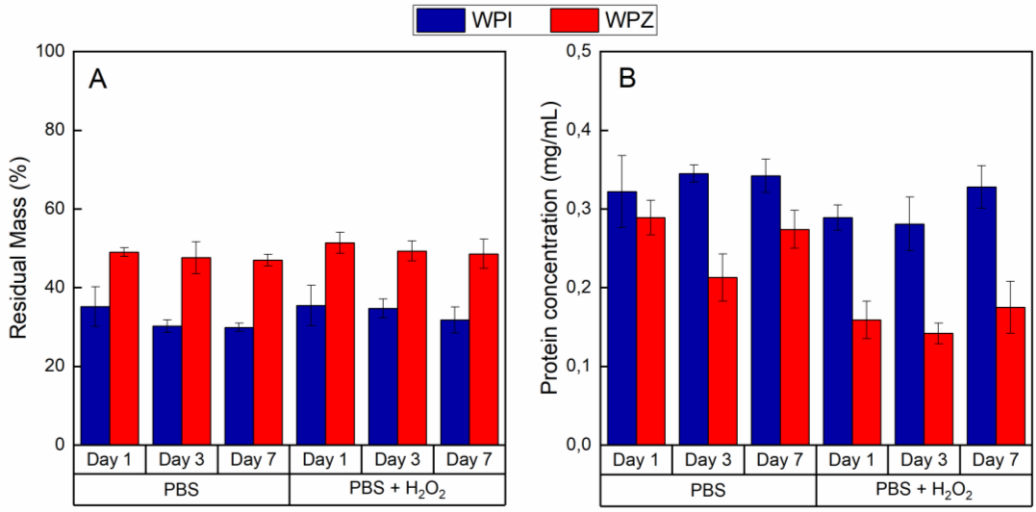


Figure 7.6: WPI and WPZ film degradation after 1, 3 and 7 days in two different media - PBS and PBS added with H2O2 - expressed in terms of (A) residual film mass and (B) concentration of proteins released in the medium (mean values ± s.e.; n = 3).

Despite the stability manifested across one week, the degradation of half of the initial mass after just one day may not be optimal, as degradation times more compatible with wound regeneration times would be more desirable. Chronic wounds have healing times longer than 12 weeks. While this is a very long time, being able to replace the dressing fewer times would definitely be preferable. To this end, the combination of proteins with polysaccharides might be a promising avenue toward the development of wound dressings with slower degradation, thanks to the interactions between the two molecules (Ghosh et al., 2012).

7.3.5 Antimicrobial test

The microbicide effect (ME) of WPZ with respect to WPI against *S. aureus* and *E. coli* is reported in Table 7.1. For both the microorganisms considered, WPZ film showed a microbicide effect higher than WPI film; in particular, a more marked antimicrobial effect of WPZ film was observed on *E. coli*.

Table 7.1: Microbicide effect (ME) of WPZ after 5 and 24h incubation with *S. aureus* and *E. coli*; WPI was used as control (CV % < 12%; n = 3).

	6 h	**24 h**
S. aureus	0,67	1,30
E. coli	2,85	4,94

These results confirm the well-known antibacterial properties of nanostructured zinc oxide. In a work by Charoensri et al., the inclusion of 4 wt% of a mixture of ZnO and silica-based diatomaceous earth into injection-molded high-density polyethylene films resulted into a ME of 1.5 and 1.3 against *S. aureus* and *E. coli* respectively (Charoensri et al., 2022). Darvish and coworkers prepared a low-density polyethylene film incorporated with 3% wt, 20-nm size ZnO nanoparticles and reported a ME of 1 and 1.5 against *E. coli* (DH5α) and *S. aureus* (ATCC 6538P) respectively (Darvish & Ajji, 2021). 6% wt ZnO nanoparticles were also dispersed into polyethylene films fabricated by Mania (Mania et al., 2020), who reported ME of 2.10 and 2.73 against *S. aureus* (ATCC 25923) and *E. coli* (NCTC 10538) respectively.

In Chapter 4, WPI and WPZ bionanocomposites were tested against two non-pathogen strains, i.e., Gram-positive *S. epidermidis*, LMG 10474, and Gram-negative *E. coli*, LMG 08063. The antibacterial effect was more marked against the former, in accordance with the majority of scientific literature reporting a lower efficacy on Gram-negatives as a result of the outer membrane that these species possess, contrary to Gram-positive ones, as extensively explained in Chapter 2 (Sirelkhatim et al., 2015).

However, for the experiment described in this section, WPZ showed a stronger effect against the Gram-negative, as also observed in a minority of other works already cited in Chapter 2 (Bharathi et al., 2019; Hezma et al., 2019; Thanusha et

al., 2018), where the greater resistance of the Gram-positive to nano-ZnO was attributed to their thicker peptidoglycan layer. While the results shown in this section cannot provide a definitive answer to this highly debated issue (for instance, the *S. aureus* strain used might be somehow more resistant against our nZnO), they can at least suggest that the root causes of the differences observed on various microbial species should be researched beyond the overarching differences between Gram+ and Gram-, venturing into the very specific features of each strain. In other words, something other than the outer membrane of Gram- or the thicker peptidoglycan layer of Gram+ must be playing a role in their response to nZnO or bionanocomposites. Another possible explanation might lie in the different test conditions. While in Chapter 4 WPI and WPZ films were tested with the disk diffusion method, this time a different protocol was used. This might have had implications on the final results as each method can have a different influence on the antibacterial mechanism of the bionanocomposites, as explained in Chapter 2 and as also pointed out by several researchers (Cunliffe et al., 2021; Gallant-Behm et al., 2005; Limo et al., 2018; Wiegand et al., 2015). The same holds for bare nZnO, which in Chapter 3 was shown to be more effective against *S. epidermidis* rather than on *E. coli* following a micro-broth dilution and a modified agar disk diffusion test.

In any case, this test opened a concrete possibility that our nZnO can in fact be effective against Gram-negative bacteria too, thus overcoming what was previously considered to be one of its major limitations.

7.3.6 *In vitro* cytocompatibility test

The results of the MTT assay carried on NHDF cells after 24 h incubation with extracts are shown in Figure 7.7. All the diluted extracts resulted cytocompatible. The non-diluted WPI extract resulted cytocompatible too, while the non-diluted WPZ extract did not.

A very high concentration of nZnO in the medium might in fact be detrimental for cells, as pointed out in several studies that raised concerns about the toxicity of metal oxide nanoparticles (Espitia et al., 2012; Limo et al., 2018). Ng and co-workers (Ng et al., 2011) reported *in vitro* cytotoxic effects of 22.5 ± 4.9 ZnO nanoparticles on BJ human skin fibroblast cells for concentrations beyond 15 μg/mL. A study by Chen (Chen et al., 2022) found that 49-nm spherical ZnO nanoparticles were cytotoxic for human gingival fibroblasts at 50 μg/mL. Meyer et al. reported an 85% reduction in human dermal fibroblasts viability after exposure to 20-nm zinc oxide nanoparticles at concentrations greater than 25 μg/mL (Meyer

et al., 2011). All the studies attributed the toxic effects to the upregulation of the p53 protein pathway in the presence of the nanoparticles, with subsequent induction of cellular apoptosis. This is considered to be a response to the oxidative stress exerted on DNA by reactive oxygen species, which have been described by several authors as the main toxicity driver in mammalian cells together with Zn^{2+} release (Chong et al., 2021; Espitia et al., 2012; Sruthi et al., 2018). In our study, assuming conservatively that all the nZnO contained in the WPZ sample was released into the extracts, cells would be exposed to a nZnO concentration equal to 22.8 μg/mL, considering the average WPZ sample weight used for the experiment of 3.4 mg. This value falls in the range of cytotoxic concentrations reported in the above-cited literature for ZnO nanoparticles of similar sizes and shapes.

However, cell viability is immediately restored with a 1:2 dilution and is preserved at control-level values for all subsequent dilutions, without showing dilution-dependent changes. In other words, the optical density (Figure 7.7) does not increase with increasing dilution after the first 1:2 dilution step. This suggests that a critical concentration must be reached before triggering cytotoxic effects, below which cell viability remains substantially unaltered. This has been observed in other reports as well (Chen et al., 2022; Ng et al., 2011). In fact, while toxic effects might arise at high concentrations of nZnO, ROS or Zn^{2+}, optimal amounts might allow to leverage the positive impact of zinc on the immune system and wound healing (M. Gupta et al., 2014; Mishra et al., 2017; Wessels et al., 2017).

Moreover, there are profound differences between *in vitro* and *in vivo* tests. In a study by Ryu (Ryu et al., 2014), 20-nm ZnO nanoparticles were repeatedly applied on the skin of rats for 90 days, and pathologic and histopathologic examinations were carried thereafter on different organ tissues. No evidence of adverse effects was found up to the extremely high concentrations of 1000 mg/kg body weight, which are not found in wound healing applications. Another study carried on human volunteers showed that no penetration or local toxicity of the epidermidis occurred after topical application of 10% w/v nano-sized zinc oxide suspension on either intact or barrier-impaired skin (Leite-Silva et al., 2016).

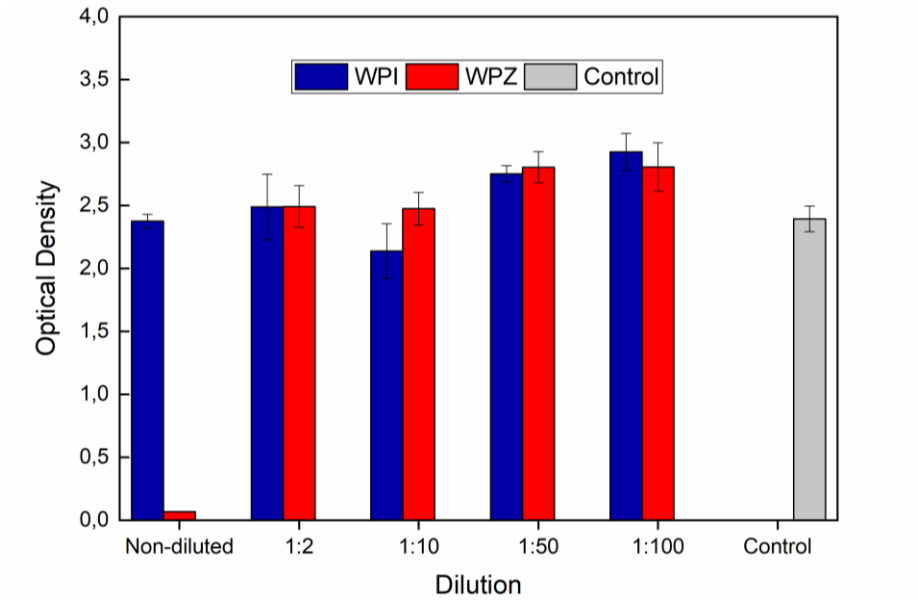


Figure 7.7: Optical density values after 24h incubation of NHDF cells with WPI and WPZ extracts, undiluted and diluted 1:2, 1:10, 1:50, 1:100 v/v in CM. Complete culture medium (CM) was considered as control (mean values ± s.e.; n = 6).

7.3.7 *In-vitro* proliferation test

Figure 7.8 shows the results of the MTT test performed after the *in-vitro* proliferation test carried on NHDF cells. The WPZ bionanocomposite induced higher proliferation compared to the protein matrix and the control sample, both for 6h and 24h extracts. This result, in accordance with the experimental evidence shown above, confirms (i) the importance of Zn^{2+} ions for fibroblast proliferation (Lansdown et al., 2007b) and (ii) the ability of WPZ composites to supply optimal levels of Zn^{2+} ions already within 6 hours. Finally, proliferation in WPI extract was higher for 24h extracts than for 6h ones, suggesting that the protein matrix itself can play a positive role in synergy with the nanomaterial.

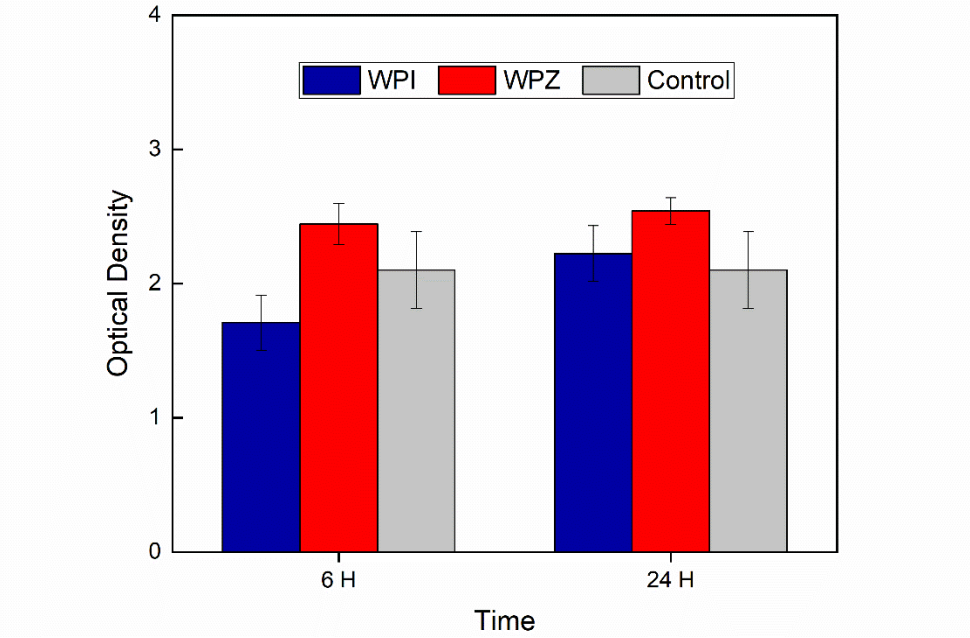


Figure 7.8: Optical density values after 6 and 24h proliferation of NHDF cells in WPI and WPZ extracts, diluted 1:2 v/v in CM. Complete culture medium (CM) was considered as control (mean values ± s.e.; n = 6).

7.3.8 *In-vivo* wound healing test

After 18 days, closure was assessed for both WPI- and WPZ-treated wounds (approximately 20% of wounded area).

Figure 7.9 shows sections of epithelial tissue after 18-days. The left column contains images of the samples stained with H&E, whereas the second and third columns contain images of the samples stained with the PSR method. In particular, the image in the second column were taken with a bright field, while those in the third column were obtained through polarized light. Picrosirius polarization method is particularly useful to reveal the organization and the heterogeneity of collagen fiber in different connective tissues. Polarizing light assessment of PSR stain identifies the old thick collagen I fibers as orange-to-red and the newly deposed fibers, rich in collagen III, as green (Junqueira et al., 1978; Lattouf et al., 2014).

Similarly to the control (Figure 7.9 a), the entire surface of the lesion treated with the dressings (Figure 7.9 c and d) was covered with new epithelium, fully restored in multiple layers of cells and with a fair degree of keratinization. Skin appendages such as hair follicles and glands were reforming. Collagen was laid

down and remodeled in an appropriate orientation to withstand the tensile stresses placed on the area of repair, suggesting that a mature remodeling phase of the healing process was reached (Agwa et al., 2022; Hemmati et al., 2018; Singer & Clark, 1999).

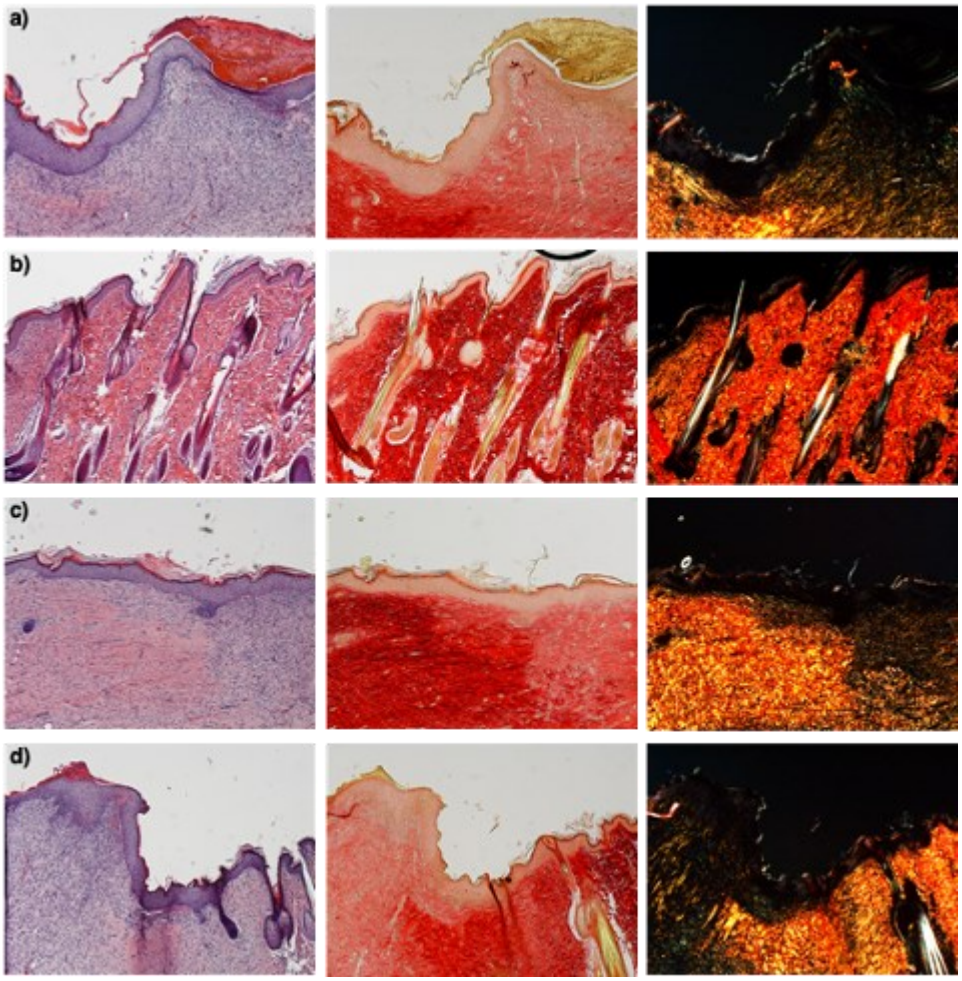


Figure 7.9: H&E (left panel) and PSR (central panel - with bright field images; right panel - with polarized light) sections of (a) lesion treated with saline solution as negative control, (b) intact skin, (c) lesion treated with WPI, (d) lesion treated with WPZ. Original magnification: 5×. Each micrograph frame has a width of 1780 μm and refers to a 18-days old lesion.

7.4 Conclusions

In this Chapter, the potential of WPI and WPZ films has been demonstrated with a thorough biopharmaceutical characterization, that showed how these have desirable wettability, hydration and degradation properties, viscoelastic behavior and cytocompatibility, coupled with their antibacterial action against pathogens. This culminated with *in-vivo* studies that confirmed their suitability to serve as wound dressings. The study also highlighted avenues to further improve their properties and overcome some of their current limitations, such as rapid degradation times, for instance through conjugation with polysaccharides like chitosan, carrageenan, or alginate. This work brought compelling and promising evidence for the advancement of this field, concluding a broader journey across bionanocomposite materials for wound healing. Some final remarks will follow in the next section.

References

Agwa, M. M., Sabra, S., Atwa, N. A., Dahdooh, H. A., Lithy, R. M., & Elmotasem, H. (2022). Potential of frankincense essential oil-loaded whey protein nanoparticles embedded in frankincense resin as a wound healing film based on green technology. *Journal of Drug Delivery Science and Technology*, *71*, 103291. https://doi.org/10.1016/J.JDDST.2022.103291

Baek, H. S., Yoo, J. Y., Rah, D. K., Han, D. W., Lee, D. H., Kwon, O. H., & Park, J. C. (2005). Evaluation of the Extraction Method for the Cytotoxicity Testing of Latex Gloves. *Yonsei Medical Journal*, *46*(4), 579–583. https://doi.org/10.3349/YMJ.2005.46.4.579

Bharathi, D., Ranjithkumar, R., Chandarshekar, B., & Bhuvaneshwari, V. (2019). Preparation of chitosan coated zinc oxide nanocomposite for enhanced antibacterial and photocatalytic activity: As a bionanocomposite. *International Journal of*

Biological Macromolecules, *129*, 989–996. https://doi.org/10.1016/J.IJBIOMAC.2019.02.061

Charoensri, K., Shin, Y. J., Kim, K. C., & Park, H. J. (2022). Active Packaging Material Based on Immobilized Diatomaceous Earth/Zinc Oxide/High-Density Polyethylene Composite for Sea Food and Products. *Polymers*, *14*(23), 5228. https://doi.org/10.3390/polym14235228

Chen, F. C., Huang, C. M., Yu, X. W., & Chen, Y. Y. (2022). Effect of nano zinc oxide on proliferation and toxicity of human gingival cells. *Human and Experimental Toxicology*, *41*, 1–10. https://doi.org/10.1177/09603271221080237/ASSET/IMAGES/LARGE/10.1177_09603271221080237-FIG2.JPEG

Chong, C. L., Fang, C. M., Pung, S. Y., Ong, C. E., Pung, Y. F., Kong, C., & Pan, Y. (2021). Current Updates On the In vivo Assessment of Zinc Oxide Nanoparticles Toxicity Using Animal Models. *BioNanoScience 2021 11:2*, *11*(2), 590–620. https://doi.org/10.1007/S12668-021-00845-2

Chopra, H., Bibi, S., Kumar, S., Khan, M. S., Kumar, P., & Singh, I. (2022). Preparation and Evaluation of Chitosan/PVA Based Hydrogel Films Loaded with Honey for Wound Healing Application. *Gels 2022, Vol. 8, Page 111*, *8*(2), 111. https://doi.org/10.3390/GELS8020111

Cunliffe, A. J., Askew, P. D., Stephan, I., Iredale, G., Cosemans, P., Simmons, L. M., Verran, J., & Redfern, J. (2021). How do we determine the efficacy of an antibacterial surface? A review of standardised antibacterial material testing methods. In *Antibiotics* (Vol. 10, Issue 9). MDPI. https://doi.org/10.3390/antibiotics10091069

Darvish, M., & Ajji, A. (2021). Effect of Polyethylene Film Thickness on the Antimicrobial Activity of Embedded Zinc Oxide Nanoparticles. *ACS Omega*, *6*(40), 26201–26209. https://doi.org/10.1021/ACSOMEGA.1C03223/ASSET/IMAGES/LARGE/AO1C03223_0009.JPEG

Espitia, P. J. P., Soares, N. de F. F., Coimbra, J. S. dos R., de Andrade, N. J., Cruz, R. S., & Medeiros, E. A. A. (2012). Zinc Oxide Nanoparticles: Synthesis, Antimicrobial Activity and Food Packaging Applications. In *Food and Bioprocess*

Technology (Vol. 5, Issue 5, pp. 1447–1464). Springer. https://doi.org/10.1007/s11947-012-0797-6

European Parliament. (2013). *Directive 86/609/EEC*. Official Journal of the European Union. https://eur-lex.europa.eu/eli/dir/1986/609/2013-01-01

Fraise, A. P., Maillard, J.-Y., & Sattar, Syed. (2013). *Russell, Hugo & Ayliffe's principles and practice of disinfection, preservation and sterilization*. https://www.wiley.com/en-us/Russell%2C+Hugo+and+Ayliffe%27s+Principles+and+Practice+of+Disinfection%2C+Preservation+and+Sterilization%2C+5th+Edition-p-9781444333251

Gallant-Behm, C. L., Yin, H. Q., Liu, S., Heggers, J. P., Langford, E., Olson, M. E., Hart, D. A., & Burrell, R. E. (2005). Comparison of in vitro disc diffusion and time kill-kinetic assays for the evaluation of antimicrobial wound dressing efficacy. *Wound Repair and Regeneration*, *13*(4), 412–421. https://doi.org/10.1111/J.1067-1927.2005.130409.X

George, D., Maheswari, P. U., & Begum, K. M. M. S. (2020). Chitosan-cellulose hydrogel conjugated with L-histidine and zinc oxide nanoparticles for sustained drug delivery: Kinetics and in-vitro biological studies. *Carbohydrate Polymers*, *236*, 116101. https://doi.org/10.1016/J.CARBPOL.2020.116101

Ghosh, A. K., Bandyopadhyay, P., Ghosh, A. K., & Bandyopadhyay, P. (2012). Polysaccharide-Protein Interactions and Their Relevance in Food Colloids. *The Complex World of Polysaccharides*. https://doi.org/10.5772/50561

Gonçalves, M. M., Carneiro, J., Justus, B., Espinoza, J. T., Budel, J. M., Farago, P. V., & de Paula, J. P. (2021). Preparation and characterization of a novel antimicrobial film dressing for wound healing application. *Brazilian Journal of Pharmaceutical Sciences*, *56*. https://doi.org/10.1590/S2175-97902020000118784

Gounga, M. E., Xu, S. Y., & Wang, Z. (2007). Whey protein isolate-based edible films as affected by protein concentration, glycerol ratio and pullulan addition in film formation. *Journal of Food Engineering*, *83*(4), 521–530. https://doi.org/10.1016/j.jfoodeng.2007.04.008

Grisoli, P., de Vita, L., Milanese, C., Taglietti, A., Fernandez, Y. D., Bouzin, M., D'alfonso, L., Sironi, L., Rossi, S., Vigani, B., Sperandeo, P., Polissi, A., & Pallavicini, P. (2021). PVA Films with Mixed Silver Nanoparticles and Gold

Nanostars for Intrinsic and Photothermal Antibacterial Action. *Nanomaterials 2021, Vol. 11, Page 1387*, *11*(6), 1387. https://doi.org/10.3390/NANO11061387

Gupta, M., Mahajan, V. K., Mehta, K. S., & Chauhan, P. S. (2014). Zinc therapy in dermatology: A review. *Dermatology Research and Practice*, *2014*. https://doi.org/10.1155/2014/709152

Hemmati, A. A., Larki-Harchegani, A., shabib, S., Jalali, A., Rezaei, A., & Housmand, G. (2018). Wound healing property of milk in full thickness wound model of rabbit. *International Journal of Surgery*, *54*, 133–140. https://doi.org/10.1016/J.IJSU.2018.04.030

Hezma, A. M., Rajeh, A., & Mannaa, M. A. (2019). An insight into the effect of zinc oxide nanoparticles on the structural, thermal, mechanical properties and antimicrobial activity of Cs/PVA composite. *Colloids and Surfaces A: Physicochemical and Engineering Aspects*, *581*, 123821. https://doi.org/10.1016/J.COLSURFA.2019.123821

ISO. (n.d.). *ISO - ISO 22196:2011 - Measurement of antibacterial activity on plastics and other non-porous surfaces*. 2011. Retrieved December 9, 2022, from https://www.iso.org/standard/54431.html

JIS. (99 C.E.). *Test method for repetitiveness of bacteria reduction activity*.

Junqueira, L. C. U., Cossermelli, W., & Brentani, R. (1978). Differential Staining of Collagens Type I, II and III by Sirius Red and Polarization Microscopy. *Archivum Histologicum Japonicum*, *41*(3), 267–274. https://doi.org/10.1679/AOHC1950.41.267

Kalantari, K., Mostafavi, E., Saleh, B., Soltantabar, P., & Webster, T. J. (2020). Chitosan/PVA hydrogels incorporated with green synthesized cerium oxide nanoparticles for wound healing applications. *European Polymer Journal*, *134*, 109853. https://doi.org/10.1016/J.EURPOLYMJ.2020.109853

Kanmani, P., & Rhim, J.-W. (2014). Properties and characterization of bionanocomposite films prepared with various biopolymers and ZnO nanoparticles. *Carbohydrate Polymers*, *106*, 190–199. https://doi.org/10.1016/J.CARBPOL.2014.02.007

Khorasani, M. T., Joorabloo, A., Moghaddam, A., Shamsi, H., & MansooriMoghadam, Z. (2018). Incorporation of ZnO nanoparticles into heparinised polyvinyl alcohol/chitosan hydrogels for wound dressing application. *International Journal of Biological Macromolecules*, *114*, 1203–1215. https://doi.org/10.1016/j.ijbiomac.2018.04.010

Lansdown, A. B. G., Mirastschijski, U., Stubbs, N., Scanlon, E., & Ågren, M. S. (2007a). Zinc in wound healing: Theoretical, experimental, and clinical aspects. *Wound Repair and Regeneration*, *15*(1), 2–16. https://doi.org/10.1111/J.1524-475X.2006.00179.X

Lansdown, A. B. G., Mirastschijski, U., Stubbs, N., Scanlon, E., & Ågren, M. S. (2007b). Zinc in wound healing: Theoretical, experimental, and clinical aspects. *Wound Repair and Regeneration*, *15*(1), 2–16. https://doi.org/10.1111/J.1524-475X.2006.00179.X

Lattouf, R., Younes, R., Lutomski, D., Naaman, N., Godeau, G., Senni, K., & Changotade, S. (2014). Picrosirius Red Staining: A Useful Tool to Appraise Collagen Networks in Normal and Pathological Tissues. *Journal of Histochemistry and Cytochemistry*, *62*(10), 751–758. https://doi.org/10.1369/0022155414545787/ASSET/IMAGES/LARGE/10.1369_0022155414545787-FIG2.JPEG

Leite-Silva, V. R., Sanchez, W. Y., Studier, H., Liu, D. C., Mohammed, Y. H., Holmes, A. M., Ryan, E. M., Haridass, I. N., Chandrasekaran, N. C., Becker, W., Grice, J. E., Benson, H. A. E., & Roberts, M. S. (2016). Human skin penetration and local effects of topical nano zinc oxide after occlusion and barrier impairment. *European Journal of Pharmaceutics and Biopharmaceutics*, *104*, 140–147. https://doi.org/10.1016/J.EJPB.2016.04.022

Limo, M. J., Sola-Rabada, A., Boix, E., Thota, V., Westcott, Z. C., Puddu, V., & Perry, C. C. (2018). Interactions between Metal Oxides and Biomolecules: From Fundamental Understanding to Applications. *Chemical Reviews*, *118*(22), 11118–11193. https://doi.org/10.1021/ACS.CHEMREV.7B00660/ASSET/IMAGES/LARGE/CR-2017-006605_0023.JPEG

Lin, L. Y., Kim, H. J., & Kim, D. E. (2008). Wetting characteristics of ZnO smooth film and nanowire structure with and without OTS coating. *Applied Surface Science*, *254*(22), 7370–7376. https://doi.org/10.1016/j.apsusc.2008.05.337

Lin, W. C., Lien, C. C., Yeh, H. J., Yu, C. M., & Hsu, S. H. (2013). Bacterial cellulose and bacterial cellulose–chitosan membranes for wound dressing applications. *Carbohydrate Polymers*, *94*(1), 603–611. https://doi.org/10.1016/J.CARBPOL.2013.01.076

Liu, X., Lin, T., Fang, J., Yao, G., Zhao, H., Dodson, M., & Wang, X. (2010). In vivo wound healing and antibacterial performances of electrospun nanofibre membranes. *Journal of Biomedical Materials Research Part A*, *94A*(2), 499–508. https://doi.org/10.1002/JBM.A.32718

Ma, X. Y., & Zhang, W. de. (2009). Effects of flower-like ZnO nanowhiskers on the mechanical, thermal and antibacterial properties of waterborne polyurethane. *Polymer Degradation and Stability*, *94*(7), 1103–1109. https://doi.org/10.1016/j.polymdegradstab.2009.03.024

Mania, S., Cieślik, M., Konzorski, M., Świecikowski, P., Nelson, A., Banach, A., & Tylingo, R. (2020). The Synergistic Microbiological Effects of Industrial Produced Packaging Polyethylene Films Incorporated with Zinc Nanoparticles. *Polymers 2020, Vol. 12, Page 1198*, *12*(5), 1198. https://doi.org/10.3390/POLYM12051198

Meyer, K., Rajanahalli, P., Ahamed, M., Rowe, J. J., & Hong, Y. (2011). ZnO nanoparticles induce apoptosis in human dermal fibroblasts via p53 and p38 pathways. *Toxicology in Vitro*, *25*(8), 1721–1726. https://doi.org/10.1016/J.TIV.2011.08.011

Mishra, P. K., Mishra, H., Ekielski, A., Talegaonkar, S., & Vaidya, B. (2017). Zinc oxide nanoparticles: a promising nanomaterial for biomedical applications. *Drug Discovery Today*, *22*(12), 1825–1834. https://doi.org/10.1016/J.DRUDIS.2017.08.006

Morgado, P. I., Aguiar-Ricardo, A., & Correia, I. J. (2015). Asymmetric membranes as ideal wound dressings: An overview on production methods, structure, properties and performance relationship. *Journal of Membrane Science*, *490*, 139–151. https://doi.org/10.1016/J.MEMSCI.2015.04.064

Mori, M., Rossi, S., Ferrari, F., Bonferoni, M. C., Sandri, G., Chlapanidas, T., Torre, M. L., & Caramella, C. (2016). Sponge-Like Dressings Based on the Association of Chitosan and Sericin for the Treatment of Chronic Skin Ulcers. I. Design of Experiments-Assisted Development. *Journal of Pharmaceutical Sciences*, *105*(3), 1180–1187. https://doi.org/10.1016/j.xphs.2015.11.047

Mujeeb Rahman, P., Abdul Mujeeb, V. M., Muraleedharan, K., & Thomas, S. K. (2018). Chitosan/nano ZnO composite films: Enhanced mechanical, antimicrobial and dielectric properties. *Arabian Journal of Chemistry*, *11*(1), 120–127. https://doi.org/10.1016/J.ARABJC.2016.09.008

Ng, K. W., Khoo, S. P. K., Heng, B. C., Setyawati, M. I., Tan, E. C., Zhao, X., Xiong, S., Fang, W., Leong, D. T., & Loo, J. S. C. (2011). The role of the tumor suppressor p53 pathway in the cellular DNA damage response to zinc oxide nanoparticles. *Biomaterials*, *32*(32), 8218–8225. https://doi.org/10.1016/J.BIOMATERIALS.2011.07.036

Podgórski, R., Wojasiński, M., & Ciach, T. (2022). Nanofibrous materials affect the reaction of cytotoxicity assays. *Scientific Reports 2022 12:1*, *12*(1), 1–12. https://doi.org/10.1038/s41598-022-13002-w

Ransy, C., Vaz, C., Lombès, A., & Bouillaud, F. (2020). Use of H2O2 to Cause Oxidative Stress, the Catalase Issue. *International Journal of Molecular Sciences 2020, Vol. 21, Page 9149*, *21*(23), 9149. https://doi.org/10.3390/IJMS21239149

Rao, K. M., Suneetha, M., Zo, S., Duck, K. H., & Han, S. S. (2019). One-pot synthesis of ZnO nanobelt-like structures in hyaluronan hydrogels for wound dressing applications. *Carbohydrate Polymers*, *223*, 115124. https://doi.org/10.1016/J.CARBPOL.2019.115124

Roy, S., & Rhim, J.-W. (2019). Carrageenan-based antimicrobial bionanocomposite films incorporated with ZnO nanoparticles stabilized by melanin. *Food Hydrocolloids*, *90*, 500–507. https://doi.org/10.1016/J.FOODHYD.2018.12.056

Ryu, H. J., Seo, M. Y., Jung, S. K., Maeng, E. H., Lee, S. Y., Jang, D. H., Lee, T. J., Jo, K. Y., Kim, Y. R., Cho, K. B., Kim, M. K., Lee, B. J., & Son, S. W. (2014). Zinc oxide nanoparticles: a 90-day repeated-dose dermal toxicity study in rats. *International Journal of Nanomedicine*, *9*(Suppl 2), 137. https://doi.org/10.2147/IJN.S57930

Schäfer, M., & Werner, S. (2008). Oxidative stress in normal and impaired wound repair. *Pharmacological Research*, *58*(2), 165–171. https://doi.org/10.1016/J.PHRS.2008.06.004

Singer, A. J., & Clark, R. A. F. (1999). Cutaneous Wound Healing. *Https://Doi.Org/10.1056/NEJM199909023411006*, *341*(10), 738–746. https://doi.org/10.1056/NEJM199909023411006

Sirelkhatim, A., Mahmud, S., Seeni, A., Kaus, N. H. M., Ann, L. C., Bakhori, S. K. M., Hasan, H., & Mohamad, D. (2015). Review on zinc oxide nanoparticles: Antibacterial activity and toxicity mechanism. *Nano-Micro Letters*, *7*(3), 219–242. https://doi.org/10.1007/s40820-015-0040-x

Sruthi, S., Ashtami, J., & Mohanan, P. V. (2018). Biomedical application and hidden toxicity of Zinc oxide nanoparticles. In *Materials Today Chemistry*. https://doi.org/10.1016/j.mtchem.2018.09.008

Tenci, M., Rossi, S., Bonferoni, M. C., Sandri, G., Boselli, C., di Lorenzo, A., Daglia, M., Icaro Cornaglia, A., Gioglio, L., Perotti, C., Caramella, C., & Ferrari, F. (2016). Particulate systems based on pectin/chitosan association for the delivery of manuka honey components and platelet lysate in chronic skin ulcers. *International Journal of Pharmaceutics*, *509*(1–2), 59–70. https://doi.org/10.1016/J.IJPHARM.2016.05.035

Thanusha, A. V., Amit Kumar, D., & Veena, K. (2018). Evaluation of nano hydrogel composite based on gelatin/HA/CS suffused with Asiatic acid/ZnO and CuO nanoparticles for second degree burns. *Materials Science and Engineering: C*, *89*, 378–386. https://doi.org/10.1016/J.MSEC.2018.03.034

Vigani, B., Rossi, S., Sandri, G., Bonferoni, M. C., Rui, M., Collina, S., Fagiani, F., Lanni, C., & Ferrari, F. (2019). Dual-Functioning Scaffolds for the Treatment of Spinal Cord Injury: Alginate Nanofibers Loaded with the Sigma 1 Receptor (S1R) Agonist RC-33 in Chitosan Films. *Marine Drugs 2020, Vol. 18, Page 21*, *18*(1), 21. https://doi.org/10.3390/MD18010021

Vigani, B., Valentino, C., Cavalloro, V., Catenacci, L., Sorrenti, M., Sandri, G., Bonferoni, M. C., Bozzi, C., Collina, S., Rossi, S., & Ferrari, F. (2021). Gellan-Based Composite System as a Potential Tool for the Treatment of Nervous Tissue Injuries: Cross-Linked Electrospun Nanofibers Embedded in a RC-33-Loaded Freeze-Dried Matrix. *Pharmaceutics 2021, Vol. 13, Page 164*, *13*(2), 164. https://doi.org/10.3390/PHARMACEUTICS13020164

Villanueva, M. E., Cuestas, M. L., Pérez, C. J., Campo Dall′ Orto, V., & Copello, G. J. (2019). Smart release of antimicrobial ZnO nanoplates from a pH-responsive

keratin hydrogel. *Journal of Colloid and Interface Science*, *536*, 372–380. https://doi.org/10.1016/J.JCIS.2018.10.067

Wessels, I., Maywald, M., & Rink, L. (2017). Zinc as a Gatekeeper of Immune Function. *Nutrients 2017, Vol. 9, Page 1286*, *9*(12), 1286. https://doi.org/10.3390/NU9121286

Wiegand, C., Abel, M., Ruth, P., Elsner, P., & Hipler, U. C. (2015). In vitro assessment of the antimicrobial activity of wound dressings: influence of the test method selected and impact of the pH. *Journal of Materials Science: Materials in Medicine*, *26*(1), 1–13. https://doi.org/10.1007/S10856-014-5343-9/FIGURES/5

Yunoki, S., Kohta, M., Ohyabu, Y., & Iwasaki, T. (2015). In vitro parallel evaluation of antibacterial activity and cytotoxicity of commercially available silver-containing wound dressings. *Chronic Wound Care Management and Research*, *2*, 1–9. https://doi.org/10.2147/CWCMR.S72101

Conclusions and Perspectives

Global health is a continuously evolving and immensely complex dimension of human life, where myriads of environmental factors, living standards, working conditions, diseases, technologies, policies, events and trends intersect and interact with each other, shaping our existence as individuals and societies. While incredible progress has been made over the decades, new challenges lie ahead that will require all our ingenuity and commitment. Chronic wounds are a *silent epidemic* that is set to become larger and larger as our median age and the incidence of the related co-morbidities keep increasing. In parallel, antimicrobial resistance will continue frustrating all our efforts to develop new antibiotics and will cause wound infections that will be increasingly harder to contrast. In other words, we are getting more vulnerable to an enemy that is getting stronger. But actions exist that can be taken now, and science and technology can come again in our rescue by providing fundamental pieces of the solution to this pressing problem.

Bionanocomposite materials can be new, promising wound dressings that combine the biocompatibility and biodegradability of biomacromolecules – which are conductive towards rapid and proper healing of wounded tissues – with the antibacterial and useful biomedical properties of nanostructured materials – which can contrast the insurgence of infections and stimulate re-epithelialization. Many biomacromolecules and nanomaterials have been investigated in the literature at the present day. While nanostructured zinc oxide can reasonably be considered one of the most promising candidates among the antimicrobial nanomaterials, many biomacromolecules exist that have not been explored yet for these applications.

In this context, a nanostructured zinc oxide has been synthesized with high specific surface area, spherical morphology and average size of 32 nm that showed marked antibacterial activity against a non-pathogen strain of Gram-positive *S. epidermidis* and a pathogen strain of a Gram-negative *E. coli*. Future studies on nZnO shall investigate its internalization by bacteria or the damage inflicted to their membranes and cell walls, as well as the production of reactive oxygen species and their role in inducing bacterial death or growth inhibition. The same should be done on epithelial cells to further understand and mitigate cytotoxicity concerns.

The nZnO was successfully introduced inside different biomacromolecule-based films obtained from whey proteins, beta-glucans, poly(3-hydroxybutyrate-co-3-hydroxyvalerate) and carboxymethylated cellulose fiber. All these natural molecules are known for their useful biomedical properties but have never been explored for the fabrication of nanoZnO-containing nanocomposites for wound healing. Plus, these biomacromolecules can be sourced through environmentally friendly processes, thus creating an opportunity to make healthcare materials sustainable.

A process was established and refined over time that allowed to systematically characterize and test all these bionanocomposites, offering a coherent baseline for mutual comparison. This addressed another important open issue in current scientific research, i.e., the lack of standards and clear protocols for the comparison of experimental wound dressings, both in terms of physico-chemical and biological properties.

PHBV films are produced rapidly, but their poor transparency, homogeneity and water affinity did not allow to obtain good antibacterial properties.

Beta-glucans films were obtained from aqueous suspensions through a simple solvent casting procedure despite their well-known poor water solubility. While this has been a good progress towards their use for the fabrication of films and membranes, they showed low transmittance and swelling ratios, and could easily be damaged while handled. However, the antibacterial activity of bionanocomposite films was very high. This should induce future efforts to focus on their combination with other materials that can provide the necessary structural support and other key functional properties.

Carboxymethylated fiber insoluble films were combined with nZnO for the first time at McGill University, showing excellent swelling ratio but a lower antibacterial activity compared to protein and glucan-based films. In this context, cellulose-based materials revealed instrumental in improving the understanding of the highly researched antibacterial mechanism of nZnO. By tuning the amount of carboxyl groups in the polymeric chain, different amounts of Zn^{2+} ions could be sequestered by the negatively charged moieties, to the point where the antimicrobial action of the bionanocomposite resulted completely suppressed. Conversely, when the degree of carboxyl group substitution is high enough to make the film water-soluble, all zinc ions are released and their transport is favored by matrix dissolution, resulting into a much higher inhibition. This helped to shed light on

another open issue in the state of the art, i.e. a limited understanding of the mechanism of action of bionanocomposites. Clarifying which are the phenomena underlying their antimicrobial activity is key to further improve their therapeutic efficacy. While many studies so far have been looking into the release of antibacterial species from the BNC matrix, few to none of them have expanded on the physico-chemical interaction of these species with the surrounding biomacromolecules as a factor controlling their diffusion and ability to suppress bacterial growth.

Finally, whey protein isolate films offered a very good combination of optical transmittance, swelling ratio, mechanical properties and antibacterial activity. Furthermore, as a by-product of the dairy industry and thanks to the simple preparation technique using water as a solvent, WPI-based products offer the potential to the fabricated cheaply, thus providing affordable solutions to patients.

For all these reasons, the WPI-nZnO composites were considered for a deep biopharmaceutical characterization with the University of Pavia that confirmed their potential as advanced wound dressings. In fact, wettability was found to be within the range for wound dressings as well as hydration. The presence of nZnO enhanced swelling and helped retain an elastic behavior of the film after a 24h hydration, demonstrating that mechanical compliance with underlying tissues can be ensured throughout application. New insights were also gained on film degradation in time, revealing that a substantial degradation tends to occur within the span of one day. This was considerably reduced by the presence of nZnO, that provides stability to the matrix. However, further improvements would be required, which pointed to the possibility of conjugating proteins with polysaccharides to further decrease degradation.

In-vitro tests carried on human dermal fibroblasts revealed the conditions of cytocompatibility of film extracts and demonstrated that extracts obtained from WPI-nZnO films promote cellular proliferation. Finally, *in-vivo* wound healing tests carried on rats showed that wounds treated with WPI and WPI-nZnO bionanocomposites undergo a regular healing process and show fully restored epithelium at the end.

These are very good premises to justify new tests and studies that can improve the current properties of this bionanocomposite while assessing its suitability for future clinical applications, in an effort to bring to fruition new, advanced wound dressings that can help us tackle the next big global health challenges that lie ahead.

While the way to go is still long, in this three-years research work conducted across three universities, two continents, and countless laboratories and facilities, a small step forward in this direction has hopefully been made.